Advances in Meteorology

Air Pollution, Air Quality, and Climate Change

Guest Editors: Sachin D. Ghude, Pavan S. Kulkarni, D. M. Chate, Mrinal Biswas, Samir Pokhrel, and Anne Boynard

Air Pollution, Air Quality, and Climate Change

Advances in Meteorology

Air Pollution, Air Quality, and Climate Change

Guest Editors: Sachin D. Ghude, Pavan S. Kulkarni,
D. M. Chate, Mrinal Biswas, Samir Pokhrel,
and Anne Boynard

Editorial Board

Contents

Hindawi Publishing Corporation
Advances in Meteorology
Volume 2014, Article ID 983426, 2 pages
http://dx.doi.org/10.1155/2014/983426

Editorial

Air Pollution, Air Quality, and Climate Change

Sachin D. Ghude,[1] Pavan S. Kulkarni,[2] D. M. Chate,[1] Mrinal Biswas,[3] Samir Pokhrel,[1] and Anne Boynard[4]

[1] *Indian Institute of Tropical Meteorology, Dr. Homi Bahbha Road, Pashan, Pune, India*
[2] *Geophysics Centre of Evora (CGE), University of Evora, 7000 Evora, Portugal*
[3] *National Center for Atmospheric Research, Boulder, CO, USA*
[4] *Laboratoire AtmosphÃ'lres, Milieux, Observations Spatiales, Guyancourt, France*

Correspondence should be addressed to Sachin D. Ghude; sachinghude@tropmet.res.in

Received 28 May 2014; Accepted 28 May 2014; Published 6 July 2014

The introduction of gases and particulate contaminants in the atmosphere due to natural or human activities causes air pollution. The concentration and toxicity of these contaminants define air quality and in the long term contribute to climate change. Both air pollution and climate change influence each other through complex interactions in the atmosphere. This issue has 9 very interesting manuscripts, touching various aspects of air pollution and air quality and their impact on climate change.

Five out of nine articles deal with aerosols studies and their contribution to air pollution, radiative transfer, and cloud properties. B. P. Singh et al. studied the effect of burning of crackers and fireworks during festive season of Diwali on aerosol properties. They found significant increase in the aerosol optical depth, aerosol absorption coefficients, and aerosol scattering coefficients during affected period as compared to nonaffected periods. S. Tiwari et al. analyzed interannual and intraseasonal variability of aerosols, particularly fine mode particles ($PM_{2.5}$) at a dense traffic intersection and in the vicinity of a thermal power plant in the megacity of Delhi, India. They observed that during the study period $PM_{2.5}$ concentration exceeds Indian National Ambient Air Quality Standards (NAAQS) on significant number of days. They also found the strong influence of different seasons and meteorological parameters on the concentration of $PM_{2.5}$. A. S. Panicker et al. used satellite data to study the effect of aerosols on UV erythemal dose over megacities of Delhi, Mumbai, Kolkata, and Chennai in India. S. N. Pereira et al. analyzed time series of aerosol absorption coefficient over Evora, Portugal. They observed a strong annual cycle in aerosol absorption coefficient with high values during winters compared to summers. They noted that it may have resulted due to the combination of several factors, with emphasis on use of biomass (wood) burning for domestic heating during winters and lower boundary layer height restricting atmospheric dispersion of aerosols. W.-S. Jung et al. analyzed satellite data to study the seasonal variability of aerosol-cloud properties and aerosol indirect effect over four different regions in Korean Peninsula during the period 2000–2009. They also estimated aerosol indirect effect for summer monsoon period to find the role in modulating precipitation. S. Dipu et al. used zenith sky transmittance and surface radiation measurements to improve the retrieval of cloud microphysical parameters and found them in good agreement with the satellite data. D. M. Lal et al. used satellite data of lightning flashes and cloud ice size during the period 2000–2012 to study the interrelation between the two. They observed that total lighting increases with increase in the cloud ice size and attends maximum at certain optimum cloud ice size and after that lightning decreases with increasing cloud ice size. S. K. Kharol et al. in their manuscript reported long-term rainfall trends during summer monsoon over six major Indian cities. They also analyzed the variation in precipitation in the upwind and downwind directions to study the urban forcing and dynamics. F. B. Vicente et al. studied the effect of wildfires in Mexico and estimated

total yearly emissions of CO_2 in Mexico during the period 1999–2010 due to wildfires.

Through this special issue on air pollution, air quality, and climate change, we tried to bring forth the current issues in the field of air pollution and climate change.

Sachin D. Ghude
Pavan S. Kulkarni
D. M. Chate
Mrinal Biswas
Samir Pokhrel
Anne Boynard

Hindawi Publishing Corporation
Advances in Meteorology
Volume 2014, Article ID 471864, 7 pages
http://dx.doi.org/10.1155/2014/471864

Research Article

Relationship between Size of Cloud Ice and Lightning in the Tropics

Deen Mani Lal,[1] Sachin D. Ghude,[1] Jagvir Singh,[2] and Suresh Tiwari[1]

[1] *Indian Institute of Tropical Meteorology, Pune 411008, India*
[2] *Ministry of Earth Sciences, Lodhi Road, New Delhi 110060, India*

Correspondence should be addressed to Deen Mani Lal; dmlal@tropmet.res.in

Received 25 November 2013; Accepted 1 February 2014; Published 20 March 2014

Academic Editor: Pavan S. Kulkarni

The association of lightning flashes with mean cloud ice size over continental and oceanic region in the tropical areas has been analyzed using the observations from various satellite platforms (MODIS, TRMM, and LIS) for the period 2000–2011. We found that frequency of lightning in general is higher over the continental region compared to oceanic region, whereas larger size of cloud ice is observed over the oceanic regions compared to the continental regions. Relationship between lighting and cloud ice size shows similar features over both continental and oceanic regions. For the first time, we show that total lighting increases with increase in the cloud ice size; attends maximum at certain cloud ice size and then decreases with increase in cloud ice size. Maximum lightning occurred for the mean cloud ice size of around 23–25 μm over the continental region and mean cloud ice size of around 24–28 μm over the oceanic region. Based on our observation we argue that the relation between lightning and mean cloud ice size follow the curve linear pattern, and not linear.

1. Introduction

Generation of lightning in atmosphere is still a matter of debate. It is a commonly established fact that ice is a key element to generate and separate the positive and negative charges inside the cloud which assists formation of lightning in the atmosphere [1]. During the occurrence of deep convection, water vapors are uplifted and condensed to form the deferent sizes of noninductive hydrometers (ice crystal, hail, drops, etc.); afterwards they are evaporated/sublimated and dispersed zonally and meridionally in the upper troposphere [2]. During upward motion, hydrometers collide with each other generating the charge on ice crystals, graupel, and liquid water [3, 4]. Some of the earlier studies [3, 5] have shown that approximately 5×10^{-4} e.s.u. (0.17 pC) charges are transferred per collision between the crystals and graupels of radius approximately 50 μm. This activity mostly takes place at the height where the temperature is colder than −10°C [6]. Similarly, in other studies based on field measurement the charge density around 1 to 10 C/km^3 at the levels between the isotherms of −10 to −25°C have been reported [7]. Carey and Rutledge [8], Petersen et al. [9, 10], and Dye et al. [11] have found that strong updraft and production of significant lightning occurs at the height where the temperature is in between 0°C to −40°C. It is also believed that most of the noninductive charges inside the thunderstorm (due to rebounding collisions between graupel and ice crystals in the presence of super-cooled liquid water) are generated in this temperature region [4, 12–18]. The separation of the charge among the particles inside a cloud depends on the relative motion of hydrometers, whereas the rate of charge transfer and polarity depends on the size of particle, temperature and the liquid water content [19–21]. In addition, charges are also generated on crystal during condensation, evaporation, and sublimation/melting of ice. The rapid growth of electrification has been reported when cloud particles are frozen and form the ice during updraft [22, 23]. Laboratory experiment [3] showed that graupel pellets gain much more charges if graupels are growing by riming and collide with ice. Some laboratory experiment also showed that during freezing of distilled water very small negative charges are generated, whereas during melting much larger negative charges are

generated [24, 25], but this effect could not be observed when water is contaminated.

Aerosol also affects the cloud ice concentration and its size by reducing the mean droplet size, which enhances the ice concentration in the region where temperature is less than zero [26]. Takahashi [27] found that increasing tendency of lightning flashes is positively correlated with increasing concentration of cloud ice as well as its size. Sherwood et al. [28] reported that occurrence of maximum lightning is associated with small size of cloud ice. In another study, decreasing size of cloud ice with increasing the aerosol concentration has also been reported [29].

In recent study over central India [30] a positive correlation has been found between ice concentration and lightning during premonsoon and monsoon seasons, whereas Deierling et al. [1] reported significant correlation between both precipitation and nonprecipitation ice mass with total lightning over Northern Alabama and Colorado/Kansas. Similar relation between lightning and cloud ice masses has also been reported in other field observations [1, 10, 17, 31–34]. The combined effect of aerosol with thermodynamic effect over India [35] and threefold enhancement of cloud-to-ground lightning flash density over Houston, Texas [36], raises the issue of pollution or heat island effect as a cause. As ice is a form of frozen cloud drops above the freezing level during deep convection, some results reported positive relation of lightning with strong updraft [11, 37–39].

Sizes of cloud ice represent the meteorological condition, aerosol effect, atmospheric dynamics, and are closely related to the cloud electrification and lightning discharge. It is still not clear whether small or large ice sizes increase the lightning flashes. Sherwood et al. [28] reported that small ice generate more lightning, whereas less cloud electrification in small cloud ice area is also reported [18, 40]. In this study we have presented the relationship between size of cloud ice and lightning flashes on global scale (over tropical regions). Lightning flashes and effective radius of cloud ice are considered over both continental as well as oceanic region.

2. Data

In this study monthly mean cloud effective radius of ice phase (cloud particle size) (QA-W) from Moderate Resolution Imaging Spectroradiometer (MODIS) Level-3, cloud ice concentration from 3A12 version 6, and area averaged lightning from Lightning Imaging Sensor (LIS) on board of Tropical Rainfall Measurement Mission's (TRMM) satellite for the period of 2000–2011 data sets have been used for analysis. MODIS Level-3 was first launched on 18 December, 1999, on board the Terra platform and subsequently on 4 May, 2002, on board the Aqua platform, which is uniquely designed (high spatial resolution, wide spectral range, and near daily global coverage) to observe and monitor cloud effective radius and other Earth changes. We have used MODIS $1^\circ \times 1^\circ$ gridded level-3 monthly averaged cloud particle size from Terra platform (2000–2011) over continental region shown in Figure 1(d) as L1 [lat. (−35)–(−22), long. (−67)–(−47)], L2 [lat. (−12)–(−8), long. 9–29], and L3 [lat. 24–34, long. 68–83] in our analysis. Similarly, we used MODIS $1^\circ \times 1^\circ$ gridded level-3 monthly average cloud particle size data set from Aqua (2002–2011) over the oceanic region shown in Figure 1(d) as O1 [lat. (−32)–(−20), long. (−146)–(−126)], O2 [lat. 12–22, long. 49–73], and O3 [lat. 0–18, long. 124–149]. We have also used MODIS, Terra platform data set, for the period of 2000-2001 for oceanic region. The agreement between MODIS monthly average cloud particle size data product from Terra and Aqua is observed to be 90% (R = 0.95) suggesting that both data sets are quite consistent. TRMM Microwave Instrument (TMI) profiling gives global vertical hydrometer profiles and surface rainfall mean on $0.5^\circ \times 0.5^\circ$ grid resolution. This data set is available at TRMM Online Visualization and Analysis System (TOVAS) web-based interface (http://gdata1.sci.gsfc.nasa.gov/daac-bin/G3/gui.cgi?instanceid=TRMM_Monthly). We have used area average monthly vertical profile of cloud ice concentration retrieved by 3A12 algorithm over the continental region (L1, L2, and L3) and oceanic region (O1, O2, and O3). We have also used lightning data from LIS which is a science instrument on board the TRMM observatory launched on 28 November, 1997. The detection efficiency of LIS is more than 80% in both daytime and nighttime with resolution (4 to 7 km) over a large region (600×600 km) of the Earth's surface for total lightning (i.e., intracloud + cloud-to-ground) [41].

2.1. Selection of Study Area. Figures 1(a) and 1(b) show the example of spatial distribution of size of cloud ice and lightning, respectively, for the year 2005. Year 2005 is neither drought year nor very heavy rainfall year. It is considered as normal rainfall year [42]. In order to study the association between size of cloud ice and lightning, we have selected three regions over the continental region as L1, L2, and L3 and over the ocean as O1, O2, and O3 shown in Figure 1(d). We have used 12 years (2000–2011) of monthly cloud ice size and lightning data over the study area (L1, L2, L3 and O1, O2, O3) for analysis.

3. Results

3.1. Spatial Distribution of Cloud Ice Size and Lightning. Figure 1 shows the spatial and seasonal pattern of lightning and cloud effective radius (cloud particle/ice size) over the tropical regions for the year 2005. A clear spatial change in lightning and cloud ice can be seen in Figure 1. It is interesting to note from Figure 1 that frequency of lightning in general is higher over the continental region compared to oceanic region. The annual average lightning flashes over the areas L1, L2, and L3 are generally greater than 500 flashes/km^2/month, whereas over the areas O1, O2, and O3 are less than 25 flashes/km^2/months. On the other hand, larger size of cloud ice is observed over oceanic region compared to continental regions. The average cloud ice size is greater than 30 μm (some places more than 40 μm) over the oceanic region (O1, O2, and O3) and less than 25 μm over the selected areas (L1, L2, and L3) on continental region. During spring months (March, April, and May; MAM), intense lightning can be seen (Figure 1(d)) over the continental

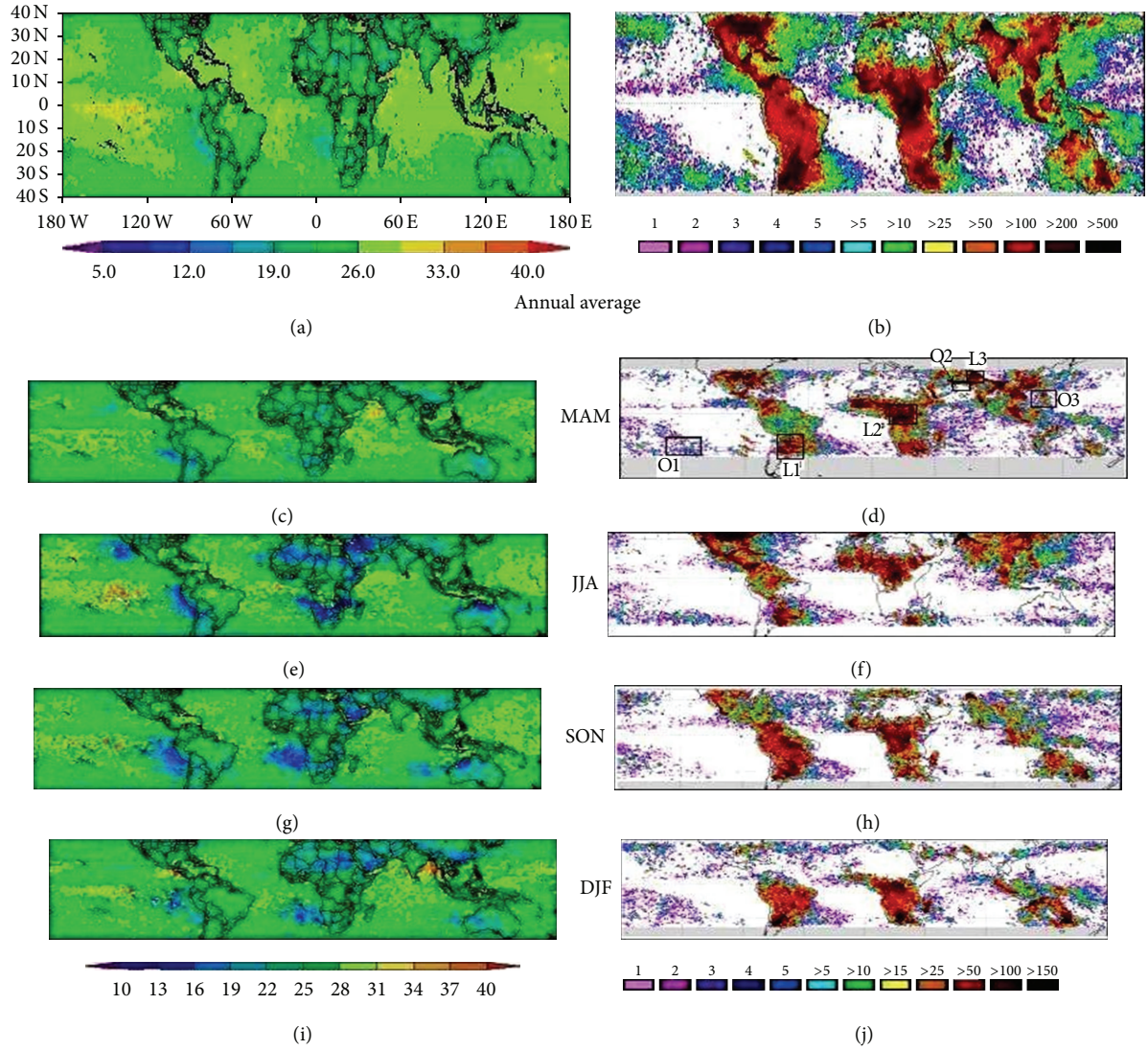

Figure 1: Spatial distribution of (a) size of cloud ice and (b) lightning for the annual average and four seasons during 2005.

regions such as Uruguay and surrounding regions (East part of Argentina and south Brazil), central part of United State, Colombia, Central African Republican and surrounding region, Democratic Republican of Congo (DRC), eastern part of South Africa, India (Indo Gangetic plain and in some other parts), South-East part of China, Thailand, and Indonesia. Lightning frequency greater than 150 flashes/km^2/month (Figure 1(d)) and the average effective cloud ice diameters between 22 and 25 μm (Figure 1(c)) have been observed over these regions. The lightning frequency over Mexico, Guatemala, Nicaragua, Angola, Namibia, and the entire part of Brazil during spring months has been observed to be less than 25 flashes/km^2/month (effective cloud ice diameter 28–31 μm). In comparison with continental regions (discussed above) the low lightning frequency (<5 flashes/km^2/month) and large ice particle size (31–40 μm) has been observed over the oceanic region. In Figure 1, the similar features are also evident during summer monsoon (June, July, and August; JJS), winter (December, January, and February; DJF), and fall months (September, October, and November; SON).

3.2. Relationship between Cloud Ice Size and Lightning. In order study the relationship between cloud ice size and lightning in detail we have analyzed the monthly mean cloud effective radius and total lightning (for the period 2000–2011) averaged over the continental (L1, L2, and L3) and oceanic (O1, O2, and O3) areas shown in Figure 1(d). Months corresponding to the cloud ice size between 19 and 34 μm are grouped in the bin size of 1 μm (we have considered all the months (12×12 = 144 months) for frequency count). We have noticed that there were hardly any months in which monthly mean cloud ice size was less that 19 μm or greater than 34 μm during the study period. Lightning corresponding to each bin (of 1 μm) is then added to obtain total lightning for every 1 μm bin between 19 and 34 μm. Figure 2 shows relationship between cloud ice size and lighting over the three different

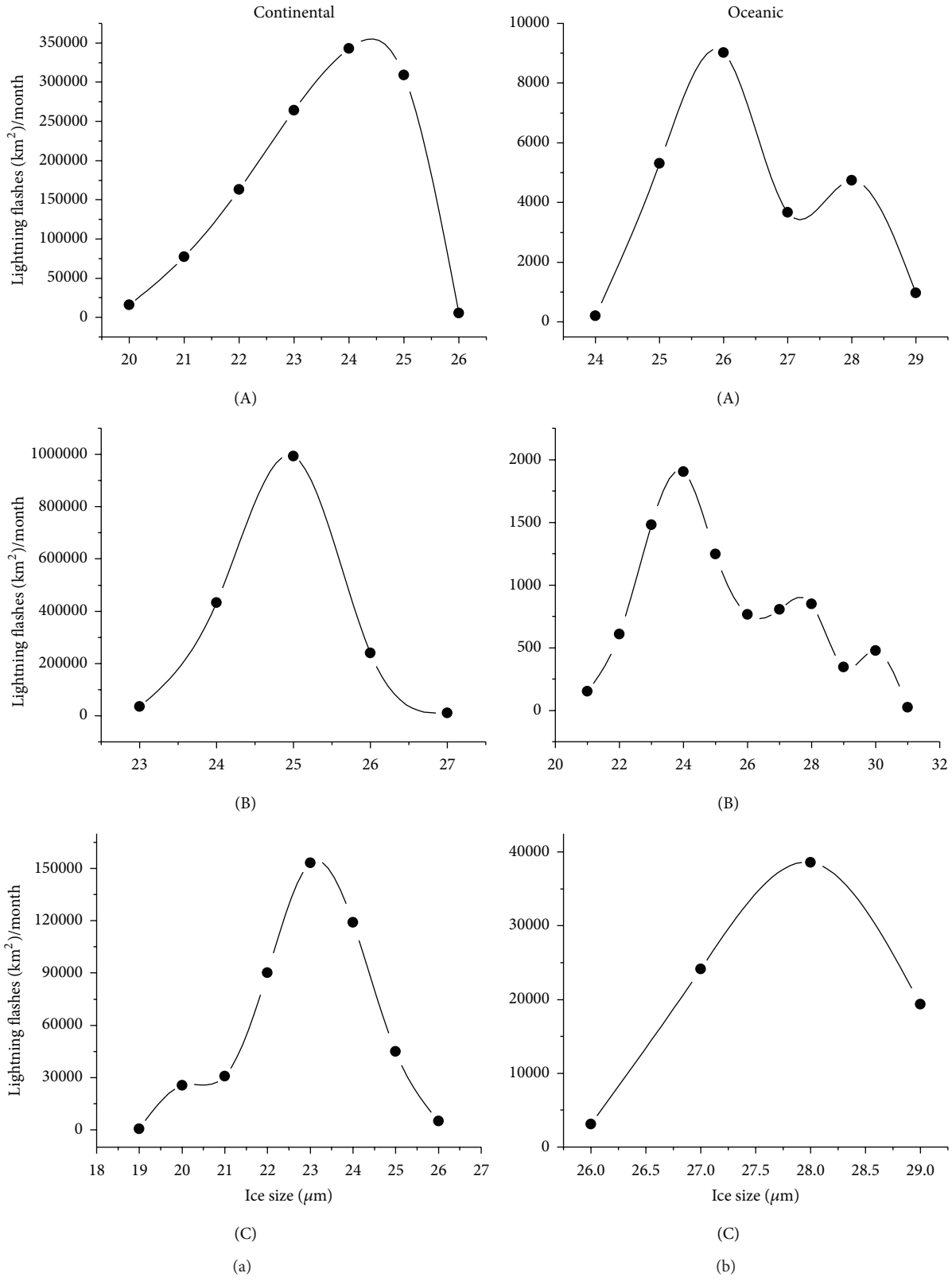

Figure 2: Relationship between mean cloud ice size and lightning over continental region (a) L1 (A), L2 (B), and L3 (C) and over oceanic region (b) O1 (A), O2 (B), and O3 (C).

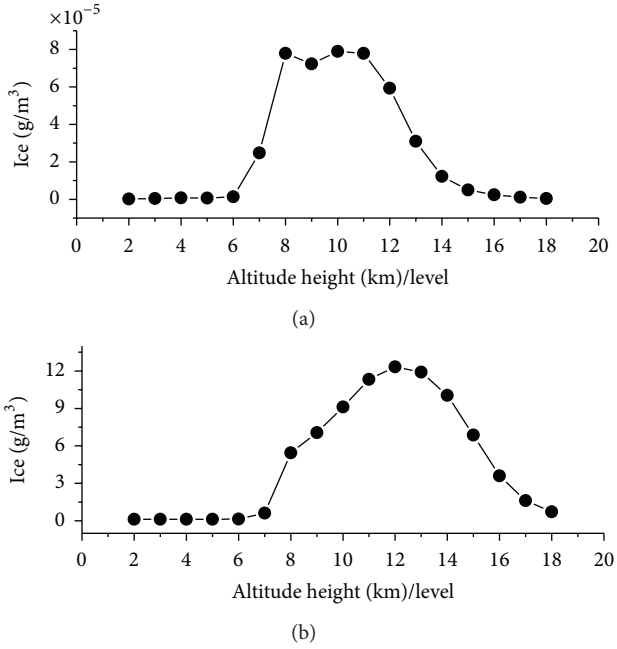

Figure 3: Distribution of cloud ice concentration as a function of altitude averaged during 2000–2011 period (a) over the continental region L1 and (b) oceanic region O2.

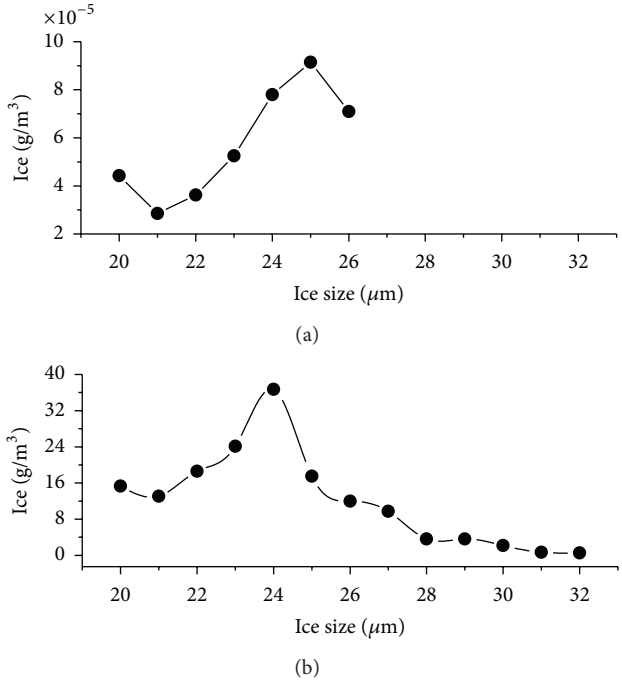

Figure 4: Relation between mean cloud ice size and cloud ice concentration averaged during 2000–2011 period at 12 km altitude (a) over the continental region L1 and (b) oceanic region O2.

continental (Figure 2(a)) and oceanic regions (Figure 2(b)). It can be seen that relationship between lighting and cloud ice size shows similar pattern over both continental and oceanic regions. Maximum lightning occurred for the mean ice cloud sizes of 24, 25, and 23 μm over the continental regions L1, L2, and L3, respectively. Similarly, over the oceanic regions O1, O2, and O3 maximum lightning occurred for the slightly greater mean cloud ice size of 26, 24, and 28 μm, respectively. It is interesting to note from Figure 2 that total lighting increases with increase in the cloud ice size, attains maximum at certain cloud ice size, and after that starts decreasing with increasing cloud ice size.

In order to understand this relationship we have analyzed vertical distribution of cloud ice concentration and relationship between cloud size with ice concentration over the continental and oceanic region. Figures 3(a) and 3(b) show the cloud ice concentration at different altitude averaged during 2000–2011 period over the continental region L1 and oceanic region O2, respectively. It can be seen that ice concentration increases from altitude of 6 km, attends maximum concentration around 8–11 km over L1 and 10–14 km over O2 region, and decreases nearly to zero concentration at 18 km. Figure 4 shows the distribution of cloud ice concentration as a function of mean cloud size at an altitude of 12 km (near to same height) over L1 and O2 regions, respectively. It can be seen from Figure 4 that ice concentration over L1 and O2 regions increases with respect to ice size up to 24 μm, attends maximum concentration at 24 μm, and ice concentration decreases with ice size above 24 μm. Similar relationship between ice concentration and ice size is also seen for the altitudes ranged between 8 and 14 km (not shown here). The charge is generated due to growth of ice size by condensation (deposition, combination of collection, etc.) and collision among them during upward motion [41, 43]. This process enhances the electric filed inside the cloud and generate lightning. During convection, cloud ice grows its size by combination of collection and condensation or deposition. The increasing ice concentration with respect to mean ice size from 19 to 24 μm in Figure 4 can be attributed to the growth of ice size. Therefore, generated charge (due to collision and condensation) increases with increasing the ice concentration and attends the maximum charge with the maximum ice concentration at 24 μm inside the cloud. Hence, increasing lightning frequency with increasing the ice concentration with respect to ice size from 19 to 24 μm with maximum lightning at 24 μm can be seen in Figure 2. Takahashi [27] has also found increase in lightning with increase in the ice concentration and ice size, compliments to our results. The latent heat is generated during condensation or deposition increases the updraft velocity of the hydrometers, which enhances the hydrometers concentration at high altitude (Figure 3) as well as electric filed inside the cloud. Ziegler and MacGorman [44] and Dey et al. [11] found that altitude range of about 7–10 km is favorable for electrification of clouds for generating lightning discharge. This is consistent with Figure 3 where we observed maximum ice concentration between 8 and 14 km altitude ranges. It can also be seen from Figure 3 that although maximum ice concentration over both land and oceanic regions are found approximately in same altitude range (8–14 km), yet less lightning occurs over oceanic region. It might be due to weak updraft velocity in mix-phase region over ocean as compared to continental region.

On the other hand, increased size of cloud ice increases its terminal velocity and thereby reduces the uplift velocity.

Therefore, larger particle descends isothermally towards the ground and begins to melt [45]. In this case charge with opposite polarity is also generated on hydrometer [43], however, unable to generate the charge to produce the lightning due to slow sublimation and low concentration of ice. Takahashi [4] also showed that the charge transfers per collision slow down with increase in ice diameter size. Therefore, the negative relationship between total lightning and mean cloud ice size which is greater than 26–28 μm instead of positive correlation for the size less than 19–25 μm can be seen in Figure 2. It is reasonable to conclude from Figures 2, 3, and 4 that the highest mean ice size of around 24 μm contributes to maximum ice concentration in the altitude range between 8 and 14 km and therefore results in the maximum lightning (over land and oceanic regions) for ice size of around 23–26 μm (seen in Figure 2). These imply that the relationship between mean ice size and lightning is curve linear.

4. Conclusions

In this work, we have analyzed 12 years (2000–2011) of monthly mean satellite observations of lightning from LIS, ice concentration from TRMM (3A12, V6), and effective diameter of cloud ice form MODIS over the Tropical Ocean and continental regions. We have examined the association of lightning flashes with mean ice size over these regions. A clear spatial change in lighting and cloud ice size from spring to winter season is seen. In general, total lightning is observed higher over the continental regions as compared to the lightning observed over oceanic region, whereas mean cloud ice size is observed higher over the oceanic region compared to the continental region during all the seasons. It is observed that the relationship between lightning and mean cloud ice size is same over both continental and oceanic regions. It is also observed that maximum lightning occurred for the mean cloud ice size of around 23–25 μm over the continental region and mean cloud ice size of around 24–28 μm over the oceanic region. However, for the first time, we found that relationship between lightning and mean cloud ice size follows the curve linear pattern and is not linear. We found that total lighting increases with increase in the cloud ice size and attends maximum at certain cloud ice size, then lightning decreases with increasing cloud ice size. The altitude profile show increase in ice concentration from 6 km, attends maximum concentration around 8–11 km over continent and 10–14 km over oceanic region, and decreases to zero concentration at around 18 km. Ice concentration within this region shows maximum around 24 μm. This concludes that maximum lightning observed around 23–25 μm over the continental region and 24–28 μm over the oceanic region is associated with the large ice concentration at around 24 μm.

Conflict of Interests

The authors declare that there is no conflict of interests regarding the publication of this paper.

Acknowledgments

The authors are gratefully thankful to Earth Observatory System and Earth System Science Program who provided the TRMM data. The authors also acknowledge the MODIS mission scientists and associated NASA personnel for the production of the data used in this research.

References

[1] W. Deierling, W. A. Petersen, J. Latham, S. Ellis, and H. J. Christian, "The relationship between lightning activity and ice fluxes in thunderstorms," *Journal of Geophysical Research: Atmospheres* , vol. 113, no. D15, Article ID D15210, 2008.

[2] R. E. Newell, Y. Zhu, E. V. Browell, W. G. Read, and J. W. Waters, "Walker circulation and tropical upper tropospheric water vapor," *Journal of Geophysical Research: Atmospheres*, vol. 101, no. D1, pp. 1961–1974, 1996.

[3] S. E. Reynolds, M. Brook, and M. F. Gourley, "Thunderstorm charge separations," *Journal of Meteorology*, vol. 14, pp. 426–436, 1957.

[4] T. Takahashi, "Riming electrification as a charge generation mechanism in thunderstorms," *Journal of the Atmospheric Sciences*, vol. 35, pp. 1536–1548, 1978.

[5] D. G. Evans and W. C. A. Hutchinson, "The electrification of freezing water droplets and of colliding ice particles," *Quarterly Journal of the Royal Meteorological Society*, vol. 89, no. 381, pp. 370–375, 1963.

[6] S. E. Reynolds, "Thunderstorm-precipitation growth and electrical-charge generation," *Bulletin of the American Meteorological Society*, vol. 34, pp. 117–123, 1953.

[7] P. R. Krehbiel, M. Brook, and R. A. McCrory, "An analysis of the charge structure of lightning discharges to ground," *Journal of Geophysical Research: Oceans*, vol. 84, no. 5, pp. 2432–2456, 1979.

[8] L. D. Carey and S. A. Rutledge, "A multiparameter radar case study of the microphysical and kinematic evolution of a lightning producing storm," *Meteorology and Atmospheric Physics*, vol. 59, no. 1-2, pp. 33–64, 1996.

[9] W. A. Petersen, S. A. Rutledge, and R. E. Orville, "Cloud-to-ground lightning observations from TOGA COARE: selected results and lightning location algorithms," *Monthly Weather Review*, vol. 124, no. 4, pp. 602–620, 1996.

[10] W. A. Petersen, S. A. Rutledge, R. C. Cifelli, B. S. Ferrier, and B. F. Smull, "Shipborne dual-Doppler operations during TOGA COARE: integrated observations of storm kinematics and electrification," *Bulletin of the American Meteorological Society*, vol. 80, no. 1, pp. 81–96, 1999.

[11] J. E. Dye, W. P. Winn, J. J. Jones, and D. W. Breed, "The electrification of New Mexico thunderstorms. 1. Relationship between precipitation development and the onset of electrification," *Journal of Geophysical Research: Atmospheres*, vol. 94, no. D6, pp. 8643–8656, 1989.

[12] S. E. Reynolds and M. Brook, "Correlation of the initial electric field and the radar echo in thunderstorms," *Journal of Meteorology*, vol. 13, no. 4, pp. 376–380, 1956.

[13] E. R. Jayaratne, C. P. R. Saunders, and J. Hallett, "Laboratory studies of the charging of soft- hail during ice crystal interactions," *Quarterly Journal of the Royal Meteorological Society*, vol. 109, no. 461, pp. 609–630, 1983.

[14] E. R. Williams, "The tripole structure of thunderstorms," *Journal of Geophysical Research: Atmospheres*, vol. 94, no. D11, pp. 13151–13167, 1989.

[15] C. P. R. Saunders and S. L. Peck, "Laboratory studies of the influence of the rime accretion rate on charge transfer during crystal/graupel collisions," *Journal of Geophysical Research: Atmospheres*, vol. 103, no. D12, pp. 13949–13956, 1998.

[16] E. R. Mansell, D. R. MacGorman, C. L. Ziegler, and J. M. Straka, "Charge structure and lightning sensitivity in a simulated multicell thunderstorm," *Journal of Geophysical Research: Atmospheres*, vol. 110, no. D12, pp. 1–24, 2005.

[17] J. Latham, W. A. Petersen, W. Deierling, and H. J. Christian, "Field identification of a unique globally dominant mechanism of thunderstorm electrification," *Quarterly Journal of the Royal Meteorological Society*, vol. 133, no. 627, pp. 1453–1457, 2007.

[18] E. J. Zipser, "Deep cumulonimbus cloud systems in the tropics with and without lightning," *Monthly Weather Review*, vol. 122, no. 8, pp. 1837–1851, 1994.

[19] E. R. Williams, R. Zhang, and J. Rydock, "Mixed-phase microphysics and cloud electrification," *Journal of the Atmospheric Sciences*, vol. 48, no. 19, pp. 2195–2203, 1991.

[20] R. G. Pereyra, E. E. Avila, N. E. Castellano, and C. P. R. Saunders, "A laboratory study of graupel charging," *Journal of Geophysical Research: Atmospheres*, vol. 105, no. D16, pp. 20803–20812, 2000.

[21] C. P. R. Saunders, H. Bax-Norman, C. Emersic, E. E. Avila, and N. E. Castellano, "Laboratory studies of the effect of cloud conditions on graupel/crystal charge transfer in thunderstorm electrification," *Quarterly Journal of the Royal Meteorological Society*, vol. 132, no. 621, pp. 2653–2673, 2006.

[22] V. N. Bringi, I. J. Caylor, J. Turk, and L. Liu, "Microphysical and electrical evolution of a convective storm using multiparameter radar and aircraft data during CaPE," in *Proceedings of the 26th International Conference on Radar Meteorology*, pp. 312–314, American Meteorological Society, May 1993.

[23] J. E. Dye, "Early electrification and precipitation development in a small, isolated Montana cumulonimbus," *Journal of Geophysical Research: Atmospheres*, vol. 91, no. D1, pp. 1231–1247, 1986.

[24] J. E. Dinger and R. Gunn, "Electrical effects associated with a change of state of water," *Terrestrial Magnetism and Atmospheric Electricity*, vol. 51, no. 4, pp. 477–494, 1946.

[25] M. Stolzenburg, T. C. Marshall, W. D. Rust, and B. F. Smull, "Horizontal distribution of electrical and meteorological conditions across the stratiform region of a mesoscale convective system," *Monthly Weather Review*, vol. 122, no. 8, pp. 1777–1797, 1994.

[26] D. Rosenfeld, U. Lohmann, G. B. Raga et al., "Flood or drought: how do aerosols affect precipitation?" *Science*, vol. 321, no. 5894, pp. 1309–1313, 2008.

[27] T. Takahashi, "Thunderstorm electrification—a numerical study," *Journal of the Atmospheric Sciences*, vol. 41, no. 17, pp. 2541–2558, 1984.

[28] S. C. Sherwood, V. T. J. Phillips, and J. S. Wettlaufer, "Small ice crystals and the climatology of lightning," *Geophysical Research Letters*, vol. 33, no. 5, Article ID L05804, 2006.

[29] S. C. Sherwood, "Aerosols and ice particle size in tropical cumulonimbus," *Journal of Climate*, vol. 15, no. 9, pp. 1051–1063, 2002.

[30] D. M. Lal and S. D. Pawar, "Relationship between rainfall and lightning over central Indian region in monsoon and premonsoon seasons," *Atmospheric Research*, vol. 92, no. 4, pp. 402–410, 2009.

[31] S. W. Nesbitt, E. J. Zipser, and D. J. Cecil, "A census of precipitation features in the tropics using TRMM: radar, ice scattering, and lightning observations," *Journal of Climate*, vol. 13, no. 23, pp. 4087–4106, 2000.

[32] W. Deierling, J. Latham, W. A. Petersen, S. M. Ellis, and H. J. Christian Jr., "On the relationship of thunderstorm ice hydrometeor characteristics and total lightning measurements," *Atmospheric Research*, vol. 76, no. 1–4, pp. 114–126, 2005.

[33] W. A. Petersen, H. J. Christian, and S. A. Rutledge, "TRMM observations of the global relationship between ice water content and lightning," *Geophysical Research Letters*, vol. 32, no. 14, Article ID L14819, 2005.

[34] K. C. Wiens, S. A. Rutledge, and S. A. Tessendorf, "The 29 June 2000 supercell observed during STEPS—part II: lightning and charge structure," *Journal of the Atmospheric Sciences*, vol. 62, no. 12, pp. 4151–4177, 2005.

[35] D. M. Lal and S. D. Pawar, "Effect of urbanization on lightning over four metropolitan cities of India," *Atmospheric Environment*, vol. 45, no. 1, pp. 191–196, 2011.

[36] S. M. Steiger, R. E. Orville, and G. Huffines, "Cloud-to-ground lightning characteristics over Houston, Texas: 1989–2000," *Journal of Geophysical Research: Atmospheres*, vol. 107, no. D11, pp. 2–13, 2002.

[37] E. J. Workman and S. E. Reynolds, "Electrical activity as related to thunderstorm cell growth," *Bulletin of the American Meteorological Society*, vol. 30, pp. 142–149, 1949.

[38] E. R. Williams and R. M. Lhermitte, "Radar tests of the precipitation hypothesis for thunderstorm electrification," *Journal of Geophysical Research: Oceans*, vol. 88, no. C15, pp. 10984–10992, 1983.

[39] S. A. Rutledge, E. R. Williams, and T. D. Keenan, "The Down Under Doppler and Electricity Experiment (DUNDEE): overview and preliminary results," *Bulletin of the American Meteorological Society*, vol. 73, no. 1, pp. 3–16, 1992.

[40] R. A. Black, J. Hellett, and C. R. P. Saunders, "Air craft study of precipitation and electrification," in *Proceeding of the 17th Conference on Severe Local Storms and Conference on Atmospheric Electricity*, pp. J20–J25, St. Louis, Mo, USA, October 1993.

[41] H. J. Christian, R. J. Blakeslee, S. J. Goodman et al., "The lightning imaging sensor," in *Proceedings of the 11th International Conference on Atmospheric Electricity*, pp. 746–749, Guntersville, Ala, USA, June 1999.

[42] *Annual Climate Summary*, IMD Government of India, 2005.

[43] J. P. Rydock and E. R. Williams, "Charge separation associated with frost growth," *Quarterly Journal of the Royal Meteorological Society*, vol. 117, no. 498, pp. 409–420, 1991.

[44] C. L. Ziegler and D. R. Macgorman, "Observed lightning morphology relative to modeled space charge and electric field distributions in a tornadic storm," *Journal of the Atmospheric Sciences*, vol. 51, no. 6, pp. 833–851, 1994.

[45] T. R. Shepherd, W. D. Rust, and T. C. Marshall, "Electric fields and charges near 0°C in stratiform clouds," *Monthly Weather Review*, vol. 124, no. 5, pp. 919–938, 1996.

Hindawi Publishing Corporation
Advances in Meteorology
Volume 2014, Article ID 958457, 8 pages
http://dx.doi.org/10.1155/2014/958457

Research Article

Estimation of Total Yearly CO_2 Emissions by Wildfires in Mexico during the Period 1999–2010

Flor Bautista Vicente,[1] Noel Carbajal,[1] and Luis Felipe Pineda Martínez[2]

[1] *División de Geociencias Aplicadas, Instituto Potosino de Investigación Científica y Tecnológica, 78216, SLP, Mexico*
[2] *Unidad de Ciencias de la Tierra, Universidad Autónoma de Zacatecas, 98600, ZAC, Mexico*

Correspondence should be addressed to Noel Carbajal; noelc@ipicyt.edu.mx

Received 1 October 2013; Revised 15 January 2014; Accepted 23 January 2014; Published 16 March 2014

Academic Editor: Sachin D. Ghude

The phenomenon of wildfires became a global environmental problem which demands estimations of their CO_2 emissions. Wildfires have deteriorated the air quality increasingly. Using available information on documented wildfires and a data set of satellite detected hot spots, total yearly emissions of CO_2 in Mexico were estimated for the period 1999–2010. A map of the main vegetation groups was used to calculate total areas for every vegetation type. The yearly number of hot spots per vegetation type was calculated. Estimates of emitted CO_2 in a wildfire were then accomplished by considering parameters such as: forest fuel load, vegetation type, burning efficiency, and mean burned area. The number of wildfires and total affected areas showed an annual variability. The yearly mean of affected area by a single wildfire varied between 0.2 and 0.3 km^2. The total affected area during the period 1999 to 2010 was 86800 km^2 which corresponds to 4.3% of the Mexican territory. Total CO_2 emissions were approximately 112 Tg. The most affected vegetation types were forest and rainforest.

1. Introduction

The enormous growth of the yearly number of forest fires of natural and anthropogenic origin has become a global environmental problem that affects worldwide ecosystems. Maps indicating the position of wildfire's occurrence practically cover a high percentage of the area of affected countries. Since there is a large variability in the characteristics of ecosystems, determined basically by topography, latitude, humidity, atmospheric and oceanic flows, soils, and so forth, the quantification of biomass per unit of area in each type of vegetation became a fundamental issue to estimate the aerosols emissions by wildfires. Biomass burning causes damages to vegetation, injuries to animal species, and land cover changes. The aerosols, produced by forest fires, influence the air quality and they alter the natural geochemical cycles in the atmosphere. Biomass burning significantly affects the ecosystems at functional level [1–3]. Practically in the whole American continent, from Alaska, Canada, until Argentina, occur a large number of wildfires where boreal forest, forest, rain forest, shrub land, grassland, and other vegetation types are devastated. In tropical regions, forest ecosystems are mostly affected by large fuel availability. In Mexico factors such as climate, incidence of hurricanes, topography, and soil bring on conditions for wildfires every year [4, 5]. These fires burn large areas of vegetation causing locally several environmental problems and in relative large distances severe conditions of air pollution [6].

Wildfires have negative impacts on the economy of affected countries. Several countries of Africa and Brazil have reported negative effects for tourism activities due to damages caused by wildfires in the vegetation of ecosystems. Countries such as India, Russia, Asia, Canada, and United States also annually reported economic losses by biomass burning [7]. In Mexico, losses of about US$ 337 million in wood and about US$ 39 million in reforestation costs have been reported for 2003 [7]. To explain this order of magnitude of economic losses in Mexico, it is convenient to analyze the statistics associated with wildfires. Between 1999 and 2010, a maximum number of about 10000 fires were reported and documented annually in Mexico, reaching the affected area values of 3000 km^2 [8]. It means that at these rates of

vegetation consumption in 20 years about 3% of the Mexican territory has been devastated by wildfires. However, a large number of wildfires that occur in inhospitable and remote areas are detected only by satellite sensors and they are not documented. The most affected regions are located in the Sierra Madre Oriental and in the southeastern part of Mexico.

There are several factors contributing to initiate the ignition in the established vegetation types. It includes basically human activities and those associated to drought periods [9]. The increase in emissions caused by biomass burning is a global scientific issue due to the generated pollution and to the potential damages associated with the greenhouse effect [2, 10, 11]. Diverse gas emissions by wildfires like carbon dioxide (CO_2), carbon monoxide (CO), NO_x, and water vapor [11–17] which are the result of vegetation burning have been documented worldwide. Kasischke and Penner [18] summarized the results of papers submitted to the meeting sponsored by Global Observation of Forest Cover/Global Observation of Land Dynamics and International Geosphere-Biosphere Program/International Global Atmospheric Chemistry/Biomass Burning Experiment. Chang and Song [19] estimated biomass burning emissions in tropical Asia. They applied burned areas estimated from newly published 1 km L3JRC and 500 m MODIS burned area products (MCD45A1). Relevant for the global warming are those of greenhouse effect like the CO_2 and methane. Another hazardous aspect is that a single wildfire plume of smoke may be transported large distances by wind effect leaving a pollution cloud over inhabited regions. Damoah et al. [20] showed that a plume of smoke from forest fires in Russia traveled over long distances from 10 to 31 of May, 2003. The plume of smoke was observed in several regions of the globe (Canada, Scandinavia, North-Atlantic, Germany, Europe, and Greenland). In this sense, biomass burning may have global implications.

It is difficult to quantify the amount of emitted pollutants into the atmosphere by wildfires, due to multiple factors involved in the ignition [2, 21]. However, there are methods to estimate the amount of produced pollutant in a wildfire by considering some parameters such as forest fuel load, vegetation type, burning efficiency, and burned area. This may represent an advantage for potential pollutant estimations in a wildfire event but may represent a problem when there is not enough information for all parameters. Nevertheless, other sources of data can be included such as satellite images, laboratory data, and field measurements [22].

Despite the complexity to quantify emitted pollutants by wildfires, different methodologies have been applied to estimate values and ranges of CO_2 emissions from biomass burning in different parts of the world. An estimation of CO_2 emissions in Greece yielded an order of magnitude of 2.2 Tg (1 Tg = 106 Ton) [21]. Calculations of emitted CO_2 by wildfires in the State of California, USA, deliver an approximated value of 6 Tg [13]. CO_2 emissions by wildfires in USA in the period 2002–2006 varied in the range 80–213 Tg [23]. An evaluation carried out for Russia and North America on CO_2 emissions by wildfires produced an order of magnitude varying between 828 and 1103 Tg [24]. A global estimation of CO_2 emissions by wildfires in 1994 yielded an approximated value of 5716 Tg

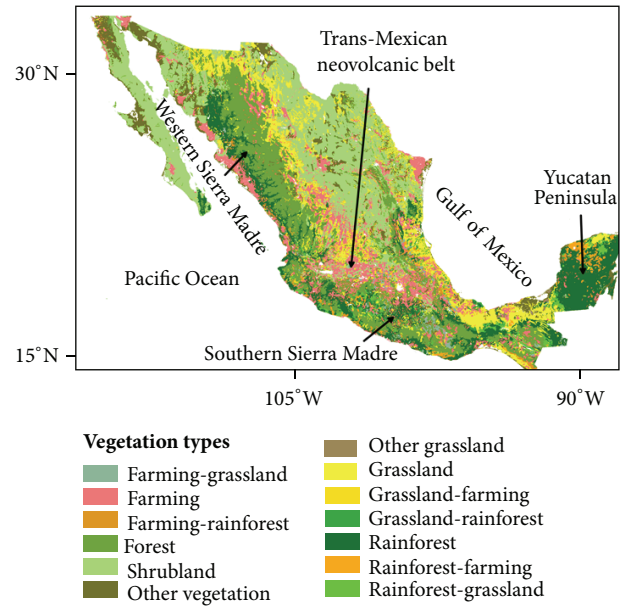

Figure 1: Main vegetation groups in Mexico. Groups of vegetation are displayed according to the floristic characteristic and vegetative development. The principal mountain chains and the peninsula of Yucatan are also indicated.

[17]. All these estimated quantities on CO_2 emissions by wildfires have implications on the chemical composition of the atmosphere. Thus it is essential to calculate CO_2 emissions in other regions of the world to understand the influence of this phenomenon, since it alters the carbon biogeochemical cycle and favors the global climate change by greenhouse effects [25–27]. In this research, we present estimations of the total CO_2 emissions by wildfires occurred in Mexico in the period from 1999 to 2010. The calculations are based on satellite information on fire hot spots, land cover, vegetation types, and other sources of information about wildfires.

2. Materials and Methods

Figure 1 shows the main vegetation groups in Mexico, according to the classification given by the National Institute for Statistics, Geography, and Informatics [28]. Different types of vegetation were grouped based on ecological floristic and physiognomic affinities. In the classification system performed by INEGI, was considered the development of vegetation by their degree of disturbance both by natural and anthropogenic causes. Mexico occupies an area of about 1964375 km^2. From this area, about 2.5% is superficial water (lakes, dams, and rivers). As a first step, the corresponding total area of each type of vegetation was calculated applying GIS (Geographical Information System). In Table 1, it is shown that shrubland occupies the largest area in Mexico with about 25.98% of the total area of Mexico. It is followed by forest with 17.51%, rainforest 14.24%, farming 13.52%, and grassland with 13.25%. These five types of vegetation embrace 84.5% of the total area. Although they were contemplated

Table 1: Available and calculated information on the considered ecosystems [29]. This data set was applied to estimate CO_2 emissions.

Vegetation type	Percentage of total area (%)	Biomass load (ton/km^2)	Burning efficiencies
Rainforest	14.24	5000–55000	0.2
Forest	17.51	5000–10000	0.3
Farming	13.52	500–10000	0.4
Grassland	13.25	150–550	0.96
Schrubland	25.98	50–200	0.95
Grassland-farming	1.24	350–5275	0.68
Rainforest-grassland	1.45	2575–27775	0.58
Farming-rainforest	1.16	2750–32500	0.30
Other vegetations	7.1	325	0.95

in the calculation, the rest of the vegetation types embrace percentages of 1-2%.

Although in Mexico thousands of wildfires are documented annually by the National Forest Commission (CONAFOR), there are enormous inaccessible regions where a large number of wildfires occur. The information given by CONAFOR considers only total number of documented wildfires and total affected areas per federal state of the country. The total number of documented wildfires and total affected areas per year for the whole country are given in Figure 2(a). Since the geographical information per federal state is not coincident with the geography of the ecosystems, yearly averaged affected areas per fire for the considered period (1999–2010) were calculated from the available data for the whole country. An alternative to fill the lack of information about all wildfires that occur in Mexico is by using satellite data. For this purpose, daily records of detected hot spots in Mexico for the period 1999–2010 were applied. The data set was obtained from reports issued by the National Commission for Knowledge and Use of Biodiversity (CONABIO). This data are obtained by CONABIO from MODIS (Moderate resolution Imaging Spectroradiometer) and from NOAA-AVHRR (National Oceanic and Atmospheric Administration-Advanced Very High Resolution Radiometer). The data set is the result of statistical analysis and verification of a real incidence of wildfires. From the original data set of hot spots, about 6% of them were eliminated [30]. Figure 2(b) shows the number of hot spots per year in the studied period. The yearly hot spots variability is due to climate factors, to anthropogenic activities, and to satellite feasibility [6, 30, 31]. Although the position of the hot spots is known, information on affected area is not available. For this reason, we applied yearly averaged affected areas from the documented wildfires. We summarize the followed methodology to estimate the emissions of CO_2 by wildfires in Mexico in the period from 1999 to 2010.

(a) A vegetation type map for México was used. This database was updated in 2005 by the National Institute for Statistics Geography and Informatics (INEGI).

(b) Historical records of documented forest fires were applied to estimate yearly means (1999–2010) of affected areas for the whole country. The data set was obtained from reports made by the National Forest Commission (CONAFOR).

(c) Daily records on the position of hot spots for the period 1999–2010 were applied (CONABIO).

(d) Applying a GIS approach, the total occupied area in the whole country by every vegetation type was established. Since the position of all hot spots is known, the total number of hot spots per vegetation type was then determined.

(e) After the statistical analysis and verification about the certainty that the applied hot spots are real wildfires [29], the corresponding yearly mean of affected area was assigned to every hot spot.

(f) Information on biomass load and biomass burning efficiencies for six types of vegetation was collected [29] (Table 1). For other combined vegetation types, average values for biomass load and burning efficiencies were calculated from the original components.

(g) The estimation of CO2 emissions was carried out as follows: the equation proposal by Seiler and Crutzen [32], actualized by Levine [29], was applied:

$$\mathrm{CO}_2(x, y) = \beta C(x, y), \tag{1}$$

where $CO_2(x, y)$ is the amount of carbon dioxide in Mg (1 Mg = 1 Ton) emitted by each forest fire (hot spot). (x, y) means the position (longitude, latitude) of the wildfire. $\beta = 0.90$ is the fraction of emitted CO_2 for tropical vegetation [29]. The variable $C(x, y)$ is written in the form $C(x, y) = \alpha \cdot M(x, y)$, where $M(x, y) = ABE$ (A = burned area in km^2, B = burned biomass load in Mg/km^2, and E = burning efficiency). $\alpha = 0.45$ is the percentage of carbon contained in the biomass [29]. From points a-6, all required information was available to estimate the CO_2 emissions by wildfires in Mexico into the atmosphere (Table 1).

3. Results and Discussion

Although the distribution of hot spots was determined for all types of vegetation and for every year applying a GIS process, this procedure is documented in Figures 3(a) and 3(b) for two

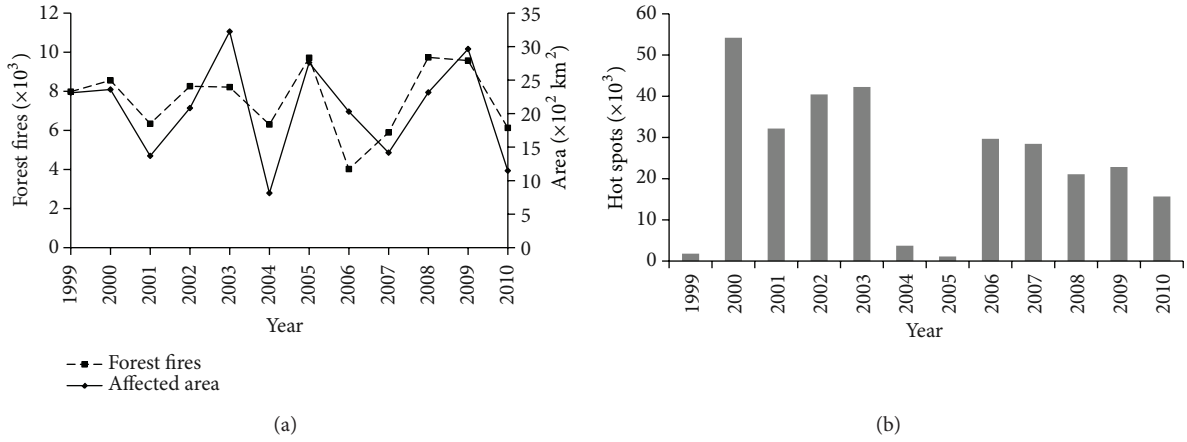

Figure 2: Documented number of forest fires and total affected area (CONAFOR) (a); reported number of hot spots (CONABIO) (b).

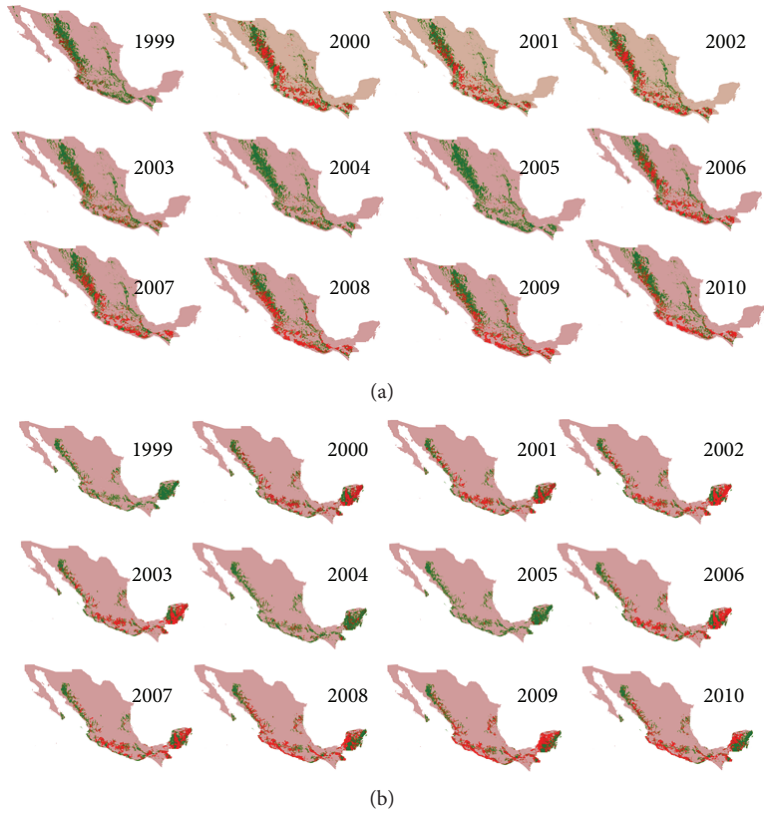

Figure 3: Incidence of wildfires in forest (a) and in rainforest (b). Green areas represent the polygon of the vegetation type and the red points symbolize the hot spots.

of the most important vegetation types for CO_2 emissions, that is, for forest and rainforest. The principal incidence of wildfires (red points) in forest (Figure 3(a)) occurs on the western side of Mexico, along the Western Sierra Madre, Southern Sierra Madre, Trans-Mexican Neovolcanic Belt, and Sierra Madre of Chiapas. In contrast, wildfires in rainforest occur dominantly in the Peninsula of Yucatan and along the coastal plains of the Gulf of Mexico and Pacific Ocean (Figure 3(b)). The number of wildfires in each vegetation type varies from year to year and the incidence of wildfires in different types of vegetation is not necessarily correlated. For example, in 2003 occurred relatively few wildfires in forest but in rainforest the incidence of wildfires was especially high. Even within the same type of vegetation, the distribution of wildfires strongly changes from year to year. It seems that climatic factors like rainfall, humidity, drought periods, and hurricanes influence regionally the potential incidence of wildfires. These climatic factors are reflected in parameters

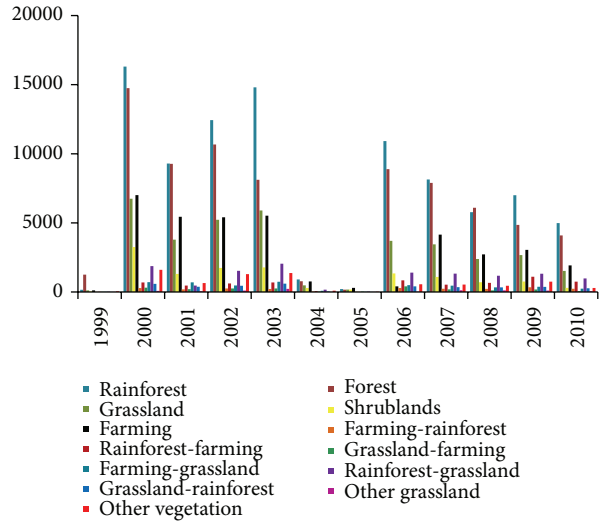

Figure 4: Time series of the yearly number of hot spots (wildfires) per vegetation type.

like normalized difference vegetation index (NDVI), relative humidity, relative green maps, fuel availability, and others which are applied to predict conditions for incidence of wildfires and to explain its regional variability. In the Peninsula of Yucatan, in the years 1999, 2004, and 2005, the number of wildfires was small compared with the rest of the years where the density of wildfires was always very high. This analysis reveals the importance of separating the incidence of wildfires in each type of vegetation. This kind of analysis could also provide strategies to prevent the occurrence of wildfires or to be prepared for a possible large incidence of fires. Another important aspect to be analyzed in the question of wildfires is its occurrence in the different types of vegetation. Once the polygons for all considered vegetation types were determined (see Figure 3 for forest and rain forest), the number of hot spots in each type of vegetation was calculated. In order to complete the discussion on the incidence of wildfires in the different types of vegetation, a histogram of yearly accumulated number of hot spots in every vegetation type is given in Figure 4. Although the variability in the number of hot spots seems to be correlated for all vegetation types, there are large changes in the number of hot spots for each vegetation type. For example, for rainforest, the number of hot spots varied from about 16 000 in the year 2000 to only a few hundred in 2005. It is also of interest to remark that there are years with a large number of wildfires in all vegetation types and years where the number of wildfires decreases dramatically. In the period of time considered (1999–2010), a recurrent minimum in the number of wildfires seems to occur every 5-6 years. In years with a minimum number of detected hot spots, there are even vegetation types without any incidence of wildfires.

Once the total yearly number of wildfires was determined for every type of vegetation, the corresponding yearly mean of affected area was then applied. In Figure 5(a), yearly means of affected areas, calculated from the total documented wildfires by the National Forest Commission, are displayed. Due to the scarce regional information about affected areas by every wildfire, we had to calculate a yearly mean affected area for the whole country. With the information on yearly mean affected area and with the yearly number of wildfires, it was possible to estimate the yearly affected area for every type of vegetation and the total yearly affected area. Comparison of yearly mean affected area and total yearly affected area considering all wildfires in all types of vegetation indicates that these two variables are occasionally positively and sometimes negatively correlated (Figures 5(a) and 5(b)). In 2004, a small yearly mean affected area coincided with a small total affected area by all wildfires. On the contrary, in 2005, a relative large yearly mean affected area is negatively correlated with a very small total affected area. The number of hot spots in 2005 was the smallest in the considered period. Considering that the CONAFOR documented in this year about 9000 wildfires, it is obvious that there were problems with the detection or availability of hot spots for CONABIO. In the years 2003 and 2006, a positive correlation takes place; that is, large yearly means affected areas coincide with large total affected areas considering all wildfires. From this analysis on affected areas, for example, large yearly mean affected areas and very small total yearly affected areas, the importance of regionally well-documented wildfires acquires relevance. The total yearly affected area seems to have a large variability, whereas the yearly mean affected area per wildfire remains dominantly in the same order of magnitude, about 0.2-0.3 km^2. The total affected area during the period 1999 to 2010 was approximately 86800 km^2 which corresponds to about 4.3% of the Mexican territory.

By applying (1) and using the number of wildfires, yearly means of affected areas, the biomass load, and burning efficiencies for each vegetation type, the total yearly emissions of CO_2 into the atmosphere by wildfires were estimated. It is important to mention that due to the wide variety of vegetations in Mexico, there is still insufficient information about total forest fuel per area for each type of vegetation. However, we consider that the collected information about biomass load and burning efficiencies could yield a good order of magnitude of total yearly emissions of CO_2. The total yearly emissions of CO_2, T_E were then calculated from the sum of all emissions. To analyze the role played by every type of vegetation in the total yearly emissions (T_E), time series of the percentage of emissions of CO_2 for every type of vegetation is given in Figure 6. Whereas for rainforest, forest, and grassland, their percentages in the total emissions remain largely the same, and there are other vegetation types with a growing influence like grassland-rainforest, rainforest-farming, and rainforest-grassland. The principal problem in Mexico related to wildfires is in rainforest regions where about 50–60% of the total emissions of CO_2 to the atmosphere occur. It is followed by forest regions with about 20% of the total emissions. The emissions by the vegetation type rainforest-farming grew from about 2% in 1999 to 7% in 2010, and this could be a warn signal for the CONAFOR. Although the percentages of emissions by farming areas show some oscillations, they remain approximately between 6 and 10%. Other vegetation types, farming-grassland, and shrubland reach values around 1%. Although the available

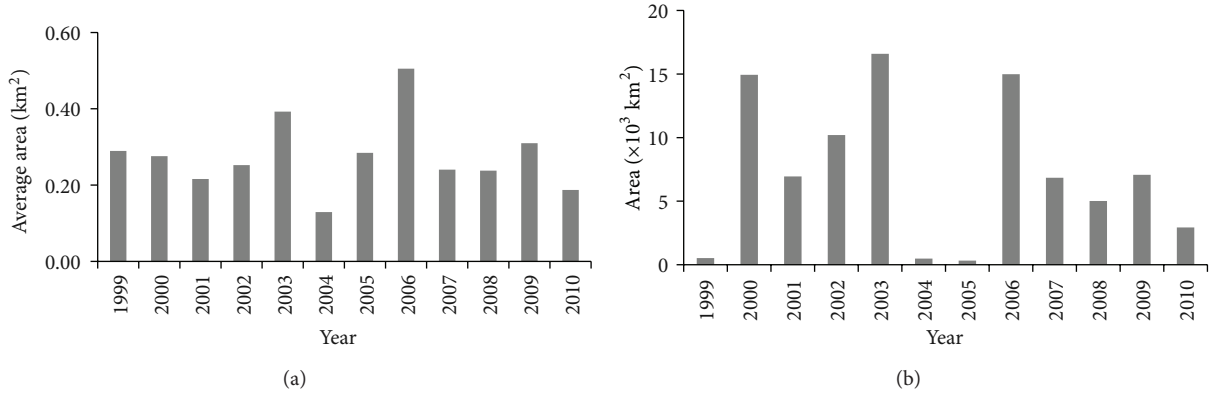

Figure 5: Mean affected area per fire obtained from documented wildfires (CONAFOR) (a) and total affected area considering all reported hot spots in all vegetation types (CONABIO) (b).

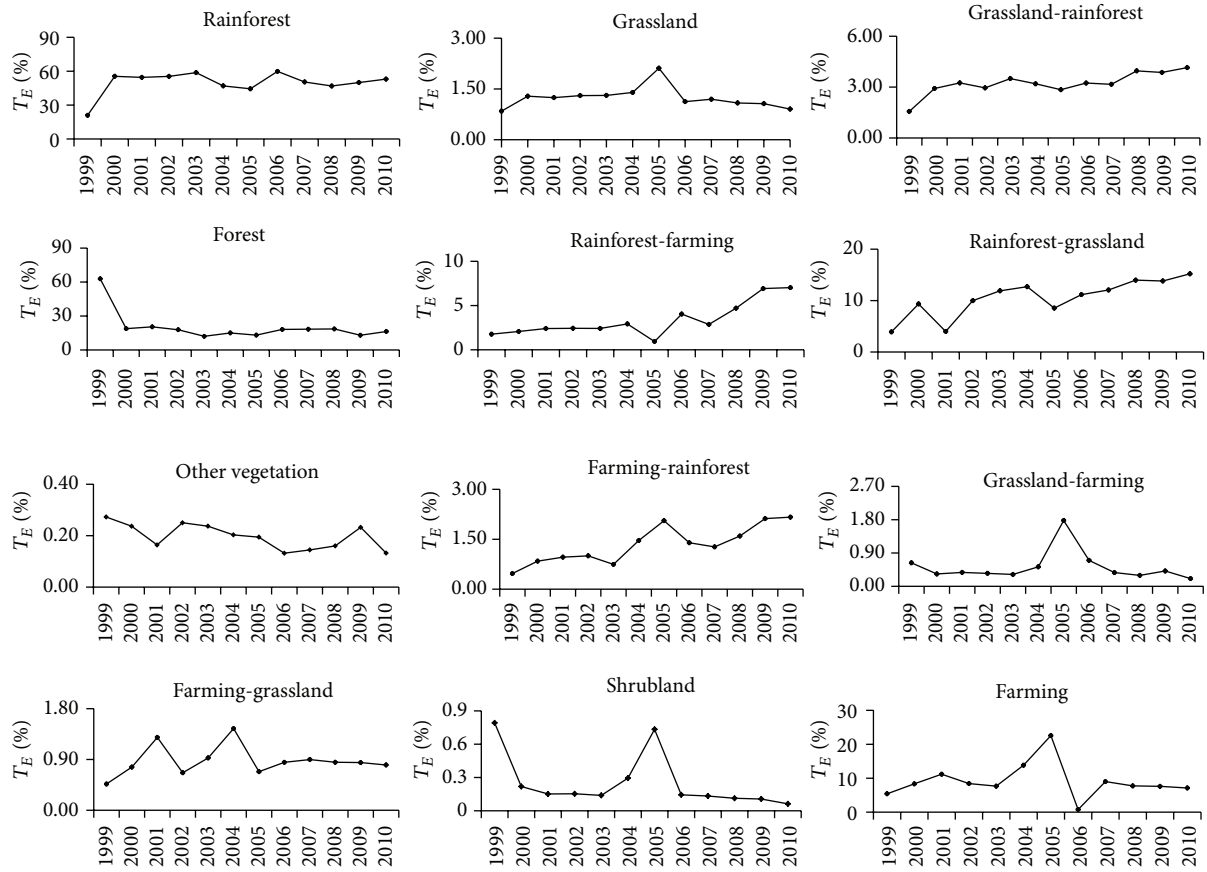

Figure 6: Time series of the percentages of each vegetation type in relation to the total yearly emissions. The considered period is from 1999 to 2010.

information is scarce, we think that this analysis reveals very well what is happening in the; therefore it could be relevant to the design of firefighting strategies.

3.1. Total Emissions of CO_2. We have carried out a careful analysis on the distribution of wildfires in the different ecosystems and we have discussed about the relative importance of the vegetation types in the emissions of CO_2 to the atmosphere. It allowed for obtaining information on the tendencies in the incidence of wildfires in the vegetation types. It was possible to determine total affected areas separately, that is, in every vegetation type and for every year in the considered period. The principal aim of this research work was to estimate the total emissions of CO_2 considering the incidence of the wildfires for the main groups of vegetation in Mexico. In Figure 6, the percentage of yearly emissions of CO_2 for every ecosystem was displayed. It provided relevant

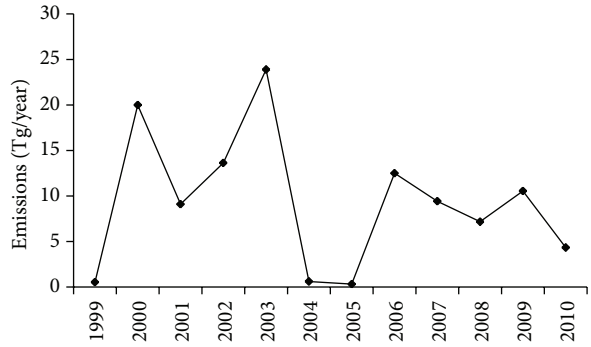

Figure 7: Total yearly emissions of CO_2 in Mexico during the period 1999 to 2010 considering all vegetation types.

evidence about the tendencies related to the emissions by wildfires in every type of vegetation. We consider that the knowledge about the tendency of damages of vegetation types by wildfires is very important to establish policies to protect threatened areas. In Figure 7, the time series of the yearly total emission of CO_2 by wildfires during the period 1999–2010 in Mexico is given. The total emission of CO_2 for this period is 112 Tg and the annual mean is 9.3 Tg with a standard deviation of 7.5 Tg. The estimated quantities in this work are relevant because it gives an idea about the tons of CO_2 emitted into the atmosphere and its impact on the greenhouse effect. The most affected regions due to these emissions are located in the southern part and in the peninsula of Yucatan. It corresponds to areas with forest and rainforest (see Figure 3). The results reflect the magnitude of the problem of air pollution, principally in the months with major presence of wildfires which regularly occur from January to May, although in some years it extends until August [6]. It is important to mention that the presented results may have uncertainties in the estimation of total yearly emissions of CO_2, due to the lack of information or due to the form in which available data were applied. The documentary sources provide only the available information but it is not the required, and it is incomplete. However, the results are relevant because they provide a quantitative idea about the emissions of CO_2 generated by forest fires that occur in Mexico every year. We are aware that currently there is a degree of uncertainty about the magnitude of CO_2 emissions by biomass burning. The same occurs with the pollution affecting the air quality in urban areas near regions with a high incidence of forest fires with the corresponding CO_2 emissions. The difficulties that we found to estimate the CO_2 emissions by wildfires in Mexico have been with approximations ridded, but the principal barrier was that wildfires are not well documented. Finally in Table 2, we compare the results obtained in this work with other estimations realized in different parts of de world and with different methodology.

4. Conclusions

Using available data like documented wildfires, the position of satellite-detected hot spots, biomass load for every type of vegetation, and biomass burning efficiencies, important information on yearly variability and distribution of wildfires was obtained. We found that emissions of carbon dioxide (CO_2) due to wildfires represent a problem that affects predominantly the vegetation types: rainforest, forest, grassland, and farming in Mexico. The total CO_2 emissions to the atmosphere during the period 1999 to 2010 were of the order of 112 Tg, with a yearly mean emission of about 9.3 Tg. According to our results, the emissions of CO_2 to the atmosphere by wildfires are in the order of magnitude of those reported in other studies realized in different parts of the world. In the same period, an area of approximately 86800 km^2 was affected by the wildfires. The analysis on the incidence of wildfires in different types of vegetation revealed interesting aspects about the relative importance of each ecosystem. We found that the relative significance of forest and rainforest in the question of wildfires remained approximately constant in the period 1999–2010. In contrast, the relative importance of rainforest-farming and rainforest-grassland is continuously growing. Since there are in Mexico vast inaccessible regions where also a large number of wildfires occur, our estimations acquire importance because the whole Mexican territory was considered through the detected hot spots in the calculation of total yearly emissions of CO_2. We are aware that there is a lot of work to be in a position where better estimations for the emissions of CO_2 can be carried out, but we consider our results as an important first step in that direction.

Table 2: Reported values of CO_2 emissions by forest fires in different parts of the world.

CO_2 emissions in Tg	Site
2.2	Greece [21]
6	California (USA) [13]
112	This work—Mexico (1999–2010)
147	USA [23]
966	Russia North America [24]
5716	Global [17]

Conflict of Interests

The authors declare that there is no conflict of interests regarding the publication of this paper.

Acknowledgment

The authors thank the Consejo Nacional de Ciencia y Tecnología (CONACYT) for the partial support of this research CB-2011-C01-168011.

References

[1] M. A. Cochrane, "Fire science for rainforests," *Nature*, vol. 421, no. 6926, pp. 913–919, 2003.

[2] J. S. Levine, T. Bobbe, N. Ray, A. Singh, and R. G. Witt, "Wildland fires and the environment: a global synthesis," Tech. Rep. UNEP/DEIAEW/TR. 99-1, 1999.

[3] C. N. Skinner and C. Chang, "Fire regimes, past and present. Vol II. Assessments and scientific basis for management options," Wildland Resources Center Report 37, Centers for Water and Wildland Resources, University of California, Davis, Calif, USA, 1996.

[4] J. Sarukhán, *Capital Natural de México. Síntesis: Conocimiento Actual, Evaluación y Perspectivas de Sustentabilidad*, Comisión Nacional para el Conocimiento y Uso de la Biodiversidad, Tlalpan, México, 2009.

[5] V. Sosa and P. Davila, "Una evaluacion del conocimiento floristico de Mexico," *Annals of the Missouri Botanical Garden*, vol. 81, no. 4, pp. 749–757, 1994.

[6] L. Villers-Ruiz and J. López-Blanco, *Incendios Forestales en México. Métodos de Evaluación*, Centro de Ciencias de la Atmósfera, Universidad Nacional Autónoma de México, Distrito Federal, México, 2004.

[7] Food and Agriculture Organization of the United Nations (FAO), *Fire Management Global Assessment*, 2006.

[8] Comisión Nacional Forestal (CONAFOR), "Reports issued weekly," 2010, http://www.cnf.gob.mx:8080/snif/portal/las-demas/reportes-de-incendios-forestales.

[9] M. J. McPhaden, "El Niño and La Niña: causes and Global Consequences. Volume I, the Earth System: physical and chemical dimensions of global environmental change," in *Encyclopedia of Global Environmental Change*, M. C. MacCracken and J. S. Perry, Eds., pp. 353–370, 2002.

[10] M. A. Cochrane, "Synergistic interactions between habitat fragmentation and fire in evergreen tropical forests," *Conservation Biology*, vol. 15, no. 6, pp. 1515–1521, 2001.

[11] J. Contreras-Moctezuma, D. A. Rodríguez-Trejo, A. Retama-Hernández, and J. J. M. Sánchez-Rodríguez, "Gases del humo de incendios en bosques de pinus hartwegii," *Agrociencia*, vol. 37, no. 3, pp. 309–316, 2003.

[12] J. M. Lobert, D. H. Scharffe, W. M. Hao et al., "Experimental evaluation of biomass burning emissions: nitrogen and carbon containing compounds," in *Global Biomass Burning: Atmospheric, Climatic and Biospheric Implications*, J. S. Lavine, Ed., pp. 289–304, MIT Press, Cambridge, Mass, USA, 1991.

[13] N. E. Clinton, P. Gong, and K. Scott, "Quantification of pollutants emitted from very large wildland fires in Southern California, USA," *Atmospheric Environment*, vol. 40, no. 20, pp. 3686–3695, 2006.

[14] D. F. Hurst, D. W. T. Griffith, J. N. Carras, D. J. Williams, and P. J. Fraser, "Measurements of trace gases emitted by Australian savanna fires during the 1990 dry season," *Journal of Atmospheric Chemistry*, vol. 18, no. 1, pp. 33–56, 1994.

[15] M. O. Andreae and P. Merlet, "Emission of trace gases and aerosols from biomass burning," *Global Biogeochemical Cycles*, vol. 15, no. 4, pp. 955–966, 2001.

[16] T. J. Christian, B. Kleiss, R. J. Yokelson et al., "Comprehensive laboratory measurements of biomass-burning emissions: 1. Emissions from Indonesian, African, and other fuels," *Journal of Geophysical Research D*, vol. 108, no. 23, article 16, 2003.

[17] J. J. Hoelzemann, M. G. Schultz, G. P. Brasseur, C. Granier, and M. Simon, "Global Wildland Fire Emission Model (GWEM): evaluating the use of global area burnt satellite data," *Journal of Geophysical Research D*, vol. 109, no. D14, article 27, 2004.

[18] E. S. Kasischke and J. E. Penner, "Improving global estimates of atmospheric emissions from biomass burning," *Journal of Geophysical Research D*, vol. 109, no. 14, pp. D14–S01, 2004.

[19] D. Chang and Y. Song, "Estimates of biomass burning emissions in tropical Asia based on satellite-derived data," *Atmospheric Chemistry and Physics*, vol. 9, pp. 19599–19640, 2009.

[20] R. Damoah, N. Spichtinger, C. Forster et al., "Around the world in 17 days—hemispheric-scale transport of forest fire smoke from Russia in May 2003," *Atmospheric Chemistry and Physics*, vol. 4, no. 5, pp. 1311–1321, 2004.

[21] M. Lazaridis, M. Latos, V. Aleksandropoulou, O. Hov, A. Papayannis, and K. Tørseth, "Contribution of forest fire emissions to atmospheric pollution in Greece," *Air Quality, Atmosphere and Health*, vol. 1, no. 3, pp. 143–158, 2008.

[22] J. S. Levine, "Global Biomass Burning: a case study of the gaseous and particulate emissions released to the atmosphere during the 1997 fires in Kalimantan and Sumatra, Indonesia," in *Biomass Burning and Its Inter-Relationships with the Climate System*, vol. 3 of *Advances in Global Change Research*, pp. 15–31, 2000.

[23] C. Wiedinmyer and J. C. Neff, "Estimates of CO_2 from fires in the United States: implications for carbon management," *Carbon Balance and Management*, vol. 2, no. 1, article 10, 2007.

[24] E. S. Kasischke and L. P. Bruhwiler, "Emissions of carbon dioxide, carbon monoxide, and methane from boreal forest fires in 1998," *Journal of Geophysical Research D*, vol. 108, no. 1, pp. 2–14, 2003.

[25] J. W. Raich and W. H. Schlesinger, "The global carbon dioxide flux in soil respiration and its relationship to vegetation and climate," *Tellus B*, vol. 44, no. 2, pp. 81–99, 1992.

[26] P. M. Fearnside, "Global warming and tropical land-use change: greenhouse gas emissions from biomass burning, decomposition and soils in forest conversion, shifting cultivation and secondary vegetation," *Climatic Change*, vol. 46, no. 1-2, pp. 115–158, 2000.

[27] N. Gruber and J. N. Galloway, "An Earth-system perspective of the global nitrogen cycle," *Nature*, vol. 451, no. 7176, pp. 293–296, 2008.

[28] INEGI (Instituto Nacional de Estadística, Geografía e Informática), *Guía Para la Interpretación de Mapa de Usos de Suelo y Vegetación*, Escala 1:250000: Series III/ INEGI, Aguascalientes, México, 2009.

[29] J. S. Levine, "Biomass burning: the cycling of gases and particulates from the biosphere to the atmosphere," in *Treatise on Geochemistry, the Atmosphere*, R. F. Keeling, Ed., Elsevier, 2003.

[30] R. Ressl, G. Lopez, I. Cruz et al., "Operational active fire mapping and burnt area identification applicable to Mexican Nature Protection Areas using MODIS and NOAA-AVHRR direct readout data," *Remote Sensing of Environment*, vol. 113, no. 6, pp. 1113–1126, 2009.

[31] S. J. Wright, "Tropical forests in a changing environment," *Trends in Ecology and Evolution*, vol. 20, no. 10, pp. 553–560, 2005.

[32] W. Seiler and P. J. Crutzen, "Estimates of gross and net fluxes of carbon between the biosphere and the atmosphere from biomass burning," *Climatic Change*, vol. 2, no. 3, pp. 207–247, 1980.

Hindawi Publishing Corporation
Advances in Meteorology
Volume 2014, Article ID 849279, 8 pages
http://dx.doi.org/10.1155/2014/849279

Research Article

Assessment and Validation of i-Skyradiometer Retrievals Using Broadband Flux and MODIS Data

S. Dipu,[1,2] G. Pandithurai,[1] A. S. Panicker,[1] T. Takamura,[3] Dong-In Lee,[4] and Dongchul Kim[5]

[1] *Indian Institute of Tropical Meteorology, Pune 411008, India*
[2] *Leipzig Institute for Meteorology, 04103 Leipzig, Germany*
[3] *CEReS, Chiba University, Inage-ku, Chiba 263-8522, Japan*
[4] *Department of Environmental Atmospheric Sciences, Pukyong National University, Busan 608737, Republic of Korea*
[5] *Universities Space Research Association, Columbia, MD 21044, USA*

Correspondence should be addressed to S. Dipu; dipuss@gmail.com and Dong-In Lee; leedi@pknu.ac.kr

Received 25 November 2013; Accepted 3 January 2014; Published 17 February 2014

Academic Editor: Sachin D. Ghude

Ground-based network of cloud measurements is presently limited and there exists uncertainty in the cloud microphysical parameters derived from ground-based measurements. Bias in the i-skyradiometer derived cloud optical depth (τ_c) and droplet effective radius (R_{eff}) and the importance of these parameters in the parameterization of clouds in climate models have made us intend to develop a possible method for improving these parameters. A new combination method, which uses zenith sky transmittance and surface radiation measurements, has been proposed in the present study to improve the retrievals. The i-skyradiometer derived parameters τ_c and R_{eff} have been provided as a first guess to a radiative transfer model (SBDART) and a new retrieval algorithm has been implemented to obtain the best combination of τ_c and R_{eff} having minimum bias (−0.09 and −2.5) between the simulated global and diffuse fluxes at the surface with the collocated surface radiation measurements. The new retrieval method has improved τ_c and R_{eff} values compared to those derived using the transmittance only method and are in good agreement with the MODIS satellite retrievals. The study therefore suggests a possible improvement of the i-skyradiometer derived cloud parameters using observed radiation fluxes and a radiative transfer model.

1. Introduction

The main challenges in numerical weather prediction using general circulation models are the representation of clouds and cloud related small-scale processes. Out of many cloud microphysical parameters, cloud optical depth (τ_c) and cloud droplet effective radius (R_{eff}) are the key parameters, which determine the radiative properties of clouds such as reflection, transmission, and absorption of solar radiation [1]. The effects of the cloud related subgrid scale processes are mainly parameterized in terms of these bulk model variables, R_{eff} and τ_c. However, the climate models poorly simulate these variables [2, 3], but a better representation of R_{eff} is essential to parameterize cloud microphysical process in numerical weather prediction and climate models [4, 5]. Sparse observations of cloud microphysical parameters using both ground-based instruments and remote sensing methods make it more difficult to improve the model simulations of these parameters. Even though satellite retrievals provide cloud microphysical properties globally, its coarse spatial and temporal resolution makes it insufficient to study the cloud microphysical properties in detail. Hence, accurate ground-based measurements of the cloud microphysical parameters on both local and global scales are important for validation of satellite retrievals, aerosol indirect effect estimates, and also for the improvement of model predictions [6].

Several methods have been used to retrieve cloud optical properties using ground-based and aircraft measurements. [7] derived τ_c from aircraft mounted solar radiometric measurements. The main drawback of this method

includes limited temporal coverage and increased expense. Retrievals of cloud optical depth and effective cloud fraction using ground-based measurements of zenith radiance have been reported by [8]. Total liquid water path measured by microwave radiometer has also been used to obtain the R_{eff} and this retrieval was applied to ARM (atmospheric radiation measurement) data to derive τ_c [9]. Recently, [10] reported that the τ_c retrieved from AERONET (AErosol RObotic NETwork) zenith radiance observations at 440 and 870 nm compared well with ARM MFRSR (multifilter rotating shadowband radiometer) observations.

The i-skyradiometer (POM-02) used in SKYNET is a unique instrument that can measure zenith transmittances at 1.6 and 2.2 μm wavelengths similar to those of MODIS (moderate resolution imaging spectroradiometer) and can derive τ_c and R_{eff} simultaneously. [11] compared R_{eff} retrieved from the i-skyradiometer channels 1.6 and 2.2 μm with R_{eff} retrieved from radar reflectivity alone, radar reflectivity constrained with microwave radiometer (MWR) column liquid water path (LWP), and MODIS satellite and reported a bias in the POM-02 retrievals of R_{eff} compared to the cloud radar and MODIS retrievals. Their study points towards the need for improvement of τ_c and R_{eff} derived from i-skyradiometer. The present study is therefore aimed at providing a new method to improve the retrievals of τ_c and R_{eff} from i-skyradiometer (POM-02) using a radiative transfer model in conjunction with collocated ground-based measurements of global and diffuse shortwave fluxes.

2. Data and Instrumentation

Observations of zenith sky transmittance and global and diffuse short-wave radiative fluxes carried out over two stations, (i) Chiba (35.7°N, 139.7°E), an urban site in Japan, and (ii) Cape Hedo (26.87°N, 128.25°E), a marine environment as part of the SKYNET (http://atmos.cr.chiba-u.ac.jp/) programme, [12] have been used in the present study. The study also utilizes measurements of cloud base and top heights and transmittance measurements. In this study, nonprecipitating water clouds with base below 2 km have been considered. For Chiba station, observations, during 4 days in April, May, and July of 2007 and, in Cape Hedo, 10 days during February, March, and April of 2008, have been considered for the analysis.

Shortwave pyranometer (made by Kipp and Zonen (model CM21)) has been used to measure global radiation over Chiba. It measures the global radiation in the spectral range 0.3 to 3.0 μm on a plane surface, which results from the direct and diffuse solar radiation incident from the hemisphere above, with a spectral sensitivity of 7 to 14 μV/W/m^2. Since the diffuse radiation was not available over Chiba during the analysis period, global solar radiation measurements were used in the study. A shaded Pyranometer (made by Kipp and Zonen (model CM21)) under a shading ball is used to measure the diffused radiation over Cape Hedo. Cloud base and cloud top heights were derived from frequency modulated continuous millimeter wave cloud radar (FMCW); a threshold radar reflectivity of −15 dBZ was used for selection of nonprecipitating clouds. Detailed technical description of FMCW radar and its comparison with a monostatic 95 GHz cloud radar SPIDER can be obtained from [13].

τ_c and R_{eff} were retrieved from the ground-based measurements of the transmitted solar radiation using Sun/Sky scanning radiometer called i-skyradiometer (POM-02). The POM Sun/Sky radiometer is manufactured by Prede Co., Ltd., Tokyo, which comes under the Asia-Pacific SKYNET network for aerosol monitoring and satellite ground-truth around the world. It has a narrow field of view (1.2°) that makes measurements in several narrow spectral bands in the ultraviolet visible and near-infrared parts of the spectrum. POM includes a dedicated sun tracker, which can follow the sun for direct radiation measurements and can also make programmed scans across the sky at defined angles away from the sun. There exist two versions of the POM sky radiometer, POM-01 and POM-02. The POM-01 sky radiometer uses a single detector and a rotating filter wheel to measure radiation in seven narrow bands from 0.315 μm to 1.020 μm (0.315, 0.4, 0.5, 0.675, 0.87, 0.940, and 1.02 μm). It is connected to a computer running the operating software in order to make measurements and store data. The POM-02 has all the features of the POM-01, but with an extended wavelength range and has a second optical system with an indium gallium arsenide infrared detector. The filter has 11 wavebands, such that it can measure sky radiance and transmittance at 1.02, 1.6, and 2.2 μm. For simultaneous determination of τ_c and R_{eff} from transmittance measurements, it is necessary to adopt both absorbing and nonabsorbing wavelength. At water-absorbing wavelength, water droplet absorbs more solar radiation as particle increases in size compared to nonabsorbing wavelength, which absorbs less solar radiation. Among the three near-infrared wavelengths (1.02, 1.6 and 2.2 μm), 1.02 μm has been adopted as nonabsorbing wavelength, while the other two are water-absorbing wavelengths. Zenith sky cloud transmittance measurements at 1.02, 1.6 and 2.2 μm were used to derive τ_c and R_{eff} [1]. The retrieval procedure compares measurements of the cloud transmittance from the ground at water-absorbing and nonabsorbing wavelengths with look-up tables of the transmittance precomputed for plane-parallel, vertically homogeneous clouds using a radiative transfer code *r-star4b* [14]. Details of the retrieval algorithm are available in [1].

The i-skyradiometer is a radiance-based instrument, which works best for overcast conditions; hence overcast cases are considered in the study. The accurate determination of sky condition is desirable for identifying cloud type and cloud coverage. The whole sky imager (WSI) is a ground-based system, which enables temporal and spatial high-resolution sky observations. It provides real time processing and display of daytime sky conditions using common image processing algorithm, which estimate the cloud cover fraction. The WSI consists of a web camera, which looks down at a slowly rotating mirror that has a black strip to occlude the direct solar irradiance from the camera. The images of the sky are collected by a local computer and processed into percent cloud cover data. The digital image analysis was based on red to blue ratio, which is used to distinguish between

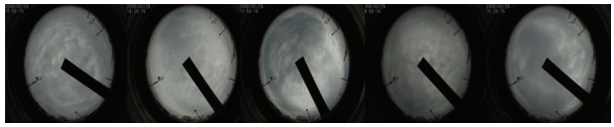

Figure 1: Whole sky images for April 4, 2008, over Cape Hedo, Japan.

clear and cloud pixels [15]. WSI data captured at every 10 minutes were used for selecting cloud cases. Figure 1 shows an example of cloud cases selected for April 4, 2008 at Cape Hedo, Japan. Further, satellite measurements are the only means of getting the global coverage of τ_c and R_{eff}. Hence, a comparison of the improved retrieval has been carried out with MODIS (Terra) level 2 products, with a spatial resolution of 1 km (MOD06). The swath data is averaged over an area of 4 km with experimental site as center and is compared with the improved retrieval.

3. Methodology

An assessment of the retrieval of cloud microphysical parameters from POM-02 and a new retrieval procedure has been proposed for improving the retrievals of τ_c and R_{eff} in conjunction with ground-based radiation measurements. A radiative transfer model, Santa Barbara discrete-ordinate atmospheric radiative transfer code (SBDART) [16], which simulates global and diffuse solar radiative fluxes at the surface and the collocated surface radiation measurements, has been used in the study [17–19]. A detailed description of SBDART uncertainty is available in [20–22]. The cloud optical parameters, τ_c and R_{eff} retrieved from i-skyradiometer were assumed as a first guess (retrieval from skyradiometer) for the SBDART model. In addition, cloud base and top heights derived from a Frequency modulated continuous wave millimeter wave cloud radar (MMCR), MODIS column integrated water vapor, TOMS ozone, and climatological values of green house gasses such as CO_2, CH_4, and N_2O were also constrained as inputs to the model [16]. Integrated water vapor is an important constituent of the atmosphere, which has high absorptivity of solar radiation. Its effect on aerosol optical depth and surface irradiance should be considered if the data from different months are mixed together [23]. Due to the complexity in the distribution of green house gases across the globe and the lack of availability of these parameters, we used default values, which is independent of season and geographic location.

Global and diffuse fluxes simulated by SBDART model (global fluxes over Chiba and diffuse fluxes over Cape Hedo) are compared with observed fluxes for different combinations of τ_c and R_{eff}. The new retrieval algorithm has been introduced for obtaining different combinations of the cloud microphysical parameters. Considering the fact that there is an underestimation in R_{eff}, the initial value of R_{eff} has been incremented up to 8 μm at an interval of 1 μm. Several studies have reported a threshold value of R_{eff} less than 12 μm for nonprecipitating clouds [24]. Since only nonprecipitating clouds have been considered in the study, R_{eff} greater than

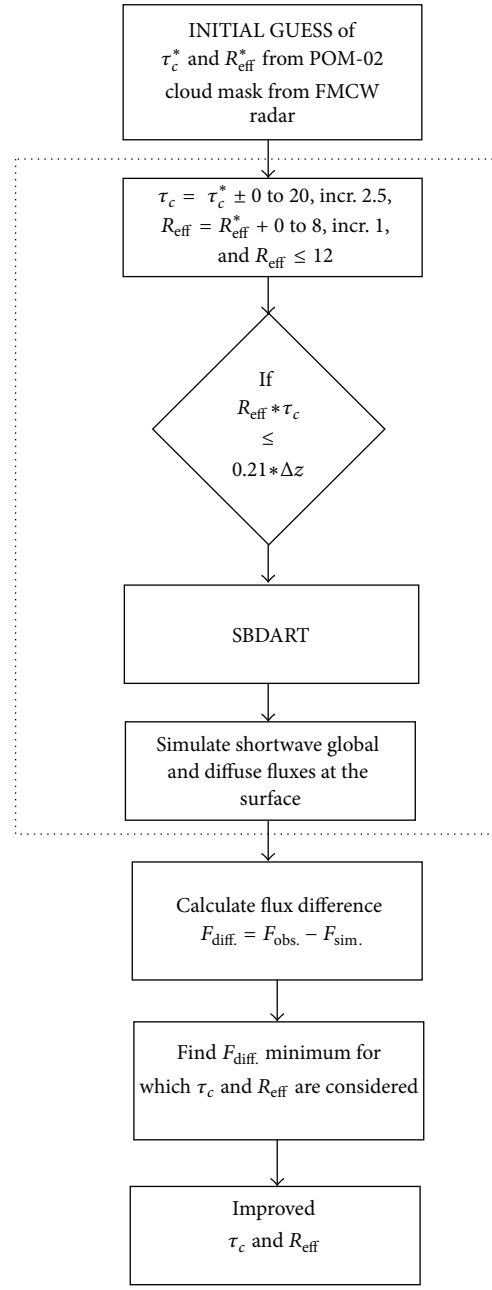

Figure 2: Flow chart of new retrieval algorithm for improved τ_c and R_{eff}.

12 μm is ignored during each step procedure [25]. The R_{eff} computation was performed only in forward direction as the R_{eff} values obtained from POM-02 (initial guess) were mostly found to be in the lower range; also the lower limit for R_{eff} in SBDART model is 2 μm. However, forward and backward step have been performed for τ_c up to 20 at an interval of 2.5. Earlier studies reveal that R_{eff} and τ_c are related through the equation $\tau_c = 1.5 * \text{LWP}/\rho_l * R_{\text{eff}}$ [26], where ρ_l is density of liquid water and LWC can be obtained through the equation $\text{LWP} = 0.14 * \Delta z$ [27], where Δz is cloud depth. Hence, R_{eff} and τ_c computed after each step are checked for whether

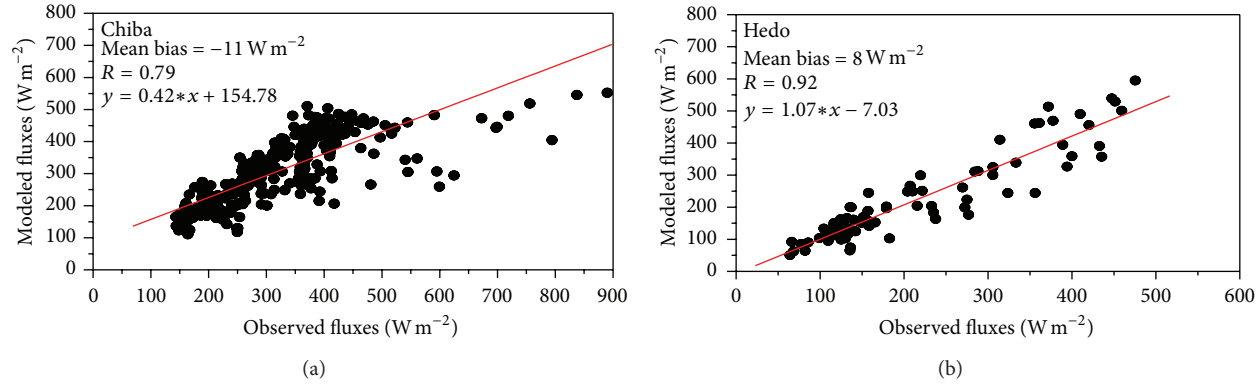

FIGURE 3: Comparison of observed and model simulated fluxes using initial guess of τ_c and R_{eff} over (a) Chiba (global fluxes) and (b) Hedo (diffuse fluxes).

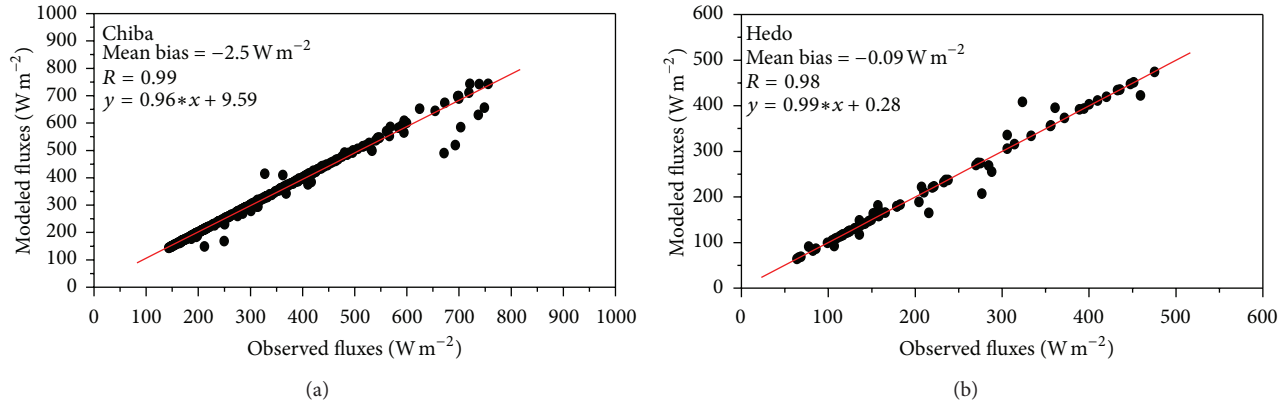

FIGURE 4: Comparison of observed and model simulated fluxes using the best combinations of τ_c and R_{eff} over (a) Chiba (global fluxes) and (b) Hedo (diffuse fluxes).

the parameters hold the relationship, $\tau_c * R_{\text{eff}} \leq 0.21 * \Delta z$, obtained from the above equations provided by [26, 27]. After each iteration, SBDART simulated short-wave global and diffuse sky fluxes at the surface using different combinations of τ_c and R_{eff} that are compared with the observed fluxes and the best combination of τ_c and R_{eff}, which simulates the fluxes having the least bias with observations, were selected as the most accurate retrievals. A flow chart illustrating the new retrieval procedure using the radiative transfer model, SBDART, is shown in Figure 2.

4. Results and Discussions

Initial retrievals of τ_c and R_{eff} from i-skyradiometer using [1] have been used as first guess in SBDART to simulate shortwave fluxes (diffuse and global) at the surface and the comparison of SBDART simulated global (over Chiba) and diffuse fluxes (over Cape Hedo) with that of observation is presented in Figure 3. It can be noted from the figure that there is large difference between the observed and model derived initial fluxes (from initial guess values) over both regions. The mean bias in the model simulated fluxes was found to be $-11\,\text{Wm}^{-2}$ over Chiba and $8\,\text{Wm}^{-2}$ over Cape Hedo while the correlation coefficients between the observed and model simulated initial fluxes were obtained as 0.79 and 0.92 over Chiba and Cape Hedo, respectively. The large bias indicates that there is an uncertainty in retrieved products of τ_c and R_{eff}.

In the improved retrieval algorithm, the i-skyradiometer derived cloud optical properties (τ_c and R_{eff}) were used as the first guess for SBDART model (Figure 2) and the combination of τ_c and R_{eff} having the least bias in simulated fluxes has been estimated as the best combination. The fluxes simulated by the radiative transfer model using the best estimates of τ_c and R_{eff} over Chiba and Cape Hedo have shown good agreement with observation (Figure 4). The improved retrieval algorithm has made a reduction in mean bias of simulated flux over Chiba from −11 to $-2.5\,\text{Wm}^{-2}$ (global) and also over Cape Hedo from $8\,\text{Wm}^{-2}$ to $-0.09\,\text{Wm}^{-2}$ (diffuse). The correlation coefficients between the improved and observed fluxes have been increased to 0.99 and 0.98 over Chiba and Cape Hedo, respectively. The best estimated values of τ_c and R_{eff} from the new retrieval method were found to be improved as compared to those of the transmittance only retrievals obtained from POM-02. A better comparison of the improved retrievals of τ_c and R_{eff} with that of initial retrievals can be obtained from Figures 5 and 6. The R_{eff} retrieval from transmittance method [1] is found to be lower as compared

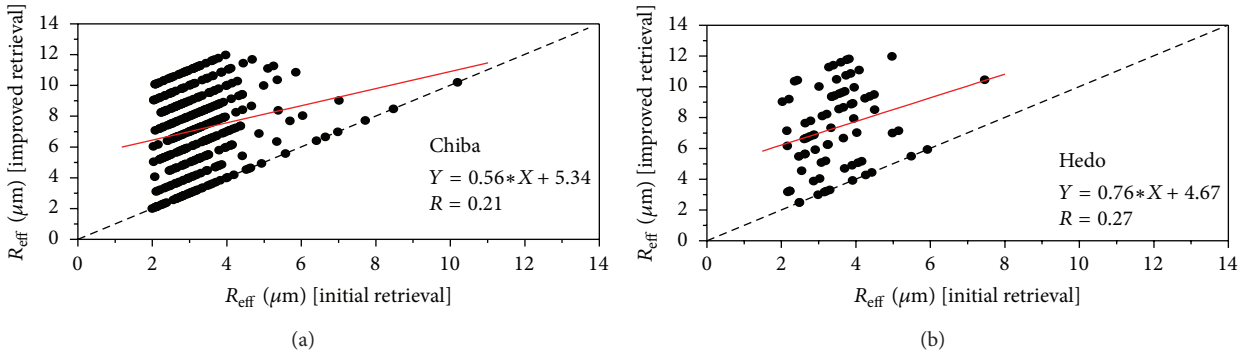

Figure 5: Initial and improved retrievals of cloud droplet effective radius over (a) Chiba and (b) Cape Hedo.

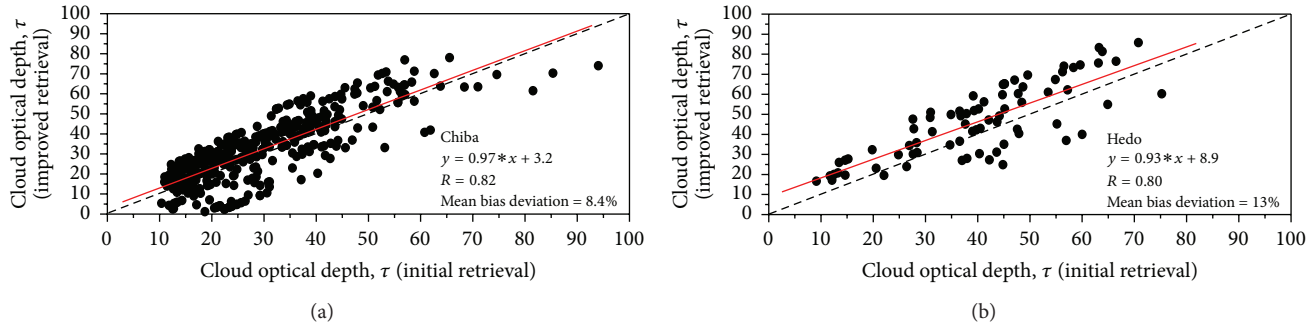

Figure 6: Initial and improved retrievals of cloud optical depth over (a) Chiba and (b) Cape Hedo.

to improved retrievals (Figure 5). The increase in improved retrievals of R_{eff} is almost about double, which is in good agreement with radar and satellite retrievals reported by [11]. The improved retrievals for τ_c values have shown an increase of 8.4% over Cape Hedo and 13% over Chiba (Figure 6).

The retrievals of R_{eff} and τ_c from both methods are compared with satellite retrievals and four cases (two from Chiba site (11 April and 18 May, 2007) and two from Cape Hedo site (28 February and 10 April, 2008)) are presented in Figures 7 and 8, respectively. The R_{eff} derived using [1] method has shown values, between 2 and 4 μm, much lower than the MODIS derived R_{eff}, between 6 and 11 μm. The improved retrieval of R_{eff} has shown considerable increase from the initial values [1] in all the cases over both stations, with a magnitude between 3 and 12 μm (Figure 7). In all of the four days, the satellite had overpass during morning hours between 10:30 and 11:50 over the sites and improved retrievals have shown good agreement with the MODIS derived cloud effective radius during those hours. Comparison of the improved retrieval of τ_c has been carried out with the initial and satellite derived τ_c and is provided in Figure 8. In all of the four cases, the values of τ_c from improved retrieval method are found to be comparable with those derived from MODIS. Over Chiba station, the MODIS derived τ_c is found to be 20 on May 18. 2007. But the initial value derived by [1] method is much lower (14.5) and new retrieval technique has improved τ_c to 17.25, more close to the MODIS derived value. However, on April 11, 2007, τ_c derived using the three methods was comparable, the MODIS observation and the τ_c derived using [1] method were in good agreement, and the improved algorithm has not made any considerable change in the initial value. The new retrieval method has improved τ_c over Cape Hedo station also. On April 10, 2008, the MODIS derived τ_c over Cape Hedo was 19 and the initial value was 10. The new retrieval method has made an increase in τ_c to 20, which is closer to MODIS observation. Even though the new retrieval method produced considerable improvements in R_{eff} on February 28, 2008, the method could not improve τ_c considerably (Figure 8).

Further, sensitivity of the retrieved cloud microphysical parameters to the errors in observed fluxes used for improving the initial guess has also been carried out for understanding the robustness of the retrieved parameters. A sensitivity experiment has been conducted by introducing an error of 5% in the observed flux and found that it can induce an error of 2.5 units in the retrieved τ_c (with constant R_{eff}), whereas in R_{eff} an error of 2.0 μm can occur (with constant τ_c). The error associated with the assumption of vertical inhomogeneity in the retrieval of τ_c using Kikuchi et al. [1] method is within 2% and it is argued that the cloud optical depth could be derived accurately from the measurements of transmittance [1]. Our analysis suggests that the POM-02 derived τ_c and R_{eff} can be improved by utilizing collocated radiation measurements. The methodology proposed here for finding the best combination of τ_c and R_{eff} using POM-02 retrievals as first guess and radiative fluxes as reference can

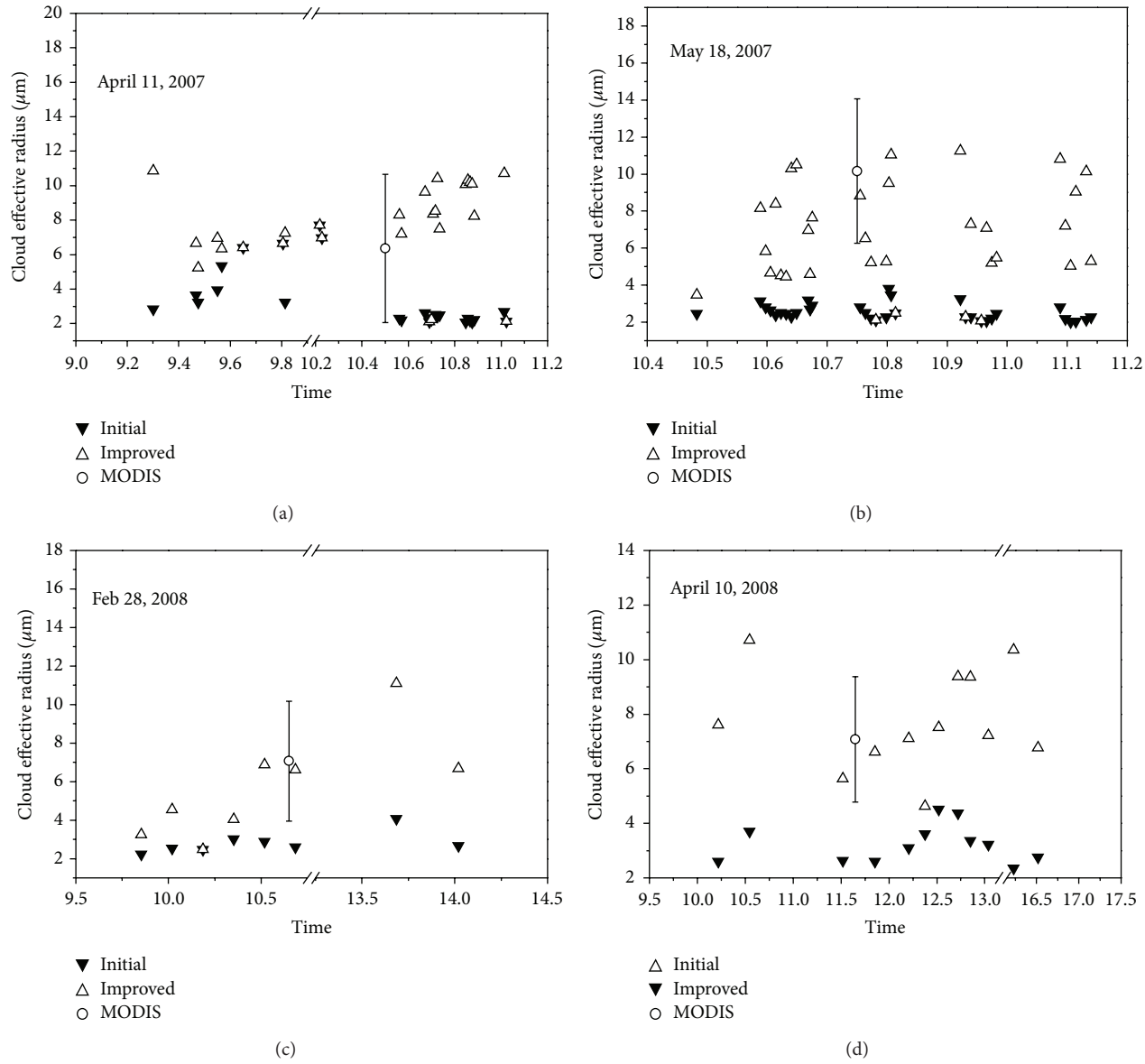

Figure 7: Initial, improved and satellite derived cloud droplet effective radius for Chiba (11 April and 18 May, 2007) and Cape Hedo (28 February and 10 April, 2008).

be used for improving the POM-02 retrievals, as accurate radiative flux observations are available in SKYNET sites.

5. Summary

Clouds remain the greatest source of uncertainty in global climate change research. Limited observations using ground-based instruments and the course resolution of satellite measurements add more uncertainty in the estimation and prediction of cloud microphysical parameters. Bias in the cloud parameters, τ_c and R_{eff}, derived using i-skyradiometer (a unique instrument that can measure zenith sky transmittances at 1.6 and 2.2 μm wavelengths and can derive τ_c and R_{eff} simultaneously) made it important to provide a technique for improving these parameters. A new combination method, which uses zenith sky transmittance and surface radiation (global and diffuse) measurements, has been proposed to improve the retrievals of τ_c and R_{eff}. The method uses a radiative transfer model (SBDART) and the i-skyradiometer derived τ_c and R_{eff} have been provided as first guess. Further, a new retrieval method has been implemented to obtain the best combination of τ_c and R_{eff} having less bias between the simulated global and diffuse fluxes at the surface with the collocated surface radiation measurements.

The τ_c and R_{eff} derived using the new retrieval method have shown considerable improvement compared to the parameters derived using [1] method and the instantaneous values are seen in good agreement with the MODIS satellite observations. The new retrieval of R_{eff} has shown an increase in the magnitude of R_{eff} with values between 3 and 12 μm,

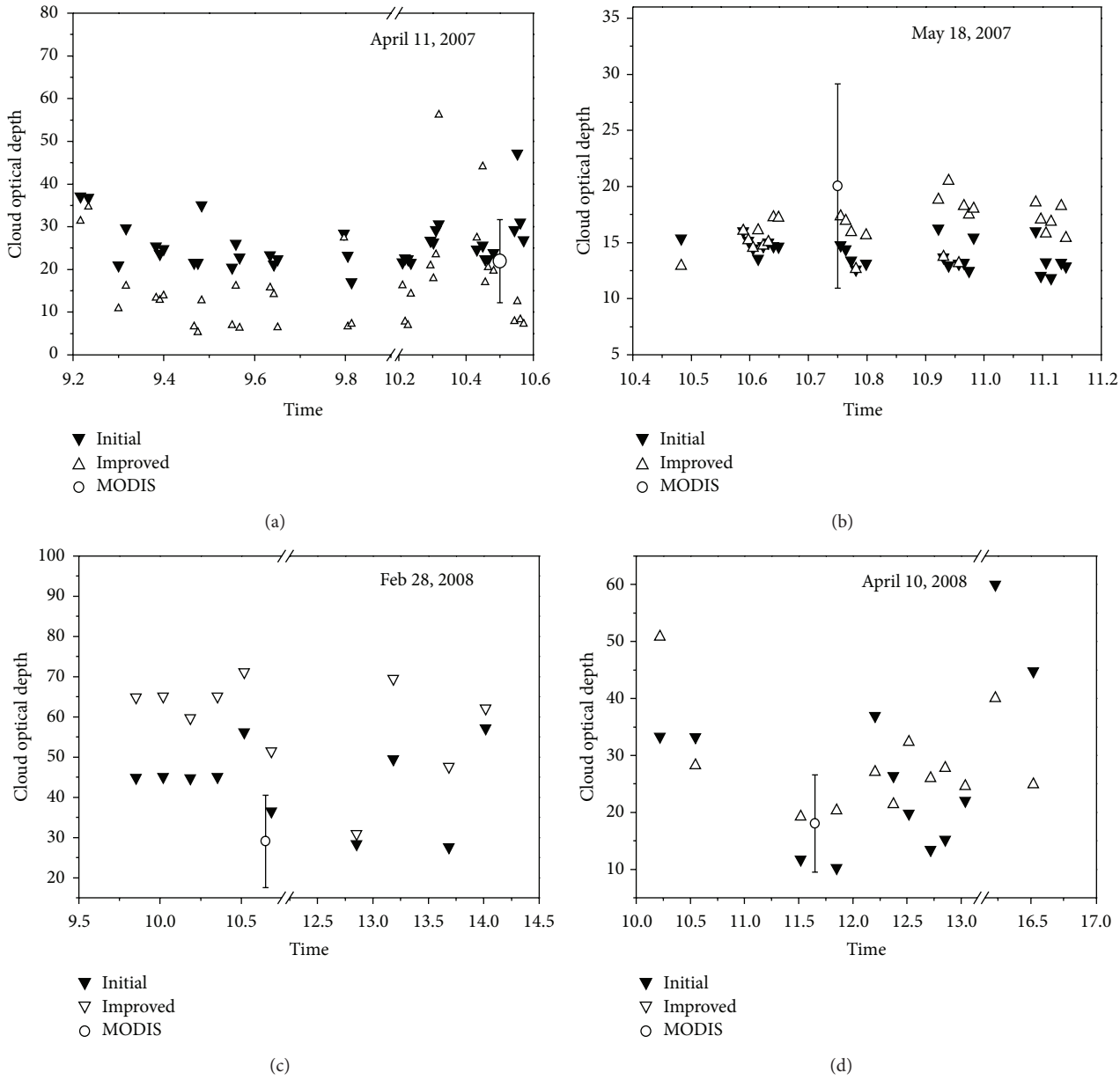

Figure 8: Initial, improved and satellite derived cloud optical depth for Chiba (11 April and 18 May, 2007) and cape Hedo (28 February and 10 April, 2008).

which is more closer to the MODIS derived R_{eff} between 6 and 11 μm, while the R_{eff} derived using [1] method is in the range of 2 to 4 μm. The MODIS satellite observed τ_c lies between 15 and 30 and the τ_c derived using the improved retrieval method has been found to be closer to MODIS observations compared to that obtained from [1] method. Our study therefore suggests that the POM-02 derived τ_c and R_{eff} can be improved. The retrieval method suggests that POM-02 derived τ_c and R_{eff} can be improved by utilizing the collocated radiation measurements. Indeed, this result may also used to improve the retrieval algorithm of skyradiometer for more robust cloud retrievals and hence, better retrievals of cloud parameters especially in SKYNET; an Asian surface network for aerosol-radiation measurements can be achieved.

Conflict of Interests

The authors declare that there is no conflict of interests regarding the publication of this paper.

Acknowledgments

Indian Institute of Tropical Meteorology (IITM) and Centre for Climate Change Research (CCCR) are fully funded by Ministry of Earth Sciences (MoES), Government of India.

The authors thank SKYNET and CHAMMPS and Cape Hedo for maintaining the experimental facilities at the site. The authors also thank Global Earth Observation System of Systems (GEOSS) and Ministry of Education, Culture, Sports, Science and Technology (MEXT), Japan. S. Dipu gratefully acknowledges CSIR, Government of India, for Research Fellowship. G. Pandithurai acknowledges the Japan Society for Promotion of Science (JSPS) for Invitation Fellowship. This work is supported by National Research Foundation of Korea (NRF) through a Grant provided by the Korean Ministry of Education, Science and Technology (MEST) 2013 (no. 200603874).

References

[1] N. Kikuchi, T. Nakajima, H. Kumagai et al., "Cloud optical thickness and effective particle radius derived from transmitted solar radiation measurements: comparison with cloud radar observations," *Journal of Geophysical Research D*, vol. 111, no. 7, Article ID D07205, 2006.

[2] M. H. Zhang, W. Y. Lin, S. A. Klein et al., "Comparing clouds and their seasonal variations in 10 atmospheric general circulation models with satellite measurements," *Journal of Geophysical Research D*, vol. 110, no. 15, Article ID D15S02, 2005.

[3] F. A. Bender, H. Rodhe, R. J. Charlson, A. M. L. Ekman, and N. Loeb, "22 views of the global albedo—comparison between 20 GCMs and two satellites," *Tellus A*, vol. 58, no. 3, pp. 320–330, 2006.

[4] G. L. Stephens, "Radiation profiles in extended water clouds. II parameterization schemes," *Journal of the Atmospheric Sciences*, vol. 35, no. 11, pp. 2123–2132, 1978.

[5] A. Slingo and H. M. Schrecker, "On the shortwave radiative properties of stratiform water clouds," *Quarterly Journal, Royal Meteorological Society*, vol. 108, no. 456, pp. 407–426, 1982.

[6] S. J. Evans and J. D. Haigh, "The retrieval of total optical depth and effective droplet radius of clouds from solar reflection measurements using the along track scanning radiometer-2 (ATSR-2)," *Geophysical Research Letters*, vol. 22, no. 6, pp. 695–698, 1995.

[7] H. W. Barker, A. Marshak, W. Szyrmer, A. Trishchenko, J. Blanchet, and Z. Li, "Inference of cloud optical depth from aircraft-based solar radiometric measurements," *Journal of the Atmospheric Sciences*, vol. 59, no. 13, pp. 2093–2111, 2002.

[8] J. C. Chiu, A. Marshak, Y. Knyazikhin et al., "Remote sensing of cloud properties using ground-based measurements of zenith radiance," *Journal of Geophysical Research D*, vol. 111, no. 16, Article ID D16201, 2006.

[9] Q. L. Min and L. C. Harrison, "Cloud properties derived from surface MFRSR measurements and comparison with GOES results at the ARM SGP site," *Geophysical Research Letters*, vol. 23, no. 13, pp. 1641–1644, 1996.

[10] J. C. Chiu, C. H. Huang, A. Marshak et al., "Cloud optical depth retrievals from the aerosol robotic network (AERONET) cloud mode observations," *Journal of Geophysical Research D*, vol. 115, no. 14, Article ID D14202, 2010.

[11] G. Pandithurai, T. Takamura, J. Yamaguchi et al., "Aerosol effect on cloud droplet size as monitored from surface-based remote sensing over East China Sea region," *Geophysical Research Letters*, vol. 36, no. 13, Article ID L13805, 2009.

[12] T. Takamura, N. Sugimoto, A. Shimizu et al., "Aerosol radiative characteristics at Gosan, Korea, during the atmospheric brown cloud East Asian regional experiment 2005," *Journal of Geophysical Research D*, vol. 112, no. 22, Article ID D22S36, 2007.

[13] T. Takano, K. Akita, H. Kubo et al., "Observations of clouds with the newly developed cloud profiling FM-CW radar at 95 GHz," in *10th Remote Sensing of Clouds and the Atmosphere*, vol. 5979 of *Proceedings of SPIE*, Bruges, Belgium, September 2005.

[14] T. Nakajima and M. Tanaka, "Matrix formulations for the transfer of solar radiation in a plane-parallel scattering atmosphere," *Journal of Quantitative Spectroscopy and Radiative Transfer*, vol. 35, no. 1, pp. 13–21, 1986.

[15] G. Pfister, R. L. Mckenzie, J. B. Liley, A. Thomas, B. W. Forgan, and C. N. Long, "Cloud coverage based on all-sky imaging and its impact on surface solar irradiance," *Journal of Applied Meteorology*, vol. 42, no. 10, pp. 1421–1434, 2003.

[16] P. Ricchiazzi, S. Yang, C. Gautier, and D. Sowle, "SBDART: a research and teaching software tool for plane-parallel radiative transfer in the rarth's atmosphere," *Bulletin of the American Meteorological Society*, vol. 79, no. 10, pp. 2101–2114, 1998.

[17] W. C. Conant, "An observational approach for determining aerosol surface radiative forcing: results from the first field phase of INDOEX," *Journal of Geophysical Research D*, vol. 105, no. 12, pp. 15347–15360, 2000.

[18] G. Pandithurai, R. T. Pinker, T. Takamura, and P. C. S. Devara, "Aerosol radiative forcing over a tropical urban site in India," *Geophysical Research Letters*, vol. 31, no. 12, Article ID L12107, 2004.

[19] A. S. Panicker, G. Pandithurai, T. Takamura, and R. T. Pinker, "Aerosol effects in the UV-B spectral region over Pune, an urban site in India," *Geophysical Research Letters*, vol. 36, no. 10, Article ID L10802, 2009.

[20] A. S. Panicker, G. Pandithurai, P. D. Safai, and S. Kewat, "Observations of enhanced aerosol longwave radiative forcing over an urban environment," *Geophysical Research Letters*, vol. 35, no. 4, Article ID L04817, 2008.

[21] A. S. Panicker, G. Pandithurai, P. D. Safai, S. Dipu, and D. I. Lee, "On the contribution of black carbon to the composite aerosol radiative forcing over an urban environment," *Atmospheric Environment*, vol. 44, no. 25, pp. 3066–3070, 2010.

[22] A. S. Panickera, S.-H. Park, D.-I. Leeb et al., "Observations of black carbon characteristics and radiative forcing over a global atmosphere watch supersite in Korea," *Atmospheric Environment*, vol. 77, pp. 98–104, 2013.

[23] Z. Li and A. Trishchenko, "Quantifying the uncertainties in determining SW cloud radiative forcing and cloud absorption due to variability in atmospheric condition," *Journal of the Atmospheric Sciences*, vol. 58, no. 4, pp. 376–389, 2001.

[24] M. O. Andreae, D. Rosenfeld, P. Artaxo et al., "Smoking rain clouds over the Amazon," *Science*, vol. 303, no. 5662, pp. 1337–1342, 2004.

[25] D. Rosenfeld, "Suppression of rain and snow by urban and industrial air pollution," *Science*, vol. 287, no. 5459, pp. 1793–1796, 2000.

[26] D. D. Turner, A. M. Vogelmann, R. T. Austin et al., "Thin liquid water clouds: their importance and our challenge," *Bulletin of the American Meteorological Society*, vol. 88, no. 2, pp. 177–190, 2007.

[27] A. V. Korolev, G. A. Isaac, J. W. Strapp, S. G. Cober, and H. W. Barker, "In situ measurements of liquid water content profiles in midlatitude stratiform clouds," *Quarterly Journal of the Royal Meteorological Society*, vol. 133, no. 628, pp. 1693–1699, 2007.

Hindawi Publishing Corporation
Advances in Meteorology
Volume 2014, Article ID 830349, 8 pages
http://dx.doi.org/10.1155/2014/830349

Research Article

Multiyear Measurements of the Aerosol Absorption Coefficient Near the Surface in a Small-Sized Urban Area in Portugal

Sérgio Nepomuceno Pereira,[1,2] Frank Wagner,[1,3] and Ana Maria Silva[1]

[1] *Évora Geophysics Centre (CGE), Rua Romão Ramalho 59, 7000 Évora, Portugal*
[2] *Andalusian Institute for Earth System Research (IISTA-CEAMA), Avenida del Mediterráneo s/n, 18006 Granada, Spain*
[3] *Hohenpeißenberg Meteorological Observatory, Albin-Schwaiger-Weg 10, 82383 Hohenpeißenberg, Germany*

Correspondence should be addressed to Sérgio Nepomuceno Pereira; sergiopereira@uevora.pt

Received 12 September 2013; Accepted 19 December 2013; Published 3 February 2014

Academic Editor: Mrinal Biswas

Measurements of the aerosol absorption coefficient, between 2007 and 2013, were made at the ground level in Évora, a Portuguese small town located in the southwestern Iberia Peninsula. Such a relatively long time series of absorbing aerosols is unique in Portugal and uncommon elsewhere. The average aerosol absorption coefficient was close to 9 Mm^{-1} and clear cycles at both daily and seasonal time scales were found. An average increase by a factor of two (from 6 to 12 Mm^{-1}) was observed in winter if compared to summer season. The daily variations were similarly shaped for all seasons, with two morning and afternoon peaks, but with magnitudes modulated by the seasonal evolution. That was not the case if Sundays were considered. These variations can be explained in terms of the impact of local particle sources, related mainly to traffic and biomass burning and upward mixing of the aerosol due to variable mixing layer heights, either daily or seasonally. Also, a strong negative correlation between the aerosol absorption coefficient and the wind speed was verified, and an exponential decay function was found to fit very well to the data. The wind direction seems to be not correlated with the aerosol absorption coefficient.

1. Introduction

It is recognized that light absorbing aerosol particles influence directly the radiative balance and exert a net warming effect on the atmosphere [1–4]. Hence, they can eventually counterbalance the radiative cooling effect of the other aerosol types which are mostly light scatterers [5, 6]. The radiative warming induced by absorbing particles can even be as important as the effect due to greenhouse gases [7, 8]. However, the discrepancies between different scientific contributions in terms of quantifying their importance to the radiative forcing (e.g., [8, 9]) keep the uncertainties high. The influence of absorbing particles seems to be more important at the regional than at the global scale [10]. Changes in the regional atmospheric stability due to atmospheric heating, in the presence of absorbing particles, can cause changes in the hydrological cycle [2, 8, 11].

Other effects, for example, observations of reduced albedo resulting from long-range transported particles into Arctic areas, were reported by Stohl et al. [12]. Recently, it was estimated that absorbing particles may have contributed to more than half of the observed Arctic warming since 1890, most of this occurring during the last decades [13].

Additionally, these absorbing particles exert an indirect radiative effect due to their influence in modifying cloud properties [14, 15]. Furthermore, their absorption of sunlight contributes to degraded visibility in polluted regions [16] and also to adverse effects on human health [17–19] as their size is mostly in the fine size range (e.g., [20, 21]). They also have impact on atmospheric chemistry and photochemistry (e.g., [22]) and through absorption of solar radiation [23]. In urban areas, the absorption of radiation in the visible spectrum is dominated by black carbon (BC) [24, 25], which is primarily introduced in the atmosphere as primary particles from combustion processes. Motor vehicles constitute the main source of black carbon in many European urban areas [26–29]; the emission levels of absorbing particles depend on multiple factors, for example, type of fuel and engine

characteristics; for this reason its prediction is difficult and measurements must be carried out.

Globally, biomass burning, fuel burned for cooking and heating, on-road and off-road diesel engines and industrial activities of many kinds represent the largest contribution for the emitted BC mass. The difficulty in quantifying emissions from such diverse sources is a basic contribution to the uncertainty in evaluating BC's climate role. Bond et al. [30] provide a large uncertainty range of 2000 to 29000 Ggy^{-1} for its global emissions which inevitably reflects in the large uncertainty bonds (90%) related to the recent estimates for the total climate forcing of BC.

The absorption coefficient of atmospheric particles is a fundamental optical parameter that needs to be known with good accuracy in order to improve our knowledge of the effects of aerosols on the climate. Models of radiative transfer require the amount of absorption (and scattering) by particles in the atmosphere. Therefore, long-term measurements of this aerosol optical property are important for improving our understanding of aerosol climatology and predictive modeling capabilities.

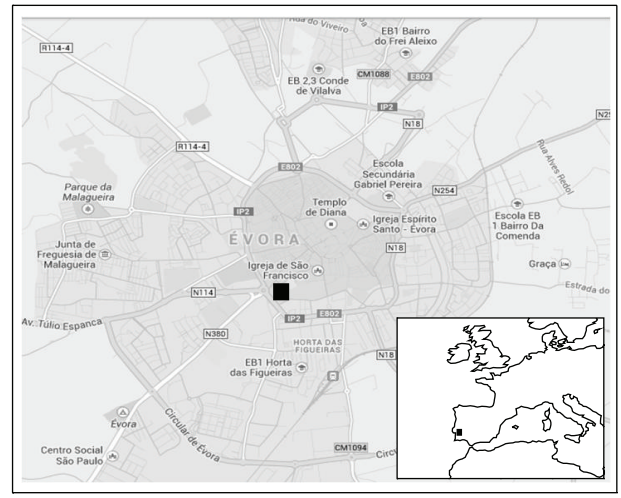

Figure 1: Map of the Iberian Peninsula showing Évora and map of Évora showing the location of Évora Geophysics Centre (CGE/black square) monitoring site within the city core as well as the main traffic roads.

2. Measurements

Évora, Portugal (38.5 N, 7.9 W, 290 m a.s.l), is located in the southwestern region of the Iberian Peninsula as shown in Figure 1. It is a Portuguese municipality with less than 60000 inhabitants. More than 40000 inhabitants reside in the urban area of the city itself, which is the biggest one within a vast rural and sparsely populated region. The distance from the capital, Lisbon, is some 130 km. The regional landscape is of low altitude (average height is below 250 m a.s.l.) and it consists primarily of wide plains. There are no significant polluting industries, neither in the city nor in the regional vicinity; for that reason the local regular production of absorbing particles should be to a large extent related to traffic circulation; during the colder periods of winter and fall wood burning is often used for domestic heating [31]. Regarding traffic circulation, the information obtained from the municipality is sparse; nevertheless, it is possible to estimate the number of vehicles entering the city as being 12000–15000 day^{-1}. The city spreads over a smooth prominence while its buildings are not elevated (mainly comprising one to three floors) thus allowing the city to be, in principle, well ventilated.

The light absorption coefficient of aerosols, $\sigma_{ap}(\lambda)$ at the wavelength $\lambda = 670$ nm, was measured with a Multiangle Absorption Photometer (MAAP 5012, Thermo ESM Andersen Instruments, Erlangen, Germany). Aerosol particles are deposited on a quartz fiber filter; a laser illuminates the filter matrix perpendicularly, and simultaneous measurements of radiation penetrating through the filter and scattered back at four detection angles are made. The determination of the aerosol absorption coefficient is made via radiative transfer calculations including the scattering effects from the filter matrix and the light scattering aerosol component. The scattering measurements allow the correction for multiple scattering processes involving the deposited particles and the filter matrix, which improves considerably the determination of aerosol absorption coefficient over other filter-based methods, as demonstrated by comparison with a reference method [32, 33]. The absolute measurement uncertainty of the MAAP has been estimated to be 12% [32, 34], while laboratory intercomparisons of multiple MAAP instruments suggested a unit-to-unit variability below 3% [35]. The aerosol was sampled at about 10 m above ground surface, at the Évora Geophysics Centre (CGE) facilities located within the urban centre of the city (Figure 1). The measurements span the period between April 2007 and April 2013. Measurements were taken every minute and further averaged to hourly values which were the basis for the data analysis, at different timescales, presented in the following sections.

Regarding the seasonal statistics the usual periods of winter (DJF), summer (JJA), spring (MAM), and fall (SON) were considered. Basic meteorological quantities were also recorded at the same site, namely, the wind speed and direction as well as the temperature in an hourly basis.

3. Results and Discussion

3.1. General Overview. The temporal evolution of the absorption coefficient, measured between April 2007 and April 2013, is presented in Figure 2; daily, monthly and yearly values are shown. The seasonal temperature is also depicted for the different seasons. Figure 3 shows the frequency distribution of hourly values of the absorption coefficient, the frequency distribution of the wind direction, and the absorption coefficient as function of both the wind speed and wind direction. The measurements show that $\sigma_{ap}(670)$ was most frequently observed with magnitudes below 10 Mm^{-1} (the third quartile is about this value), even if a few hourly values of $\sigma_{ap}(670)$ as high as 120 Mm^{-1} could be detected. Only 1% of the data were above 50 Mm^{-1}. The mean absorption coefficient for the

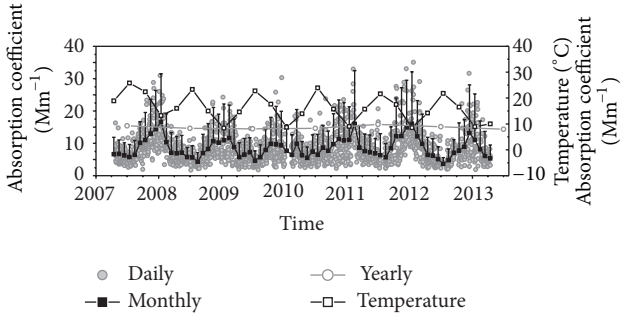

FIGURE 2: Time series of the absorption coefficient (daily and monthly values in the left scale; yearly values in the right scale) and seasonal temperature measured in Évora between April 2007 and April 2013.

whole period was found to be $8.7 \pm 9.9\ \mathrm{Mm}^{-1}$, with a respective median value of $6.2\ \mathrm{Mm}^{-1}$; the relatively high standard deviation originates from the hourly values which were used for the statistical computations. Mean values for different years were in the range of 8–10 Mm^{-1} and of 6-7 Mm^{-1} for the respective median values and no interannual trend is evident. The magnitudes of the absorbing coefficient reported here are comparable to the findings of Mogo et al. [36] for the absorption coefficient (at 660 nm) in a similar sized and populated small Portuguese town during a nine-month period (October 2009 to July 2010); in a city such as Granada, in the south of Spain and with a population one order of magnitude larger, the mean $\sigma_{ap}(670)$, during two years of measurements (December 2005 to November 2007), was reported to be $21\ \mathrm{Mm}^{-1}$ by Lyamani et al. [37]. However, in a background site, located in the Spanish Mediterranean Basin, the measured absorption coefficient was about three times lower ($2.8\ \mathrm{Mm}^{-1}$ at 637 nm) [38]. Some examples of measurements performed in other parts of the world show the high variability that can be observed in areas of different human impact. Absorption measurements in large world urban areas can be one order of magnitude higher than the ones observed in this study [39–42]. In areas with low human impact the absorption coefficient can be several times lower or even one order of magnitude lower in the case of remote areas as in [43–45].

Also, as Figure 3 shows, the distribution of the absorption coefficient is clearly asymmetric, right skewed, and it is well characterized by a lognormal curve (with modal value $6.6\ \mathrm{Mm}^{-1}$), which is often observed in diverse extensive aerosol properties [46–50]. The measured wind speed was moderate, as it rarely exceeded the $4\ \mathrm{ms}^{-1}$ (mean value of $2\ \mathrm{ms}^{-1}$); however, a significant influence in the magnitude of the absorption coefficient is clearly observed (Figure 3(c)). The strong negative correlation between wind speed and $\sigma_{ap}(670)$ levels indicates the predominance of local particle sources. Low wind speeds keep the pollution close to the source and hence local pollution levels rise while strong winds favor particle dispersion out of the source region which in turn leads to lower pollution levels close to the source. In Section 3.2 we show that the relation between the absorption coefficient and the wind speed is very well accounted by an exponential decay pattern. The prevailing wind directions measured at the site (Figure 3(b)) are mainly westerly because of the dominant winds in the extra tropical northern latitudes where the Portuguese territory is located. As one could expect the wind direction seems not to be correlated with the aerosol absorption coefficient as one can observe between the wind speed and the aerosol absorption coefficient. This noncorrelation between wind direction and the absorption coefficient is the consequence of the predominance of local particle sources and of the location of CGE inside the ring road where significant traffic circulates.

3.2. Seasonal Variations. The temporal evolution of $\sigma_{ap}(670)$ previously presented in Figure 2 reveals a clear annual cycle; higher values and variability were observed during winter and autumn periods with the maximum values being attained, every year, during the winter months. This regularity is shown in Figure 4 where the monthly statistics of the absorption coefficient are considered. In Table 1 several statistical parameters are presented in terms of monthly and seasonal timescales. The annual cycle should result from the combination of several factors, related both to particle production and meteorology. On the one hand, the additional input of soot during the colder period, due to domestic heating, is a main contribution as wood is often used as the main fuel. Additionally, we cannot discard the possibility of some increase in traffic during autumn/winter, due to worse weather conditions, contributing to the observed increase in $\sigma_{ap}(670)$; although no trustworthy information on that issue was available, the empirical observations suggest this fact. On the other hand, during the colder seasons the boundary layer height is generally smaller, with lower capacity for atmospheric dispersion, and temperature inversions are more frequent due mainly to the long wave radiative losses during the winter clear sky nights, typical in this region; hence, the concentrations of particles near the ground are expected to be higher. During the warmer periods the intense convective activity due to the solar heating of the ground surface induces the opposite effect. As Table 1 shows, the monthly absorption coefficient remains around $6\ \mathrm{Mm}^{-1}$ ($5\ \mathrm{Mm}^{-1}$ if median values are considered) between April and August, and then it increases during September until maximum mean values, 12-13 Mm^{-1}, are reached during the winter months (December to February). This variation represents a twofold increase if summer and winter, which are the most dissimilar seasons, are compared in terms of magnitudes of the absorption coefficient. The standard deviation increased even by a larger factor (Table 1). The upper quartile is also much higher during winter but not the lower quartile which is relatively constant throughout the year. In the following section it will be shown that this increased variability is mainly caused by the amplitude of the daily cycles observed in each season.

A clear negative correlation between local wind speed and absorption coefficient, already noticed in Section 3.1, was verified in all the seasons. The increase in wind speed causes an increase in ventilation; the dispersion of particles in the ambient air is enhanced and consequently causes a decrease

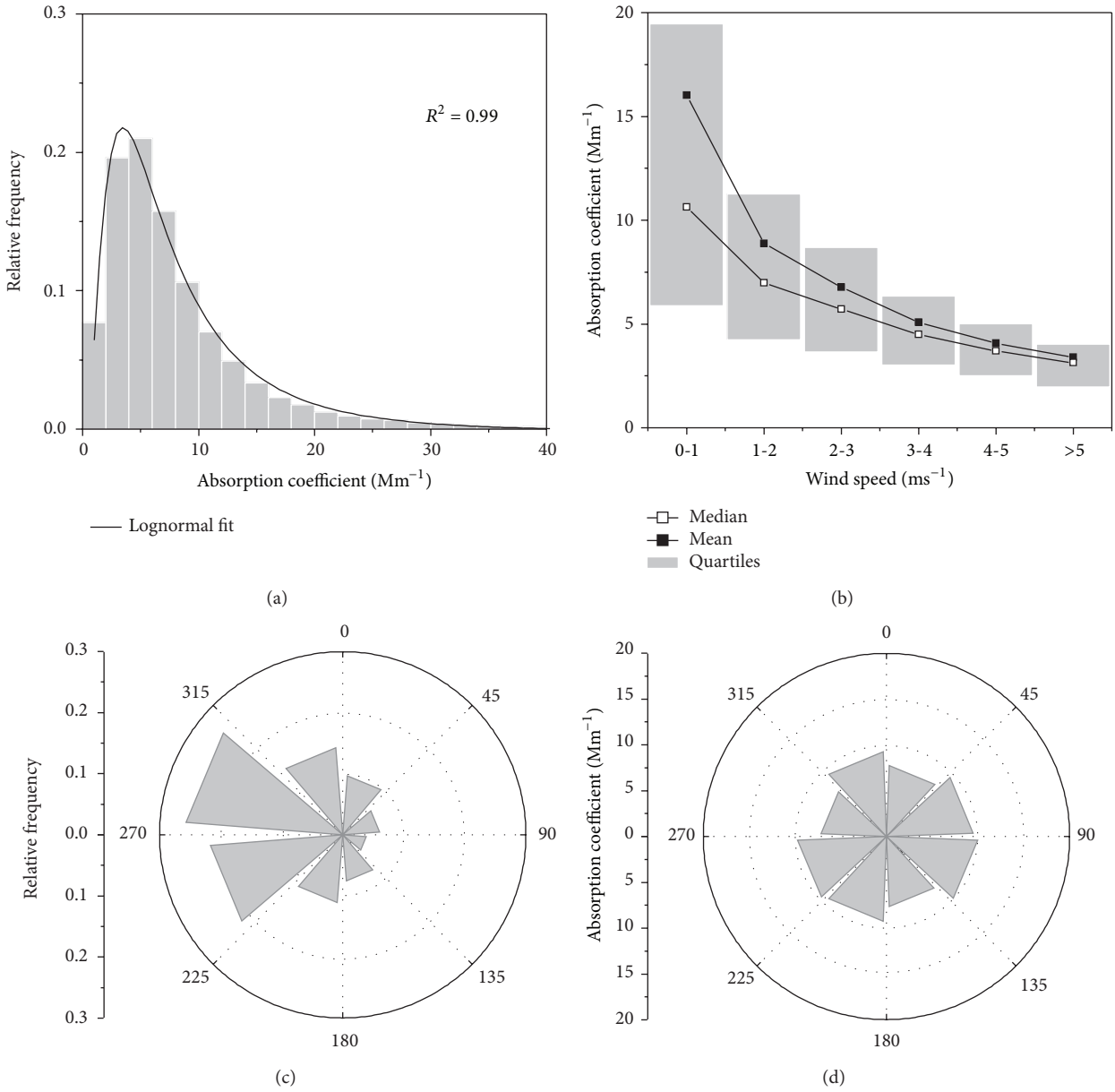

FIGURE 3: Relative frequency distributions of the hourly (a) absorption coefficient, with the respective lognormal fitting, and (b) wind direction. Absorption coefficient as function of (c) wind speed (including the quartiles) and (d) wind direction.

in the observed particle concentration and thus in the absorption coefficient. Exponential decay curve fittings apply very well to the observed dependency between $\sigma_{ap}(670)$ and wind speed. These features are shown in Figure 5 including the exponential fittings applied for the case of winter and summer and also for the whole data between 2007 and 2013 (see also Table 2). These types of curves were also used by Wang et al. [51] for absorbing particles. Such decreasing trends are an indication of the closeness of the air pollution sources which is the case of urban/suburban environments. It is worth mentioning the similarity of the year and seasonal decay constants (Table 2) and the fact that for high wind speeds the concentration of particles is almost independent of the season.

3.3. Diurnal Variation. The diurnal variation of the absorption coefficient is characterized by two distinct and prominent peaks, in the morning and in the afternoon, as shown in Figure 6. These sharp enhancements seem to be driven by vehicular emissions as they are coincident with the morning and afternoon traffic rush hours. This type of daily evolution is often found within urban areas (e.g., [37, 52–56]). During the afternoon, the decrease in traffic circulation, before the following afternoon rush hour, and the typical daytime development of a convective boundary layer lead to a decrease in the $\sigma_{ap}(670)$ levels. During the night period, traffic is weakly present and thus the levels of suspended particles attain the minimum, which is perceptible in Figure 6. Also, the morning peak is lower than the late afternoon peak,

Table 1: Basic statistical properties of $\sigma_{ap}(670)$ organized for each month and season between 2007 and 2013. Q1 and Q3 indicate the quartiles; P1 and P99 indicate the 1st and 99th percentiles.

	Mean (Mm^{-1})	SD (Mm^{-1})	Q1 (Mm^{-1})	Median (Mm^{-1})	Q3 (Mm^{-1})	P1 (Mm^{-1})	P99 (Mm^{-1})
Month							
Jan.	12.9	13.6	4.8	8.6	15.7	0.7	73.6
Feb.	11.1	11.2	4.5	7.6	13.1	0.7	61.7
Mar.	8.4	8.5	3.9	6.2	9.8	0.7	47.5
Apr.	6.5	4.9	3.2	5.2	8.4	0.7	23.4
May.	6.6	4.9	3.5	5.4	8.4	0.9	25.1
Jun.	6.4	4.3	3.5	5.5	8.2	0.9	20.9
Jul.	5.6	4.7	3.0	4.6	6.8	0.8	22.4
Aug.	6.0	4.7	3.2	4.9	7.4	0.7	23.1
Sep.	8.1	6.2	4.2	6.5	10.0	1.2	31.2
Oct.	9.9	9.3	4.4	7.3	12.0	0.8	48.7
Nov.	11.1	11.8	4.5	7.6	13.2	0.7	65.1
Dec.	12.2	12.6	4.8	8.6	14.7	0.6	70.1
Season							
Winter	12.2	12.6	4.8	8.3	14.6	0.6	70.0
Spring	7.2	6.4	3.5	5.6	8.8	0.7	31.5
Summer	6.1	4.6	3.2	5.0	7.6	0.8	22.2
Autumn	9.7	9.5	4.4	7.1	11.6	0.8	50.3

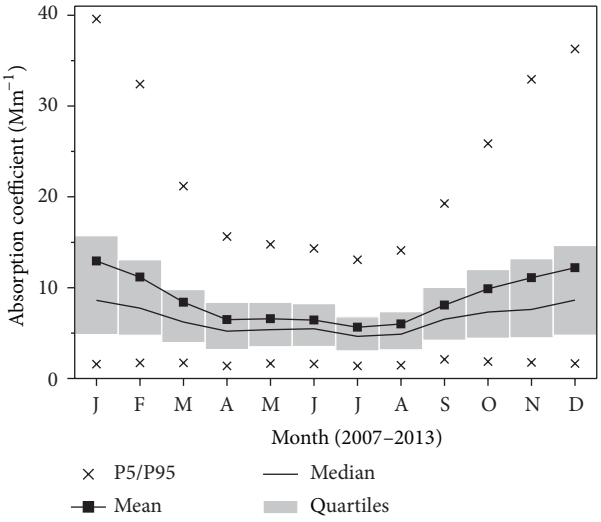

Figure 4: Basic statistics of the absorption coefficient measured between April 2007 and April 2013. Computations were based on the hourly values. The quartiles are depicted and P5 and P95 indicate the 5th and 95th percentiles.

and a higher rate of decrease in $\sigma_{ap}(670)$ is observed. This is likely related to the afternoon rush hour being broader, temporally, and maybe also to the effect of the mixed layer during, afternoon in the dispersion of the pollutants, which is not the case later in the evening and in the nighttime periods. These features are common to all the working days (Monday to Friday). However, Saturday presents less prominent peaks, particularly in the morning, and during Sundays the morning peak in $\sigma_{ap}(670)$ is virtually absent, corresponding to the typical lack of activity and very low traffic levels in this period of the week.

Table 2: Parameters (±standard errors) of the exponential fitting ($y = y_0 + a * \exp(bx)$) between the wind speed and the absorption coefficient for 2007–2013 and for winter and summer seasons.

	y_0 (Mm^{-1})	a (Mm^{-1})	b ($m^{-1}s$)	R^2
2007–2013	3.4 ± 0.5	17.9 ± 0.9	−0.7 ± 0.1	0.99
Winter	3.7 ± 0.6	22.8 ± 0.9	−0.6 ± 0.1	0.99
Summer	3.7 ± 0.4	10.4 ± 0.8	−0.7 ± 0.1	0.98

The features above described apply regardless of the season, and they are visible in the "average" curve of Figure 6 which considers all the measurement periods (2007–2013). However the magnitude and variability observed in the three curves (average and the seasonal values) of the absorption coefficient are significantly different if summer and winter seasons are compared (spring and autumn can be found in between). The daily evolution of $\sigma_{ap}(670)$ is similar in both seasons but larger values of $\sigma_{ap}(670)$ are observed in winter and the differences between maxima and minima are noticeably larger during that season.

In winter the absorption coefficient can increase by a factor up to six, in the week days, between the early morning minima and the late afternoon maxima. During summer the variability is much lower as the differences observed between minima and maxima are related roughly by a factor of two.

Also, the abovementioned average difference between the first and the second peaks is in fact mainly accounted for by the winter data because during summer both peaks are fairly similar.

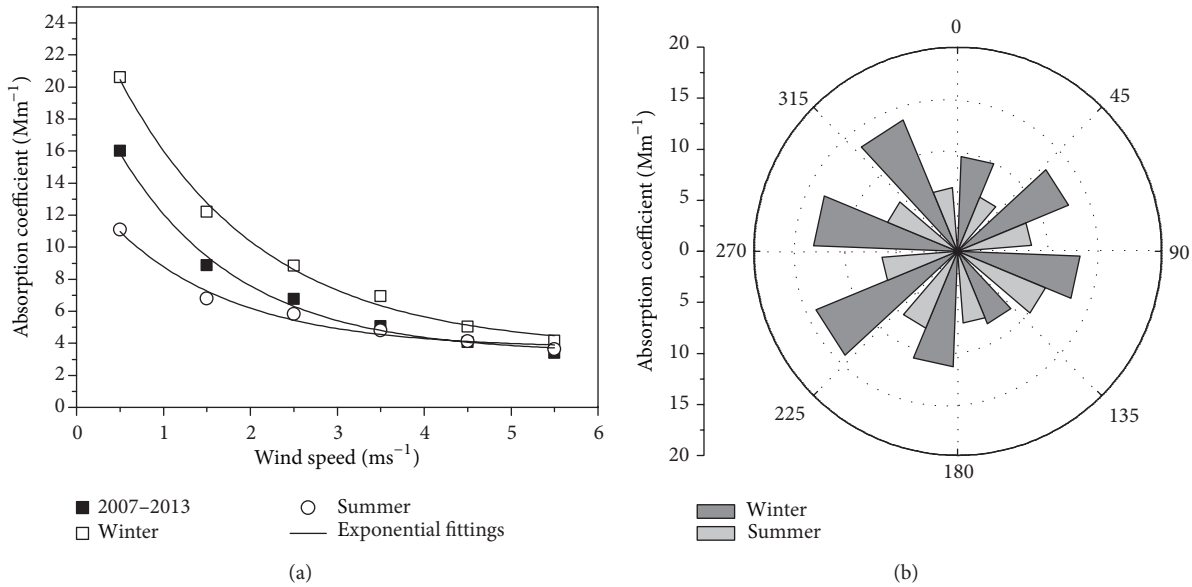

Figure 5: Dependence of the absorption coefficient on (a) the wind speed and (b) direction for summer and winter seasons.

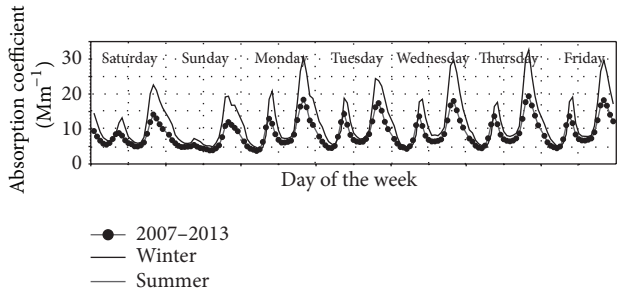

Figure 6: Average daily variations of the absorption coefficient, measured between 2007 and 2013, throughout the days of a week. Winter and summer seasonal values are also shown individually.

These facts are consistent with the discussion previously presented in the context of the seasonal evolution of the absorption coefficient (see Section 3.2), namely, on the additional input of aerosols due to domestic heating during winter and the lower capacity of the atmosphere for dispersing the pollutants due to the temperature inversions.

4. Conclusions

Measurements of the absorption coefficient in the visible range (670 nm) made in a small Portuguese town, located in the southwestern Iberia Peninsula, are analyzed. The time series upon which this work is made is unique in Portugal as it spans over a relatively large period of time, between 2007 and 2013.

The average absorption coefficient, $\sigma_{ap}(670)$, was 8.7 ± 9.9 Mm^{-1} with a lower median value of 6.2 Mm^{-1}, as the distribution of $\sigma_{ap}(670)$ was shaped log normally. Its temporal variation was characterized by both clear seasonal and daily cycles. The seasonal cycle revealed that the highest and lowest values of $\sigma_{ap}(670)$ were observed in winter and summer periods, respectively. Thus, winter and summer were the most dissimilar seasons, while spring and autumn could be found in between; therefore, the analysis was more detailed in extracting the differences between summer and winter. An average increase by a factor of two in the absorption coefficient (from 6 to 12 Mm^{-1}) was observed in winter if compared to summer season. This fact was attributed to the additional input of aerosols, particularly due to domestic heating, and also to the average atmospheric conditions, namely, the lower boundary layer height and frequent temperature inversions.

Concerning the daily variations, the influence of local activities in the absorbing particle levels, namely, due to traffic, was shown with morning and afternoon peaks being related to the traffic rush hours of the day; also, the reduction in human activities in Sunday mornings was particularly evident.

A strong dependence of the absorption coefficient on the wind speed was found and an exponential decay function fitted very well to the data. This indicates an increase in the atmospheric particle dispersion as the wind speed increases.

In spite of some differences, the wind direction was less influent, likely because the sampling site is located within the city centre, inside the ring road, and hence traffic pollution is transported to the measurement site from all directions; thus, all the quadrants are able to influence the measurement site.

Conflict of Interests

The authors declare that there is no conflict of interests regarding the publication of this paper.

Acknowledgment

This work was supported by FCT (Fundação para a Ciência e a Tecnologia) within the following Grants and Projects: SFRH/BD/29008/2006, SFRH/BPD/81132/2011, and PTDC/CEO-MET/4222/2012.

References

[1] M. O. Andreae, "The dark side of aerosols," *Nature*, vol. 409, no. 6821, pp. 671–672, 2001.

[2] V. Ramanathan, P. J. Crutzen, J. T. Kiehl, and D. Rosenfeld, "Atmosphere: aerosols, climate, and the hydrological cycle," *Science*, vol. 294, no. 5549, pp. 2119–2124, 2001.

[3] C. E. Chung, V. Ramanathan, D. Kim, and I. A. Podgorny, "Global anthropogenic aerosol direct forcing derived from satellite and ground-based observations," *Journal of Geophysical Research: Atmospheres*, vol. 110, no. 24, Article ID D24207, 2005.

[4] K. V. S. Badarinath and K. Madhavi Latha, "Direct radiative forcing from black carbon aerosols over urban environment," *Advances in Space Research*, vol. 37, no. 12, pp. 2183–2188, 2006.

[5] S. E. Schwartz, "The White house effect—shortwave radiative forcing of climate by anthropogenic aerosols: an overview," *Journal of Aerosol Science*, vol. 27, no. 3, pp. 359–382, 1996.

[6] J. M. Haywood and K. P. Shine, "Multi-spectral calculations of the direct radiative forcing of tropospheric sulphate and soot aerosols using a column model," *Quarterly Journal of the Royal Meteorological Society*, vol. 123, no. 543, pp. 1907–1930, 1997.

[7] M. Z. Jacobson, "Strong radiative heating due to the mixing state of black carbon in atmospheric aerosols," *Nature*, vol. 409, no. 6821, pp. 695–697, 2001.

[8] V. Ramanathan and G. Carmichael, "Global and regional climate changes due to black carbon," *Nature Geoscience*, vol. 1, no. 4, pp. 221–227, 2008.

[9] P. Foster, V. Ramaswamy, P. Artaxo et al., "Changes in atmospheric constituents and in radiative forcing," in *Climate Change 2007. the Physical Science Basis, Contribution of Working Group I to the Fourth Assessment Report of the Intergovernmental Panel on Climate Change*, S. Solomon, D. Qin, M. Manning et al., Eds., Cambridge University Press, Cambridge, UK, 2007.

[10] C. Wang, "A modeling study on the climate impacts of black carbon aerosols," *Journal of Geophysical Research D: Atmospheres*, vol. 109, no. 3, Article ID D03106, 2004.

[11] S. Menon, J. Hansen, L. Nazarenko, and Y. Luo, "Climate effects of black carbon aerosols in China and India," *Science*, vol. 297, no. 5590, pp. 2250–2253, 2002.

[12] A. Stohl, E. Andrews, J. F. Burkhart et al., "Pan-Arctic enhancements of light absorbing aerosol concentrations due to North American boreal forest fires during summer 2004," *Journal of Geophysical Research D: Atmospheres*, vol. 111, no. 22, Article ID D22214, 2006.

[13] D. Shindell and G. Faluvegi, "Climate response to regional radiative forcing during the twentieth century," *Nature Geoscience*, vol. 2, no. 4, pp. 294–300, 2009.

[14] A. S. Ackerman, O. B. Toon, D. E. Stevens, A. J. Heymsfield, V. Ramanathan, and E. J. Welton, "Reduction of tropical cloudiness by soot," *Science*, vol. 288, no. 5468, pp. 1042–1047, 2000.

[15] Y. J. Kaufman, D. Tanré, and O. Boucher, "A satellite view of aerosols in the climate system," *Nature*, vol. 419, no. 6903, pp. 215–223, 2002.

[16] H. Horvath, "Estimation of the average visibility in central Europe," *Atmospheric Environment*, vol. 29, no. 2, pp. 241–246, 1995.

[17] B. R. Gurjar, A. Jain, A. Sharma et al., "Human health risks in megacities due to air pollution," *Atmospheric Environment*, vol. 44, no. 36, pp. 4606–4613, 2010.

[18] J. Löndahl, E. Swietlicki, E. Lindgren, and S. Loft, "Aerosol exposure versus aerosol cooling of climate: what is the optimal emission reduction strategy for human health?" *Atmospheric Chemistry and Physics*, vol. 10, no. 19, pp. 9441–9449, 2010.

[19] H. J. Kim, X. D. Liu, T. Kobayashi et al., "Ultrafine carbon black particles inhibit human lung fibroblast-mediated collagen gel contraction," *American Journal of Respiratory Cell and Molecular Biology*, vol. 28, no. 1, pp. 111–121, 2003.

[20] J. H. Seinfeld and S. N. Pandis, *Atmospheric Chemistry and Physics: From Air Pollution to Climate Change*, John Wiley & Sons, New York, NY, USA, 1998.

[21] S. Ruellan and H. Cachier, "Characterisation of fresh particulate vehicular exhausts near a Paris high flow road," *Atmospheric Environment*, vol. 35, no. 2, pp. 453–468, 2001.

[22] W. Fendel, D. Matter, H. Burtscher, and A. Schmidt-Ott, "Interaction between carbon or iron aerosol particles and ozone," *Atmospheric Environment*, vol. 29, no. 9, pp. 967–973, 1995.

[23] G. Li, R. Zhang, J. Fan, and X. Tie, "Impacts of black carbon aerosol on photolysis and ozone," *Journal of Geophysical Research: Atmospheres*, vol. 110, no. 23, Article ID D23206, 2005.

[24] T. C. Bond and R. W. Bergstrom, "Light absorption by carbonaceous particles: an investigative review," *Aerosol Science and Technology*, vol. 40, no. 1, pp. 27–67, 2006.

[25] H. Moosmüller, R. K. Chakrabarty, and W. P. Arnott, "Aerosol light absorption and its measurement: a review," *Journal of Quantitative Spectroscopy and Radiative Transfer*, vol. 110, no. 11, pp. 844–878, 2009.

[26] R. S. Hamilton and T. A. Mansfield, "Airborne particulate elemental carbon: its sources, transport and contribution to dark smoke and soiling," *Atmospheric Environment A*, vol. 25, no. 3-4, pp. 715–723, 1991.

[27] A. Berner, S. Sidla, Z. Galambos et al., "Modal character of atmospheric black carbon size distributions," *Journal of Geophysical Research D: Atmospheres*, vol. 101, no. 14, pp. 19559–19565, 1996.

[28] T. A. Pakkanen, V.-M. Kerminen, C. H. Ojanen, R. E. Hillamo, P. Aarnio, and T. Koskentalo, "Atmospheric black carbon in Helsinki," *Atmospheric Environment*, vol. 34, no. 9, pp. 1497–1506, 2000.

[29] T. C. Bond, D. G. Streets, K. F. Yarber, S. M. Nelson, J.-H. Woo, and Z. Klimont, "A technology-based global inventory of black and organic carbon emissions from combustion," *Journal of Geophysical Research D: Atmospheres*, vol. 109, no. 14, Article ID D14203, 2004.

[30] T. C. Bond, S. J. Doherty, D. W. Fahey et al., "Bounding the role of black carbon in the climate system: a scientific assessment," *Journal of Geophysical Research: Atmospheres*, vol. 118, pp. 5380–5552, 2013.

[31] S. Pereira, F. Wagner, and A. M. Silva, "Long term black carbon measurements in the southwestern Iberia Peninsula," *Atmospheric Environment*, vol. 57, pp. 63–71, 2012.

[32] A. Petzold, H. Schloesser, P. J. Sheridan, W. P. Arnott, J. A. Ogren, and A. Virkkula, "Evaluation of multiangle absorption photometry for measuring aerosol light absorption," *Aerosol Science and Technology*, vol. 39, no. 1, pp. 40–51, 2005.

[33] P. J. Sheridan, W. Patrick Arnott, J. A. Ogren et al., "The reno aerosol optics study: an evaluation of aerosol absorption measurement methods," *Aerosol Science and Technology*, vol. 39, no. 1, pp. 1–16, 2005.

[34] A. Petzold and M. Schönlinner, "Multi-angle absorption photometry—a new method for the measurement of aerosol light absorption and atmospheric black carbon," *Journal of Aerosol Science*, vol. 35, no. 4, pp. 421–441, 2004.

[35] T. Müller, J. S. Henzing, G. de Leeuw et al., "Characterization and intercomparison of aerosol absorption photometers: result of two intercomparison workshops," *Atmospheric Measurement Techniques*, vol. 4, no. 2, pp. 245–268, 2011.

[36] S. Mogo, V. E. Cachorro, A. de Frutos, and A. Rodrigues, "Absorption ångström exponents of aerosols and light absorbing carbon (lac) obtained from in situ data in Covilhã, central Portugal," *Journal of Environmental Monitoring*, vol. 14, pp. 3174–3181, 2012.

[37] H. Lyamani, F. J. Olmo, and L. Alados-Arboledas, "Physical and optical properties of aerosols over an urban location in Spain: seasonal and diurnal variability," *Atmospheric Chemistry and Physics*, vol. 10, no. 1, pp. 239–254, 2010.

[38] M. Pandolfi, M. Cusack, A. Alastuey, and X. Querol, "Variability of aerosol optical properties in the Western Mediterranean Basin," *Atmospheric Chemistry and Physics*, vol. 11, no. 15, pp. 8189–8203, 2011.

[39] S. Eidels-Dubovoi, "Aerosol impacts on visible light extinction in the atmosphere of Mexico City," *Science of the Total Environment*, vol. 287, no. 3, pp. 213–220, 2002.

[40] X. He, C. C. Li, A. K. H. Lau et al., "An intensive study of aerosol optical properties in Beijing urban area," *Atmospheric Chemistry and Physics*, vol. 9, no. 22, pp. 8903–8915, 2009.

[41] G. Paredes-Miranda, W. P. Arnott, J. L. Jimenez, A. C. Aiken, J. S. Gaffney, and N. A. Marley, "Primary and secondary contributions to aerosol light scattering and absorption in Mexico City during the MILAGRO 2006 campaign," *Atmospheric Chemistry and Physics*, vol. 9, no. 11, pp. 3721–3730, 2009.

[42] A.-P. Hyvärinen, H. Lihavainen, M. Komppula et al., "Aerosol measurements at the Gual Pahari EUCAARI station: preliminary results from in-situ measurements," *Atmospheric Chemistry and Physics*, vol. 10, no. 15, pp. 7241–7252, 2010.

[43] D. J. Delene and J. A. Ogren, "Variability of aerosol optical properties at four North American surface monitoring sites," *Journal of the Atmospheric Sciences*, vol. 59, no. 6, pp. 1135–1150, 2002.

[44] C. Junker, S. G. Jennings, and H. Cachier, "Aerosol light absorption in the North Atlantic: trends and seasonal characteristics during the period 1989 to 2003," *Atmospheric Chemistry and Physics*, vol. 6, no. 7, pp. 1913–1925, 2006.

[45] A. Virkkula, J. Backman, P. P. Aalto et al., "Seasonal cycle, size dependencies, and source analyses of aerosol optical properties at the SMEAR II measurement station in Hyytiälä, Finland," *Atmospheric Chemistry and Physics*, vol. 11, no. 9, pp. 4445–4468, 2011.

[46] A. R. Deacon, R. G. Derwent, R. M. Harrison, D. R. Middleton, and S. Moorcroft, "Analysis and interpretation of measurements of suspended particulate matter at urban background sites in the United Kingdom," *Science of the Total Environment*, vol. 203, no. 1, pp. 17–36, 1997.

[47] N. T. Oneill, A. Ignatov, B. N. Holben, and T. F. Eck, "The lognormal distribution as a reference for reporting aerosol optical depth statistics; empirical tests using multi-year, multi-site AERONET sunphotometer data," *Geophysical Research Letters*, vol. 27, no. 20, pp. 3333–3336, 2000.

[48] E. Gerasopoulos, M. O. Andreae, C. S. Zerefos et al., "Climatological aspects of aerosol optical properties in Northern Greece," *Atmospheric Chemistry and Physics*, vol. 3, no. 6, pp. 2025–2041, 2003.

[49] S. Pereira, F. Wagner, and A. M. Silva, "Scattering properties and mass concentration of local and long-range transported aerosols over the South Western Iberia Peninsula," *Atmospheric Environment*, vol. 42, no. 33, pp. 7623–7631, 2008.

[50] M. A. Obregón, S. Pereira, F. Wagner, A. Serrano, M. L. Cancillo, and A. M. Silva, "Regional differences of column aerosol parameters in western Iberian Peninsula," *Atmospheric Environment*, vol. 62, pp. 208–219, 2012.

[51] Y. Wang, P. K. Hopke, O. V. Rattigan, and Y. Zhu, "Characterization of ambient black carbon and wood burning particles in two urban areas," *Journal of Environmental Monitoring*, vol. 13, no. 7, pp. 1919–1926, 2011.

[52] M. A. Pohjola, A. Kousa, J. Kukkonen et al., "The spatial and temporal variation of measured urban PM10 and PM2. 5 in the Helsinki metropolitan area," *Water, Air, & Soil Pollution*, vol. 2, pp. 189–201, 2002.

[53] S. Sharma, J. R. Brook, H. Cachier, J. Chow, A. Gaudenzi, and G. Lu, "Light absorption and thermal measurements of black carbon in different regions of Canada," *Journal of Geophysical Research D: Atmospheres*, vol. 107, no. 24, article 4771, 2002.

[54] K. Madhavi Latha and E. J. Highwood, "Studies on particulate matter (PM10) and its precursors over urban environment of Reading, UK," *Journal of Quantitative Spectroscopy and Radiative Transfer*, vol. 101, no. 2, pp. 367–379, 2006.

[55] K. K. Moorthy and S. S. Babu, "Aerosol black carbon over Bay of Bengal observed from an island location, Port Blair: temporal features and long-range transport," *Journal of Geophysical Research D: Atmospheres*, vol. 111, no. 17, Article ID D17205, 2006.

[56] H. Lyamani, F. J. Olmo, and L. Alados-Arboledas, "Light scattering and absorption properties of aerosol particles in the urban environment of Granada, Spain," *Atmospheric Environment*, vol. 42, no. 11, pp. 2630–2642, 2008.

Hindawi Publishing Corporation
Advances in Meteorology
Volume 2014, Article ID 197072, 8 pages
http://dx.doi.org/10.1155/2014/197072

Research Article

Radiative Impact of Fireworks at a Tropical Indian Location: A Case Study

B. P. Singh,[1] A. K. Srivastava,[2] S. Tiwari,[2] S. Singh,[3] R. K. Singh,[1] D. S. Bisht,[1,2] D. M. Lal,[1,2] A. K. Singh,[4] R. K. Mall,[5] and Manoj K. Srivastava[1]

[1] *Department of Geophysics, Banaras Hindu University, Varanasi 221005, India*
[2] *Indian Institute of Tropical Meteorology (Branch), Prof. Ram Nath Vij Marg, New Delhi 110060, India*
[3] *Radio and Atmospheric Sciences Division, National Physical Laboratory, New Delhi 110012, India*
[4] *Department of Physics, Banaras Hindu University, Varanasi 221005, India*
[5] *Institute of Environment and Sustainable Development, Banaras Hindu University, Varanasi 221005, India*

Correspondence should be addressed to Manoj K. Srivastava; mksriv@gmail.com

Received 22 August 2013; Accepted 21 October 2013; Published 22 January 2014

Academic Editor: Sachin D. Ghude

During Diwali festival, extensive burning of crackers and fireworks is made. Weeklong intensive observational campaign for aerosol study was carried out at a representative urban location in the eastern Indo-Gangetic Plain (IGP), Varanasi (25.3°N, 83.0°E), from October 29 to November 04, 2005 (Diwali on November 01, 2005), to investigate behavioral change of aerosol properties and radiative forcing between firework affected and nonaffected periods. Results show a substantial increase (~27%) in aerosol optical depth, aerosol absorption coefficients, and aerosol scattering coefficients during affected period as compared to non-affected periods. Magnitudes of radiative forcing at top of atmosphere during affected and non-affected periods are found to be $+10 \pm 1$ and $+12 \pm 1\ \mathrm{Wm}^{-2}$, respectively, which are -31 ± 7 and $-17 \pm 5\ \mathrm{Wm}^{-2}$, respectively, at surface. It suggests an additional cooling of ~20% at top of atmosphere, ~45% cooling at surface, and additional atmospheric heating of $0.23\ \mathrm{Kday}^{-1}$ during fireworks affected period, which is ~30% higher than the non-affected period average.

1. Introduction

Importance of aerosols in regional and global climate has gained wide knowledge base during the last couple of decades. General impact of these aerosols is to cool the atmosphere and to compensate the atmospheric warming caused due to enhanced greenhouse gases. However, atmospheric warming due to aerosols is also noticed when absorbing particles, such as black carbon (soot) and/or mineral dust, are present [1, 2]. Significant heating to the atmosphere may play a crucial role in various boundary layer processes under favorable atmospheric conditions [3]. The presence of such aerosols is higher in the atmospheric boundary layer [4], but they are also reported in the free troposphere till stratosphere. Boundary layer aerosols are characterized as short-lived and showed spatiotemporal variation in mass and number concentrations. Depending on weather condition and location, the regional variability in physical, chemical, and optical characteristics of aerosols is influenced by mixing various types of aerosols, produced by different natural and/or anthropogenic processes [3, 5], for example, aerosol production from biomass burning [6], biogenic production [7], industrial effluents [8], and so forth. The impact of aerosol is also found to be associated with climatic elements [9].

During recent decades, there have been a number of studies to characterize aerosols on local scale; however, studies on instant increment of aerosols within 1-2 days, due to fireworks, are available for only a few locations, for example, during New Year event [10], Millennium festival [11], Diwali festival [12–14], and so forth. Further, studies reported for firework generated aerosols are more inclined towards the impact of firework generated, gaseous as well as particulate, pollutants on health [15, 16], air quality [12–14, 16, 17], number and mass concentration [10, 11], and

interrelationship between gaseous pollutants and particles [10, 18], but the impact of fireworks generated aerosols on climate in terms of atmospheric forcing has never been assessed for any location so far.

The present study is an attempt to understand the changes in optical characteristics of aerosols and also to understand changes in radiative impacts that are caused due to mixing firework generated aerosols in the ambience. Data for this intensive observation period (IOP) was collected for an urban location in Indo-Gangetic Plain (IGP), Varanasi (25.3N, 83.0E, 76 above mean sea level), during October 29 to November 04, 2005 (Diwali was celebrated on November 01). The objectives of the work are to broaden our understanding towards the effect of fireworks on climate and also to quantify their impact in terms of radiative forcing. To the best of our knowledge, this is the first time to report the impact of firework generated aerosol on radiative balance and heating of the atmosphere.

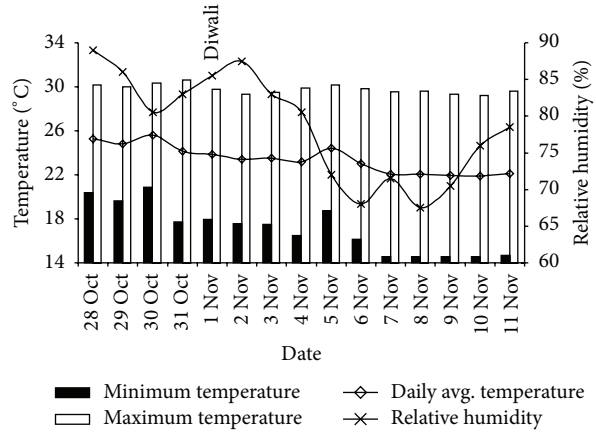

Figure 1: Weather parameters from October 28 till November 11, 2005 at Varanasi.

2. Site Description, Weather, and Data

Varanasi is a representative urban station in the central part of IGP. Varanasi is amongst few locations in India for which the column ozone and solar ultraviolet radiation are observed along with surface weather parameters, by the office of India Meteorological Department (IMD) at BHU, Varanasi, for the purpose of global database at World Ozone and Ultraviolet Radiation Data Centre (WOUDC). Weather parameters for the present study are obtained from surface weather observatory being managed by IMD, BHU, Varanasi.

Surface weather parameters and aerosol optical depths (AODs) are collected at every half-to-one hour interval during the entire campaign that includes the pre- and post-Diwali period. Weather was mostly calm and stable during the IOP. Mean sea level pressure during this period varied from 1011 to 1016 hPa and wind was mostly calm. For the IOP, daily maximum and daily minimum surface temperature and relative humidity varied from 29.0 to 31.0°C, 11.1 to 19.0°C, and 67% to 89%, respectively. General weather of Varanasi during IOP is, however, shown in Figure 1.

Multiwavelength AODs have been collected using MicroTOPS-II. The MicroTOPS-II used in this study was compared with another set of MicroTOPS-II at the National Physical Laboratory, New Delhi (NPL), before IOP. MicroTOPS-II at NPL was calibrated at Solar Light Company, USA, in 2004. More details for comparison, however, can be found elsewhere [19]. AODs were measured at 340, 500, and 870 nm wavelengths (full width at half maximum: ±2–10 nm) and signals at 936 and 1020 nm are used to compute columnar water vapor (CWV). As per Morys et al. [20], pointing accuracy of the MicroTOPS-II is better than 0.10 and long-term stability of the filter used in the instrument is better than 0.1 nm per year. In order to check the repeatability of the instrument, frequent observations were taken at about 11 seconds interval on a fairly clear forenoon of October 30, 2005. This series of observation showed average and standard deviations of AODs at 340, 500, and 870 nm as 1.213 ± 0.013, 0.967 ± 0.009, and 0.403 ± 0.005, respectively, over ~7 minutes of continuous measurements. This suggests that the observations made during IOP are consistent and can be considered as possessing good quality.

The spectral variations of AODs provide useful information on columnar size distribution of aerosols, which can be represented by Ångström power law [21] as,

$$\tau_a(\lambda) = \beta\lambda^{-\alpha}, \quad (1)$$

where $\tau_a(\lambda)$ is AOD at wavelength λ (in μm), β is turbidity coefficient, and α is Ångström exponent (AE). α is a good indicator of size range of the dominant particle population in an aerosol sample [22, 23], and turbidity coefficient (β) indicates total aerosol loading, which is equal to aerosol optical depth (τ_a) at 1.0 μm wavelength.

First order derivative of α (i.e., α') is a derived parameter, which is calculated using more than two wavelengths. This parameter is useful for the estimation of type of aerosols [19]. In the present study, α' is computed using AODs obtained at central wavelengths of 340, 500, and 870 nm.

3. Methodology

AODs, single scattering albedo (SSA), and asymmetric parameter (AP) are crucial aerosol properties for the estimation of aerosol direct radiative forcing (DRF). Since direct measurements of SSA and AP were not available at Varanasi, these parameters have been estimated using standard procedures (described in next section) of Optical Properties of Aerosols and Clouds (OPAC) model [24].

3.1. Estimation of Aerosol Optical Parameters. OPAC model provides wide range of optical and microphysical properties of aerosols pertaining to 61 discrete wavelengths (between 0.3 and 40 μm), eight values of RH, and various aerosol compositions. We have followed an approach that uses the available measurements as anchoring point in standard continental average aerosol model of OPAC, which is then fine-tuned to match the measurement in order to derive optical properties of aerosols (see [5] for details). As measured

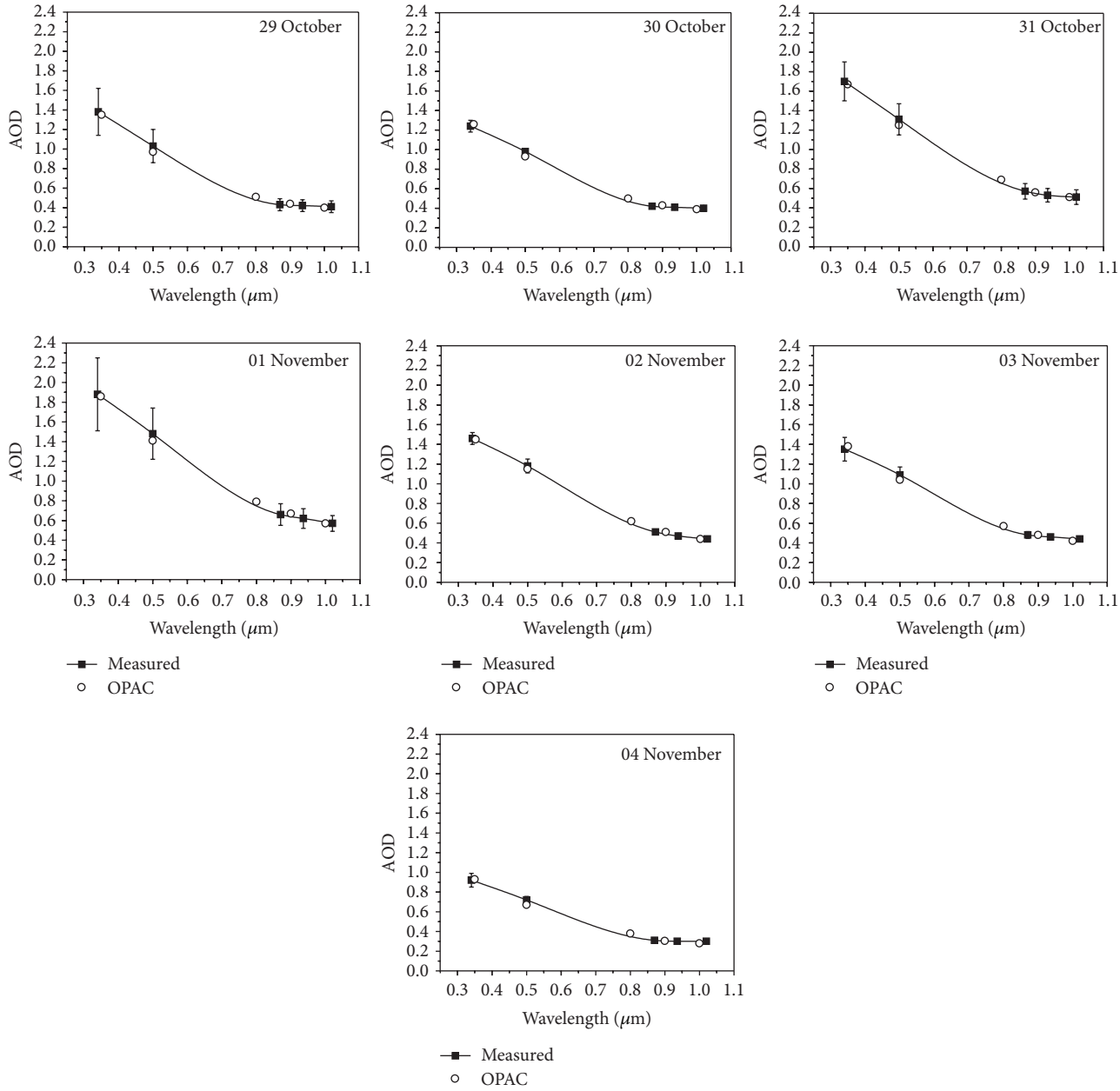

Figure 2: Comparison between measured and model (OPAC) derived spectral AODs for intensive observation period (IOP, October 29 to November 04, 2005).

aerosol composition over the station was not available during the study period, we have assumed possible composition in the OPAC model. Once an appropriate atmosphere is generated in OPAC model, measured AODs from MicroTOPS-II were used as a reference to constrain other crucial aerosol optical parameters (i.e., SSA and AP). Comparison of OPAC derived and measured spectral AODs are shown in Figure 2. Modelled spectral AOD values were found to be lying within standard deviations of measured spectral AODs, for all the days during IOP. Difference between observed and modelled values was found within 5%.

Using the above-mentioned approach, OPAC model is run for each day of IOP. Though this is an alternative method to derive crucial aerosol optical parameters in the absence of observations, it is an established and widely used method in the literature ([5] and references therein). In this method, however, there are chances of uncertainties due to vertical aerosol distribution. In the absence of vertical aerosol profiles, as in the present case, the surface aerosol properties are attributed to column properties, assuming vertical profiles in OPAC model, as suggested by Srivastava et al. [5]. Additionally, uncertainties may also be generated due to OPAC accounted external mixtures of different aerosol components to form aerosol types. Being an urban station in the central part of IGP, the probability of internal mixing or coating of aerosols may be possible, which can deliver certain uncertainties in the end result.

3.2. Estimation of Aerosol Direct Radiative Forcing. Aerosols are significant contributors to direct radiative forcing (DRF). Some of these particles, for example, BC and mineral dust, show absorbing nature [1, 2] and contribute significantly to the warming of lower atmosphere due to short-wave absorption [25]. In the present study, net flux is computed in the shortwave region (0.30–3.0 μm), separately for top of atmosphere (TOA) and surface, with and without aerosols, using the Santa Barbara DISORT atmospheric radiative transfer (SBDART) model [26]. The input parameters for SBDART model are spectral AOD, SSA, and AP, which are either measured or obtained by OPAC model. SBDART uses six standard atmospheres to consider vertical profiles of atmospheric parameters, such as average temperature, pressure, water vapor, and ozone density [26]. Location of Varanasi falls in the tropical classification, which is characterized by average water vapor of 4.117 g cm^{-2} and average columnar ozone of 253 DU. These data are close to observations over Varanasi during October-November months. Surface albedo over the station was considered to be 0.18, which is slightly less in comparison to Kanpur (an industrial city situated ~300 km away from Varanasi) [27].

Diurnal average of aerosol direct radiative forcing (DRF) at TOA and at surface is estimated by computing the difference in net radiative fluxes, with and without aerosol, respectively, at TOA and surface. The difference between TOA and surface forcing is considered as atmospheric forcing (ΔF), which represents the amount of energy trapped or absorbed by aerosols within the atmosphere and which is available to be transformed into heat.

4. Results and Discussion

4.1. Aerosol Optical Characteristics. Figure 3 shows measured AOD at 340, 500, and 870 nm wavelengths, along with the Ångström exponents (α), computed for the wavelength pair of 340–870 nm and α' (computed with the help of wavelength pairs 340–500 nm and 500–870 nm). By and large, opposite behavior is observed between AOD and α [12, 28, 29]. AOD was found to increase (with decreasing α) from October 30 till November 01 (Diwali) and decrease (with increasing α) on subsequent days (Table 1 and Figure 3). Results suggest enhanced loading of aerosols during Diwali period, most probably due to excessive burning of firework and crackers [10–12, 30]. α' is a parameter that provides information on types of aerosol in the aerosol population [19]. Positive α' is an indicator of fine/accumulation-mode particles dominance, whereas negative α' suggests dominance of coarse-mode aerosol particles [19, 31–34]. Table 1 shows that α' is positive during IOP indicating persistent dominance of fine-mode particles during all these days; however, it was the lowest on Diwali. It suggests that IOP is dominated by fine mode particle; but there is inclusion of other fine mode particles due to burning of fireworks during Diwali day. Babu and Moorthy [30] also found enhanced AODs during the event of firework, which was caused due to enhanced presence of black and organic carbon, generated by burning of different types of crackers and fireworks during

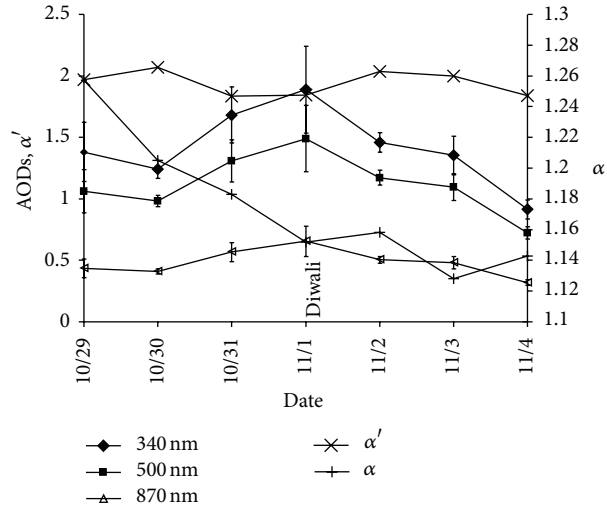

Figure 3: Day-to-day variability in AODs (340 nm, 500 nm, and 870 nm), AE (α, 340–870 nm), and α' for IOP.

Diwali. Singh et al. [12] have reported enhancement of 5.7% and 5.5% for AOD_{340} and AOD_{500}, respectively, during Diwali at Kanpur.

The variations in OPAC derived parameters, such as absorption coefficients, scattering coefficient, and SSA at 500 nm (SSA_{500}), are also shown in Table 1. In general, the behavior of scattering coefficient was found similar to that of absorption coefficient and AOD, but it was different to that of AE. Scattering and absorption coefficients were found to be maximum (461.6 and 24.2 Mm^{-1}, resp.) on Diwali. The type of aerosols which contribute maximum to the scattering coefficient may include water-soluble inorganic species, such as sulfates and nitrates, arising from emissions of SO_2 and NO_x, and contributions from fossil fuel and biomass combustion sources. However, those aerosol types that contribute maximum to the absorbing coefficient may include BC, which is largely associated with firework [30].

Since scattering and absorbing type of aerosols are well mixed in the real atmosphere, their ultimate effect in terms of heating/cooling of the atmosphere depends on SSA of aerosol population. For the present case, minimum value of SSA_{500} (≈0.95) was observed on November 02, the next day of Diwali. It suggests extended influence of absorbing particles emitted due to burning of fireworks during Diwali night [10, 11, 30], which was affective till the next day. Absorbing aerosols are found to be associated with lower SSA values [35].

Spectral variations of average AOD, absorption coefficient, scattering coefficient, and SSA are shown in Figures 4(a)–4(d), respectively, for affected (October 31, November 01 and 02) and nonaffected (October 29, 30, November 03 and 04) periods. Significant differences in all the parameters were observed at all the wavelengths, for affected and nonaffected periods. It is found that AOD increased with the advent of Diwali and reached to its maximum value on November 01 (Diwali) for each wavelength (Figure 3). The burning of fireworks and crackers invariably contributes to the anthropogenic aerosols [12, 14]

Table 1: Daily mean values of AOD, column water vapor and AE, absorption coefficients, scattering coefficients, and SSA from October 29, 2005, to November 04, 2005.

Days (2005)	Category	AOD_{500}	$AE_{340-870}$	CWV (cm)	Abs. coeff.$_{500}$ (Mm^{-1})	Scatt. coeff.$_{500}$ (Mm^{-1})	SSA_{500}
October 29	NA	1.06	1.26	1.63	15.58	320.20	0.954
October 30	NA	0.98	1.21	1.34	15.01	303.20	0.953
October 31	AF	1.31	1.18	1.39	20.80	406.20	0.951
November 01	AF	1.49	1.15	1.61	24.23	461.60	0.950
November 02	AF	1.17	1.16	1.58	18.70	351.10	0.950
November 03	NA	1.10	1.13	1.51	17.03	338.10	0.952
November 04	NA	0.72	1.14	1.45	14.08	218.10	0.954

NA: nonaffected, AF: affected.

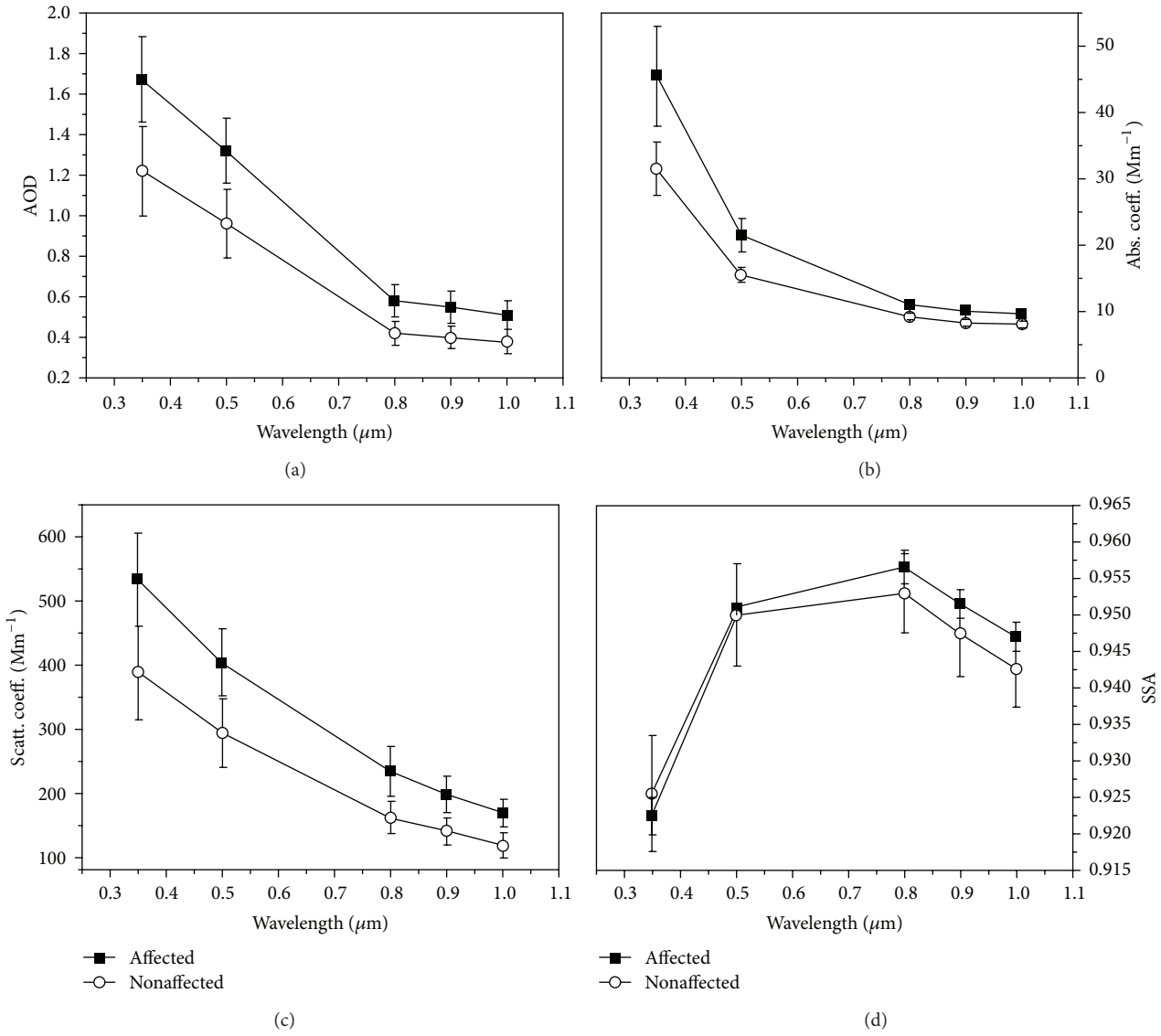

Figure 4: Spectral variation of (a) AOD, (b) absorption coefficient, (c) scattering coefficient, and (d) SSA for firework affected (October 31, November 01 and 02, 2005) and nonaffected periods (October 29, 30, November 03 and 04, 2005).

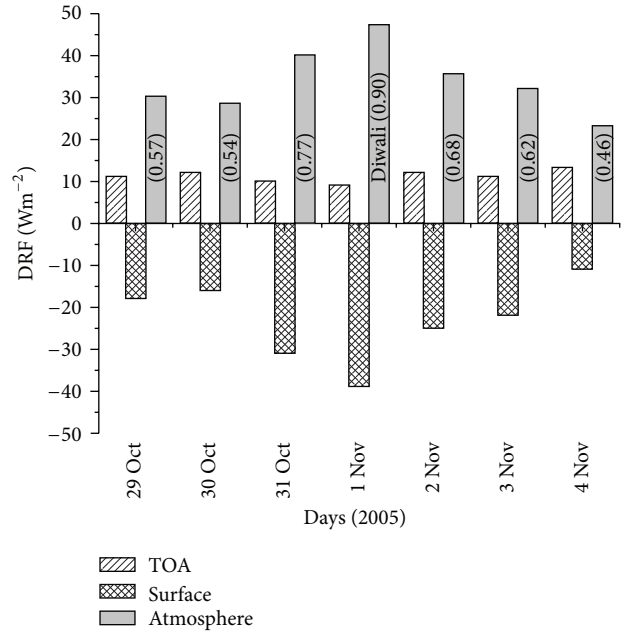

Figure 5: Day-to-day variability in the estimated direct radiative forcing at the TOA, surface, and in the atmosphere. The heating rate values are given in parentheses within respective bars.

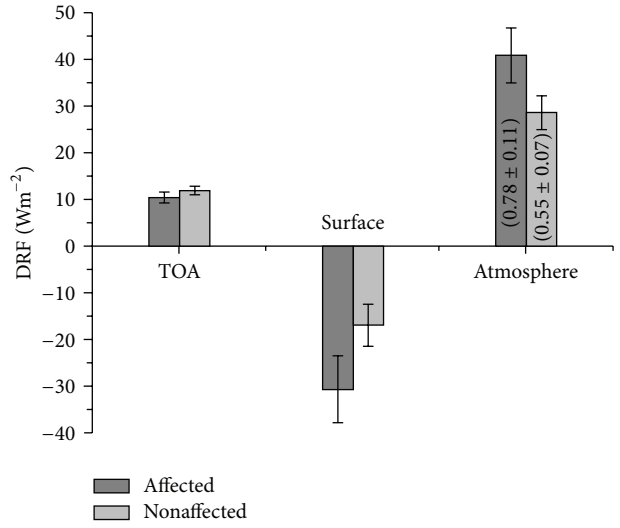

Figure 6: Comparison of estimated direct radiative forcing at the TOA, surface, and in the atmosphere for firework affected and nonaffected periods. Atmospheric heating rates are given in parentheses in the respective atmospheric forcing bars.

and increases AODs [36]. AODs at all other wavelengths were found to increase for firework affected period (Figure 3). Average AOD_{500} for affected period shows the value of 1.3, which is ~27% higher than the nonaffected period average. Similar increment in absorption coefficient (21.2 Mm^{-1}, increase of 27.4%) and scattering coefficient (406 Mm^{-1}, increase of 27.4%) was also noticed for firework affected period in comparison to nonaffected period. It is to be mentioned here that, apart from the emissions of absorbing aerosols, different water-soluble species (like sulfate, nitrate, etc.) are also emitted from fire crackers burning, which are of scattering in nature. As a result, an enhancement in both absorption and scattering coefficients was observed. For the same period, however, AE had decreased by 6.2%.

4.2. Aerosol Radiative Forcing and Implications to Atmospheric Heating Rate. Broadband aerosol direct radiative forcing (DRF) at the TOA, surface, and in the atmosphere for each day during IOP is shown in Figure 5. Negative value of surface forcing implies a net cooling effect, whereas positive value for TOA and within atmospheric implies a net warming effect. Significant day-to-day variability was observed in surface and atmospheric forcing values. The surface and atmospheric forcing was maximum (−38 and 47 Wm^{-2}, resp.) on Diwali (November 01), whereas aerosol DRF at TOA was minimum (9 Wm^{-2}) on Diwali.

Average aerosol DRF estimated at TOA, surface, and in the atmosphere, during affected and nonaffected period, is shown in Figure 6. Magnitudes of forcing at TOA during the affected and nonaffected periods were +10 ± 1 and +12 ± 1 Wm^{-2}, respectively; however, the forcing at surface was −31 ± 7 and −17 ± 5 Wm^{-2}, respectively. These estimates indicated an additional cooling of 2 Wm^{-2} at the TOA (~20%) and 14 Wm^{-2} at the surface (~45%) during firework affected period. Results could be due to enhanced loading of aerosols (absorbing and/or scattering type) over the station during firework period. Apart from the aerosol loading of absorption/scattering type aerosols, TOA and surface forcing are also sensitive to the albedo of the underlying surface [37]. The atmospheric forcing values during affected and nonaffected periods were estimated to be +41 ± 6 and +29 ± 4 Wm^{-2}, respectively, which translate to an additional atmospheric warming of +12 Wm^{-2} during firework affected period.

The higher value of surface cooling and strong atmospheric heating in the atmosphere suggests their association with various aerosol properties, for example, size range and chemical composition of aerosol population, and raises several climatic issues [4, 9, 38, 39]. An important aspect in this regard is the aerosol-generated atmospheric heating rates, which can be calculated from the first law of thermodynamics and hydrostatic equilibrium as

$$\frac{\partial T}{\partial t} = \frac{g}{C_p}\frac{\Delta F}{\Delta P} \times 24\,(\text{hr/day}) \times 3600\,(\text{sec/hr})\,, \qquad (2)$$

where $\partial T/\partial t$ is heating rate in kelvin per day ($Kday^{-1}$), g/C_p is lapse rate, g is acceleration due to gravity, C_p is specific heat capacity of air at constant pressure (1006 $Jkg^{-1}\,K^{-1}$), ΔF is atmospheric forcing due to aerosols, and ΔP is atmospheric pressure difference, which was considered to be 300 hPa in the present case.

The estimated atmospheric daily heating rates during the study period are also shown in Figure 5 (in parenthesis). Heating rates are found to be increased to higher magnitudes (0.90 $Kday^{-1}$) on Diwali, which decreased afterwards to attain a lower magnitude (0.46 $Kday^{-1}$) on November 04. Average atmospheric heating rate was found to be

$0.78 \pm 0.11\,\mathrm{Kday}^{-1}$ for the affected period, which is approximately 30% higher than the nonaffected period (average about $0.55 \pm 0.07\,\mathrm{Kday}^{-1}$). Considering the nonaffected period to represent normal atmospheric conditions, atmosphere is found to be heated up by $0.23\,\mathrm{Kday}^{-1}$ due to enhanced aerosol loading related to burning of fireworks.

5. Conclusions

Increase of particulate number density is a common feature during fireworks burning event. During Diwali festival, fireworks are burnt in peak duration of 1-2 hours. An intensive observation program was conducted from October 29 to November 04, 2005 (Diwali on November 01.) at an urban location in Indo-Gangetic Plain, Varanasi, India, to study the optical properties of aerosols, radiative forcing, and atmospheric heating rates caused due to Diwali fireworks.

Study shows enhancement of ~27% in the values of AOD_{500}, absorption coefficients, and scattering coefficients for firework affected period in comparison to nonaffected period. Estimated top of atmosphere and surface forcing were found to be $+10 \pm 1$ and $-31 \pm 7\,\mathrm{Wm}^{-2}$, respectively, for firework affected period and $+12 \pm 1$ and $-17 \pm 5\,\mathrm{Wm}^{-2}$, respectively, for nonaffected periods. The estimated forcing caused an additional cooling of ~20% at top of atmosphere and ~45% at surface due to enhanced loading of aerosols (absorbing and/or scattering type) over the station during firework period. The resultant atmospheric forcing was $+41 \pm 6$ and $+29 \pm 4\,\mathrm{Wm}^{-2}$ during firework affected and nonaffected periods, respectively, which exerted an additional atmospheric heating of $\sim 0.23\,\mathrm{Kday}^{-1}$ during firework affected period. In view of increasing population and extensive use of fireworks (and crackers) in major urban locations, the routine measurements of aerosols will certainly be helpful to understand the additional burden of aerosols caused due to fireworks burning. Such observations are also useful for understanding their impact on regional climate.

Conflict of Interests

The authors declare that there is no conflict of interests regarding the publication of this paper.

Acknowledgments

Authors Manoj K. Srivastava, B. P. Singh, and A. K. Singh are thankful for financial support from ISRO-ARFI and R. K. Singh is thankful to BHU and UGC for financial support. A. K. Singh, S. Tiwari, D. S. Bisht, and D. M. Lal are thankful to Director, IITM, for support and encouragement. IMD is acknowledged for proving supportive weather data. Authors are grateful to the anonymous reviewers for their constructive comments and suggestions towards the improvement of paper.

References

[1] V. Ramanathan, F. Li, M. V. Ramana et al., "Atmospheric brown clouds: hemispherical and regional variations in long-range transport, absorption, and radiative forcing," *Journal of Geophysical Research D*, vol. 112, no. 22, 2007.

[2] IPCC, *Climate Change 2007: The Physical Science Basis*, chapter 2, Cambridge University Press, Cambridge, UK, Contribution of Working Group I to the Fourth Assessment Report of the Intergovernmental Panel on Climate Change, 2007.

[3] A. K. Srivastava, D. S. Bisht, and S. Tiwari, "Boundary layer aerosol characteristics at Mahabubnagar during CAIPEEX-IGOC: modeling the optical and radiative properties," *Science of the Total Environment*, vol. 468-469, pp. 1093–1102, 2014.

[4] J. Schneider and R. Eixmann, "Three years of routine Raman lidar measurements of tropospheric aerosols: backscattering, extinction, and residual layer height," *Atmospheric Chemistry and Physics*, vol. 2, no. 4, pp. 313–323, 2002.

[5] A. K. Srivastava, S. Singh, S. Tiwari, and D. S. Bisht, "Contribution of anthropogenic aerosols in direct radiative forcing and atmospheric heating rate over Delhi in the Indo-Gangetic Basin," *Environmental Science and Pollution Research*, vol. 19, no. 4, pp. 1144–1158, 2012.

[6] K. Ram, M. M. Sarin, and S. N. Tripathi, "Temporal trends in atmospheric PM2.5, PM10, elemental carbon, organic carbon, water-soluble organic carbon, and optical properties: impact of biomass burning emissions in the Indo-Gangetic Plain," *Environmental Science and Technology*, vol. 46, no. 2, pp. 686–695, 2012.

[7] R. J. Charlson, J. E. Lovelock, M. O. Andreae, and S. G. Warren, "Oceanic phytoplankton, atmospheric sulphur, cloud albedo and climate," *Nature*, vol. 326, no. 6114, pp. 655–661, 1987.

[8] R. J. Charlson, J. Langner, H. Rodhe, C. B. Leovy, and S. G. Warren, "Perturbation of the northern hemisphere radiative balance by backscattering from anthropogenic sulfate aerosols," *Tellus*, vol. 43, no. 4, pp. 152–163, 1991.

[9] S.-W. Kim, S.-C. Yoon, A. Jefferson et al., "Observation of enhanced water vapor in Asian dust layer and its effect on atmospheric radiative heating rates," *Geophysical Research Letters*, vol. 31, no. 18, 2004.

[10] F. Drewnick, S. S. Hings, J. Curtius, G. Eerdekens, and J. Williams, "Measurement of fine particulate and gas-phase species during the New Year's fireworks 2005 in Mainz, Germany," *Atmospheric Environment*, vol. 40, no. 23, pp. 4316–4327, 2006.

[11] B. Wehner, A. Wiedensohler, and J. Heintzenberg, "Submicrometer aerosol size distributions and mass concentration of the millennium fireworks 2000 in Leipzig, Germany," *Journal of Aerosol Science*, vol. 31, no. 12, pp. 1489–1493, 2000.

[12] R. P. Singh, S. Dey, and B. Holben, "Aerosol behaviour in Kanpur during Diwali festival," *Current Science*, vol. 84, no. 10, pp. 1302–1304, 2003.

[13] U. C. Kulshrestha, T. Nageswara Rao, S. Azhaguvel, and M. J. Kulshrestha, "Emissions and accumulation of metals in the atmosphere due to crackers and sparkles during Diwali festival in India," *Atmospheric Environment*, vol. 38, no. 27, pp. 4421–4425, 2004.

[14] S. Tiwari, D. M. Chate, M. K. Srivastava et al., "Statistical evaluation of PM_{10} and distribution of PM_1, $PM_{2.5}$, and PM_{10} in ambient air due to extreme fireworks episodes (Deepawali festivals) in megacity Delhi," *Natural Hazards*, vol. 61, no. 2, pp. 521–531, 2012.

[15] J. M. Becker, S. Iskandrian, and J. Conkling, "Fatal and near-fatal asthma in children exposed to fireworks," *Annals of Allergy, Asthma and Immunology*, vol. 85, no. 6, pp. 512–513, 2000.

[16] T. Moreno, X. Querol, A. Alastuey et al., "Recreational atmospheric pollution episodes: inhalable metalliferous particles from firework displays," *Atmospheric Environment*, vol. 41, no. 5, pp. 913–922, 2007.

[17] K. Ravindra, S. Mor, and C. P. Kaushik, "Short-term variation in air quality associated with firework events: a case study," *Journal of Environmental Monitoring*, vol. 5, no. 2, pp. 260–264, 2003.

[18] A. K. Attri, U. Kumar, and V. K. Jain, "Formation of ozone by fireworks," *Nature*, vol. 411, no. 6841, p. 1015, 2001.

[19] N. K. Lodhi, S. N. Beegum, S. Singh, and K. Kumar, "Aerosol climatology at Delhi in the western indo-gangetic plain: microphysics, long-term trends, and source strengths," *Journal of Geophysical Research*, vol. 118, no. 3, pp. 1361–1375, 2013.

[20] M. Morys, F. M. Mims III, S. Hagerup et al., "Design, calibration, and performance of MICROTOPS II handheld ozone monitor and Sun photometer," *Journal of Geophysical Research D*, vol. 106, no. 13, pp. 14573–14582, 2001.

[21] A. Ångström, "The parameters of atmospheric turbidity," *Tellus*, vol. 16, pp. 64–75, 1964.

[22] A. K. Srivastava, P. C. S. Devara, Y. J. Rao, Y. Bhavanikumar, and D. N. Rao, "Aerosol optical depth, ozone and water vapor measurements over Gadanki, a tropical station in peninsular India," *Aerosol and Air Quality Research*, vol. 8, no. 4, pp. 459–476, 2008.

[23] G. V. Pawar, P. C. S. Devara, S. D. More, P. Pradeep Kumar, and G. R. Aher, "Determination of aerosol characteristics and direct radiative forcing at Pune," *Aerosol and Air Quality Research*, vol. 12, pp. 1166–1180, 2012.

[24] M. Hess, P. Koepke, and I. Schult, "Optical properties of aerosols and clouds: the software package OPAC," *Bulletin of the American Meteorological Society*, vol. 79, no. 5, pp. 831–844, 1998.

[25] P. Alpert, Y. J. Kaufman, Y. Shay-El et al., "Quantification of dust-forced heating of the lower troposphere," *Nature*, vol. 395, no. 6700, pp. 367–370, 1998.

[26] P. Ricchiazzi, S. Yang, C. Gautier, and D. Sowle, "SBDART: a research and teaching software tool for plane-parallel radiative transfer in the earth's atmosphere," *Bulletin of the American Meteorological Society*, vol. 79, no. 10, pp. 2101–2114, 1998.

[27] A. K. Prasad, S. Singh, S. S. Chauhan, M. K. Srivastava, R. P. Singh, and R. Singh, "Aerosol radiative forcing over the Indo-Gangetic plains during major dust storms," *Atmospheric Environment*, vol. 41, no. 29, pp. 6289–6301, 2007.

[28] S. More, P. Pradeep Kumar, P. Gupta, P. C. S. Devara, and G. R. Aher, "Comparison of aerosol products retrieved from AERONET, MICROTOPS and MODIS over a tropical urban city, Pune, India," *Aerosol and Air Quality Research*, vol. 13, pp. 107–121, 2013.

[29] G. Pandithurai, R. T. Pinker, P. C. S. Devara, T. Takamura, and K. K. Dani, "Seasonal asymmetry in diurnal variation of aerosol optical characteristics over Pune, western India," *Journal of Geophysical Research D*, vol. 112, no. 8, Article ID D08208, 2007.

[30] S. S. Babu and K. K. Moorthy, "Anthropogenic impact on aerosol black carbon mass concentration at a tropical coastal station: a case study," *Current Science*, vol. 81, no. 9, pp. 1208–1214, 2001.

[31] T. F. Eck, B. N. Holben, J. S. Reid et al., "Wavelength dependence of the optical depth of biomass burning, urban, and desert dust aerosols," *Journal of Geophysical Research D*, vol. 104, no. 24, pp. 31333–31349, 1999.

[32] N. T. O'Neill, T. F. Eck, B. N. Holben, A. Smirnov, A. Royer, and Z. Li, "Optical properties of boreal forest fire smoke derived from Sun photometry," *Journal of Geophysical Research*, vol. 107, no. 11, pp. AAC 6-1–AAC 6-19, 2002.

[33] D. G. Kaskaoutis, H. D. Kambezidis, A. D. Adamopoulos, and P. A. Kassomenos, "On the characterization of aerosols using the Ångström exponent in the Athens area," *Journal of Atmospheric and Solar-Terrestrial Physics*, vol. 68, no. 18, pp. 2147–2163, 2006.

[34] K. Soni, S. Singh, T. Bano, R. S. Tanwar, S. Nath, and B. C. Arya, "Variations in single scattering albedo and angstrom absorption exponent during different seasons at Delhi, India," *Atmospheric Environment*, vol. 44, no. 35, pp. 4355–4363, 2010.

[35] O. Dubovik, B. Holben, T. F. Eck et al., "Variability of absorption and optical properties of key aerosol types observed in worldwide locations," *Journal of the Atmospheric Sciences*, vol. 59, no. 3, pp. 590–608, 2002.

[36] B. M. Vyas and V. Saraswat, "Studies of atmospheric aerosol's parameters during pre-diwali to post–Diwali festival period over Indian semi arid station i.e., Udaipur," *Applied Physics Research*, vol. 4, no. 2, pp. 40–55, 2012.

[37] J. Meier, I. Tegen, B. Heinold, and R. Wolke, "Direct and semi-direct radiative effects of absorbing aerosols in Europe: results from a regional model," *Geophysical Research Letters*, vol. 39, no. 9, 2012.

[38] J. T. Houghton, Y. Ding, D. J. Griggs et al., Eds., *Climate Change 2001: The Scientific Basis*, Cambridge University Press, New York, NY, USA, 2001.

[39] Y. J. Kaufman, O. Boucher, D. Tanre, M. Chin, L. A. Remer, and T. Takemura, "Aerosol anthropogenic component estimated from satellite data," *Geophysical Research Letters*, vol. 32, no. 17, 2005.

Hindawi Publishing Corporation
Advances in Meteorology
Volume 2014, Article ID 202868, 5 pages
http://dx.doi.org/10.1155/2014/202868

Research Article

Aerosol Modulation of Ultraviolet Radiation Dose over Four Metro Cities in India

A. S. Panicker,[1] G. Pandithurai,[1] G. Beig,[1] Dongchul Kim,[2] and Dong-In Lee[3]

[1] *Indian Institute of Tropical Meteorology, Pashan, Pune 411008, India*
[2] *Universities Space Research Association, Columbia, MD 21044, USA*
[3] *Department of Environmental Atmospheric Sciences, Pukyong National University, Busan 608737, Republic of Korea*

Correspondence should be addressed to A. S. Panicker; abhilashpanicker@gmail.com and Dong-In Lee; leedi@pknu.ac.kr

Received 12 September 2013; Revised 20 November 2013; Accepted 21 November 2013; Published 2 January 2014

Academic Editor: Pavan S. Kulkarni

This paper discusses the influence of aerosols on UV erythemal dose over four metro cities in India. Tropospheric Emission Monitoring Internet Service (TEMIS), archived UV-index (UV-I), and UV daily erythemal dose obtained from SCIAMACHY satellite were used in this study during June 2004 and May 2005 periods covering four important Indian seasons. UV-Index (UV-I), an important parameter representing UV risk, was found to be in the high to extreme range in Chennai (8.1 to 15.33), moderate to extreme range in Mumbai and Kolkata (5 to 16.5), and low to extreme over Delhi (3 to 15). Average UV erythemal dose showed seasonal variation from 5.9 to 6.3 KJm^{-2} during summer, 2.9 to 4.4 KJm^{-2} during postmonsoon, 3 to 4.5 KJm^{-2} during winter, and 5.1 to 6.19 KJm^{-2} during premonsoon seasons over the four cities. To estimate the influence of aerosols on reducing UV dose, UV aerosol radiative forcing and forcing efficiency were estimated over the sites. The average aerosol forcing efficiency was found to be from -1.38 ± 0.33 to -3.01 ± 0.28 KJm^{-2} AOD^{-1} on different seasons. The study suggests that aerosols can reduce the incoming UV radiation dose by 30–60% during different seasons.

1. Introduction

Ultraviolet radiation, in spite of its nominal presence in solar spectrum, is important in human health perspectives. The UV region of the spectrum mainly consists of UV-C (200–280 nm), UV-B (280–315 nm), and UV-A (315–400 nm). Out of these UV-B is the most important spectral range, as it directly influences the human health. Enhanced exposure to UV-B can damage both terrestrial and oceanic organisms and also results in increases in the incidences of cataracts and skin cancer in humans [1, 2]. Very high levels of UV radiation also are reported to result in the extinction of minute biological species [3]. The impact of UV irradiance on human skin is characterized with UV erythemal dose. UV-index (UV-I) serves as a primary indicator of impact of UV radiation on human health. The UV radiation reaching the earth surface is modulated by the ozone concentration, cloud cover, solar zenith angle, and aerosols. The influences of ozone on UV radiation are well documented [4]. Several studies report the influence of cloud cover on UV radiation. Reference [5] reported that, for a solar zenith angle of 50°, average UV-B transmission was observed to be 30% for overcast skies and found to be ranging between 61 and 79% according to cloud amount. The paper [6] has shown that the effect of cloud for UV wavelengths is less than that for the whole solar spectrum and less than that for the visible part of the spectrum. However studies on influence of aerosols on UV are sparse, especially across Indian subcontinent [7–9]. A few studies reported the variation of UV radiation and UV-index over Indian region [10, 11]. However most of the studies ignore the aerosol component and its influence on UV radiative transfer. The role played by aerosols on the UV radiative transfer in the atmosphere is also uncertain [9]. Reference [12] has suggested that aerosol vertical (height) distribution can also affect surface UV irradiances by 2–5% for optical depth observations at visible wavelengths. And [13] has shown that the increase of anthropogenic aerosols has significantly decreased the biologically active UV radiation (5 to 18%) in nonurban areas of industrialized countries. It is suggested that aerosols are partially efficient to reduce UV radiation

increase due to ozone depletion [14, 15]. Hence in this paper, the modulation of UV radiation by aerosols, quantified through aerosol forcing efficiency over four metro cities in India (Chennai, Mumbai, Delhi, and Kolkata), is discussed. The data and methodology are explained in Section 2. A detailed description of variations of UV erythemal dose, UV-I, AOD, and forcing estimates is explained in Section 3 and conclusions are provided in Section 4.

2. Data and Methodology

The locations selected for this study are four metro cities in India, which are characterized with high industrialization and high population density. Chennai (13.08°N; 80.27°E) is situated in south of India and is characterized with typical tropical conditions, namely, high solar irradiance and high humidity, throughout the year. Mumbai (18.97°N; 72.83°E) is in the western part of India and is the financial capital of India. It is a highly urbanized and industrialized area and is a peak point of air pollution. Kolkata (22.57°N; 88.37°E) is in the eastern part of India, located on the bank of river Ganges. New Delhi (28.61°N; 77.23°E) is the political capital of India and is characterized by extreme weather events especially during premonsoon and winter seasons.

The Tropospheric Emission Monitoring Internet Service (TEMIS) archived daily datasets of UV erythemal (UVE) dose rate and UV-index (UV-I) are used in this study. TEMIS (http://www.temis.nl/general/index.html) provides global datasets of trace gases, aerosols, and UV products obtained from satellite instruments such as SCHIAMACHY (SCanning Imaging Absorption SpectroMeter for Atmospheric CHartographY), GOME (Global Ozone Monitoring Experiment), and ATSR (Along-Track Scanning Radiometer). UV-I and UVE used in the study are obtained from SCHIMACHY satellite products. The data are available for selected specific locations on http://www.temis.nl/uvradiation/SCIA/stations_uv.html. UV-I is a measure of UV risk to human health. The clear-sky UV-I is the effective UV irradiance (1 unit equals 25 mWm^{-2}) reaching the Earth's surface. The clear-sky UV-I is based on the CIE action spectrum for the susceptibility of the Caucasian skin to sunburn (erythemal) and it is valid for cloud-free conditions. The convention regarding UV-I is that, index values between 1 and 2 (minimal), between 3 and 4 (low), 5 and 6 (moderate), 7 and 9 (high) and above 10 (very high or extreme), which may be vulnerable to sensitive skin [9, 16]. UV erythemal dose (UVE) represents the UV irradiance weighted to represent the incoming UV radiation affecting human skin. It is the integration of the erythemal UV-I from sunrise to sunset, with a time step of 10 minutes. The integration takes cloud cover into account and hence estimates the daily erythemal UV dose, the total amount of UV radiation absorbed by human skin during the day, and is expressed in KJm^{-2}. Aerosol concentration is generally represented by aerosol optical depth (AOD) [17]. We used AOD at 550 nm obtained from MODIS level-3 products at a resolution of $1^\circ \times 1^\circ$ over the study regions for this analysis.

There are several methods suggested in the literature to estimate radiative forcing [18–23]. To estimate the UV radiative forcing and hence forcing efficiency, we used the differential method suggested by [21]. In this method, the day with lowest AOD (highest UVE) is selected as a clear-sky day (no aerosol condition). The UV radiative forcing (UVRF) is estimated for each day using the equation as suggested in [24]:

$$\text{UVRF} = [F\downarrow - F\uparrow]_{\text{UVEeachday}} - [F\downarrow - F\uparrow]_{\text{UVEclearday}}, \quad (1)$$

where downward fluxes were obtained from TEMIS archived UVE irradiances. Upward fluxes were derived as product of average albedo in UV region (0.07) [25, 26] and downward UV erythemal radiation. The downward flux during day with minimum AOD (maximum UVE) was chosen as "clear-sky day" and upward fluxes for clear-sky day also were derived using albedo as explained above. The difference is calculated to obtain radiative forcing for each day as shown in the equation. In a month, we used only days whose AOD observations lie in condition suggested by [27] that is, AOD values falling within mean AOD $\pm 3\sigma$ condition. The UVE also was considered only for the corresponding days.

Since radiative forcing estimates in each day differ according to AOD conditions, it is standardized by estimating forcing efficiency (F_{eff}), defined as radiative forcing per unit increase in AOD [19, 21]. Generally F_{eff} is estimated by regressing between daily radiative forcing and daily mean AOD. However this method may not provide a representative value of surface forcing because of the day-to-day variation in the aerosol absorbing characteristics and scattering direction changes [21]. Hence we used the ratio method suggested by [19] by taking ratio of daily mean radiative forcing and AOD, to estimate forcing efficiency from radiative forcing over the four experimental locations.

3. Results and Discussions

3.1. Variations of UV Erythemal Dose, UV-Index, and AOD. Figure 1 shows the monthly variation of UV erythemal dose and UV-I over different metro cities in India. UVE dose and UV-I were found to be high during June over all the four sites. The reason for this high UV irradiance could be associated with the lower solar elevation during summer periods. The minimum values of UV-I and UVE were observed during December-January. This also could be mainly associated with high solar elevation angles of irradiance during winter compared to other factors such as cloud cover or ozone concentration variation [3]. The highest value of UVE was found to be up to 6.85 KJm^{-2} during June 2004 (over Mumbai). It steadily decreased and reached its minimum during December. The erythemal dose showed a steady increase from January 2005 and was found to reach a value of 6.7 KJm^{-2} (over Mumbai) during the month of May in 2005. The seasonal mean UVE was found to be 5.95 to 6.4 KJm^{-2} during monsoon months over the four locations. The seasonal mean UV erythemal dose values ranged between 2.86 and 4.36 KJm^{-2}, 2.04 and 4.45 KJm^{-2}, and 5.11 and 6.26 KJm^{-2}, respectively, during post-monsoon, winter and premonsoon over different locations (Table 1). In all seasons, Chennai showed higher UV

Table 1: Variation of UV erythemal dose, UV-aerosol forcing efficiency, and percentage of UVE reduction over Chennai, Mumbai, Kolkata, and Delhi.

Station	UV erythemal dose (KJm^{-2})			F_{eff} (KJm^{-2} AOD^{-1})			UVE reduction in %		
	Postmonsoon 04	Winter 04-05	Premonsoon 05	Postmonsoon 04	Winter 04-05	Premonsoon 05	Postmonsoon 04	Winter 04-05	Premonsoon 05
Chennai	4.36 ± 0.34	4.45 ± 0.77	6.19 ± 0.06	−2.06 ± 0.44	−1.31 ± 0.34	−2.07 ± 0.33	47.1	30	33.5
Mumbai	4.08 ± 0.58	3.82 ± 0.71	6.26 ± 0.54	−1.67 ± 0.23	−1.56 ± 0.32	−1.93 ± 0.23	41	41	31
Delhi	2.86 ± 0.39	2.04 ± 0.51	5.11 ± 0.99	−1.38 ± 0.33	−1.21 ± 0.34	−1.78 ± 0.3	48.3	60	35
Kolkata	3.72 ± 0.14	3.06 ± 0.67	5.48 ± 0.77	−1.86 ± 0.33	−1.71 ± 0.34	−3.01 ± 0.28	50.3	55.8	54.9

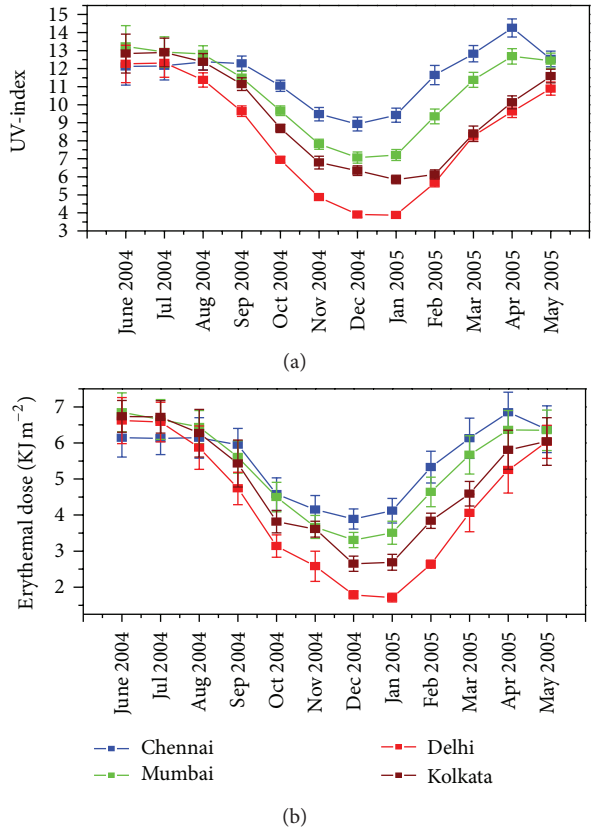

Figure 1: Monthly variation of (a) UV-index and (b) UV erythemal dose irradiance over Chennai, Mumbai, Kolkata, and Delhi.

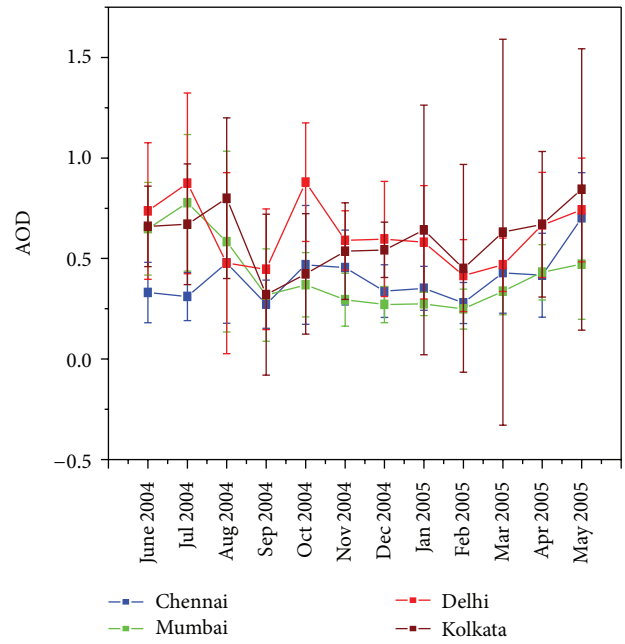

Figure 2: Monthly variation of AOD over Chennai, Mumbai, Kolkata, and Delhi.

erythemal values (except during winter) and Delhi showed lower values. This implies that solar inclination is the major factor for variation of UVE in various selected locations.

UV-I also followed the same pattern as of UV erythemal dose (Figure 1). UV-I was found to be in extreme range (greater than 10) in premonsoon (March–May) and in early monsoon months (June, July). It steadily decreased and was found to be in high range (7–9) during postmonsoon (October and November) (except over Delhi). The UV-I was found to be lowest in December. The UV-I over Delhi was found to be in moderate to low range in postmonsoon and winter (December–February) months. However it still pertained in moderate to high range over the other three locations, indicating high UV risk throughout the year.

The variation of aerosol loading represented by AOD is shown in Figure 2. AOD showed higher values in the months of June and July and then showed a sharp decrease in August and September over all the four locations. It is expected to have lower AOD in monsoon due to rain and washout. However, 2004 was a below-normal monsoon year [28] and rains intensified in August and September over the subcontinent. This could be the major reason for higher aerosol loading in early monsoon months. The AOD showed a substantial increase in postmonsoon seasons. Lower AOD values were observed during winter season (except over Kolkata). High AOD values in premonsoon season are majorly associated with the high convection and associated surface lifting of particles [29–31].

3.2. Aerosol—UV Forcing and UV Reduction. Aerosol UV radiative forcing and forcing efficiency were calculated as explained in Section 2. We confined our forcing calculations to post-monsoon, winter, and premonsoon seasons only, as the AOD in monsoon season could be contaminated due to cloud cover in active monsoon conditions. The estimated radiative forcing efficiency (UV radiative forcing per

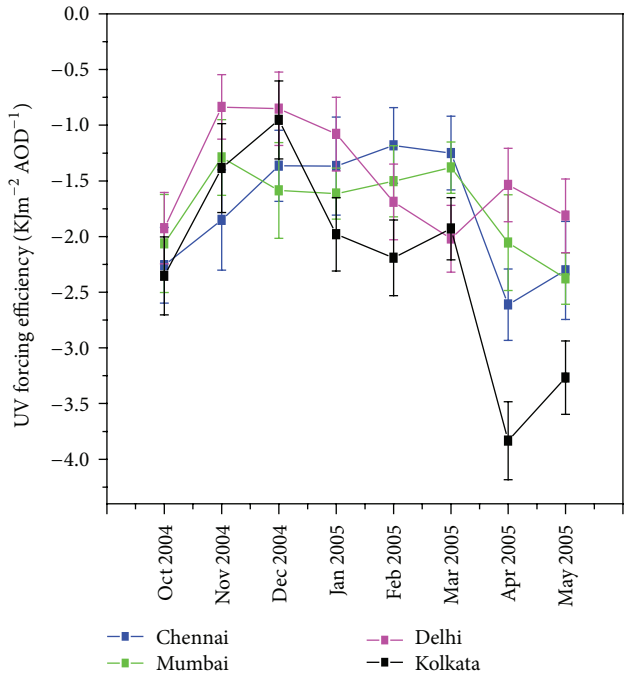

Figure 3: Monthly variation of aerosol-UV forcing efficiency over Chennai, Mumbai, Kolkata, and Delhi.

unit optical depth) is depicted in Figure 3. Monthly mean F_{eff} ranged from −0.75 to −3.9 KJm^{-2} AOD^{-1} on different seasons. Table 1 depicts the total erythemal dose variations and aerosol forcing efficiency values in different seasons. The forcing efficiency was found to be varying proportional to AOD. The F_{eff} over Chennai was up to −2.07 ± 0.33 KJm^{-2} AOD^{-1} during premonsoon. The F_{eff} varied between −1.56 and −1.93 KJm^{-2} AOD^{-1} over Mumbai, −1.21 and −1.78 KJm^{-2} AOD^{-1} over Delhi, and −1.71 and −3.01 KJm^{-2} AOD^{-1} over Kolkata. It can be seen from Table 1 that the total UV erythemal dose over Chennai during postmonsoon was 4.36 ± 0.34 KJm^{-2}, and it can be observed that F_{eff} was −2.06 KJm^{-2} AOD^{-1}. This implies that a unit increase in AOD is able to reduce the UV erythemal dose rate by 47.1%. The lower reduction in UV erythemal in winter over Chennai (30%) is associated with lower AOD observed during the season. Over Mumbai, it can be seen that unit increase in AOD can reduce the UV erythemal dose rate by 31 to 41% during different seasons proportional to aerosol loading. The UV reduction was found to be highest over Delhi during postmonsoon (60%). It varied between 35 and 60% over Delhi on different seasons. The aerosol-induced UV reduction was 50.3 to 55.8% over Kolkata during different seasons. The results obtained here are in accordance with the earlier findings. Reference [32] suggested that aerosols can reduce UV radiation with more than 50% in cloud-free conditions. Reference [33] found a reduction of UV by 40–50% caused by smoke aerosols. Reference [9], using a hybrid method, has reported a UV reduction of 40–56% over another Indian city, Pune, during 2004-2005. Reference [3] found a reduction of 40–50% in UV-B on biomass burning days and a reduction of UV-B by 35–40% on dusty days over Hyderabad, another urban location in India.

4. Conclusions

(1) Tropospheric Emission Monitoring Internet Service (TEMIS) archived UV-index, UV daily erythemal dose obtained from SCIAMACHY satellite, and AOD from MODIS satellite were used to study the variation of UV parameters and its aerosol-induced reduction.

(2) The analysis was carried out over four highly urbanized metro cities of India, namely, Chennai, Mumbai, Delhi, and Kolkata.

(3) UV erythemal dose and UV-index were found to be high during June over all the sites and were found to be minimum in December-January. The reason for this UV irradiance variation could mainly be associated with the lower solar elevation during summer periods than other factors such as aerosol, cloud cover, or albedo.

(4) Over the four locations, UV-Index was found to be in extreme range (greater than 10) in premonsoon (March–May) and in early monsoon months (June, July). It steadily decreased and was found to be in high range (7–9) during postmonsoon (October, November) (except over Delhi).

(5) The aerosol UV radiative forcing and forcing efficiency (forcing per unit AOD) were estimated using differential method that is, utilizing observed fluxes and minimum AOD conditions.

(6) The average aerosol forcing efficiency was found to be varying from −1.38 to −3.01 KJm^{-2} AOD^{-1} on different seasons.

(7) Our study suggests that aerosols can reduce the incoming UV radiation dose by 30–60% during different seasons.

Conflict of Interests

The authors declare that there is no conflict of interests regarding the publication of this paper.

Acknowledgments

The authors acknowledge Professor B. N. Goswami, Director IITM, for encouragements. IITM is funded by the Ministry of Earth Sciences, Government of India. This work is supported by the National Research Foundation of Korea (NRF) through a Grant provided by the Korean Ministry of Education, Science & Technology (MEST) 2013 (no. 200603874).

References

[1] R. L. McKenzie, P. J. Aucamp, A. F. Bais, L. O. Björn, and M. Ilyas, "Changes in biologically-active ultraviolet radiation reaching the Earth's surface," *Photochemical and Photobiological Sciences*, vol. 6, no. 3, pp. 218–231, 2007.

[2] P. M. Udelhofen, P. Gies, C. Roy, and W. J. Randel, "Surface UV radiation over Australia, 1979–1992: effects of ozone and cloud cover changes on variations of UV radiation," *Journal of Geophysical Research D*, vol. 104, no. 16, pp. 19135–19159, 1999.

[3] K. V. S. Badarinath, S. K. Kharol, V. Krishna Prasad et al., "Influence of natural and anthropogenic activities on UV Index variations—a study over tropical urban region using ground based observations and satellite data," *Journal of Atmospheric Chemistry*, vol. 59, no. 3, pp. 219–236, 2008.

[4] E. Koubek, "The absorption of UV light by ozone," *Journal of Chemical Education*, vol. 66, no. 4, p. 338, 1989.

[5] J. S. Schafer, V. K. Saxena, B. N. Wenny, W. Barnard, and J. J. de Luisi, "Observed influence of clouds on ultraviolet-B radiation," *Geophysical Research Letters*, vol. 23, no. 19, pp. 2625–2628, 1996.

[6] I. Foyo-Moreno, I. Alados, F. J. Olmo, and L. Alados-Arboledas, "The influence of cloudiness on UV global irradiance (295–385 nm)," *Agricultural and Forest Meteorology*, vol. 120, no. 1–4, pp. 101–111, 2003.

[7] M. K. Srivastava, S. Singh, A. Saha et al., "Direct solar ultraviolet irradiance over Nainital, India, in the central Himalayas for clear-sky day conditions during December 2004," *Journal of Geophysical Research D*, vol. 111, no. 8, Article ID D08201, 2006.

[8] K. V. S. Badarinath, S. K. Kharol, T. R. K. Chand, and K. M. Latha, "Characterization of aerosol optical depth, aerosol mass concentration, UV irradiance and black carbon aerosols over Indo-Gangetic plains, India, during fog period," *Meteorology and Atmospheric Physics*, vol. 111, no. 1, pp. 65–73, 2011.

[9] A. S. Panicker, G. Pandithurai, T. Takamura, and R. T. Pinker, "Aerosol effects in the UV-B spectral region over Pune, an urban site in India," *Geophysical Research Letters*, vol. 36, no. 10, p. L10802, 2009.

[10] N. D. Ganguly and K. N. Iyer, "Long-term trend in Ozone and Erythemal UV at Indian latitudes," *Journal of Atmospheric Chemistry*, vol. 55, pp. 227–239, 2006.

[11] R. Bhattacharya, S. Pal, A. Bhoumick, and P. Barman, "Annual variability and distribution of ultraviolet Index over India using temis data," *International Journal of Engineering Science and Technology*, vol. 4, no. 11, p. 4577, 2012.

[12] J. P. Diaz, F. J. Exposito, C. J. Torres, and V. Carreno, "Simulation of mineral dust effects on UV radiation levels," *Journal of Geophysical Research D*, vol. 105, no. 4, pp. 4979–4991, 2000.

[13] S. C. Liu, S. A. McKeen, and S. Madronich, "Effect of anthropogenic aerosols on biologically active ultraviolet radiation," *Geophysical Research Letters*, vol. 18, no. 12, pp. 2265–2268, 1991.

[14] J. E. Frederick, E. K. Koob, A. D. Alberts, and E. C. Weatherhead, "Empirical studies of tropospheric transmission in the ultraviolet: broadband measurements," *Journal of Applied Meteorology and Climatology*, vol. 32, pp. 1883–1892, 1993.

[15] C. Meleti and F. Cappellani, "Measurements of aerosol optical depth at Ispra: analysis of the correlation with UV-B, UV-A, and total solar irradiance," *Journal of Geophysical Research D*, vol. 105, no. 4, pp. 4971–4978, 2000.

[16] J. P. Kinney and C. S. Long, "The ultraviolet index: a useful tool," *Dermatology Online Journal*, vol. 6, no. 1, article 2, 2000.

[17] A. S. Panicker, G. Pandithurai, P. D. Safai, S. Dipu, and D.-I. Lee, "On the contribution of black carbon to the composite aerosol radiative forcing over an urban environment," *Atmospheric Environment*, vol. 44, no. 25, pp. 3066–3070, 2010.

[18] A. Jayaraman, D. Lubin, S. Ramachandran et al., "Direct observations of aerosol radiative forcing over the tropical Indian Ocean during the January-February 1996 pre-INDOEX cruise," *Journal of Geophysical Research D*, vol. 103, no. 12, pp. 13827–13836, 1998.

[19] G. Pandithurai, R. T. Pinker, T. Takamura, and P. C. S. Devara, "Aerosol radiative forcing over a tropical urban site in India," *Geophysical Research Letters*, vol. 31, no. 12, Article ID L12107, 4 pages, 2004.

[20] G. Pandithurai, S. Dipu, K. K. Dani et al., "Aerosol radiative forcing during dust events over New Delhi, India," *Journal of Geophysical Research D*, vol. 113, no. 13, Article ID D13209, 2008.

[21] W. C. Conant, "An observational approach for determining aerosol surface radiative forcing: results from the first field phase of INDOEX," *Journal of Geophysical Research D*, vol. 105, no. 12, pp. 15347–15360, 2000.

[22] A. K. Srivastava, K. Ram, P. Pant, P. Hegde, and H. Joshi, "Black carbon aerosols over Manora Peak in the Indian Himalayan foothills: implications for climate forcing," *Environmental Research Letters*, vol. 7, no. 1, Article ID 014002, 8 pages, 2012.

[23] A. K. Srivastava, S. Tiwari, P. C. S. Devara et al., "Pre-monsoon aerosol characteristics over the Indo-Gangetic Basin: implications to climatic impact," *Annales Geophysicae*, vol. 29, no. 5, pp. 789–804, 2011.

[24] A. S. Panicker, G. Pandithurai, P. D. Safai, and S. Kewat, "Observations of enhanced aerosol longwave radiative forcing over an urban environment," *Geophysical Research Letters*, vol. 35, no. 4, Article ID L04817, 2008.

[25] R. Chadyšien and A. Girgždys, "Ultraviolet radiation albedo of natural surfaces," *Journal of Environmental Engineering and Landscape Management*, vol. 16, no. 2, pp. 83–88, 2008.

[26] U. Feisterand and R. Grew, "Spectral albedo measurements in the UV and visible region over different types of surfaces," *Photochemistry and Photobiology*, vol. 62, no. 4, pp. 736–744, 1995.

[27] S. Ramachandran, R. Rengarajan, A. Jayaraman, M. M. Sarin, and S. K. Das, "Aerosol radiative forcing during clear, hazy, and foggy conditions over a continental polluted location in north India," *Journal of Geophysical Research D*, vol. 111, no. 20, Article ID D20214, 2006.

[28] A. S. Panicker, G. Pandithurai, and S. Dipu, "Aerosol indirect effect during successive contrasting monsoon seasons over Indian sub continent: using MODIS data," *Atmospheric Environment*, vol. 44, no. 15, pp. 1937–1943, 2010.

[29] A. S. Panicker, D. I. Lee, Y. V. Kumkar, D. Kim, M. Maki, and H. Uyeda, "Decadal climatological trends of aerosol optical parameters over three different environments in South Korea," *International Journal of Climatology*, vol. 33, no. 8, pp. 1909–1916, 2013.

[30] A. S. Panicker, S.-H. Park, D.-I. Lee et al., "Observations of black carbon characteristics and radiative forcing over a global atmosphere watch supersite in Korea," *Atmospheric Environment*, vol. 77, pp. 98–104, 2013.

[31] S.-H. Park, A. S. Panicker, D.-I. Lee et al., "Characterization of chemical properties of atmospheric aerosols over anmyeon (South Korea), a super site under global atmosphere watch," *Journal of Atmospheric Chemistry*, vol. 67, no. 2-3, pp. 71–86, 2010.

[32] N. A. Krotkov, P. K. Bhartia, J. R. Herman, V. Fioletov, and J. Kerr, "Satellite estimation of spectral surface UV irradiance in the presence of tropospheric aerosols 1. Cloud-free case," *Journal of Geophysical Research D*, vol. 103, no. 8, pp. 8779–8793, 1998.

[33] O. V. Kalashnikova, F. P. Mills, A. Eldering, and D. Anderson, "Application of satellite and ground-based data to investigate the UV radiative effects of Australian aerosols," *Remote Sensing of Environment*, vol. 107, no. 1-2, pp. 65–80, 2007.

Hindawi Publishing Corporation
Advances in Meteorology
Volume 2013, Article ID 976813, 8 pages
http://dx.doi.org/10.1155/2013/976813

Research Article

Estimates of Aerosol Indirect Effect from Terra MODIS over Republic of Korea

Woon-Seon Jung,[1] A. S. Panicker,[2] Dong-In Lee,[1] and Sung-Hwa Park[3]

[1] *Department of Environmental Atmospheric Sciences, Pukyong National University, 599-1 Daeyeon-dong, Nam-gu, Busan 608-737, Republic of Korea*
[2] *Indian Institute of Tropical Meteorology, Pune 411-008, India*
[3] *Atmospheric Environmental Research Institute, Pukyong National University, 599-1 Daeyeon-dong, Nam-gu, Busan 608-737, Republic of Korea*

Correspondence should be addressed to Dong-In Lee; leedi@pknu.ac.kr

Received 13 September 2013; Revised 4 November 2013; Accepted 5 November 2013

Academic Editor: Samir Pokhrel

Moderate resolution imaging spectroradiometer (MODIS) data have been analyzed over four different regions (Yellow sea, Korean inland, East Sea, and South Sea) in Republic of Korea to investigate the seasonal variability of aerosol-cloud properties and aerosol indirect effect during the past decade (2000–2009). Aerosol optical depth (AOD) was found to be consistently high during spring. Cloud ice radius (CIR) also showed higher values during spring, while an enhancement in cloud water radius (CWR) and fine mode fraction (FMF) was observed during summer. AOD and aerosol index (AI) were found to be higher during January to June. However, FMF and CWR showed enhancement during July to December. Aerosol indirect effect (AIE) in each year has been estimated and found to be showing positive and negative indirect effects. The AIE for fixed cloud ice path (CIP) showed positive indirect effect (Twomey effect) over Yellow sea, while the AIE for fixed cloud water path (CWP) showed a major negative indirect effect (anti-Twomey effect) over all regions. During Changma (summer monsoon) period, the AIE for both CIP and CWP showed dominant anti-Twomey effect in middle and low level clouds, indicating the growth of cloud droplet radius with changes in aerosols, enhancing the precipitation.

1. Introduction

Aerosols are known to impact the formation and the life cycle of clouds by acting as cloud condensation nuclei (CCN) or ice nuclei (IN). A wide range of measurements shows that anthropogenic aerosols induce changes in clouds and their optical properties. These changes are popularly known as aerosol indirect effect (AIE) [1–3]. It is important to understand and quantify the microphysical impact of both natural and anthropogenic aerosols on clouds, in order to understand and predict climate change. The main identified AIEs include the cloud albedo effect [4] and cloud life time effect [5]. The "Twomey effect" (positive indirect effect) refers to a decrease in a cloud effective radius with increasing aerosol content for a fixed liquid water path. Contrary to this effect, an increase in the cloud droplet size with the aerosol load, or an "anti-Twomey effect" (negative indirect effect), was also reported in some parts of the world for certain environmental conditions [6]. It has also been reported that the AIE could be an important factor in modulating the response of large scale systems such as monsoons [7–9]. However, studies on AIE and its influence on precipitation are sparse across the world [10–12].

Aerosols in Asian regions are known to be an important factor in modulating different weather phenomenon. Korean peninsula is surrounded by oceanic areas on its three territories. Hence aerosol-cloud properties have been analyzed over three oceanic and the continental region over Republic of Korea. Aerosols in wet environment have a great significance in the development of clouds and precipitation. Especially, heavy rainfalls in East Asian monsoon region are related to Changma/Baiu/Meiyu frontal system [13] and interaction

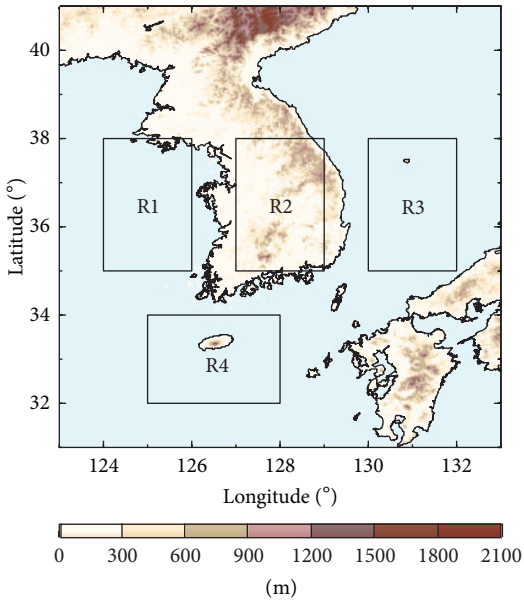

Figure 1: Topographic map of Republic of Korea with selected regions from R1 to R4.

between aerosol and clouds in monsoon is a main important factor [14]. Summer monsoon in Korea is characterized with humid, moist environment [13] and hence aerosol indirect effect could be different as compared with dry period. Clouds in East Asian monsoon region also show different structures and components according to the cloud levels or height [15]. Especially, cloud height and type are shown to be as important as cloud cover in modifying the radiation field of the earth-atmosphere system [16].

In this study, we investigate the seasonal and monthly variability of aerosol-cloud properties and associated indirect effect using Terra moderate resolution imaging spectroradiometer (MODIS) satellite data for four different regions in Korean peninsula. Also the AIE has been exclusively estimated during summer monsoon (Changma) period in different cloud types to find the possible role of AIE in modulating precipitation.

2. Data and Methodology

Oceans exert a strong influence on precipitation development over Korea. The aerosol-cloud properties and their variations were investigated over three oceanic and one continental regions in Korea. The selected regions include Yellow sea (R1, 124°–126°E & 35°–38°N), Korean inland (R2, 127°–129°E & 35°–38°N), East sea (R3, 130°–132°E & 35°–38°N), and South sea (R4, 125°–128°E & 32°–34°N) (Figure 1).

In this study, we used MODIS level 3 daily data sets of aerosol optical depth (AOD), fine mode fraction (FMF), cloud ice radius (CIR), cloud water radius (CWR), cloud ice path (CIP), cloud water path (CWP), Angstrom exponent (ANG), and cloud top pressure (CTP) over Korean peninsula for a period of 10 years (from 2000 to 2009). We also used total ozone mapping spectrometer (TOMS) level 3 daily data sets of aerosol index (AI) over Korean peninsula for 5 years (from 2000 to 2004) and ozone monitoring instrument (OMI) for 5 years (from 2005 to 2009) because of absence of satellite data. The daily data have been averaged to find monthly variations during different seasons namely, spring (March–May), summer (June–August), autumn (September–November), and winter (December–February).

For AIE estimation, each of the selected regions was further subdivided into grids of 1° × 1° and analyses were performed for each grid. The MODIS 1° × 1° derived daily CWP and CIP have been divided into 14 different bins, ranging between 1 and 350 at an interval of 25. The indirect effect for each bin has been calculated using the below expression as explained in [17], that is,

$$\mathrm{AIE} = -\frac{d \ln r_e}{d \ln \tau_\alpha}, \tag{1}$$

where τ_α is aerosol optical depth and r_e is the cloud effective radius (r_e: cloud ice radius for fixed CIP and cloud water radius for fixed CWP). Simple linear regression has been performed between AOD and CIR (for fixed CIP bins) and AOD and CWR (for fixed CWP bins) to estimate the AIE for cloud water and cloud ice radii, respectively.

In addition, back-trajectories were analysed to determine the pathways and origins of aerosol to Korea using hybrid single-particle Lagrangian integrated trajectory (HYSPLIT) from air resources laboratory (ARL). Vertical motion calculation method was isobaric and meteorological data were obtained from national centers for environmental prediction (NCEP), global data assimilation system (GDAS). Back-trajectories were generated for 120 hours back in time from central point in each region.

3. Results and Discussion

3.1. Seasonal Variability of Aerosol Cloud Properties. Regional and monthly variations of aerosol-cloud parameters have been analyzed over the period 2000–2009 and are depicted in Figures 2 and 3. It is found that the aerosol parameters show significant variability, which in turn influences the cloud properties. The AOD, indicating the aerosol loading, [18] is found to have the highest average value (0.45) over R1 compared to other regions (Figure 2(a)). The long-range transport of aerosols from adjacent deserts in Mongolia and China [19–21] could be the main reason for this higher aerosol loading over R1. The AOD values were found to be higher during the period from January to June and were found to have consistently lower values from July to December in all regions. The AOD values were found to be consistently high during spring season (March–May). The average AI (Figure 2(b)), an indicator of absorbing aerosol concentration, also showed higher value (0.77) over R1 compared to other regions. Furthermore, the trend of AI was similar to that of AOD, suggesting the long range transport of more absorbing aerosols from adjacent deserts in Mongolia and China over the January–May period (Figure 4). The AI had a consistently high value from March to June in all regions for every year, except in 2009. R2 showed high

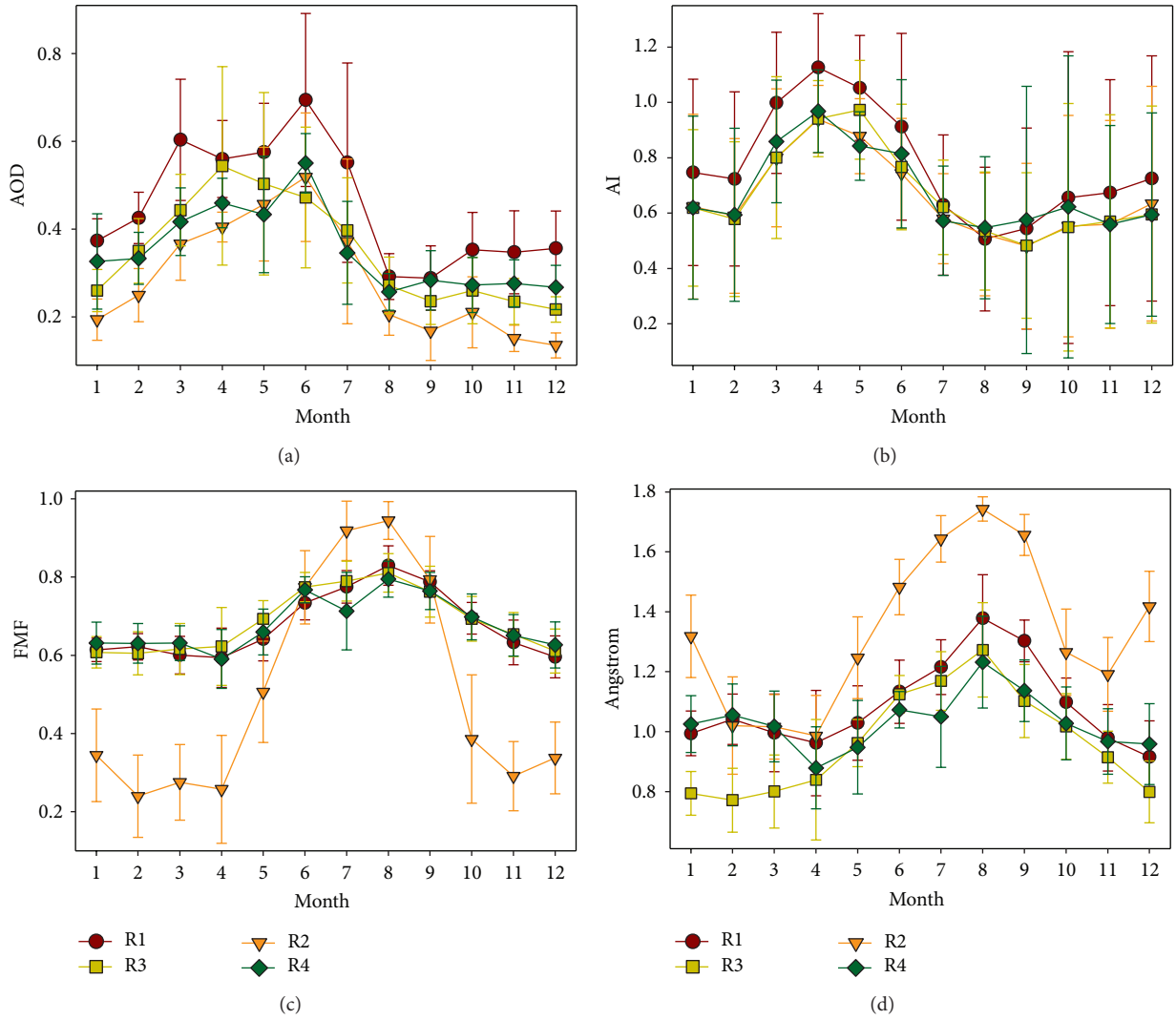

Figure 2: Monthly variability of (a) AOD, (b) AI (c) FMF and (d) Angstrom in R1 (red circle), R2 (orange inverted triangle), R3 (yellow square), and R4 (green diamond).

fluctuations in FMF variations compared to other regions (Figure 2(c)). In summer, FMF values were found to be high over R2 compared with oceanic area and it could be because of transported air pollutants from urban areas and strong convection current. In other seasons, FMF showed relatively low value over R2 compared with ocean and it could be due to stable condition of atmosphere. It was conjectured that R2 indicated the characteristics of inland area. All oceanic areas showed a higher average value of FMF compared to Korean inland (except during summer season). This indicates an abundance of sea salt accumulation mode aerosols over oceans, which have the highest probability of acting as CCN [22]. FMF values were found to be high during summer for all regions in all the years. The climatological mean of ANG, which indicates the size distribution of aerosols, is shown in Figure 2(d). ANG is found to be lower during spring season over all the regions (except over R2). Lower values of angstrom exponent indicate the dominance of larger coarse mode particles. Reference [20] has shown that there is a significant reduction in ANG over Korean region in past decade. Hence lower Angstrom exponent over all three regions affirms the influx of transported coarse mode dust aerosols from adjacent arid regions of Mongolia and China. The reason for higher AOD over R1 region compared to R2, in spite of having similar sources of transport, could be associated with the abundance of sea salt aerosols over R1 region, which further grows due to its hygroscopic nature [23]. Along with this, the significant reduction in aerosol concentration in past decade due to controlled anthropogenic activities over Korean inland [20] could be another reason for lower AOD over R2.

The average CIR was also higher (25.9 μm) over the R1 region (Figure 3(a)), compared to all other regions, indicating strong ice nucleation. This CIR enhancement could be associated with increase in transported dust particles from arid regions, which are reported as ideal cloud ice nuclei [11, 24, 25]. High concentrations of dust particles acting as ice nuclei in clouds could lead to changes in a cloud's microphysical

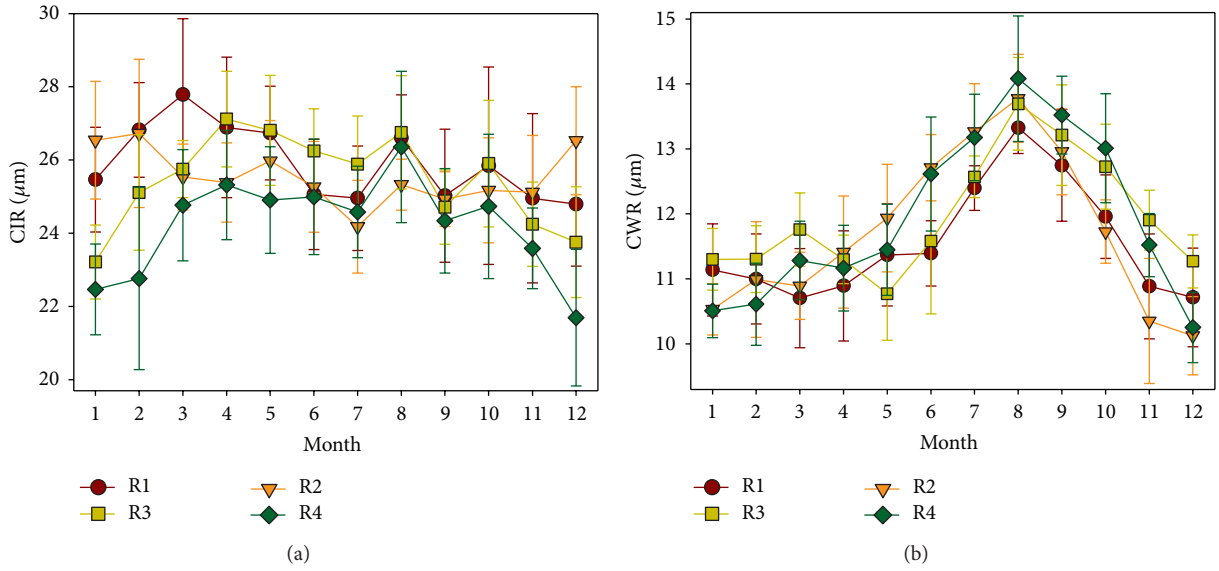

Figure 3: Same as Figure 2 but for (a) CIR and (b) CWR.

and radiative properties. Dust sources are mostly the deserts, dry lake beds, and agricultural areas with soil disturbance. Analogous to the FMF, the CWR consistently had higher values during the summer months for all years (Figure 3(b)). This could be associated with the changes in wind patterns during the Changma period (summer monsoon), bringing sea salt aerosol CCN to land and hence increasing the CWR (Figure 4(b)). R2 showed high fluctuations in FMF variations compared to other regions. It had a value of almost one during summer. It is assumed that there were transport of air pollutants and strong convection current over R2 region. The similarity in FMF and CWR trends indicates larger cloud water droplet nucleation due to sea salt fractions [26, 27]. On the other hand, FMF and CWR showed lower values during winter (December–February) (Figures 2 and 3), characterized with higher atmospheric stability as compared with summer. Additionally, cloud water nuclei were more dominant in winter than ice nuclei.

A climatological mean back trajectory image for different selected regions in different seasons is shown in Figures 4(a)–4(d). The simulations of HYSPLIT have shown that the long range transports of dust aerosols from continent of China are the major responsible component for this aerosol enhancement. The main path of air mass with aerosols transported over a long-range begins from the Taklamakan Desert through the Gobi Desert and Shandong Peninsula, and ends in the central region of the Korean peninsula (except during summer).

3.2. Aerosol Indirect Effect Estimates. The AIE which is the principal source of uncertainties in climate predictions [28] has been estimated for both CIP (Figure 5(a)) and CWP bins (Figure 5(b)) for each season from 2000 to 2009 as explained in Section 2. The climatological mean AIE values during 2000–2009 for fixed CIP and CWP bins in different seasons are shown in Figure 5. The AIE of ice droplets during different seasons showed Twomey (positive indirect effect) and anti-Twomey (negative indirect effect) effects (Figure 5(a)). R1 in spring showed a climatologically dominant Twomey effect and had a positive value of 0.09. This is related to an increase in aerosol particles from dry areas, forming clouds with more droplets and less precipitation efficiency, which in turn leads to high reflection of solar radiation. Oceanic regions in summer also showed dominant Twomey effect. It may be associated with an increase in the cloud amount. R2 showed a dominant anti-Twomey effect in summer and was found to have an average negative indirect effect value of −0.04. This could be related to the growth of cloud droplets and increased precipitation during the Changma period (summer monsoon). All regions except R2 showed an anti-Twomey effect in autumn. The AIE of cloud water droplets in each season generally had a negative value and showed an anti-Twomey effect (Figure 5(b)). This could be associated with an increase in water droplet nucleation, which would result from the high transport of sea salt aerosols from the oceans, subsequently working as efficient CCN. Sea salt can act as giant CCN (GCCN) which trigger early onset of precipitation [26]. R1 in spring showed a Twomey effect and had a positive AIE value of 0.02. This is related to an increase in aerosol particles transported from dry areas, resulting in high reflection and increased cloud lifetime.

Especially in Changma (summer monsoon in June-July) period, there persists strong moist environment. Hence aerosol indirect effect could be different as compared to dry period. Cloud in this Asian monsoon region also shows different structures and components according to the cloud levels or height. Especially, cloud height and type are shown to be as important as cloud cover in modifying the radiation field of the earth-atmosphere system [16].

Hence the climatological mean AIE during Changma period is investigated during 2000 to 2009 by considering the cloud level height. The cloud levels have been divided into

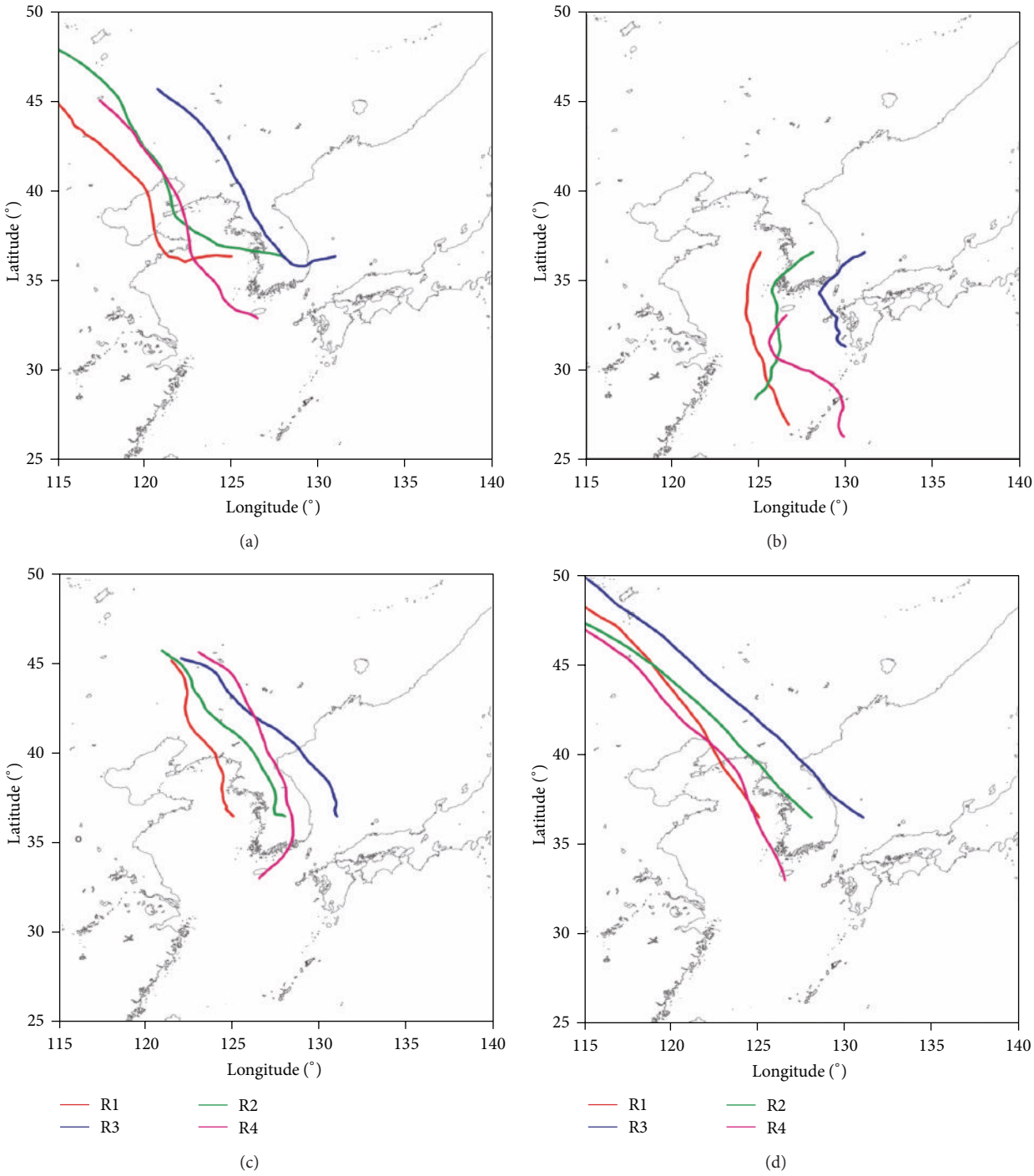

Figure 4: Climatological mean back-trajectories of the air mass arrived over R1 (red), R2 (green), R3 (blue), and R4 (pink) in (a) spring, (b) summer, (c) autumn, and (d) winter.

three intervals of cloud top pressure (high cloud, Pc ≥ 440 mb; middle cloud, 440 mb < Pc ≤ 680 mb; and low cloud, Pc > 680 mb) [29]. The AIE has been estimated for both CIP and CWP bins during Changma period in each region for all three types of cloud during 2000 to 2009 and hence climatological mean value is computed (Figure 6). Since low clouds do not contain ice droplets, AIE for ice droplets has been estimated only for high and middle clouds (Figure 6(a)). The AIE for ice droplets in each cloud level also showed a dominant anti-Twomey effect (negative indirect effect), indicating the increase in cloud drop size with enhanced aerosols. Middle clouds also showed a strong anti-Twomey effect (except over R3). However, high cloud in R1 showed a Twomey effect and had a positive value of 0.01. This could be associated

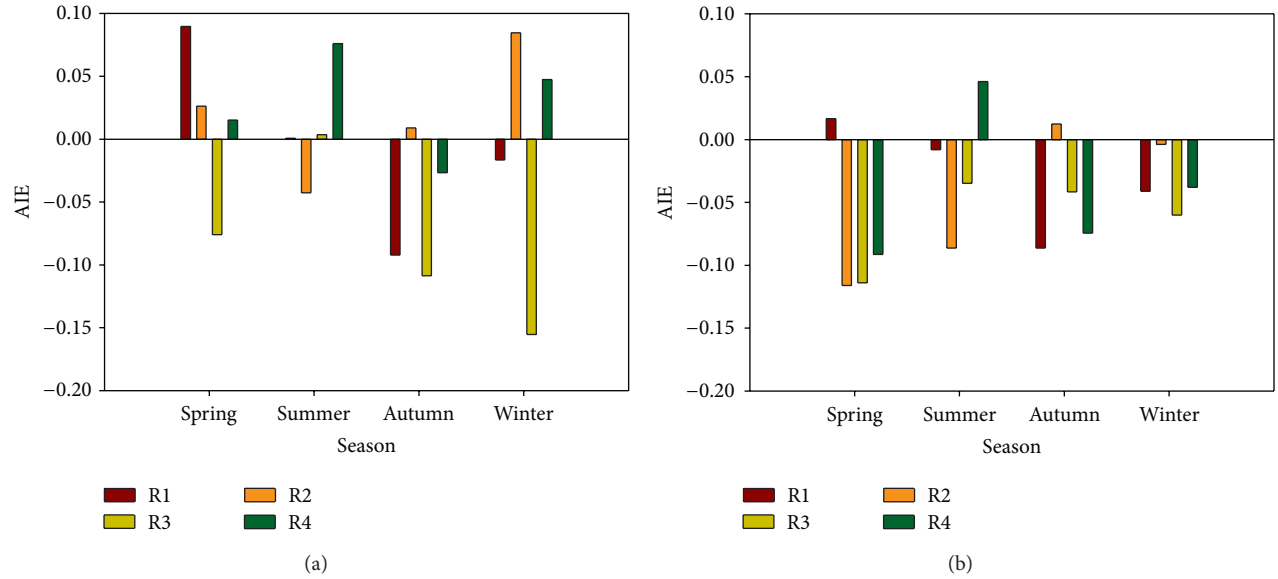

Figure 5: Seasonal climatological mean of aerosol indirect effect of (a) ice and (b) water particle in R1 (red), R2 (orange), R3 (yellow), and R4 (green).

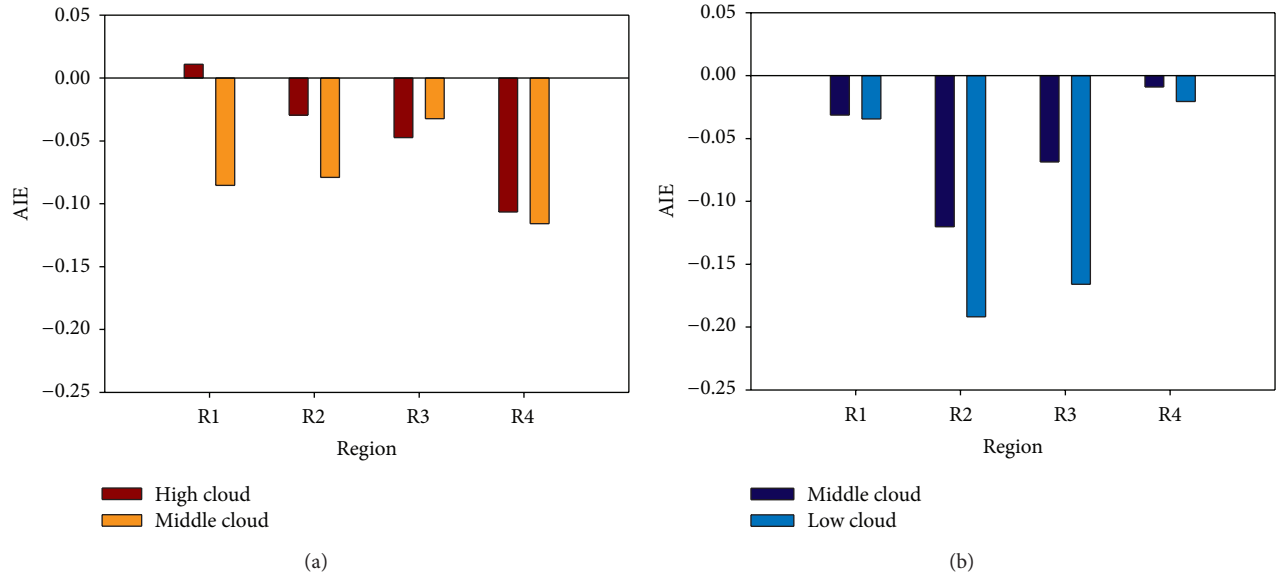

Figure 6: Regional climatological mean aerosol indirect effect during Changma period for (a) ice in high (red) and middle cloud (orange) and (b) water particle in middle (blue) and low cloud (sky blue).

with high reflection at the cloud top. The AIE for CWP bins has been estimated for middle and low clouds, since high cloud has fewer amounts of water drops compared to ice pellets (Figure 6(b)). In particular, low clouds in each region showed a strong anti-Twomey effect and it could be associated with the development of precipitation in comparison with middle cloud. The enhanced anti-Twomey effect could be attributed to enhanced moisture content available to individual hygroscopic aerosols, increasing cloud drop growth, resulting in precipitation. The R2 region showed a strong anti-Twomey effect in middle (−0.12) and low clouds (−0.19). This clearly indicates that the development of precipitation during Changma is influenced by an anti-Twomey effect over Korean inland. The differences in AIE during entire summer and exclusively during Changma period could be due to the fact that Korean summer consists of dry clear sky periods and wet Changma periods. The AIE for ice droplets (for fixed CIP bins) during Changma period also showed a dominant anti-Twomey effect. In particular, the AIE value at low clouds showed a strong anti-Twomey effect, indicating

higher probability of precipitation development compared to middle clouds. Finally, the AIE during the Changma period could be considered as a clear indicator for precipitation predictions.

Several studies report AIE estimates over different parts of the world. The AIE values reported in this study are in agreement with those reported in earlier studies. It reported indirect effect values of 0.07 to 0.11 on different experimental days using ground based method over Oklahoma [17]. It also obtained similar AIE values using ground based observations [30]. AIE value is reported between 0.13 and 0.19 in Alaska region [31]. It also found AIE values of 0.03 to 0.71 over East China Sea region [2]. Even though positive AIE values have been majorly reported, few studies report negative indirect values in certain environmental conditions [6, 24]. AIE was studied on two contrasting monsoon seasons over Indian region [10]. It is found that the AIE values were positive during bad monsoon years and were negative during good monsoon years. The negative indirect values ranged between −0.007 and −0.22 over different regions in good monsoon conditions, indicating the increase in cloud effective radii with changes in aerosol loading and hence inducing precipitation. However the positive indirect effect values were found to be ranging between 0.15 to 0.37 in bad monsoon condition, which reduces the cloud effective radii and precipitation.

4. Summary and Conclusions

This study presents the seasonal variability of aerosols and cloud properties by using Terra MODIS satellite data for four different regions in Korean peninsula over 10 years. The selected regions include Yellow sea (R1, 124°–126°E & 35°–38°N), Korean inland (R2, 127°-129°E & 35°-38°N), East sea (R3, 130°–132°E & 35°–38°N), and South sea (R4, 125°–128°E & 32°–34°N). It is found that aerosol parameters show significant seasonal and monthly variability, which in turn influences cloud properties.

The AOD and AI values were found to be higher during January to June for all years. This obviously is associated with the long range transport of aerosols from deserts and continent of China, indicated by small Angstrom exponent values, representing the presence of large dust aerosols. The CIR also showed higher values during spring, while the CWR and FMF showed an increase during summer in all years. This is related to an abundance of accumulation mode aerosols which influence condensation, formation, and enhancement of cloud droplet size. The AOD, CIR, and AI were found to be higher in R1 than other regions. The FMF over R2 is higher in summer as compared with other seasons.

The AIE values for ice droplets in each year were estimated for different seasons and found to have both positive and negative indirect effects. However, the AIE of cloud water droplets in each season generally had a negative value. The AIE during the Changma period at different cloud levels showed a strong anti-Twomey effect, especially in low cloud for water droplets. This portrays that aerosols play an important role in increasing cloud drop size and hence precipitation during Changma period.

Acknowledgments

This research was supported by the National Research Foundation of Korea (NRF) through a Grant provided by the Korean Ministry of Education, Science & Technology (MEST) in 2013 (no. 200603874). MODIS and TOMS/OMI data used in this study were produced with the Giovanni online data system, developed, and maintained by the NASA-GES DISC which is acknowledged with thanks. One of the authors, A. S. Panicker, acknowledges director of IITM, Professor Goswami and Dr. Beig for their encouragements.

References

[1] A. S. Ackerman, O. B. Toon, D. E. Stevens, A. J. Heymsfield, V. Ramanathan, and E. J. Welton, "Reduction of tropical cloudiness by soot," *Science*, vol. 288, no. 5468, pp. 1042–1047, 2000.

[2] G. Pandithurai, T. Takamura, J. Yamaguchi et al., "Aerosol effect on cloud droplet size as monitored from surface-based remote sensing over East China Sea region," *Geophysical Research Letters*, vol. 36, no. 13, Article ID L13805, 2009.

[3] M. G. Manoj, P. C. S. Devara, S. Joseph, and A. K. Sahai, "Aerosol indirect effect during the aberrant Indian Summer Monsoon breaks of 2009," *Atmospheric Environment*, vol. 60, no. 1, pp. 153–163, 2012.

[4] S. Twomey, "The influence of pollution on the shortwave albedo of clouds," *Journal of Atmospheric Sciences*, vol. 34, no. 7, pp. 1149–1152, 1977.

[5] B. A. Albrecht, "Aerosols, cloud microphysics, and fractional cloudiness," *Science*, vol. 245, no. 4923, pp. 1227–1230, 1989.

[6] T. Yuan, Z. Li, R. Zhang, and J. Fan, "Increase of cloud droplet size with aerosol optical depth: an observation and modeling study," *Journal of Geophysical Research D*, vol. 113, no. 4, Article ID D04201, 2008.

[7] P. K. Patra, S. K. Behera, J. R. Herman, S. Maksyutov, H. Akimoto, and T. Yamagata, "The Indian summer monsoon rainfall: interplay of coupled dynamics, radiation and cloud microphysics," *Atmospheric Chemistry and Physics*, vol. 5, no. 8, pp. 2181–2188, 2005.

[8] V. R. Kiran, M. Rajeevan, S. V. B. Rao, and N. P. Rao, "Analysis of variations of cloud and aerosol properties associated with active and break spells of Indian summer monsoon using MODIS data," *Geophysical Research Letters*, vol. 36, no. 9, Article ID L09706, 2009.

[9] R. L. Bhawar and P. C. S. Devara, "Study of successive contrasting monsoons (2001-2002) in terms of aerosol variability over a tropical statio Pune, India," *Atmospheric Chemistry and Physics*, vol. 10, no. 1, pp. 29–37, 2010.

[10] A. S. Panicker, G. Pandithurai, and S. Dipu, "Aerosol indirect effect during successive contrasting monsoon seasons over Indian subcontinent using MODIS data," *Atmospheric Environment*, vol. 44, no. 15, pp. 1937–1943, 2010.

[11] P. Chylek, M. K. Dubey, U. Lohmann et al., "Aerosol indirect effect over the Indian Ocean," *Geophysical Research Letters*, vol. 33, no. 6, Article ID L06806, 2006.

[12] A. K. Srivastava, S. Tiwari, P. C. S. Devara et al., "Pre-monsoon aerosol characteristics over the Indo-Gangetic Basin: implications to climatic impact," *Annales Geophysicae*, vol. 29, no. 5, pp. 789–804, 2011.

[13] J.-H. Jeong, D.-I. Lee, C.-C. Wang, S.-M. Jang, C.-H. You, and M. Jang, "Environment and morphology of mesoscale convective systems associated with the Changma front during 9-10 July 2007," *Annales Geophysicae*, vol. 30, no. 8, pp. 1235–1248, 2012.

[14] A. Jayaraman, "Aerosol radiation cloud interactions over the tropical Indian Ocean prior to the onset of the summer monsoon," *Current Science*, vol. 81, no. 11, pp. 1437–1445, 2001.

[15] E.-K. Seo, "Characteristics of summer rainfall over East Asia as observed by TRMM PR," *Journal of Korean Earth Science Society*, vol. 32, no. 1, pp. 33–45, 2011.

[16] T. Chen, W. B. Rossow, and Y. Zhang, "Radiative effects of cloud-type variations," *Journal of Climate*, vol. 13, no. 1, pp. 264–286, 2000.

[17] G. Feingold, W. L. Eberhard, D. E. Veron, and M. Previdi, "First measurements of the Twomey indirect effect using ground-based remote sensors," *Geophysical Research Letters*, vol. 30, no. 6, p. 1287, 2003.

[18] A. K. Srivastava, K. Ram, P. Pant, P. Hegde, and H. Joshi, "Black carbon aerosols over Manora Peak in the Indian Himalayan foothills: implications for climate forcing," *Environmental Research Letters*, vol. 7, no. 1, Article ID 014002, 2012.

[19] K. O. Ogunjobi, Y. J. Kim, and Z. He, "Aerosol optical properties during Asian dust storm episodes in South Korea," *Theoretical and Applied Climatology*, vol. 76, no. 1-2, pp. 65–75, 2003.

[20] A.-S. Panicker, D.-I. Lee, Y.-V. Kumkar, D. Kim, M. Maki, and H. Uyeda, "Decadal climatological trends of aerosol optical parameters over three different environments in South Korea," *International Journal of Climatology*, vol. 33, no. 8, pp. 1909–1916, 2012.

[21] S.-H. Park, A. S. Panicker, D.-I. Lee et al., "Characterization of chemical properties of atmospheric aerosols over anmyeon (South Korea), a super site under global atmosphere watch," *Journal of Atmospheric Chemistry*, vol. 67, no. 2-3, pp. 71–86, 2010.

[22] G. C. Roberts, M. O. Andreae, J. Zhou, and P. Artaxo, "Cloud condensation nuclei in the Amazon Basin: "Marine" conditions over a continent?" *Geophysical Research Letters*, vol. 28, no. 14, pp. 2807–2810, 2001.

[23] C. A. Randles, L. M. Russell, and V. Ramaswamy, "Hygroscopic and optical properties of organic sea salt aerosol and consequences for climate forcing," *Geophysical Research Letters*, vol. 31, no. 16, Article ID L16108, 2004.

[24] G. Myhre, F. Stordal, M. Johnsrud et al., "Aerosol-cloud interaction inferred from MODIS satellite data and global aerosol models," *Atmospheric Chemistry and Physics*, vol. 7, no. 12, pp. 3081–3101, 2007.

[25] S. Dipu, T. V. Prabha, G. Pandithurai et al., "Impact of elevated aerosol layer on the cloud macrophysical properties prior to monsoon onset," *Atmospheric Environment*, vol. 70, no. 1, pp. 454–467, 2013.

[26] M. Konwar, R. S. Maheskumar, J. R. Kulkarni, E. Freud, B. N. Goswami, and D. Rosenfeld, "Aerosol control on depth of warm rain in convective clouds," *Journal of Geophysical Research*, vol. 117, no. 13, Article ID D13204, 2012.

[27] J. R. Kulkarni, R. S. Maheskumar, S. B. Morwal et al., "The Cloud Aerosol Interaction and Precipitation Enhancement Experiment (CAIPEEX): overview and preliminary results," *Current Science*, vol. 102, no. 3, pp. 413–425, 2012.

[28] Intergovernmental Panel on Climate Change (IPCC), S. Solomon, D. Qin et al., *Climate Change 2007, The Physical Science Basis*, Cambridge University Press, New York, NY, USA, 2007.

[29] W. B. Rossow and R. A. Schiffer, "Advances in understanding clouds from ISCCP," *Bulletin of the American Meteorological Society*, vol. 80, no. 11, pp. 2261–2287, 1999.

[30] B.-G. Kim, S. E. Schwartz, M. A. Miller, and Q. Min, "Effective radius of cloud droplets by ground-based remote sensing: relationship to aerosol," *Journal of Geophysical Research D*, vol. 108, no. 23, p. 4740, 2003.

[31] T. J. Garrett, C. Zhao, X. Dong, G. G. Mace, and P. V. Hobbs, "Effects of varying aerosol regimes on low-level Arctic stratus," *Geophysical Research Letters*, vol. 31, no. 17, Article ID L17105, 2004.

Hindawi Publishing Corporation
Advances in Meteorology
Volume 2013, Article ID 740453, 9 pages
http://dx.doi.org/10.1155/2013/740453

Research Article

Interannual and Intraseasonal Variability in Fine Mode Particles over Delhi: Influence of Meteorology

S. Tiwari,[1] D. S. Bisht,[1] A. K. Srivastava,[1] G. P. Shivashankara,[2] and R. Kumar[3]

[1] *Indian Institute of Tropical Meteorology (Branch), Prof Ramnath Vij Marg, New Delhi 110060, India*
[2] *Department of Environmental Engineering, P. E. S. College of Engineering, Mandya, Karnataka 571401, India*
[3] *Sharda University, Knowledge Park III, Greater Noida 201306, India*

Correspondence should be addressed to D. S. Bisht; dsbisht@tropmet.res.in

Received 23 May 2013; Revised 26 September 2013; Accepted 3 October 2013

Academic Editor: D. M. Chate

Fine mode particles (i.e., $PM_{2.5}$) were collected at Delhi, India, for three consecutive years from January 2007 to December 2009 and were statistically analyzed. Daily mean mass concentration of $PM_{2.5}$ was found to be $108.81 \pm 75.5\,\mu g\,m^{-3}$ ranged from 12 to $367.9\,\mu g\,m^{-3}$, which is substantially higher than the Indian National Ambient Air Quality Standards (NAAQS). Among the measurements, ~69% of $PM_{2.5}$ samples exceeded 24 h Indian NAAQS of $PM_{2.5}$ level ($\mu g\,m^{-3}$); however, ~85% samples exceeded its annual level ($40\,\mu g\,m^{-3}$). Approximately 30% of PM2.5 mass was in the range of 40–80 $\mu g\,m^{-3}$, indicating abundance of fine particles over Delhi. Intraseasonal variability of $PM_{2.5}$ indicates highest mass concentration during postmonsoon ($154.31 \pm 81.62\,\mu g\,m^{-3}$), followed by winter ($150.81 \pm 74.65\,\mu g\,m^{-3}$), summer ($70.86 \pm 29.31\,\mu g\,m^{-3}$), and monsoon ($45.06 \pm 18.40\,\mu g\,m^{-3}$). In interannual variability, it was seen that in 2008, the fine mode particle was ~23% and ~36% higher as compared to 2007 and 2009, respectively. Significantly negative correlation was found between $PM_{2.5}$ and temperature (−0.59) as well as wind speed (−0.38). Higher concentration of $PM_{2.5}$ ($173.8\,\mu g\,m^{-3}$) was observed during calm conditions whereas low concentration ($79.18\,\mu g\,m^{-3}$) was observed when wind speed was >5 Km/hr. In winter, greater exposure risk is expected, as the pollutant often gets trapped in lower atmosphere due to stable atmospheric conditions.

1. Introduction

Aerosols, suspended in the atmosphere, are distributed through turbulence and direct atmospheric transport of air masses. These aerosols interact with Earth's energy budget, directly as well as indirectly. As a direct effect, aerosols scatter, absorb, and reflect solar energy that enters and exits in the Earth's atmosphere, while as an indirect effect, they altered the size, shape, and location of clouds and affected the precipitation in lower atmosphere [1–4]. Apart from this, atmospheric aerosols, especially fine particles, have received much attention during the last two decades due to their potential adverse impacts on human health and agricultural production. Particulate matters with aerodynamic diameters less than 2.5 μm (i.e., $PM_{2.5}$), called fine particles, have especially been found to be associated with increasing respiratory illness, carcinogens [5], asthma [6], and ultimately in increasing the number of premature deaths [7–9]. Many epidemic studies have linked airborne concentrations of $PM_{2.5}$ and PM_{10} with a variety of health problems, including morbidity and mortality [10].

Due to industrial and population growth, increased transportation system, burning of fossil fuel, high rate of urbanizations, and migrations are unavoidable in a developing country. India is the world's seventh largest country, second to China in its population. Rapid growth in megacities, especially in Delhi and Mumbai, is a cause of concern for air quality. Note that Delhi is the fourth most polluted and the seventh most populous metropolis in the world. According to a local survey, 30% of Delhi's population was found suffering from respiratory disorders due to air pollution, and this number is about 12 times the national average [11]. Over the station, the presence of industrial activity and traffic emissions are likely to be the most important sources of air pollutants. Increasing particulate matter has already noted to affect human health in megacities [12, 13]. As $PM_{2.5}$

particles have relatively large surface to volume ratio and longer residence times in the atmosphere, they possess a higher proportion of persistent organic compounds than larger particles [14]. In addition to this, high levels of $PM_{2.5}$ have been associated with amenity problems such as visibility degradation associated with haze [15].

The problem of pollution is not only the issue for Delhi, but also it is the case for several megacities of the entire world. Some studies on air quality assessment in Delhi have been carried out for PM emissions, effect of CNG regulations, air toxicity, and air quality index [16–18]. According to these studies, the transport sector of Delhi shares ~72% of the total airborne pollutants [16, 19]; however, major sources of air pollution in Delhi are emissions from vehicles (67%), coal based thermal power plants (13%), industrial units (12%), and domestic exhaust (8%). In 1991, the air pollutants daily emission loads over Delhi were ~1,450 metric tons (http://envfor.nic.in/divisions/cpoll/delpolln.html), which is still in the higher range exceeding prescribed standards of the World Health Organization [20]. The magnitude and urgency of the problem as a global environmental issue need a systematic understanding of the potential causes of pollution and their contribution to air quality. Mostly, in megacities, the main sources of fine particles are the combustion of fossil fuels from automobiles, construction equipments (mobile sources), furnaces, and power plants (stationary sources), where such particles are produced by combustion processes and mixed in the ambient air by mechanical processes [13, 21].

In the present study, fine mode particles (i.e., $PM_{2.5}$ mass concentrations) were obtained from Central Pollution Control Board (CPCB) during the period from January 2007 to December 2009 in Delhi. The observed aerosol data was analyzed and presented in the present study with objectives (i) to assess interannual and intraseasonal variability of $PM_{2.5}$ mass concentration over Delhi and its possible sources and (ii) to understand the effect of ambient meteorological parameters on aerosol formation and existence during different atmospheric conditions.

2. Data Collection and Sampling Site

Delhi, situated between 28°21′17″ to 28°53′ latitude and 76°20′37″ to 77°20′37″ longitude with height of ~218 meter above mean sea level, is around 160 km away in the south from the southern part of the Himalayas. It is bounded by the Thar desert of Rajasthan in the west, plains of central India in the south, and Indo-Gangetic Plains (IGP) in the east. The area of the city is 1,483 km^2 with ~18 million inhabitants. It experiences severe weather conditions between different seasons from hot and humid weather in summer to cold and dry weather in winter [22]. During the whole year, the prevailing wind was found to be easterly, northerly, and northwesterly, and to be strongest wind was in summer. Apart from such swings of weather in annual cycle, the whole northern part of India, especially the IGP, experiences thick foggy conditions during winter with lower boundary layer. More details about the station and the meteorological conditions are discussed elsewhere [23].

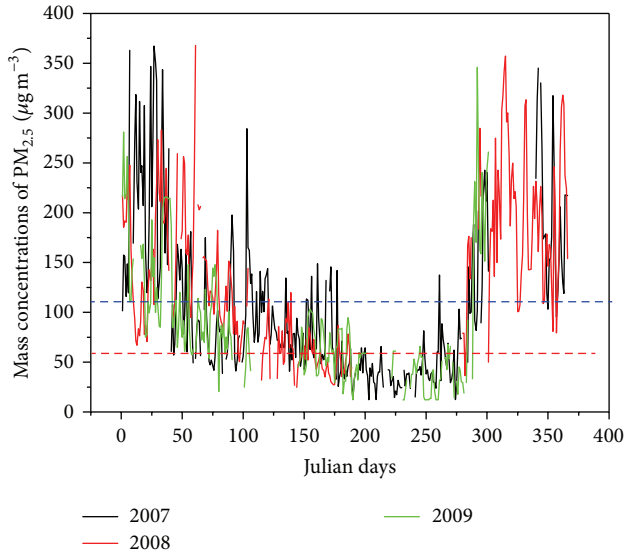

Figure 1: Day to day variability of mass concentrations of $PM_{2.5}$, during 2007 to 2009 (blue dash line—mean concentration of $PM_{2.5}$; red dash line—NAAQS).

Hourly mass concentrations of $PM_{2.5}$ were collected for a period of three years from January 2007 to December 2009 which was monitored by CPCB (http://www.cpcb.nic.in/) at the Income Tax Office (ITO) intersection. CPCB is an independent governmental body which is responsible for monitoring the pollution levels at different environments across the country, including Delhi, under its National Ambient Air Quality Monitoring Network (NAAQMN). The sampling site is one of the highest traffic intersection zones, and a thermal power plant (747 MW) called "Indraprastha Thermal Power station" is located at about 500 m in the southeast azimuth. Further, the corresponding ambient meteorological parameters such as temperature, relative humidity (RH), and wind speed (WS) were collected from the India Meteorological Department (http://www.imd.gov.in/), Lodhi Road.

3. Results and Discussion

3.1. Temporal Variability in Fine ($PM_{2.5}$) Mode Particle. Day to day variability in mass concentrations of fine mode particle ($PM_{2.5}$) during the study period from January 2007 to December 2009 was plotted and depicted in Figure 1. The daily mean mass concentration of $PM_{2.5}$ over Delhi during the study period was $108.81 \pm 75.5\ \mu g\ m^{-3}$ that ranged from 12 to 367.9 $\mu g\ m^{-3}$ which is substantially higher and far in excess of their annual averages stipulated by the Indian National Ambient Air Quality Standards (NAAQS; http://cpcb.nic.in/National_Ambient_Air_Quality_Standards.php; 40 $\mu g\ m^{-3}$) and the US National Ambient Air Quality Standards (http://www.epa.gov/air/criteria.html; US NAAQS; 15 μgm^{-3}). During the study period, ~69% $PM_{2.5}$ samples were found to exceed the 24 h limit of NAAQS for $PM_{2.5}$ standard (60 $\mu g\ m^{-3}$). Mass concentrations of $PM_{2.5}$ show considerable

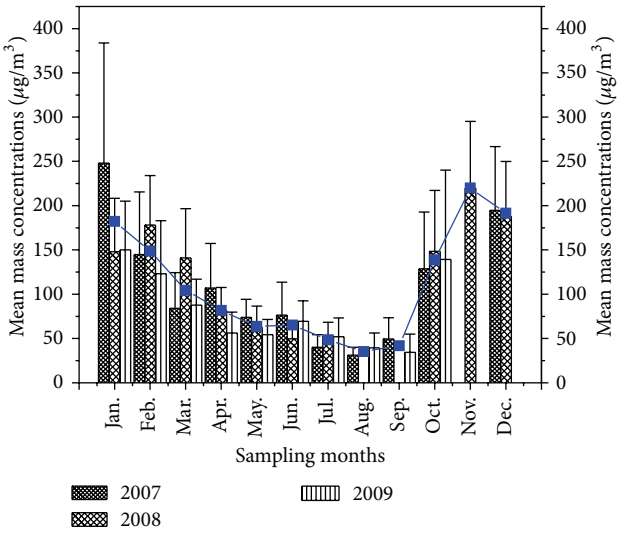

Figure 2: Yearwise monthly mean mass concentrations of $PM_{2.5}$, during 2007 to 2009.

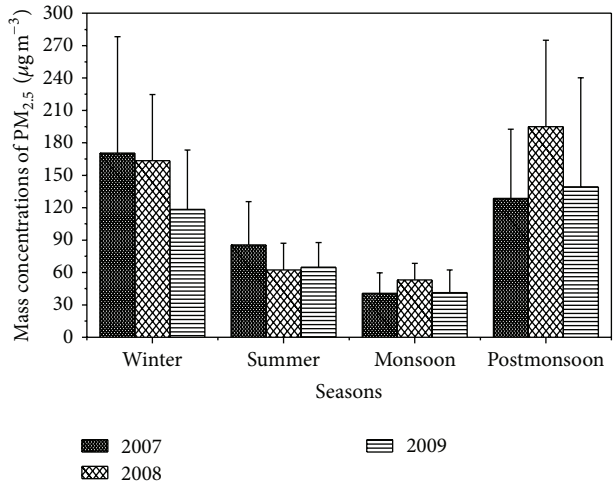

Figure 3: Seasonal variation of mass $PM_{2.5}$ concentrations during study period over Delhi.

day to day variability, with the lowest value of 12 $\mu g\,m^{-3}$ (on 18th August 2009) and the highest of 368 $\mu g\,m^{-3}$ (on 1st March 2008), which could be due to the meteorological effect.

Interannual monthly mean mass concentrations of $PM_{2.5}$ and its standard deviation during 2007 to 2009 were plotted and shown in Figure 2. Monthly mass concentrations of $PM_{2.5}$ were observed to be in the following order: January > February > October > April > March > June > May > September > July > August (2007), November > December > February > October > January > March > April > May > June > July (2008), and December > January > October > February > March > June > April > May > July > August > September (2009). On the basis of monthly analysis, $PM_{2.5}$ indicates the highest concentrations in winter and postmonsoon months. Also, we analyzed interannual variation of fine mode particles and were found the highest value during 2008 (135.44 ± 77 $\mu g\,m^{-3}$, varying from 12.0 to 367.9 $\mu g\ m^{-3}$) followed by 2007 (103.7 ± 77.5 $\mu g\,m^{-3}$, varying from 12.2 to 367.9 $\mu g\,m^{-3}$) and 2009 (87.1 $\mu g\,m^{-3}$, varying from 12.0 to 345.9 $\mu g\,m^{-3}$). In 2008, the fine mode particle was higher by ~23% and 36% as compared to 2007 and 2009, respectively, which could be due to synoptic meteorological changes over the station (see Section 3.2). Intraseasonal variability of mass $PM_{2.5}$ was studied and shown in Figure 3. On the basis of annually season, the highest mass $PM_{2.5}$ concentrations were during postmonsoon (154.31 ± 81.62 $\mu g\,m^{-3}$) followed by winter (150.81 ± 74.65 $\mu g\,m^{-3}$), summer (70.86 ± 29.31 $\mu g\,m^{-3}$), and monsoon (45.06 ± 18.40 $\mu g\,m^{-3}$). In overall, the lower mass concentration of fine particle was observed during monsoon due to washout effect, whereas the higher concentration was during winter due to low level inversion. $PM_{2.5}$ concentrations during monsoon in 2007 and 2009 were nearly equal to the annual mean NAAQS except in 2008 (53.13 $\mu g\,m^{-3}$); however, it was approximately four times higher during postmonsoon and winter whereas during summer, it was approximately double the NAAQS.

Very high mass concentration of $PM_{2.5}$ during winter and postmonsoon is basically due to meteorological and emission effects [24, 25]. The mixing height is observed to be lower due to low temperature and calm winds during these periods. On the other hand, burning of fire crackers during Deepawali festival, which is generally celebrated in the last week of October or in the first week of November every year all over India, is another important cause of generation of particulate matters during postmonsoon season [26–29]. Minima were observed during monsoon season due to washout effect [24]. Bach et al. [30] reported an increase in total suspended particulate matters (TSPM) on an average by 300% at 14 locations; however, they also reported at one location that, due to fireworks on New Year's Eve, the lung penetrating size ranges particles increases up to 700%. Increase in particle number is witnessed in the accumulation mode range (>100 nm) during the Millennium Fireworks in Leipzig, Germany [31]. Further, Liu et al. [32] reported the chemical composition and particle size of typical firework mixtures. An enhancement in $PM_{2.5}$ up to 6 times and PM_{10} up to 4 times on a lantern day (fireworks) in Beijing (China) is found relative to those over normal days [33].

Frequency distribution of $PM_{2.5}$ mass concentrations over Delhi during study period was also studied (Figure 4). It is divided into nine different categories of 40 $\mu g\,m^{-3}$ intervals within the limit of NAAQS from 0 to 360 $\mu g\,m^{-3}$. In overall study, mass concentration of $PM_{2.5}$ skewed toward higher to lower concentrations in respect of corresponding spectrum except 0–40 $\mu g\,m^{-3}$ (15%). The highest contribution was 30% (40–80 $\mu g\,m^{-3}$) followed by 17% (80–120 $\mu g\,m^{-3}$), 14% (120–160 $\mu g\,m^{-3}$), 10% (160–200 $\mu g\,m^{-3}$), 9% (200–240 $\mu g\,m^{-3}$), 3% (240–280 $\mu g\,m^{-3}$), 2% (280–320 $\mu g\,m^{-3}$), and 1% (320–360 $\mu g\,m^{-3}$). It clearly indicated that mass concentrations of $PM_{2.5}$ was higher (85%) than their National Ambient Air Quality Standard limits (40 $\mu g\,m^{-3}$); however, ~30% of

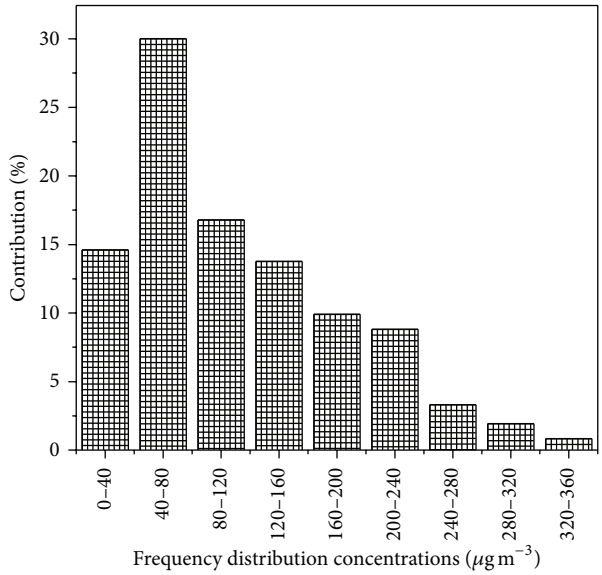

FIGURE 4: Frequency distribution of $PM_{2.5}$ over Delhi during study period.

samples (significant fraction) were observed between 40 and 80 $\mu g\,m^{-3}$ ranges, which indicates that the environment of Delhi is more dangerous in the health point of view due to high loadings of fine particles into the atmosphere of Delhi. This feature is basically due to emissions from anthropogenic sources and climatic conditions of Delhi.

Meteorological parameters such as temperature, relative humidity, wind speed, rainfall, and mixing height play crucial role in dispersion, transportation, and accumulation of the atmospheric pollutants. In general the atmosphere of Delhi during winter season is characterized by low relative humidity and low solar heating of land accompanied by low ventilation coefficients that result in less dispersion of aerosols, which in turn leads to an increase in the concentrations of fine mode particles. Due to this process, there is a greater exposure risk in trapping the air pollutants in the lower layer of the atmosphere thereby resulting in high mass concentrations of PM near to the surface. In such conditions, the probability of the formation of secondary aerosols is higher ([34] and references therein). Apart from this, long range transport of fine particles may also play crucial role during postmonsoon [24, 34]. Crop harvest and clearing agricultural land by burning the biomass during postmonsoon are common practices in the largely agricultural surroundings. The burning smoke reaches Delhi contributing to substantial smog formation and enhancement in PM and ozone levels [35]. In a recent study, Awasthi et al. [36] reported higher concentrations of $PM_{2.5}$ (69 $\mu g\,m^{-3}$) as compared to NAAQS, which varied from 44 to 147 $\mu g\,m^{-3}$ at Patiala district of India, which is located northwest of Delhi near the foothills of the Himalayas. They found that the concentration of fine particulate matter was increased substantially (78%) during postmonsoon (October to November) due to burning of crop residue with the maxima observed from 100 to 147 $\mu g\,m^{-3}$ in 2009. Similar results with higher concentrations of aerosols are also reported by Badarinath et al. [37] using satellite-based measurements during exhaustive burning of rice crop residue in IGP region in the months of October to November. Therefore, the significantly high concentrations of fine size aerosols observed over Delhi have larger influence of certain anthropogenic activities related to agriculture during the winter season [24].

The daily mean mass concentration of PM (108.81 ± 75.5 $\mu g\,m^{-3}$) during the study period at Delhi is found to be relatively lower than the previously reported values (171 $\mu g\,m^{-3}$) by Khillare et al. [38] during 2004, which can be attributed to introduction of metro-rail and use of CNG for public transport in Delhi. Lowering in the concentrations of $PM_{2.5}$ may increase in the proportion of petrol-fueled four- and two-wheeler vehicles, three-wheeler converted to CNG, and poor CNG kit in three-wheeler public transport system, which was first generation of CNG three-wheeler vehicles introduced in Delhi. Apart from these, the other significant fallout of the ruling was in the industrial sector—approximately 500 heavy industries were either shut down or relocated to areas outside the Delhi administrative boundaries. Yet, there remains a tremendous amount of potential to reduce the air pollution impacts in Delhi as the demand rises for infrastructure and services. Reynolds and Kandlikar [39] examined the opportunities for combined benefits of Delhi's fuel switching strategy—not only for local air pollution but also for climate related affects—and evaluated the potential for extending such services to other cities. Gadde et al. [40] have identified the contribution of ~14% (globally) of the open burnt rice straw in the states of Punjab, Haryana, and Uttar Pradesh. In addition to this, Delhi's low nighttime temperature during the winter (~2°C) and indoors and outdoors heating of biofuels for heating purpose are accomplished with small coal-burning boilers, stoves, and open burning of leaves and woods [41]. Guttikunda and Calori [42] have done a GIS-based emissions inventory at 1 km × 1 km spatial resolution for air pollution analysis in Delhi and found the mass concentrations of $PM_{2.5}$ (123 ± 87 $\mu g\,m^{-3}$) which is higher to present study. Dey et al. [43] have also reported higher outdoor fine particulate ($PM_{2.5}$) mass concentrations (148.4 ± 67 $\mu g\,m^{-3}$) over Delhi. Overall, the level of $PM_{2.5}$ in Delhi is comparable to Beijing, China (115 $\mu g\,m^{-3}$) [44], and to the wintertime in California's San Joaquin Valley, USA (138 $\mu g\,m^{-3}$) [45], and is higher than the Belgrade City (75 $\mu g\,m^{-3}$) [46].

Recent increase in the proportion of diesel cars and diesel light trucks appears to be the cause of increase of PM concentrations. Besides this, the particulate pollutants in Delhi environment are also contributed to nonexhaust particles originating from wear and corrosion of road pavements, vehicle components, and particles originating in surroundings as well as industrial processes, increasing construction activities, loss of vegetation, and thermal power plants. The four wheelers, which were converted from petrol to compressed natural gas (CNG), are characterized by poor quality of piston rings as well as the improper maintenance of air filters, which generate white smoke, causing increase in PM levels [47]. Apart from generation of particles in the vicinity

Table 1: Yearly mean mass concentrations of $PM_{2.5}$, temperature, relative humidity, and wind speed along with their standard deviation (std.) and minimum (min) and maximum (max) values in Delhi during 2007 to 2009.

	Mass concentration of $PM_{2.5}$ ($\mu g\,m^{-3}$)			Temperature (°C)			Relative humidity (%)			Wind speed (km/hr)		
Year	2007	2008	2009	2007	2008	2009	2007	2008	2009	2007	2008	2009
Mean	77.5	135.4	87.1	25.4	25.1	26.0	64.2	63.9	59.1	5.0	5.2	4.7
Std.	88.8	77.8	62.2	7.0	6.5	6.9	45.9	15.2	15.9	3.4	3.5	3.9
Max	367.3	367.9	345.9	39.0	35.0	37.8	88.0	97.0	97.0	18.9	18.9	19.4
Min	12.2	24.7	12.0	9.4	9.2	11.8	24	25	20	Calm	Calm	Calm

of the city, particles from nearby thermal power plants also contribute significantly to the particle level of Delhi. Note that three major power plants, namely, Badarpur, Indraprastha, and Rajghat with the total electricity generation capacity of 1,087 MWs, are situated in the vicinity of measurement location. These power plants produce nearly 6,000 metric tons (Badarpur 3,500–4,000, Indraprastha 1,200–1,500, and Rajghat 600–800) of fly ash per day and are responsible for as much as 10% of the total air pollution load. Furthermore, Delhi is also dealing with massive dust due to continuous constructional activities and a failed effort to control burning of garbage and biomass.

3.2. Effect of Meteorology on $PM_{2.5}$ Mass Concentrations. Yearly mean mass concentrations of $PM_{2.5}$, temperature (Temp.), relative humidity (RH), and wind speed (WS) along with their standard deviation, minimum, and maximum values in Delhi during 2007 to 2009 are assembled in Table 1. Large variations were seen in interannual and intraseasonal (as discussed in Section 3.1) mass concentrations of fine mode particles over Delhi during the study period, which is directly influenced by ambient meteorological conditions. The annual mean mass concentration of $PM_{2.5}$ during 2008 was higher than in 2007 and 2009, although very good agreement was seen between mass concentrations and meteorological parameters such as WS, temperature, and RH. The highest mean WS (5.2 Km/hr) was observed in 2008, whereas the lowest was in 2009 (4.7 Km/hr) and the intermediate was in 2007 (5.0 Km/hr). Seasonwise occurrence of calm conditions was studied and higher occurrence of calm conditions was observed during winter period of 2008 as compared to 2007 and 2009; however, there are less calm conditions observed in other seasons. The RH was found similar to WS with lower in 2009 (mean RH: 59%) as compared to 2007 (mean RH: 64%) and 2008 (mean RH: 63%). There is no significant relationship seen during interannual variability between mass concentrations with RH; however, good agreement was seen on intraseasonal variability on mass concentrations and RH. Seasonwise variations between them have been studied and higher concentration of fine particles was observed during winter period as in 2007 (171 $\mu g\,m^{-3}$), 2008 (163 $\mu g\,m^{-3}$), and 2009 (118 $\mu g\,m^{-3}$) and corresponding RH was 72%, 62%, and 64%, respectively. In another study, Singh [48] suggested that RH plays a very crucial role in altering the radiative properties of atmospheric aerosols as hygroscopic nature. A very good agreement between columnar aerosol optical depth and RH over Rajkot was observed by Ranjan et al. [49]. Devara and Raj [50] observed that the higher relative humidity and lower temperature during monsoon period at Pune caused the growth of cloud droplets which results in higher rainfall. In the case of temperature, it was higher during 2009 (Mean: 26°C) compared to 2007 (Mean: 25.4°C) and 2008 (Mean: 25.1°C). Also, large variation was observed between maximum and minimum temperature during interannual variability and varied from 9.4 to 39.0°C in 2007, 9.2 to 35.0°C in 2008, and 11.8 to 37.8°C in 2009. Statistically, the variability in temperature was seen during intraseasonal with highest magnitude during summer (31.5°C) followed by monsoon (31.0°C), postmonsoon (23.5°C), and winter (18.0°C).

Regression analysis between daily mass concentrations of $PM_{2.5}$ and meteorological parameters such as WS, temperature, and RH during study period was performed and depicted in Figure 5 (Figure 5(a): WS; Figure 5(b): temperature, and Figure 5(c): RH). Very good agreement was observed between mass concentrations with WS and temperature; however, very week relationships were seen between PM and RH in the overall study due to large variability in RH during different seasons. A good agreement was seen during intraseasonal which was discussed earlier. Significant correlation between $PM_{2.5}$ and WS over Delhi was observed (−0.38 (r), slope: $Y = 6.97725 - 0.01784X$; $N = 755$; $P < 0.0001$), which is significant at 99% confidence level (Figure 5(a)). The mass concentrations were separated in different WS (calm conditions and WS ≤ 5 Km/hr and ≥5 Km/hr). Very high mass concentrations (173.8 $\mu g\,m^{-3}$) of PM were observed when WS was in calm conditions; however, when the WS was in <5 Km/hr, it was still showing higher mass concentration (124.77 $\mu g\,m^{-3}$) which is three times higher than NAAQS. Very low PM mass concentrations (79.18 $\mu g\,m^{-3}$) were observed in higher WS (>5 Km/hr). Also, it was seen that the concentrations of pollutants decrease effectively with increasing wind speed, suggesting the dilution of pollutants through dispersion. Similarly to WS, the correlation between PM and temperature was also observed to be very high (−0.58 (r)), which is also significant at 99% confidence level (slope: $Y = 31.21856 - 0.05543X$; $N = 755$; $P < 0.0001$) (Figure 5(b)). We also separated the concentrations against temperature (indicated as vertical line) and found that the higher concentrations (164.66 $\mu g\,m^{-3}$) were observed when the temperature was less than 22.5°C; however, very low concentrations (77.14 $\mu g\,m^{-3}$) were observed to be >22.5°C. Wallace and Kanaroglou [51] studied the relationship between temperature and fine particulate matter during day and night at Ontario, Canada, for the

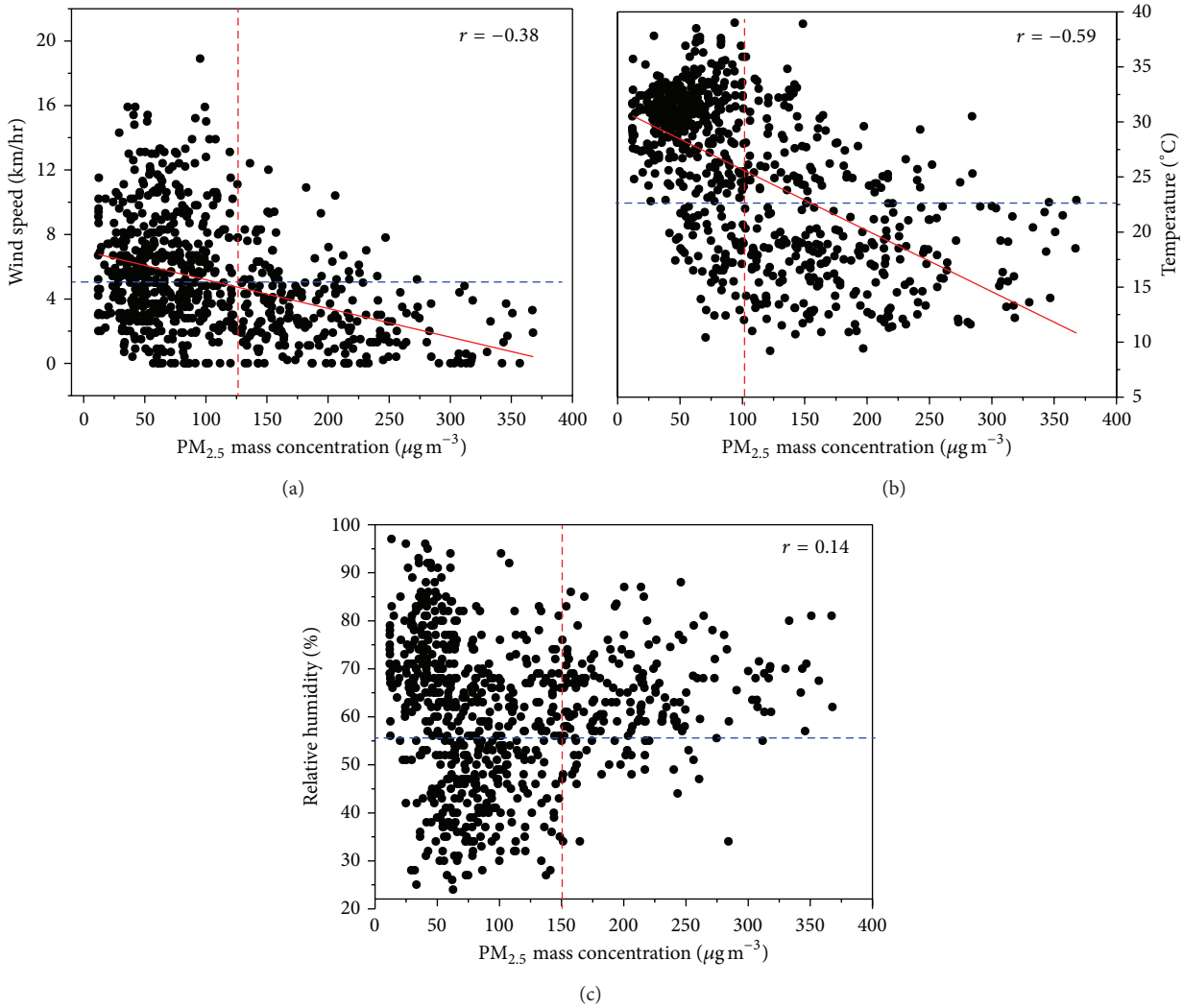

FIGURE 5: Day to day relation between wind speed and $PM_{2.5}$ (a), temperature and $PM_{2.5}$ (b), and relative humidity and $PM_{2.5}$ (c) during 2007 to 2009. Vertical and horizontal lines indicate the dominance of the metrological parameters and $PM_{2.5}$ mass concentration.

period from 2003 to 2007. They found that in nighttime, the 54% concentrations of fine particles increased due to low level inversion and lower temperature but it was found opposite during daytime and the concentration decreased about 14% during daytime. Due to large variability during day and night temperature along with interannual and intraseasonal variability, very poor relationship (0.14) between RH and mass concentrations of PM was observed during the study period. Interesting results were seen in the separation of lower (<55%) and higher (>55%) RH; in case of <55% RH, the lower mass concentration (96.96 $\mu g\,m^{-3}$) was observed; however, in >55% RH, the mass concentration was found to be relatively higher (114.6 $\mu g\,m^{-3}$). High wind speed was associated with lower pollutant levels in most of the cases, whereas in the case of RH and temperature, it was opposite. On the basis of these relationships, it can be mentioned that the interplay of meteorological variables with pollution plays a key role in assessing the impact of pollution for a region. Seasonal correlation analysis between fine particle and meteorological parameters was also performed and depicted in Table 2. The WS and temperature was found to be negatively correlated during winter and post-monsoon seasons; however, a poor correlation was observed during summer and monsoon. Very interesting results were seen in the case of RH having positive relationship (=0.35) during postmonsoon whereas significant negative correlation (−0.48) was seen during summer. No relationship was observed during monsoon and winter. It is clearly indicated that meteorological parameters play a vital role in dispersion and accumulation of aerosols in different seasons. Chate and Devara [52] studied the impact of RH on nucleation mode particle during winter of 1997 and 1998 and found that they have positive impact on growth in submicron aerosols (0.013 to 0.133 $\mu g\,m^{-3}$) during cold season; however, during the same period in the present study, we have not found any significant relation in larger particle (2.5 $\mu g\,m^{-3}$) as compared to nucleation aerosols. In an other study, Cheng and Lam [53] investigated the impact of wind on TSP concentrations in Hong Kong and found a similar relationship. Also, Chaloulakou et al. [54] investigated the relationship among PM and meteorological parameters such

Table 2: Interannual and intraseasonal correlation coefficient between $PM_{2.5}$, and meteorological parameters (wind speed: WS, temperature: Temp., and relative humidity: RH) in Delhi during 2007 to 2009.

	2007 $PM_{2.5}$	2008 $PM_{2.5}$	2009 $PM_{2.5}$	Overall $PM_{2.5}$
WS	−0.30	−0.56	−0.30	−0.38
Temp.	−0.60	−0.54	−0.56	−0.59
RH	0.03	0.11	−0.01	0.14
	Winter $PM_{2.5}$	Summer $PM_{2.5}$	Monsoon $PM_{2.5}$	Postmonsoon $PM_{2.5}$
WS	−0.50	−0.16	−0.09	−0.58
Temp.	−0.58	−0.02	−0.11	−0.51
RH	0.19	−0.48	−0.18	0.35

as wind speed over Athens, Greece, and found very good agreement with wind speed ($r = -0.43$) and mass PM. They also found good agreement between temperature and fine particles below 10°C (−0.36) and found a positive correlation above 30°C (0.41). Further, $PM_{2.5}$ concentrations measured near a highly trafficked road in Paris were found to be inversely proportional to the wind speed [55].

4. Conclusions

Mass concentrations of $PM_{2.5}$ were collected during three consecutive years over Delhi at a busy traffic intersection at I.T.O., from January 2007 to December 2010. The data were analyzed for annual and seasonal variations of $PM_{2.5}$ mass concentration and their results are summarized and given below.

The capital of India, Delhi, is found to be heavily loaded with fine particulate matter ($PM_{2.5}$) showing daily mean mass concentration ($108.81 \pm 75.5\,\mu g\,m^{-3}$) that ranged from 12 to $367.9\,\mu g\,m^{-3}$ which is substantially higher than the Indian NAAQS. Approximately 69% samples of $PM_{2.5}$ mass were exceeded to 24 h Indian NAAQS $PM_{2.5}$ level ($60\,\mu g\,m^{-3}$) whereas 85% samples were exceeded to its annual level ($40\,\mu g\,m^{-3}$). Most of the samples existed between 40 and $80\,\mu g\,m^{-3}$ (~30%) and indicated that the environment of Delhi is susceptible to a health point of view, generated due to anthropogenic emissions and meteorological conditions over Delhi. Intraseasonal variability of $PM_{2.5}$ indicates the highest mass concentrations during postmonsoon ($154.31 \pm 81.62\,\mu g\,m^{-3}$) followed by winter ($150.81 \pm 74.65\,\mu g\,m^{-3}$), summer ($70.86 \pm 29.31\,\mu g\,m^{-3}$), and monsoon ($45.06 \pm 18.40\,\mu g\,m^{-3}$). In 2008, the fine mode particle was ~23% and ~36% higher as compared to 2007 and 2009, respectively; these large interannual variations are found due to synoptic meteorological changes. Significant negative correlations are found between $PM_{2.5}$ and temperature (−0.59) as well as wind speed (−0.38). Higher concentrations of $PM_{2.5}$ ($173.8\,\mu g\,m^{-3}$) were observed during calm conditions, whereas $124.77\,\mu g\,m^{-3}$ was observed when WS was below 5 Km/hr. Very low PM mass concentrations ($79.18\,\mu g\,m^{-3}$) were observed in higher WS (>5 Km/hr). The high correlation is expected due to the cause that concentrations of pollutants decrease effectively with increasing WS and temperature, which suggests the dilution of pollutants into the atmosphere. In winter, greater exposure risk is expected, as the pollutant often gets trapped in lower atmosphere due to stable atmospheric conditions, thereby leading to higher levels. On the basis of the present study, it can be concluded that the interplay of meteorological variables with pollution plays crucial role in assessing the impact of pollution.

Acknowledgments

The authors gratefully thank Professor B. N. Goswami, Director of the Indian Institute of Tropical Meteorology, Pune for their encouragement and support during the preparation of this paper. Authors also thank the Central Pollution Control Board and the India Meteorological Department for data generation.

References

[1] S. Dey, S. N. Tripathi, R. P. Singh, and B. Holben, "Influence of dust storms on the aerosol optical properties over the Indo-Gangetic basin," *Journal of Geophysical Research D*, vol. 109, no. 20, Article ID D20211, 13 pages, 2004.

[2] S. Singh, S. Nath, R. Kohli, and R. Singh, "Aerosols over Delhi during pre-monsoon months: characteristics and effects on surface radiation forcing," *Geophysical Research Letters*, vol. 32, no. 13, Article ID L13808, 4 pages, 2005.

[3] G. Pandithurai, S. Dipu, K. K. Dani et al., "Aerosol radiative forcing during dust events over New Delhi, India," *Journal of Geophysical Research D*, vol. 113, Article ID D13209, 13 pages, 2008.

[4] K. A. Srivastava and S. N. Tripathi, "Numerical study for production of space charge within the stratiform cloud," *Journal of Earth System Science*, vol. 119, no. 5, pp. 627–638, 2010.

[5] D. W. Dockery and C. A. Pope, "Acute respiratory effects of particulate air pollution," *Annual Review of Public Health*, vol. 15, pp. 107–132, 1994.

[6] W. P. Anderson, C. M. Reid, and G. L. Jennings, "Pet ownership and risk factors for cardiovascular disease," *Medical Journal of Australia*, vol. 157, no. 5, pp. 298–301, 1992.

[7] J. Chen, R. P. Wildman, D. Gu et al., "Prevalence of decreased kidney function in Chinese adults aged 35 to 74 years," *Kidney International*, vol. 68, no. 6, pp. 2837–2845, 2005.

[8] F. Dominici, R. D. Peng, M. L. Bell et al., "Fine particulate air pollution and hospital admission for cardiovascular and respiratory diseases," *Journal of the American Medical Association*, vol. 295, no. 10, pp. 1127–1134, 2006.

[9] G. E. R. Schwartz, L. G. S. Russek, L. A. Nelson, and C. Barentsen, "Accuracy and replicability of anomalous after-death communication across highly skilled mediums," *Journal of the Society for Psychical Research*, vol. 65, no. 862, pp. 1–25, 2001.

[10] Y. Wang, C. Lee, S. Tiep et al., "Peroxisome-proliferator-activated receptor δ activates fat metabolism to prevent obesity," *Cell*, vol. 113, no. 2, pp. 159–170, 2003.

[11] M. Kandlikar, "The causes and consequences of particulate air pollution in urban India: a synthesis of the science," *Annual Review of Energy and the Environment*, vol. 25, pp. 629–684, 2000.

[12] Central pollution Control Board (CPCB), 2008 Epidemiological study on effect of air pollution on human health (adults) in Delhi. Environmental Health Series: EHS/1/2008, http://www.cpcb.nic.in.

[13] S. Madronich, "Chemical evolution of gaseous air pollutants down-wind of tropical megacities: Mexico City case study," *Atmospheric Environment*, vol. 40, no. 31, pp. 6012–6018, 2006.

[14] R. Jaenicke, "Protein folding and Protein Association," *Angewandte Chemie*, vol. 23, no. 6, pp. 395–413, 1984.

[15] J. W. Milne, D. B. Roberts, S. J. Walk, and D. J. William, "Sources of Sydney brown haze," in *The Urban Atmosphere—Sydney. A Case Study*, CSIRO, Highett, Australia, 1982.

[16] P. Goyal and S. Sidhartha, "Present scenario of air quality in Delhi: a case study of CNG implementation," *Atmospheric Environment*, vol. 37, no. 38, pp. 5423–5431, 2003.

[17] A. Kumar and T. C. Foster, "Shift in induction mechanisms underlies an age-dependent increase in DHPG-induced synaptic depression at CA3-CA1 synapses," *Journal of Neurophysiology*, vol. 98, no. 5, pp. 2729–2736, 2007.

[18] B. Bishoi, A. Prakash, and V. K. Jain, "A comparative study of air quality index based on factor analysis and US-EPA methods for an urban environment," *Aerosol and Air Quality Research*, vol. 9, no. 1, pp. 1–17, 2009.

[19] V. Kathuria, "Impact of CNG on Delhi's air pollution," *Economic and Political Weekly*, vol. 40, pp. 1907–1916, 2005.

[20] B. R. Gurjar, J. A. Van Aardenne, J. Lelieveld, and M. Mohan, "Emission estimates and trends (1990–2000) for megacity Delhi and implications," *Atmospheric Environment*, vol. 38, no. 33, pp. 5663–5681, 2004.

[21] A. Faiz, C. Weaver, K. Sinha, M. Walsh, and J. Carbajo, *Air Pollution from Motor Vehicles: Issues and Options for Developing Countries*, The World Bank, Washington, DC, USA, 1992.

[22] A. K. Srivastava, S. Singh, S. Tiwari, V. P. Kanawade, and D. S. Bisht, "Variation between near-surface and columnar aerosol characteristics during the winter and summer at Delhi in the Indo-Gangetic Basin," *Journal of Atmospheric and Solar-Terrestrial Physics*, vol. 77, pp. 57–66, 2012.

[23] S. Tiwari, A. K. Srivastava, D. S. Bisht, P. Parmita, M. K. Srivastava, and S. D. Attri, "Diurnal and seasonal variations of black carbon and $PM_{2.5}$ over New Delhi, India: influence of meteorology," *Atmospheric Research*, vol. 125-126, pp. 50–62, 2013.

[24] S. Tiwari, D. M. Chate, P. Pragya, K. Ali, and D. S. Bisht, "Variations in mass of the PM_{10},$PM_{2.5}$ and PM_1 during the monsoon and the winter at New Delhi," *Aerosol and Air Quality Research*, vol. 12, no. 1, pp. 20–29, 2012.

[25] S. Tiwari, A. K. Srivastava, D. S. Bisht, and P. D. Safai, "Assessment of carbonaceous aerosol over Delhi in the Indo-Gangetic Basin: characterization, sources and temporal variability," *Natural Hazards*, vol. 65, pp. 1745–1764, 2013.

[26] S. Tiwari, D. M. Chate, M. K. Srivastava et al., "Statistical evaluation of PM_{10} and distribution of PM_1, $PM_{2.5}$, and PM_{10} in ambient air due to extreme fireworks episodes (Deepawali festivals) in megacity Delhi," *Natural Hazards*, vol. 61, no. 2, pp. 521–531, 2012.

[27] A. K. Attri, U. Kumar, and V. K. Jain, "Formation of ozone by fireworks," *Nature*, vol. 411, no. 6841, pp. 1015–1021, 2001.

[28] R. P. Singh, S. Dey, and B. Holben, "Aerosol behaviour in Kanpur during Diwali festival," *Current Science*, vol. 84, no. 10, pp. 1302–1303, 2003.

[29] S. C. Barman, R. Singh, M. P. S. Negi, and S. K. Bhargava, "Fine particles ($PM_{2.5}$) in ambient air of Lucknow city due to fireworks on Diwali festival," *Journal of Environmental Biology*, vol. 30, no. 5, pp. 625–632, 2009.

[30] W. Bach, A. Daniels, L. Dickinson et al., "Firework's pollution and health," *International Journal of Environmental Studies*, vol. 7, pp. 183–192, 1975.

[31] B. Wehner, A. Wiedensohler, and J. Heintzenberg, "Submicrometer aerosol size distributions and mass concentration of the Millennium fireworks 2000 in Leipzig, Germany," *Journal of Aerosol Science*, vol. 31, no. 12, pp. 1489–1493, 2000.

[32] D. Liu, D. Rutherford, M. Kinsey, and K. A. Prather, "Real-time monitoring of pyrotechnically derived aerosol particles in the troposphere," *Analytical Chemistry*, vol. 69, no. 10, pp. 1808–1814, 1997.

[33] Y. Wang, G. Zhuang, C. Xu, and Z. An, "The air pollution caused by the burning of fireworks during the lantern festival in Beijing," *Atmospheric Environment*, vol. 41, no. 2, pp. 417–431, 2007.

[34] A.-P. Hyvärinen, H. Lihavainen, M. Komppula et al., "Aerosol measurements at the Gual Pahari EUCAARI station: preliminary results from in-situ measurements," *Atmospheric Chemistry and Physics*, vol. 10, no. 15, pp. 7241–7252, 2010.

[35] NASA (National Aeronautics and Space Administration), Top Science, Exploration and Discovery Stories of 2008.

[36] A. Awasthi, R. Agarwal, S. K. Mittal, N. Singh, K. Singh, and P. K. Gupta, "Study of size and mass distribution of particulate matter due to crop residue burning with seasonal variation in rural area of Punjab, India," *Journal of Environmental Monitoring*, vol. 13, no. 4, pp. 1073–1081, 2011.

[37] K. V. S. Badarinath, T. R. K. Chand, and V. K. Prasad, "Agriculture crop residue burning in the Indo-Gangetic Plains: a study using IRS-P6 AWiFS satellite data," *Current Science*, vol. 91, no. 8, pp. 1085–1089, 2006.

[38] P. S. Khillare, T. Agarwal, and V. Shridhar, "Impact of CNG implementation on PAHs concentration in the ambient air of Delhi: a comparative assessment of pre- and post-CNG scenario," *Environmental Monitoring and Assessment*, vol. 147, no. 1–3, pp. 223–233, 2008.

[39] C. C. O. Reynolds and M. Kandlikar, "Climate impacts of air quality policy: switching to a natural gas-fueled public transportation system in New Delhi," *Environmental Science and Technology*, vol. 42, no. 16, pp. 5860–5865, 2008.

[40] B. Gadde, S. Bonnet, C. Menke, and S. Garivait, "Air pollutant emissions from rice straw open field burning in India, Thailand and the Philippines," *Environmental Pollution*, vol. 157, no. 5, pp. 1554–1558, 2009.

[41] K. Ali, G. A. Momin, S. Tiwari, P. D. Safai, D. M. Chate, and P. S. P. Rao, "Fog and precipitation chemistry at Delhi, North India," *Atmospheric Environment*, vol. 38, no. 25, pp. 4215–4222, 2004.

[42] S. K. Guttikunda and G. Calori, "A GIS based emissions inventory at 1 km × 1 km spatial resolution for air pollution analysis in Delhi, India," *Atmospheric Environment*, vol. 67, pp. 101–111, 2013.

[43] S. Dey, L. D. Girolamo, A. V. Donkelaar, S. N. Tripathi, T. Gupta, and M. Mohan, "Variability of outdoor fine particulate ($PM_{2.5}$) concentration in the Indian Subcontinent: a remote sensing approach," *Remote Sensing of Environ*, vol. 127, pp. 153–161, 2012.

[44] K. He, F. Yang, Y. Ma et al., "The characteristics of $PM_{2.5}$ in Beijing, China," *Atmospheric Environment*, vol. 35, no. 29, pp. 4959–4970, 2001.

[45] J. G. Watson, "Visibility: science and regulation," *Journal of the Air and Waste Management Association*, vol. 52, no. 6, pp. 628–713, 2002.

[46] S. F. Rajšić, M. D. Tasić, V. T. Novaković, and M. N. Tomašević, "First assessment of the PM_{10} and $PM_{2.5}$ particulate level in the ambient air of Belgrade City," *Environmental Science and Pollution Research*, vol. 11, no. 3, pp. 158–164, 2004.

[47] EPCA report number 9 (November 2004) Report on the increase in the number of three-wheelers in Delhi, In response to the Hon'ble Supreme Court Order Dated October 8, 2004, In response to the I.A. 217 of 2003.

[48] N. Singh, *Role of atmospheric ions on condensation and cloud formation processes [Ph.D. thesis]*, University of Roorkee, Roorkee, India, 1985.

[49] R. R. Ranjan, H. P. Joshi, and K. N. Iyer, "Spectral variation of total column aerosol optical depth over Rajkot: a tropical semi-arid Indian station," *Aerosol and Air Quality Research*, vol. 7, no. 1, pp. 33–45, 2007.

[50] P. C. S. Devara and P. E. Raj, "A lidar study of atmospheric aerosols during two contrasting monsoon seasons," *Atmosfera*, vol. 11, no. 4, pp. 199–204, 1998.

[51] J. Wallace and P. Kanaroglou, "The effect of temperature inversions on ground-level nitrogen dioxide (NO_2) and fine particulate matter ($PM_{2.5}$) using temperature profiles from the Atmospheric Infrared Sounder (AIRS)," *Science of the Total Environment*, vol. 407, no. 18, pp. 5085–5095, 2009.

[52] D. M. Chate and P. C. S. Devara, "Growth properties of submicron aerosols during cold season in India," *Aerosol and Air Quality Research*, vol. 5, no. 2, pp. 127–140, 2005.

[53] S. Cheng and K. Lam, "An analysis of winds affecting air pollution concentrations in Hong Kong," *Atmospheric Environment*, vol. 32, no. 14-15, pp. 2559–2567, 1998.

[54] A. Chaloulakou, P. Kassomenos, N. Spyrellis, P. Demokritou, and P. Koutrakis, "Measurements of PM_{10} and $PM_{2.5}$ particle concentrations in Athens, Greece," *Atmospheric Environment*, vol. 37, no. 5, pp. 649–660, 2003.

[55] S. Ruellan and H. Cachier, "Characterisation of fresh particulate vehicular exhausts near a Paris high flow road," *Atmospheric Environment*, vol. 35, no. 2, pp. 453–468, 2001.

Hindawi Publishing Corporation
Advances in Meteorology
Volume 2013, Article ID 572954, 15 pages
http://dx.doi.org/10.1155/2013/572954

Research Article

Long-Term (1951–2007) Rainfall Trends around Six Indian Cities: Current State, Meteorological, and Urban Dynamics

Shailesh Kumar Kharol,[1] D. G. Kaskaoutis,[2] Anu Rani Sharma,[3] and Ramesh P. Singh[4]

[1] *Department of Physics and Atmospheric Science, Dalhousie University, Halifax, NS, Canada B3H 3J5*
[2] *Department of Physics, School of Natural Sciences, Shiv Nadar University, Dadri 203207, India*
[3] *Department of Natural Resources, TERI University, Vasant Kunj, New Delhi 110 070, India*
[4] *School of Earth and Environmental Sciences, Schmid College of Science and Technology, Chapman University, Orange, CA 92866, USA*

Correspondence should be addressed to Ramesh P. Singh; rsingh@chapman.edu

Received 18 July 2013; Revised 18 September 2013; Accepted 3 October 2013

Academic Editor: Samir Pokhrel

The present study focuses on analyzing the precipitation trends over six Indian cities during the summer monsoon (June–September) covering the period 1951–2007 and also attempting to investigate possible urban forcing and dynamics by examining the variation in precipitation in the upwind and downwind directions. The analysis shows negative trends in the total number of rainy days over Hyderabad (−10.4%), Kanpur (−7.1%), Jaipur (−10.5%), and Nagpur (−4.8%) and positive trends over Delhi (7.4%) and Bangalore (22.9%). On the other hand, decreases of −21.3%, −5.9%, −14.2%, and −14.6% in seasonal rainfall are found over Delhi, Hyderabad, Jaipur, and Kanpur, respectively, whereas Bangalore and Nagpur show 65.8% and 13.5% increase. The lesser rainfall and rainy days, along with the mostly declining trend, in the downwind directions of the cities may imply an urban influence in precipitation associated with the increased anthropogenic emissions due to expansion of the urban areas and the increase of population. However, the large spatiotemporal variability of precipitation and the lack of statistical significance in the vast majority of the trends do not allow the extraction of safe conclusion concerning the aerosol-precipitation interactions around Indian cities.

1. Introduction

Rainfall is a key physical process that transports water from the atmosphere back to Earth's surface and links weather, climate, and hydrological cycle [1, 2]. Especially for India, precipitation has serious importance in the regional climate, annual crop, food grains, and local economy and, therefore, analysis of the long-term trends in precipitation was the subject of numerous studies [3–5]. Duhan and Pandey [5] analyzed 102 years of precipitation records in central India (Madhya Pradesh) founding a spatial-averaged decreasing trend of −2.59%, with a maximum decrease of ∼ −12%, but only 3 out of the 45 stations exhibited significant decreasing trend in annual precipitation. However, pronounced spatiotemporal differences were observed between the 45 stations on seasonal basis. Analysis of 100 years of surface rainfall observations over India suggested that the mean monsoon rainfall has not been significantly changed, but several locations across the country exhibited an increasing trend in heavy rainfall (>70 mm/day) during the summer monsoon season [6]. Furthermore, the increase in extreme rainfall (>120 mm/day) events during the Indian summer monsoon (ISM) is particularly pronounced during the last 50 years [7]. The extreme rainfall events analysis by Malik et al. [8] suggested that ISM exhibits characteristically different patterns in the year 2000 as compared to the period 1951–2000 with an increase in magnitude and frequency of extreme rainfall events and a decline in moderate ones. In contrast, Guhathakurtha et al. [9] noted decreasing trends in the frequency of monsoon rainy days in most parts of the country by examining changes in extreme rainfall events over India during the period 1901–2005. Similarly, Dash et al. [10] found

a significant decrease in the frequency of moderate and low rainy days over India during the last half century. In synopsis, the precipitation fluctuations in India are largely random over the century, with no systematic change detectable on either an annual or a seasonal scale [11].

Basistha et al. [4] noted main causes of precipitation fluctuations in India, including the global and/or regional climate change implying a weakening monsoon circulation, land use land cover (LULC) changes corresponding to reduction in forest cover and increasing irrigated agriculture, and the increasing trend of anthropogenic aerosol and pollution levels. Bawiskar [12] analyzed sixty years (1948–2007) of daily temperature and wind datasets during premonsoon season (March–May) and observed a significant decrease in temperature gradient between Indian landmass and adjoining oceanic regions as a result of global warming. This decreasing trend directly affects the kinetic energy and cyclonic circulation over the area and can weaken the monsoon circulation in the lower troposphere. On the other hand, Rosenfeld [13] suggested that urban aerosols and anthropogenic pollution may reduce, or even vanish, the precipitation from clouds that have temperature of about −10°C at their tops in a moderately convective situation, while they may support the occurrence of heavier precipitation in a more convective and humid environment. Aerosol particles from both natural and anthropogenic sources are among the factors that could contribute to enhanced warming and precipitation redistribution over India [14, 15].

Atmospheric aerosols may affect precipitation through their direct, semidirect, and indirect effects in solar radiation and clouds. The former mostly acts to suppress precipitation by decreasing the amount of ground-reaching solar radiation, and, hence, reducing the heat availability for evaporating water and energizing convective rain clouds. The second is defined by the strong absorbing capability of the carbonaceous aerosols, which absorb solar radiation and heat the atmosphere, leading to stabilization of the lower troposphere and suppression of convective clouds. Besides these effects, aerosols can also have important microphysical effects on clouds and precipitation through their influence on cloud drop nucleation (indirect effect), which affects cloud lifetime, cloud albedo, and precipitation [16, 17]. Anthropogenic aerosols serve as small cloud condensation nuclei (CCN), which may slow down cloud-drop coalescence as well as the ice precipitation and prolong the time required in conversion of cloud water into precipitation [18]. Givati and Rosenfeld [19] quantified the microphysical effects of air pollutants on precipitation in a regional scale and found a decrease of 15–25% in orographic precipitation in the downwind direction of the pollution sources. Similarly, Rosenfeld et al. [20] highlighted the role of air pollution in the loss of water resources in hilly areas and suggested a 30–50% decrease in precipitation during hazy conditions at the mountains. Borys et al. [21, 22] provided evidence on suppression of precipitation in winter orographic clouds due to atmospheric pollutants that increase the CCN concentration leading to formation of smaller cloud droplets. The reduced drop size caused smaller fall velocities and smaller amounts of snowfall. Furthermore, Rosenfeld et al. [23] suggested that increase in aerosol concentration beyond a threshold would decrease the vigor of convective clouds because of both direct and indirect microphysical effects. On the other hand, several studies [24–26] suggested reduction in ground-reaching solar radiation, evaporation, and daytime temperature over heavily polluted areas due to formation of fog-like haze associated with increased anthropogenic pollutants. However, to establish any link between aerosols and precipitation over India is a real challenge, since changes in ambient meteorological conditions, in intraseasonal monsoon variability, and in land cover and normalized difference vegetation index (NDVI) can also influence precipitation [27–31]. On the other hand, several studies [32–35] observed a reverse effect, that is, enhancement of precipitation with aerosols.

Furthermore, land use changes affect several atmospheric properties and processes, such as boundary layer dynamics [36], convection [37], mesoscale circulations [38], cloud properties [39], and precipitation [40–42]. A significant impact of urbanization on the spatiotemporal patterns of precipitation was also highlighted in the literature [43–45]. India has witnessed an explosive growth of population (0.3 billion in the year 1950 to 1.04 billion in the year 2002) accompanied by uncontrolled urbanization over the last five decades. The population growth is mainly detected in urban areas due to the large-scale migration of rural population. Around urban areas, natural landscapes have been modified by artificial surfaces during construction, which are more capable of storing solar energy and converting it to sensible heat resulting in an increase of temperature (Urban Heat Island, [46, 47]) compared to surrounding environments. Kaufmann et al. [48] analyzed the impact of urbanization in the Pearl River Delta, China, and suggested more than ~300% increase in urban areas, which were strongly related with reduction in rainfall causing dry winters over the region. To this respect, Lee et al. [49] suggested a significant weakening of ISM due to an increase in surface albedo and reduction in surface roughness. Modeling investigations by the same authors show that monsoon circulation and rainfall are being influenced by the major modifications of the biosphere in the Indian subcontinent, mainly caused by surface energy balance altering, the planetary boundary layer motion fields, moisture convergence, and hydrological cycle. More recently, Kishtawal et al. [50] found a significant increasing trend in the frequency of heavy rainfall over urban regions in India during the monsoon season, with this increasing trend to be more pronounced over areas with faster urbanization.

In the present study, we have analyzed the long-term (1951–2007) variations and trends in precipitation (rainfall amount and number of rainy days) over six Indian cities (namely, Delhi, Hyderabad, Bangalore, Kanpur, Nagpur, and Jaipur). In order to examine possible urban aerosol-pollution forcing on precipitation amount and trends, the analysis has been performed over the upwind and downwind directions of each city during the rainy monsoon (June–September) period. Moreover, extensive literature survey and discussions are provided for possible linkage of the long-term precipitation trends with the increasing anthropogenic aerosols and LULC changes around the urban centers.

Table 1: Upwind and downwind grids around the six selected locations along with the dominant surface wind flow and the dispersion of pollutants during the monsoon period.

Location	Upwind grid	Downwind grid	Surface wind	Dispersion of pollutants
Delhi	27.5°N–78.5°E	29.5°N–76.5°E	Mostly from southeast	Mostly to northwest
Hyderabad	16.5°N–77.5°E	18.5°N–79.5°E	Southwest	Northeast
Kanpur	25.5°N–81.5°E	27.5°N–79.5°E	Mostly from southeast	Mostly to northwest
Jaipur	25.5°N–76.5°E	27.5°N–74.5°E	Mostly from southeast	Mostly to northwest
Nagpur	20.5°N–78.5°E	22.5°N–80.5°E	Southwest	Northeast
Bangalore	11.5°N–76.5°E	13.5°N–78.5°E	Southwest	Northeast

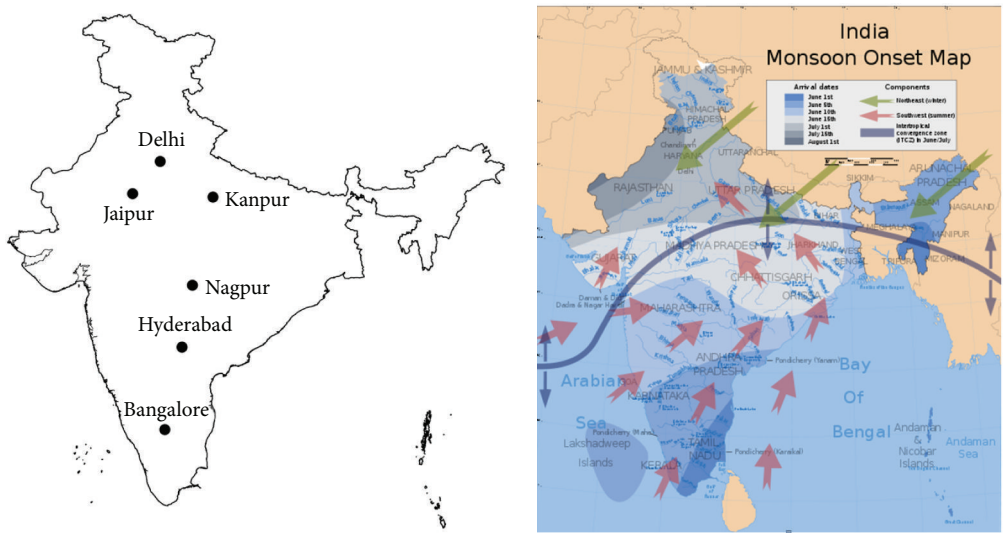

(a) (b)

Figure 1: Locations of the 6 Indian urban cities used in the analysis (a) and monsoon onset map (b) obtained from http://en.wikipedia.org/wiki/File:India_southwest_summer_monsoon_onset_map_en.svg.

2. Selected Sites and Climatology

Six urban locations at different regions of India have been considered for the analysis (Figure 1(a)). Except from the variations in the land use, topography characteristics, and meteorological conditions, the selected urban sites present large differences regarding the monsoon onset as shown in Figure 1(b). This figure shows shifting of the intertropical convergence zone (ITCZ) northwards during the summer monsoon season. The winds are from southwest (except the northwestern part of the country), while the monsoon rainfall affects primarily (beginning of June) the southeastern Indian regions and by the end of July has affected the whole territory except from the northwestern regions (Thar desert and Indian Trans-Himalaya). Detailed information about climatology, land use, and specific characteristics of the different Indian regions can be found in Ramachandran and Cherian [51]. In order to qualitatively assess the urban forcing in precipitation changes, upwind and downwind pixels around the six cities are selected based on the dominant monsoon surface wind flow (Table 1). The sites located in central-south India (Hyderabad, Nagpur, and Bangalore) are influenced by the southwest monsoon flow (Arabian Sea branch; see Figure 1(b)), while the rest sites (Delhi, Jaipur, and Kanpur) are mainly influenced by the Bay of Bengal branch and the dominant surface winds are from east-southeast direction (Figure 1(b)).

2.1. Delhi. Delhi is the capital of India situated in the northern part of the country (28.38°N, 77.12°E, 218 m ASL). It is the largest center of small industries and main commercial center in northern India. The city is densely populated and has a large number of automobiles, thus adding additional loading of industrial and urban emissions, in addition to the desert-dust transport during premonsoon and monsoon [52]. The climate of the area is monsoon-influenced subtropical with large variations in temperature and precipitation between winter and summer seasons. The prevailing winds are mainly easterly, northerly and northwesterly during the summer season [53].

2.2. Hyderabad. Hyderabad (17.47°N, 78.42°E, 547 m ASL) is the fifth largest city in India with ~5.5 million inhabitants and is also considered as one of the most polluted due to population growth and associated anthropogenic activities observed during the last decades. The decennial growth of population (1981–91) is 39.7% against the growth rate of

24.2% for the state. As a consequence, the traffic density has been increased contributing ~75% of all sources of air pollution in Hyderabad [54]. Additionally, dust transported during premonsoon and monsoon, crop residue burning in autumn, and forest fires in the dry period of the year affect the atmosphere over Hyderabad [55–57]. The climate of the region is semiarid with a total rainfall amount of ~700 mm occurring mostly during the monsoon season (June–September) under the influence of the strong south-westerly winds.

2.3. Bangalore. Bangalore (12.58°N, 77.38°E, 920 m ASL) is located in the Deccan Plateau in the southern part of India, which is influenced by the Arabian Sea and the Bay of Bengal. Due to its high elevation, Bangalore usually enjoys salubrious climate throughout the year, although freak heat waves can make life very uncomfortable during summer months. The coolest month is January with an average low temperature of 15.1°C and the hottest month is April with an average high temperature of 33.6°C. Bangalore receives rainfall from both the northeast and the southwest monsoons and the wettest months are September, October, and August [58]. The climate of the area is classed as the seasonally dry tropical savanna climate with four seasons.

2.4. Kanpur. Kanpur (26.28°N, 80.24°E, 142 m ASL) lies in the central part of the Indo-Gangetic Plains and is one of the most polluted cities in India [59]. It is characterized by a very hot summer and cold winter; the temperature during summer goes up to 40°C and in winter it is dropped below 0°C. Kanpur is the 9th most populous city in India and is highly congested, overcrowded and with high aerosol levels [60].

2.5. Jaipur. Jaipur, the capital city of Rajasthan state (26.53°N, 75.50°E, 432 m ASL) located in the northwestern India (close to Thar desert), is one of the fastest growing cities in the country. The climate of the area is extremely hot with humid summers and chilly winters, while aerosols of desert origin dominate [61]. During the monsoon months there are frequent heavy rains and thunderstorms, but flooding is not common. The winter months of November to February are mild and pleasant, with average temperatures in the 15–18°C range and little humidity. However, there are occasional cold waves that lead to temperature near freezing. Monsoon usually starts in the third week of July, but the area does not experience much of rainy days due to its semiarid climate.

2.6. Nagpur. The city of Nagpur (21.09°N, 79.09°, 310 m ASL) located in the central India has been classified under dry or semihumid climate throughout the year except the monsoon months of June–September [62]. The climate witnesses a very hot weather during April–June, while in winter the temperature hovers around 12°C and, sometimes, even dips down to zero. The rainfall is driven by the south-westerly monsoon winds. The mean annual rainfall ranges between 1000 mm and 1300 mm, of which about 80% is received during monsoon.

3. Dataset and Methodology

The daily gridded rainfall data at 1° × 1° spatial resolution from India Meteorological Department (IMD) was used [63]. The IMD product uses gauge data from 1803 stations to estimate accumulated rainfall in the 24 hours ending 08:30 IST (03:00 UTC) during the period 1951–2007. IMD uses the Shepard [64] interpolation technique for gridding data from individual stations over the Indian subcontinent (6.5°N to 37.5°N, 66.5°E to 101.5°E). In this method, the interpolated values are computed from a weighted sum of the observations. More specifically, for a given grid point, the search distance is defined as the distance from this point to a given station, while the interpolation is restricted to the radius of influence. For search distances equal to or greater than the radius of influence, the grid point value is assigned a missing code when there is no station located within this distance. More details about IMD gridded rainfall datasets have been described elsewhere [63]. In the present work, we used the gridded points over the 6 urban centers and the rainfall data in the downwind and upwind directions from the stations, based on climatology of surface wind direction during the rainy monsoon season. It should be noted that the dominant surface wind flow may differentiate during the drought monsoon years, as a response of anomalies in pressure pattern [65], without being considered in the analysis. The upwind and downwind grids remain the same during the whole study period (Table 1), and this may affect the rainfall amount and trends. Thus, for a more detailed analysis, except of the higher spatial resolution grid around the urban areas, the upwind and downwind regions have to account for the daily surface-wind flow. Furthermore, the gridded daily rainfall data over Indian region were analyzed to identify the number of rainy days for each year at the selected stations and in the upwind and downwind directions. The rainy days were detected by noting the rainfall values and the days with rainfall values above "0" were considered as rainy. The variability in precipitation at any grid point depends on large-scale dynamics and the regional/local forcing as well. Therefore, a higher resolution rainfall dataset, like APHRODITE (0.25° × 0.25° and 0.5° × 0.5° resolution), may be more effective in capturing the fluctuation in precipitation due to changes in local emissions and LULC changes [66]. Qualitative comparison between the two gridded databases (IMD and APHRODITE) has been recently performed by Krishnan et al. [67], who found an overall satisfactory agreement concerning the spatial distribution of the trends in rainfall rate over India during the summer monsoon (JJAS) season in the period 1951–2007. We may also point out that the aerosol data is not available in such a high spatial resolution similar to APHRODITE data sets.

4. Results

4.1. Regional Monsoon Meteorology. The ISM is characterized by south-westerly winds in the lower troposphere affecting the most part of the Indian subcontinent and adjoining oceanic regions from June to September being the main source of precipitation over the whole south Asia. This

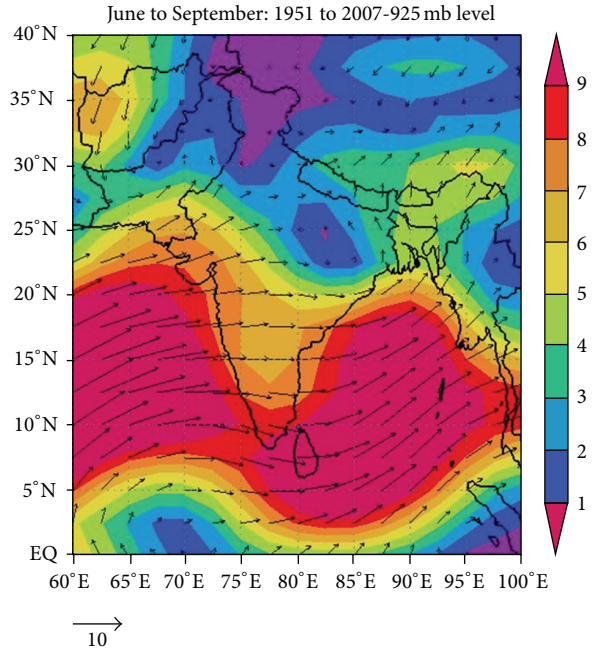

Figure 2: NCEP/NCAR reanalysis mean vector wind composite at 925 mb level for Indian summer monsoon (June–September) during 1951–2007.

system is part of a large-scale circulation pattern, which develops in response to the thermal gradients between the warm Asian continent in the north and cooler Indian Ocean in the south. A center of low-pressure system develops over the western part of India during the summer season, because of the intense heating of the landmass, while high pressure develops over the relatively cooler Indian Ocean. This pressure gradient carries moisture oceanic air masses in to mainland, which are released as precipitation [68].

The mean (1951–2007) composite vector wind at 925-mb level from NCEP/NCAR reanalysis website (http://www.cdc.noaa.gov/cgi-bin/data/composites/printpage.pl/) is shown in Figure 2 during the monsoon period. The mean wind direction is shown by the arrows, while the wind speed depends on arrow length and is color scaled. The winds are mainly south-westerly over the Bay of Bengal (BoB) and the Arabian Sea (AS), shifting towards west over the Indian mainland. The ISM has two branches, (a) the AS branch and (b) the BoB branch. The former dominates the weather scenes in central and peninsular India, while the latter controls the weather scenes in Bangladesh, northeastern India, Indo-Gangetic Plains (IGP), and the southern slopes of Himalayas. The wind speed is larger over sea (above 9 ms^{-1}), while lower speed intensities are observed in the central and northern India. The southern studied locations, that is, Bangalore, Hyderabad, and Nagpur, are influenced more by the abundant moisture from the south-westerly winds than those located in IGP, that is, Delhi and Kanpur, and as a consequence, the monsoon precipitation is larger over southern India and decreases gradually towards the northern parts of the country. This fact may also redistribute the rainfall over the study regions between intense and weak monsoon years.

4.2. Trends in Total Number of Rainy Days. Figure 3 shows the multidecadal trend (1951–2007) in total number of rainy days over the six Indian cities during summer monsoon; the mean number of rainy days is also shown in each panel. Overall, the analysis shows large heterogeneities in the number of rainy days as well as in the multidecadal variability and trends. Thus, Hyderabad, Kanpur, Jaipur, and Nagpur exhibit negative trends in the total number of rainy days; however, positive trends are observed for Delhi and Bangalore results that are in general agreement with those found by De and Prakas Rao [69]. Statistically significant trend at 95% confidence level is shown only at Bangalore strongly influenced by the large peak in 2005. According to the analysis, the total number of rainy days suggests a 7.4% and 22.9% increase over Delhi and Bangalore; however, over Hyderabad, Jaipur, Kanpur, and Nagpur a decrease of −10.4%, −10.5%, −7.1%, and −4.8%, respectively is found. Large interannual variability in the total number of rainy days is observed over all cities attributed to intense and weak monsoon years, which may, in turn, cause significant anomalies in the aerosol field [31]. The large differences in the monsoon onset, duration, and intensity over Indian subcontinent (Figure 1(b)), along with the high spatial variation in the intensity of prolonged dry or drought conditions over the country are the main reasons for the different fluctuations in precipitation dataset over the different locations and, therefore, for the different trends [67]. However, in Bangalore these fluctuations are much smoother, due to its proximity to the AS and BoB, except an abnormal increase in rainy days up to 100 in 2005. This extreme value, also detected in the rainfall amount (Figure 4), seems to be mostly attributed to topography and local forcing since in the upwind region of the city (Figure 10) the variability in rainfall is much more fluctuated with several peaks and gaps, on which the 2005 peak is not so intense. However, at the pixel over Bangalore, as well as in the downwind region, the precipitation exhibits an abnormal increase in 2005. The analysis reveals that the most rainy days are observed in Nagpur (88 ± 9) and Hyderabad (73 ± 9) corresponding to ~72% and ~60% of the total days during the monsoon season. On the other hand, the number of rainy days is less in Jaipur (50 ± 10), Delhi (55 ± 10), and Bangalore (51 ± 12).

Earlier studies suggested that tropospheric warming leads to enhancement of moisture content in the atmosphere, which is associated with an increase in heavy rainfall events [50, 70, 71]. Similarly, significant increasing trends in the frequency and magnitude of extreme rain events have been found over India; however, considerable decline was observed in the frequency of moderate events over central India during 1951–2000 monsoon season [7]. They also suggested a 10% increase in the level of heavy rainfall events per decade from 1951 to 2000, whereas the number of extreme rainfall events indicated an increase of more than double. Further study of the trends in rainy days with light, moderate, and heavy rainfall amount (not shown) also revealed large heterogeneities between the sites, with increasing, neutral, or decreasing trends, which were not statistically significant in the vast majority of the cases. The present analysis revealed an increasing trend of heavy rainfall events (>25 mm) over Bangalore (statistically significant) and Nagpur; however, Delhi,

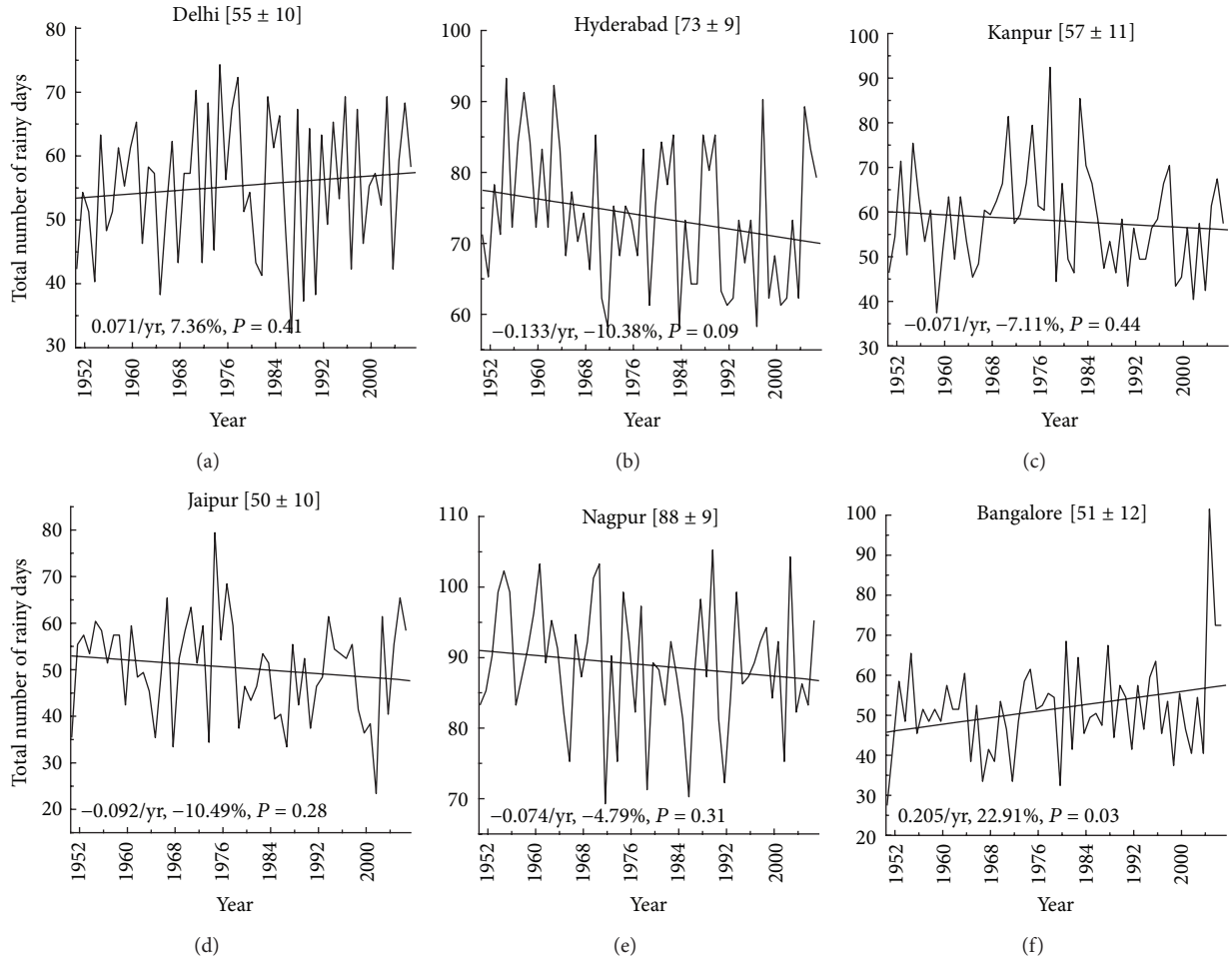

Figure 3: Long-term (1951–2007) trends of the total number of rainy days over Indian mega cities during southwest monsoon (JJAS) period. The mean values along the standard deviations as well as the results from the linear regression in the data series are given.

Jaipur and Kanpur suggested decreasing trends, whereas Hyderabad exhibited mostly neutral trend. The differences between the current results and those reported by Badarinath et al. [72] may be attributed to the different locations considered for the analysis, since we have not included any coastal urban center.

4.3. Trends in Seasonal Precipitation. The ISM rainfall is very important for the economic development, disaster management, and hydrological planning of the country, while the crop failure, drought, or famine due to deficient monsoon becomes very critical to local population [73]. The area-averaged rainfall over the whole country does not show any significant trend; however, large variations can exist at regional scale [74]. Figure 4 shows the trends in monsoonal rainfall over the 6 Indian cities during 1951–2007 accompanied with the mean seasonal rainfall amount and its standard deviation. Furthermore, the slope, the % variation, and the P value from the linear regressions are given at each panel. A general characteristic for all cities is the large year-to-year variability suggesting presence of intense and weak monsoon years [75]. Over Delhi, the seasonal rainfall ranges significantly, from a minimum of ~150 mm to a maximum of ~1000 mm (mean of 609 ± 207), while over Hyderabad it presents lesser variability (310 mm to 965 mm) with similar mean value. Kanpur exhibits a mean of 705 ± 245 mm, while Jaipur and Bangalore present the lowest amounts of rainfall (about 485 and 415 mm, resp.). The semiarid environment close to Thar desert is responsible for the low rainfall in Jaipur, while for Bangalore the main reason is the regional topography and the high mountains around the city able to receive the largest amounts of precipitation. Finally, over Nagpur the seasonal rainfall ranges from a minimum of ~500 mm to a maximum of ~1500 mm. Furthermore, the multidecadal variability exhibits significant differences between the urban sites. Large spatial distribution in monsoon rainfall was also reported by Prasad et al. [29] over Indian subcontinent, while Gautam et al. [76] observed different trends in rainfall over northern India depending on month, for example, positive trend in June and negative for the rest of the monsoon (July–September). Furthermore, no clear periodicity in the rainfall amount was found from the statistical analysis. On the other hand, negative trends in seasonal rainfall are observed over Delhi (−21.3%), Hyderabad (−5.9%), Kanpur (−14.6%), and

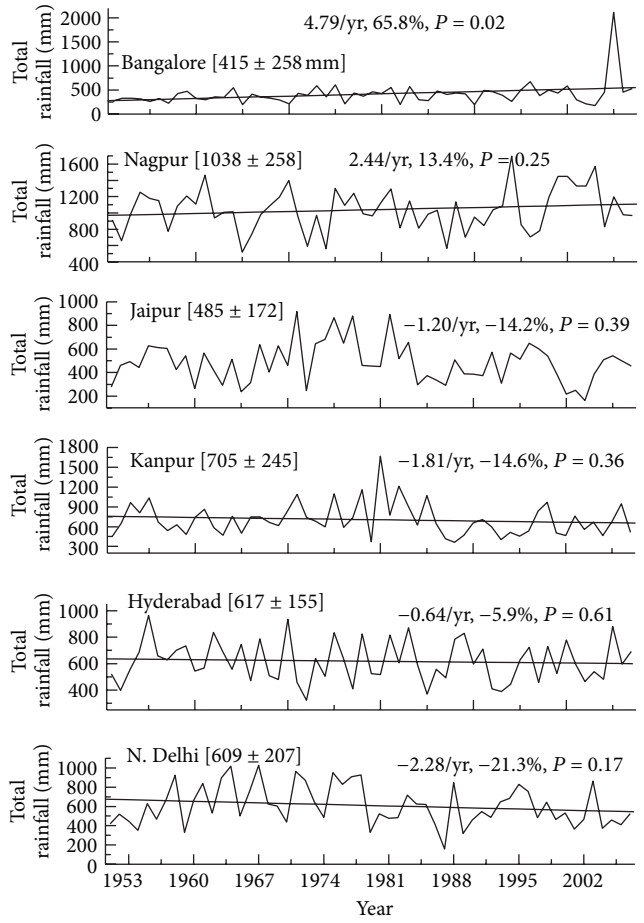

FIGURE 4: Trends in monsoonal rainfall amount (JJAS) over different Indian cities during 1951–2007. The mean values along the standard deviations as well as the results from the linear regression in the data series are given.

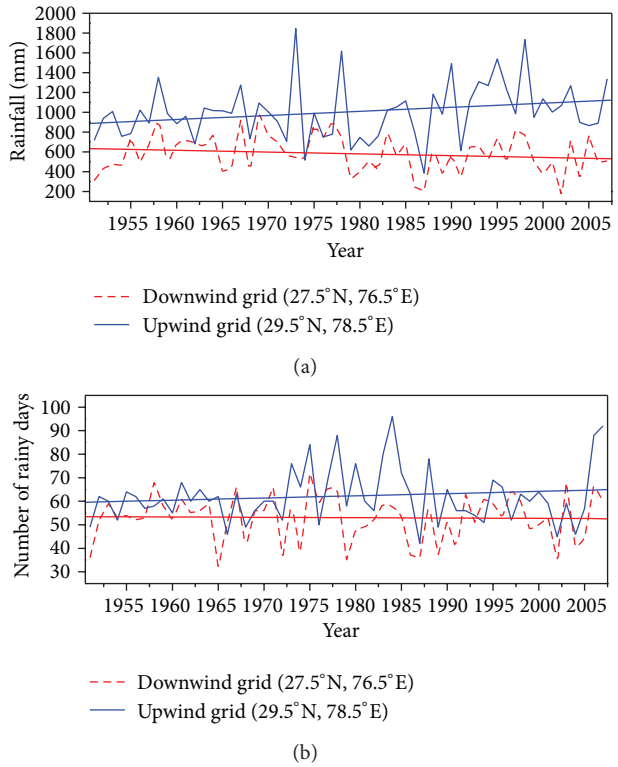

FIGURE 5: Long-term (1951–2007) trends of (a) monsoonal rainfall and (b) total number of rainy days over downwind and upwind grids around Delhi during the southwest monsoon (JJAS) period.

Jaipur (−14.2%); however, Bangalore and Nagpur exhibit increasing trend in monsoon rainfall, corresponding to 65.8% and 13.4%, respectively. Statistically significant trend is considered only in Bangalore, and influenced by the extreme value in 2005, which is even 3 times larger than the climatological mean. Similarly to our findings, De and Prakas Rao [69] observed increasing trend of rainfall over Bangalore. The rainfall trends in Delhi and Nagpur seem not to coincide well with the trends in the rainy days, that is, decrease in rainfall and increase in rainy days for Delhi and the opposite for Nagpur. This inconsistency, although can be partly explained via variations and trends in the rain intensity, may be only pixel-dependent, since in the upwind and downwind regions of both cities (Figures 5 and 9) the two parameters covary.

4.4. Trends in Number of Rainy Days and in Seasonal Precipitation at Upwind and Downwind Grids. According to Rosenfeld [13] and Toon [77] urban and industrial air pollution suppresses precipitation-forming process in convective clouds. Furthermore, Borys et al. [21] suggested that even a little amount of anthropogenic sulfate aerosols may reduce the orographic snowfall rate by up to 50% in the Colorado City Mountains. The most vulnerable regions for precipitation suppression effects are those that are in the downwind direction to the populated urban centers [19]. Thus, the precipitation was found to decrease over hills and mountains downwind of major coastal urban areas in California and Israel, while the suppression rate was found to be 15%–25% of the annual precipitation [19, 78]. In this respect, we further examine the trends in rainfall and number of rainy days in the upwind and downwind directions of the selected urban centers. It is to be noted that due to large spatial distribution of precipitation, the values may differentiate even in nearby pixels, so a qualitative rather than quantitative analysis can be revealed from the following figures.

Figure 5 shows the long-term (1951–2007) trends of (a) rainfall and (b) total number of rainy days at downwind and upwind grids around Delhi during the monsoon (JJAS) period. The seasonal rainfall exhibits a negative trend over the downwind grid. However, the total number of rainy days remains nearly constant over the region. Contrary to the downwind direction, the upwind one shows a pronounced increasing trend in both the seasonal rainfall and total number of rainy days. Note also the significant larger precipitation amount and number of rainy days in the upwind direction. Therefore, there is evidence that the large variation in rainfall, total number of rainy days, and their associated trends, even in a $2^\circ \times 2^\circ$ (~200 × 200 km) region, may be forced by

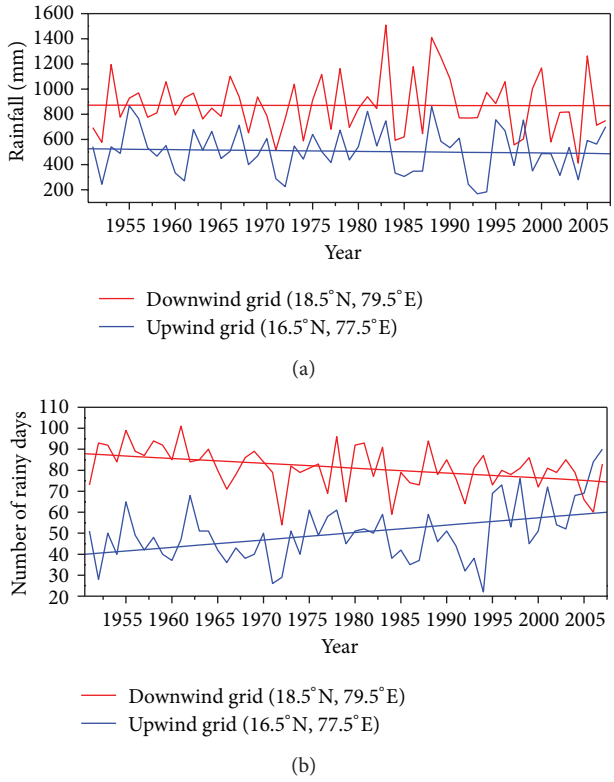

FIGURE 6: Same as in Figure 5 but for Hyderabad.

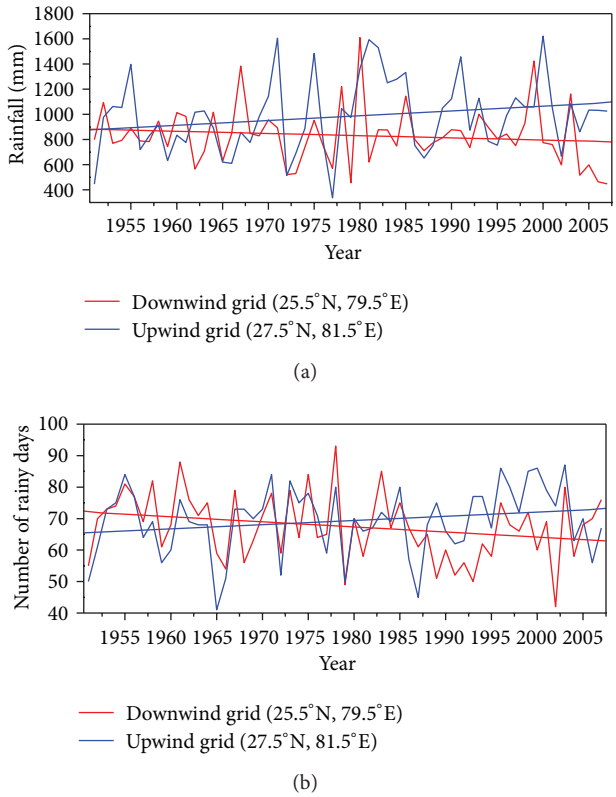

FIGURE 7: Same as in Figure 5 but for Kanpur.

the urbanized area and the local emissions of aerosols and pollutants that suppress precipitation. These results are rather contradictory to those found by Kishtawal et al. [50] who reported an increase in heavy rainfall due to urbanization, since in our case no statistically significant difference was found in the trends of rainfall and number of rainy days.

More or less similar decreasing trends of seasonal rainfall and total number of rainy days at downwind grid of the cities are observed for Hyderabad (Figure 6), Kanpur (Figure 7), Jaipur (Figure 8), and Nagpur (Figure 9). However, the trends in both rainfall and total number of rainy days in the downwind directions present significant variability, since the precipitation is a strong function of the local and regional topography, the synoptic meteorology, and wind speed. More specifically, Hyderabad presents a neutral variation in rainfall amount (for downwind pixel), but a pronounced decreasing trend in the number of rainy days. Kanpur shows similar to Hyderabad trends in rainfall and number of rainy days for the downwind pixel, while Jaipur exhibits neutral variation in the number of rainy days and a slight decrease in rainfall. On the other hand, in Nagpur the slight decreasing trend in the number of the rainy days was mostly pronounced for the heavy rainfall amounts (not shown), while a similar decreasing trend is observed in rainfall. In contrast, Bangalore exhibits slight increasing trend in seasonal rainfall and rainy days at the downwind direction, mainly driven by the large rainfall amount in 2005 (Figure 10). However, the difference in rainfall amount between upwind and downwind pixels around Bangalore is about four-fold, or even more

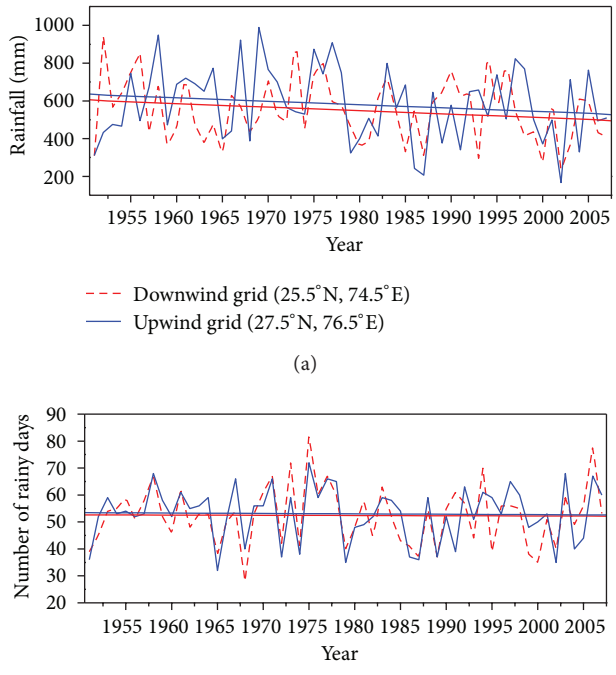

FIGURE 8: Same as in Figure 5 but for Jaipur.

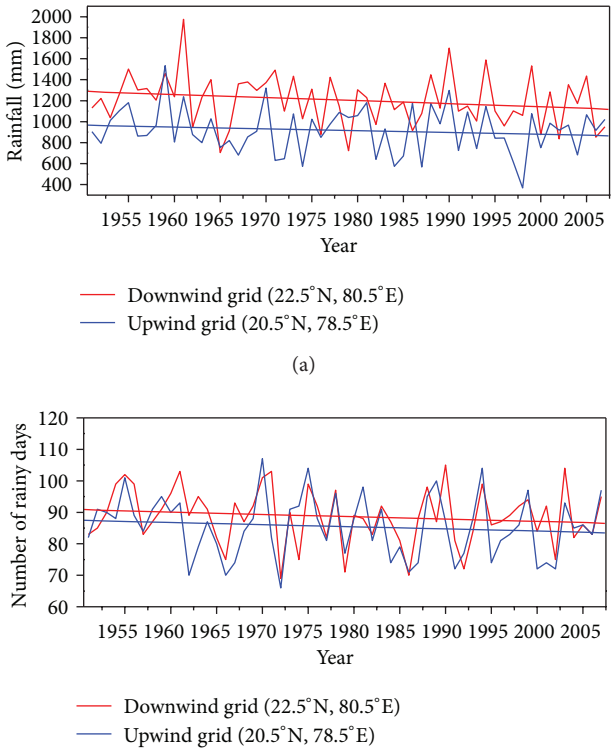

Figure 9: Same as in Figure 5 but for Nagpur.

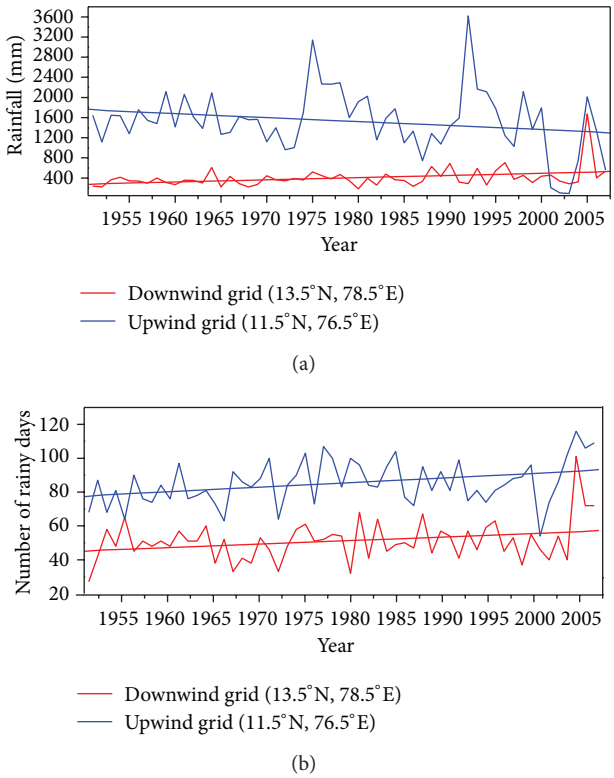

Figure 10: Same as in Figure 5 but for Bangalore.

Table 2: Percentage (%) variation in rainfall and number of rainy days in upwind (up) and downwind (down) directions of the 6 Indian cities. The statistically significant trends in 95% confidence level are defined via bold.

Station	Rainfall Direction		Number of rainy days Direction	
	up	down	up	down
Delhi	23.41	−17.84	8.56	−1.60
Hyderabad	−7.40	−0.40	**40.16**	**−16.27**
Kanpur	21.95	11.88	10.94	−13.59
Jaipur	−17.84	−19.23	−1.62	−0.87
Nagpur	−10.71	−13.60	−4.54	−4.76
Bangalore	−29.38	**60.74**	**17.77**	**22.85**

at specific years, a fact that indicates a strong influence of the regional topography also. Similar feature, that is, much lower values at the downwind pixel, is also observed for the total number of rainy days. On the other hand, increasing trends of the total number of rainy days at upwind grid of the cities are observed over Hyderabad, Kanpur, and Bangalore, while Nagpur and Jaipur exhibit slightly negative or neutral trends. Table 2 summarizes the % variations in rainfall and number of rainy days as obtained from the linear regression analysis. Despite the significant differences between the sites, the results show that the trends in rainfall and total number of rainy days at the downwind directions are mostly negative, while higher precipitation at the upwind directions occurs.

5. Discussion

This section aims to associate the multidecadal variability in precipitation amount between upwind and downwind areas around the cities with trends in anthropogenic aerosols and pollutants, the growing rate of population and LULC changes due to urbanization. Several ground-based and satellite observations highlight an increase in aerosol loading over Indian subcontinent, especially for the anthropogenic component, during the last decades [27, 79, 80]. This is a direct consequence of the increase in population density [81], demands for energy, urbanization, and industrialization being a major reason for the continuation of the solar dimming phenomenon [72, 82] and the formation of atmospheric brown clouds [83]. Increasing trends in aerosol optical depth (AOD) during the last decade have been observed over Delhi [84], Kanpur [85], Hyderabad [86], Trivandrum [87], Pune [88], and several other locations in India [51]. However, the increasing AOD trends exhibited significant spatiotemporal heterogeneity over Indian mainland and adjoining oceanic regions as revealed from the aforementioned studies. The main finding is that a large increase in anthropogenic AOD occurs in the winter season mainly due to increasing rates of Black Carbon, organics, and sulphates [89]. According to this, Ramanathan et al. [14] reported that aerosols attenuate significantly the surface heating and evaporation and slow down the hydrological cycle, while Menon et al. [90] observed a large change in the precipitation distribution over south Asia attributed to the increased anthropogenic emissions.

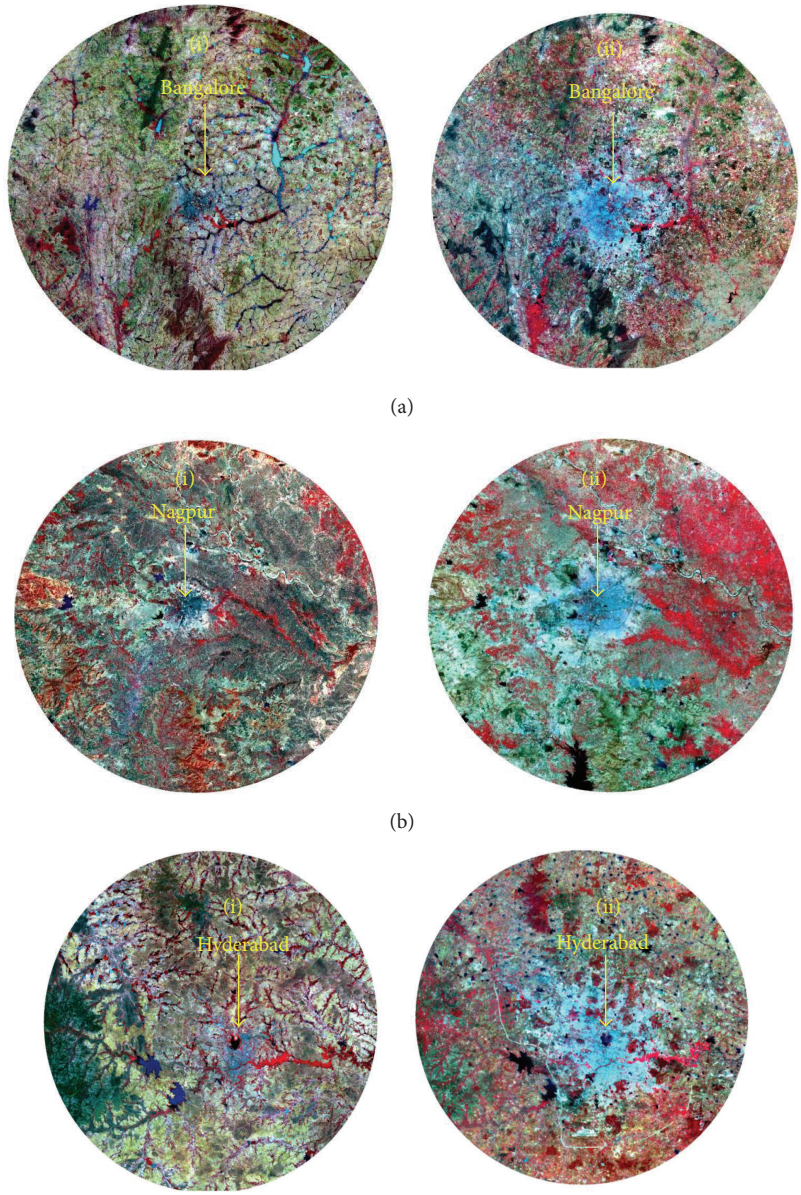

Figure 11: False color composite of (i) LANDSAT-MSS during 1972-73 and (ii) IRS-AWiFS during 2006-07 over Bangalore (a), Nagpur (b), and Hyderabad (c) cities.

More recently, Gautam et al. [91] found a strong influence of the increasing aerosol amount during premonsoon to the monsoon onset, duration, and intension. On the other hand, Lee et al. [49] noted a decrease in seasonal surface temperatures over Indian subcontinent as a result of massive irrigation that led to weakened Indian monsoon circulation.

However, several studies have shown a contrasting feature of precipitation that may increase or decrease due to anthropogenic aerosols, while the mechanisms remain mostly unclear involving microphysical, thermodynamic, and dynamic processes. Ayers [92] and Alpert et al. [93] disputed on the suppression of precipitation due to urban pollutions. Rosenfeld [94] noted suppression of rain due to forest fires in Indonesia via satellite observations, whereas Lin et al. [95] highlighted increasing rainfall trend associated with elevated aerosol layers during the biomass burning season in Amazonia. Jirak and Cotton [96] reported decrease in precipitation during the past half-century at downwind directions of Denver and Colorado Springs, contrary to other studies [97–99] that found increasing rainfall downwind of major urban areas possibly due to giant CCN from paper mills exhausts. On the other hand, Warner [100] by analyzing long-term ground measurements showed no evidence of subsequent changes in surface precipitation results that agree with

those of Woodcock and Jones [101] over Hawaii. Therefore, there are critical difficulties for the quantitative examination of the rainfall trends over the urban environments in view of the trends in aerosol loading above them, since both parameters are significantly linked to other factors as well. This is also true in the current analysis, since no clear trend was found for the precipitation variation between upwind and downwind areas. The evidence of mostly decreasing trend and lesser precipitation amount in the downwind directions are not statistically significant at the majority of the cases. The low level moisture convergence, which is not considered in the current work, may play an important role in the cloud and precipitation formation [31, 68, 102]. In depth investigation into the microphysical properties of polluted clouds over the urban environments may better explain the precipitation trends and their association with aerosols and local pollutants. This is the concept of the recent, and still ongoing, cloud aerosol interactions and precipitation enhancement experiment (CAIPEEX) campaign over selected sites in India [15, 103].

The rapid population growth, LULC changes, and accelerated socioeconomic activities have modified the environment over India during the last decades [104]. Furthermore, LULC changes can significantly contribute to overall climate change and rainfall patterns [105]. Lamptey et al. [106] have investigated climatic sensitivity to agriculture and urban land cover over northeastern United States and found an increase of more than 1 K over the urban sites during summer and winter as a result of urbanization. The urban areas in India have experienced rapid human and industrial development during the last 50 years, which caused serious environmental degradation. Figures 11(a)–11(c) show the false color composite of Bangalore, Nagpur, and Hyderabad cities, respectively, during 1972-73 (Landsat-MSS) and 2006-07 (IRS-P6 AWiFS). Bangalore represents an uneven landscape with intermingling of hill and valleys with bare rocky outcrops and falls into high elevation zone. The change analysis between false color composites during 1972-73 and 2006-07 suggests large-scale expansion of Bangalore city; however, in addition to urban expansion, increase in vegetation conditions was also observed, which may be related to the increase in total precipitation (Figure 4) and number of rainy days (Figure 3), since the increase in leaf area index increases evapotranspiration and surface heating, thus favoring precipitation [107]. Nagpur city lies on the Deccan plateau of the Indian Peninsula and the surrounding region is undulating plateau rising northward to the Satpura range from 889 to 2142 feet high and is drained by several rivers. Nagpur also experienced expansion of urbanization along with increased vegetation activities over the study period. A large dam constructed towards south of the city is evident in 2006-07 image, which did not exist during 1972-73. The slight increase in rainfall (Figure 4) can be addressed to the increase in vegetation and enhanced evaporation from the man-made lake. Figure 11(c) shows a significant expansion in the urban area of Hyderabad during the last 3 decades, as well as important changes in the LULC outside the city, directly affecting the anthropogenic emissions and AOD [86]. Therefore, the changes in rainfall patterns, and mainly those between downwind and upwind directions around the urban areas, may be associated to the large LULC changes around the Indian cities and to increased number of automobiles, industries, and anthropogenic emissions. However, the linkage between urban areas expansion, anthropogenic emissions, and rainfall trends depends also on regional meteorology, topography, aerosol properties, and concentration of undisturbed cloud-active particles [108].

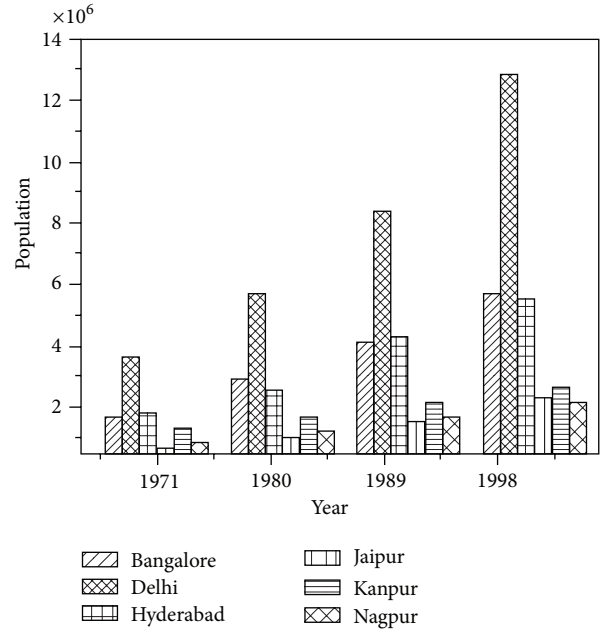

Figure 12: Population growth over the 6 Indian cities during 1971–1998.

Figure 12 shows the population growth for the six Indian cities from 1971 to 1998. A pronounced increasing trend in population is found in all cities and, especially in Delhi, closely associated with the increasing aerosol and pollutant emissions [89]. However, Figure 12 covers only a part of the studied period and, therefore, the trend in population growth is expected to be higher if the 6 last decades are taken into account. Detailed analysis of the growing in population density and associated changes in precipitation has recently been reported by Kishtawal et al. [50]. The tremendous increase in population and associated emissions along with serious land degradation and LULC changes around the Indian cities enhance the urban heat island effect and modify the urban microclimate, which may also have effects on precipitation. Thus, the variation in precipitation amount and trends at upwind and downwind regions of the urban centers may partly be explained by the LULC changes, increase in population and emissions.

6. Conclusions

In the present study, we have analyzed the trends in monsoon rainfall and number of rainy days over six major Indian cities (Delhi, Hyderabad, Kanpur, Jaipur, Nagpur, and Bangalore) during the period 1951–2007. The study also provided an extensive literature overview concerning the precipitation

trends and anthropogenic factors influencing it around the urban environments. The main results are summarized as follows.

(i) A decrease of −21.3%, −5.9%, −14.2% and −14.6%, in seasonal monsoon rainfall was observed over Delhi, Hyderabad, Jaipur, and Kanpur, respectively, whereas Bangalore and Nagpur showed 65.8% and 13.4% increase during the period 1951–2007.

(ii) The total number of rainy days showed 7.4% and 22.9% increase over Delhi and Bangalore cities; however, over Hyderabad, Jaipur, Kanpur, and Nagpur it showed −10.4%, −10.5%, −7.1%, and −4.8% decrease in the monsoon season. These findings will be helpful to the public planners and agricultural scientists to work out irrigation and water management options as well as to prevent floods and droughts. However, in the vast majority of the cases the above-mentioned trends in rainfall amount and number of rainy days are not statistically significant at 95% confidence level. Overall, the analysis did not reveal a clear trend in precipitation, which seems to be location-dependent.

(iii) The differences observed between the cities due to regional meteorology and topography and the statistical insignificance of the trends (in the vast majority of the cases) prevent us from a safe conclusion about the trend in monsoonal precipitation, although an evidence of a decreasing trend in the majority of the stations. In general, the decreasing trend seemed to be more pronounced in the downwind directions of each urban environment implying a possible anthropogenic forcing in precipitation, although such an influence cannot be quantified due to lack of statistical significance. The long-term rainfall data revealed that the suppression of precipitation exhibits a slight increasing trend during the last decades further motivated from the continuously increasing emission rates. The urban areas produce large amounts of pollutants, which increase the number of cloud condensation nuclei in the atmosphere and decrease the mean droplet radius. This creates a lack of coalescence and inhibits precipitation formation, especially in the downwind to the cities directions. On the other hand, urban pollution may increase heavy rainfall as some studies showed. Aerosol-cloud-precipitation interactions are complicated phenomena involving several microphysical, dynamic, and thermodynamic processes. Therefore, a more detailed analysis and evaluation of the results necessitate measured gauge precipitation in upwind and downwind directions of the cities as well as advanced model simulations.

Acknowledgments

The authors thank the Director of the National Remote Sensing Center (NRSC), Hyderabad and the Dy. Director of the RS&GIS-AA, NRSC for the necessary help at various stages and ISRO-GBP for funding support. The authors gratefully acknowledge Indian Meteorological Department (IMD) for providing gridded rainfall dataset over Indian region. The authors would like to thank the NCEP/NCAR science data support team for processing the meteorological data and the Landsat and IRS missions. The authors are thankful to their colleague late Dr. K. V. Badarinath for his help and suggestions in completing this work. Comments/suggestions made by three anonymous reviewers are thankfully acknowledged that have helped us to improve the earlier version of the paper.

References

[1] L. S. Kuchment, "The hydrological cycle and human impact on it," in *Water Resources ManagementEncyclopedia of Life Support Systems (EOLSS), Developed under the Auspices of the UNESCO*, A. Y. Hoekstra and H. H. G. Savenije, Eds., Eolss Publishers, Oxford, UK.

[2] D. Rosenfeld, U. Lohmann, G. B. Raga et al., "Flood or drought: how do aerosols affect precipitation?" *Science*, vol. 321, no. 5894, pp. 1309–1313, 2008.

[3] K. R. Kumar, G. B. Pant, B. Parthasarathy, and N. A. Sontakke, "Spatial and subseasonal patterns of the long-term trends of Indian summer monsoon rainfall," *International Journal of Climatology*, vol. 12, no. 3, pp. 257–268, 1992.

[4] A. Basistha, D. S. Arya, and N. K. Goel, "Analysis of historical changes in rainfall in the Indian Himalayas," *International Journal of Climatology*, vol. 29, no. 4, pp. 555–572, 2009.

[5] D. Duhan and A. Pandey, "Statistical analysis of long term spatial and temporal trends of precipitation during 1901–2002 at Madhya Pradesh, India," *Atmospheric Research*, vol. 122, pp. 136–149, 2013.

[6] K. C. Sinha Ray and A. K. Srivastava, "Is there any change in extreme events like heavy rainfall?" *Current Science*, vol. 79, no. 2, pp. 155–158, 2000.

[7] B. N. Goswami, V. Venugopal, D. Sangupta, M. S. Madhusoodanan, and P. K. Xavier, "Increasing trend of extreme rain events over India in a warming environment," *Science*, vol. 314, no. 5804, pp. 1442–1445, 2006.

[8] N. Malik, B. Bookhagen, N. Marwan, and J. Kurths, "Analysis of spatial and temporal extreme monsoonal rainfall over South Asia using complex networks," *Climate Dynamics*, pp. 1–17, 2011.

[9] P. Guhathakurtha, P. Menon, A. B. Mazumdar, and O. P. Sreejith, "Changes in extreme rainfall events and flood risk in India during last century," Research Report 14, India Met Department, National Climate Centre (NCC), Pune, 2010.

[10] S. K. Dash, J. R. Kumar, and M. S. Shekhar, "On the decreasing frequency of monsoon depressions over the Indian region," *Current Science*, vol. 86, no. 10, pp. 1404–1411, 2004.

[11] M. Lal, "Climatic change-implications for India's water resources," *Journal of Indian Water Resources Society*, vol. 21, pp. 101–119, 2001.

[12] S. M. Bawiskar, "Weakening of lower tropospheric temperature gradient between Indian landmass and neighbouring oceans and its impact on Indian monsoon," *Journal of Earth System Science*, vol. 118, no. 4, pp. 273–280, 2009.

[13] D. Rosenfeld, "Suppression of rain and snow by urban and industrial air pollution," *Science*, vol. 287, no. 5459, pp. 1793–1796, 2000.

[14] V. Ramanathan, P. J. Crutzen, J. T. Kiehl, and D. Rosenfeld, "Atmosphere: aerosols, climate, and the hydrological cycle," *Science*, vol. 294, no. 5549, pp. 2119–2124, 2001.

[15] S. Dipu, T. V. Prabha, G. Pandithurai et al., "Impact of elevated aerosol layer on the cloud microphysical properties prior to monsoon onset," *Atmospheric Environment*, vol. 70, pp. 454–467, 2013.

[16] V. Ramaswamy, "Radiative forcing of climate change," in *Climate Change 2001: The Scientific Basis, Contribution of Working Group I to the Third Assessment Report of the Intergovernmental Panel on Climate Change*, J. T. Houghton, Y. Ding, D. J. Griggs, M. Noguer, P. J. van der Linden, and X. Dai, Eds., chapter 6, Cambridge University Press, Cambridge, UK, 2001.

[17] U. Lohmann and J. Feichter, "Global indirect aerosol effects: a review," *Atmospheric Chemistry and Physics*, vol. 5, no. 3, pp. 715–737, 2005.

[18] M. O. Andreae, D. Rosenfeld, P. Artaxo et al., "Smoking Rain Clouds over the Amazon," *Science*, vol. 303, no. 5662, pp. 1337–1342, 2004.

[19] A. Givati and D. Rosenfeld, "Quantifying precipitation suppression due to air pollution," *Journal of Applied Meteorology*, vol. 43, pp. 1038–1056, 2004.

[20] D. Rosenfeld, J. Dai, X. Yu et al., "Inverse relations between amounts of air pollution and orographic precipitation," *Science*, vol. 315, no. 5817, pp. 1396–1398, 2007.

[21] R. D. Borys, D. H. Lowenthal, S. A. Cohn, and W. O. J. Brown, "Mountaintop and radar measurements of anthropogenic aerosol effects on snow growth and snowfall rate," *Geophysical Research Letters*, vol. 30, no. 10, pp. 45–1, 2003.

[22] R. D. Borys, D. H. Lowenthal, and D. L. Mitchell, "The relationships among cloud microphysics, chemistry, and precipitation rate in cold mountain clouds," *Atmospheric Environment*, vol. 34, no. 16, pp. 2593–2602, 2000.

[23] D. Rosenfeld, W. L. Woodley, D. Axisa, E. Freud, J. G. Hudson, and A. Givati, "Aircraft measurements of the impacts of pollution aerosols on clouds and precipitation over the Sierra Nevada," *Journal of Geophysical Research D*, vol. 113, no. 15, Article ID D15203, 2008.

[24] D. P. Kaiser and Y. Qian, "Decreasing trends in sunshine duration over China for 1954–1998: indication of increased haze pollution?" *Geophysical Research Letters*, vol. 29, no. 21, pp. 38–1, 2002.

[25] Q. Xu, "Abrupt change of the mid-summer climate in central east China by the influence of atmospheric pollution," *Atmospheric Environment*, vol. 35, no. 30, pp. 5029–5040, 2001.

[26] Y. Qian, W. Wang, L. R. Leung, and D. P. Kaiser, "Variability of solar radiation under cloud-free skies in China: the role of aerosols," *Geophysical Research Letters*, vol. 34, no. 12, Article ID L12804, 2007.

[27] G. Habib, C. Venkataraman, I. Chiapello, S. Ramachandran, O. Boucher, and M. Shekar Reddy, "Seasonal and interannual variability in absorbing aerosols over India derived from TOMS: relationship to regional meteorology and emissions," *Atmospheric Environment*, vol. 40, no. 11, pp. 1909–1921, 2006.

[28] Z. Levin and W. Cotton, "Aerosol pollution impact on precipitation: a scientific review," Report from the WMO/IUGG International Aerosol Precipitation Science Assessment Group (IAPSAG) (World Meteorological Organization, Geneva, Switzerland, 2007), 2007.

[29] A. K. Prasad, S. Sarkar, R. P. Singh, and M. Kafatos, "Interannual variability of vegetation cover and rainfall over india," *Advances in Space Research*, vol. 39, no. 1, pp. 79–87, 2007.

[30] S. Sarkar, L. Chiu, M. Kafatos, and R. Singh, "Sensitivity of rainfall on land cover change over South East Asia: some observational results," *Advances in Space Research*, vol. 39, no. 1, pp. 73–78, 2007.

[31] M. G. Manoj, P. C. S. Devara, P. D. Safai, and B. N. Goswami, "Absorbing aerosols facilitate transition of Indian monsoon breaks to active spells," *Climate Dynamics*, vol. 37, no. 11-12, pp. 2181–2198, 2011.

[32] A. Teller and Z. Levin, "The effects of aerosols on precipitation and dimensions of subtropical clouds: a sensitivity study using a numerical cloud model," *Atmospheric Chemistry and Physics*, vol. 6, no. 1, pp. 67–80, 2006.

[33] W.-K. Tao, X. Li, A. Khain, T. Matsui, S. Lang, and J. Simpson, "Role of atmospheric aerosol concentration on deep convective precipitation: cloud-resolving model simulations," *Journal of Geophysical Research D*, vol. 112, no. 24, Article ID D24S18, 2007.

[34] W.-K. Tao, J.-P. Chen, Z. Li, C. Wang, and C. Zhang, "Impact of aerosols on convective clouds and precipitation," *Reviews of Geophysics*, vol. 50, Article ID RG2001, 2012.

[35] G. Li, Y. Wang, K.-H. Lee, Y. Diao, and R. Zhang, "Increased winter precipitation over the North Pacific from 1984–1994 to 1995–2005 inferred from the global precipitation climatology project," *Geophysical Research Letters*, vol. 35, no. 13, Article ID L13821, 2008.

[36] D. S. Niyogi, S. Raman, and K. Alapaty, "Uncertainty in the specification of surface characteristics, part II: hierarchy of interaction-explicit statistical analysis," *Boundary-Layer Meteorology*, vol. 91, no. 3, pp. 341–366, 1999.

[37] R. A. Pielke Sr., "Influence of the spatial distribution of vegetation and soils on the prediction of cumulus convective rainfall," *Reviews of Geophysics*, vol. 39, no. 2, pp. 151–177, 2001.

[38] S. B. Roy and R. Avissar, "Impact of land use/land cover change on regional hydrometeorology in Amazonia," *Journal of Geophysical Research D*, vol. 107, no. 20, pp. 67–68, 2002.

[39] D. K. Ray, U. S. Nair, R. O. Lawton, R. M. Welch, and R. A. Pielke Sr., "Impact of land use on Costa Rican tropical montane cloud forests: sensitivity of orographic cloud formation to deforestation in the plains," *Journal of Geophysical Research D*, vol. 111, no. 2, Article ID D02108, 2006.

[40] C. H. Marshall, R. A. Pielke Sr., L. T. Steyaert, and D. A. Willard, "The impact of anthropogenic land-cover change on the Florida Peninsula Sea Breezes and warm season sensible weather," *Monthly Weather Review*, vol. 132, no. 1, pp. 28–52, 2004.

[41] E. M. Douglas, A. Beltrán-Przekurat, D. Niyogi, R. A. Pielke Sr., and C. J. Vörösmarty, "The impact of agricultural intensification and irrigation on land-atmosphere interactions and Indian monsoon precipitation—a mesoscale modeling perspective," *Global and Planetary Change*, vol. 67, no. 1-2, pp. 117–128, 2009.

[42] V. Mishra, K. A. Cherkauer, D. Niyogi et al., "A regional scale assessment of land use/land cover and climatic changes on water and energy cycle in the upper Midwest United States," *International Journal of Climatology*, vol. 30, no. 13, pp. 2025–2044, 2010.

[43] J. M. Shepherd, H. Pierce, and A. J. Negri, "Rainfall modification by major urban areas: observations from spaceborne rain radar on the TRMM satellite," *Journal of Applied Meteorology*, vol. 41, no. 7, pp. 689–701, 2002.

[44] D. Niyogi, T. Holt, S. Zhong, P. C. Pyle, and J. Basara, "Urban and land surface effects on the 30 July 2003 mesoscale convective system event observed in the southern Great Plains," *Journal of Geophysical Research D*, vol. 111, no. 19, Article ID D19107, 2006.

[45] T. L. Mote, M. C. Lacke, and J. M. Shepherd, "Radar signatures of the urban effect on precipitation distribution: a case study for Atlanta, Georgia," *Geophysical Research Letters*, vol. 34, no. 20, Article ID L20710, 2007.

[46] T. R. Oke, "The urban energy balance," *Progress in Physical Geography*, vol. 12, no. 4, pp. 471–508, 1988.

[47] X. Zhang, F. W. Zwiers, G. C. Hegerl et al., "Detection of human influence on twentieth-century precipitation trends," *Nature*, vol. 448, no. 7152, pp. 461–465, 2007.

[48] R. K. Kaufmann, K. C. Seto, A. Schneider, Z. Liu, L. Zhou, and W. Wang, "Climate response to rapid urban growth: evidence of a human-induced precipitation deficit," *Journal of Climate*, vol. 20, no. 10, pp. 2299–2306, 2007.

[49] E. Lee, T. N. Chase, B. Rajagopalan, R. G. Barry, T. W. Biggs, and P. J. Lawrence, "Effects of irrigation and vegetation activity on early Indian summer monsoon variability," *International Journal of Climatology*, vol. 29, no. 4, pp. 573–581, 2009.

[50] C. M. Kishtawal, D. Niyogi, M. Tewari, R. A. Pielke, and J. M. Shepherd, "Urbanization signature in the observed heavy rainfall climatology over India," *International Journal of Climatology*, vol. 30, no. 13, pp. 1908–1916, 2010.

[51] S. Ramachandran and R. Cherian, "Regional and seasonal variations in aerosol optical characteristics and their frequency distributions over India during 2001-2005," *Journal of Geophysical Research D*, vol. 113, no. 8, Article ID D08207, 2008.

[52] S. Singh, K. Soni, T. Bano, R. S. Tanwar, S. Nath, and B. C. Arya, "Clear-sky direct aerosol radiative forcing variations over megacity Delhi," *Annales Geophysicae*, vol. 28, no. 5, pp. 1157–1166, 2010.

[53] S. Singh, S. Nath, R. Kohli, and R. Singh, "Aerosols over Delhi during pre-monsoon months: characteristics and effects on surface radiation forcing," *Geophysical Research Letters*, vol. 32, no. 13, Article ID L13808, pp. 1–4, 2005.

[54] K. M. Latha, K. V. S. Badarinath, and K. K. Moorthy, "Impact of diesel vehicular emissions on ambient black carbon concentration at an urban location in India," *Current Science*, vol. 86, no. 3, pp. 451–453, 2004.

[55] S. K. Kharol and K. V. S. Badarinath, "Impact of biomass burning on aerosol properties over tropical urban region of Hyderabad, India," *Geophysical Research Letters*, vol. 33, no. 20, Article ID L20801, 2006.

[56] K. V. S. Badarinath, S. K. Kharol, D. G. Kaskaoutis, and H. D. Kambezidis, "Case study of a dust storm over Hyderabad area, India: its impact on solar radiation using satellite data and ground measurements," *Science of the Total Environment*, vol. 384, no. 1-3, pp. 316–332, 2007.

[57] K. V. S. Badarinath, S. Kumar Kharol, and A. Rani Sharma, "Long-range transport of aerosols from agriculture crop residue burning in Indo-Gangetic Plains—a study using LIDAR, ground measurements and satellite data," *Journal of Atmospheric and Solar-Terrestrial Physics*, vol. 71, no. 1, pp. 112–120, 2009.

[58] V. Sreekanth, "Satellite derived aerosol optical depth climatology over Bangalore, India," *Advances in Space Research*, vol. 51, no. 12, pp. 2297–2308, 2013.

[59] R. P. Singh, S. Dey, S. N. Tripathi, V. Tare, and B. Holben, "Variability of aerosol parameters over Kanpur, northern India," *Journal of Geophysical Research D*, vol. 109, no. 23, Article ID D23206, pp. 1–14, 2004.

[60] A. K. Srivastava, S. N. Tripathi, S. Dey, V. P. Kanawade, and S. Tiwari, "Inferring aerosol types over the Indo-Gangetic Basin from ground based sunphotometer measurements," *Atmospheric Research*, vol. 109-110, pp. 64–75, 2012.

[61] R. Gautam, N. C. Hsu, S. C. Tsay et al., "Accumulation of aerosols over the Indo-Gangetic plains and southern slopes of the Himalayas: distribution, properties and radiative effects during the 2009 pre-monsoon season," *Atmospheric Chemistry and Physics*, vol. 11, no. 24, pp. 12841–12863, 2011.

[62] J. Singh, M. Kumar, and B. K. Bhattacharya, "Global radiation, transmissivity and bright sunshine hour trend over Nagpur in pre-monsoon and monsoon seasons," *Atmospheric and Climate Sciences*, vol. 2, pp. 206–209, 2012.

[63] M. Rajeevan, J. Bhate, J. D. Kale, and B. Lal, "High resolution daily gridded rainfall data for the Indian region: analysis of break and active monsoon spells," *Current Science*, vol. 91, no. 3, pp. 296–306, 2006.

[64] D. Shepard, "A two-dimensional interpolation function for irregularly spaced data," in *Proceedings of the 23rd ACM National Conference*, pp. 517–523, 1968.

[65] D. G. Kaskaoutis, R. Gautam, R. P. Singh et al., "Influence of anomalous dry conditions on aerosols over India: transport, distribution and properties," *Journal of Geophysical Research*, vol. 117, Article ID D09106, 2012.

[66] A. Yatagai, K. Kamiguchi, O. Arakawa, A. Hamada, N. Yasutomi, and A. Kitoh, "Constructing a long-term daily gridded precipitation dataset for Asia based on a dense network of rain gauges," *Bulletin of the American Meteorological Society*, vol. 93, pp. 1401–1415, 2012.

[67] R. Krishnan, T. P. Sabin, D. C. Ayantika et al., "Will the South Asian monsoon overturning circulation stabilize any further?" *Climate Dynamics*, vol. 40, pp. 187–211, 2013.

[68] P. K. Patra, S. K. Behera, J. R. Herman, S. Maksyutov, H. Akimoto, and T. Yamagata, "The Indian summer monsoon rainfall: interplay of coupled dynamics, radiation and cloud microphysics," *Atmospheric Chemistry and Physics*, vol. 5, no. 8, pp. 2181–2188, 2005.

[69] U. S. De and G. S. Prakas Rao, "Urban climatic trends, 2004," *Journal of Indian Geophysical Union*, vol. 8, no. 3, pp. 199–203, 2004.

[70] M. R. Allen and W. J. Ingram, "Constraints on future changes in climate and the hydrologic cycle," *Nature*, vol. 419, no. 6903, pp. 224–232, 2002.

[71] K. E. Trenberth, A. Dai, R. M. Rasmussen, and D. B. Parsons, "The changing character of precipitation," *Bulletin of the American Meteorological Society*, vol. 84, no. 9, pp. 1205–1161, 2003.

[72] K. V. S. Badarinath, A. R. Sharma, D. G. Kaskaoutis, S. K. Kharol, and H. D. Kambezidis, "Solar dimming over the tropical urban region of Hyderabad, India: effect of increased cloudiness and increased anthropogenic aerosols," *Journal of Geophysical Research D*, vol. 115, no. 21, Article ID D21208, 2010.

[73] C. Bhuiyan, R. P. Singh, and W. A. Flügel, "Modelling of ground water recharge-potential in the hard-rock Aravalli terrain, India: a GIS approach," *Environmental Earth Sciences*, vol. 59, no. 4, pp. 929–938, 2009.

[74] P. Guhathakurta and M. Rajeevan, "Trends in the rainfall pattern over India," *International Journal of Climatology*, vol. 28, no. 11, pp. 1453–1469, 2008.

[75] R. L. Bhawar and P. C. S. Devara, "Study of successive contrasting monsoons (2001-2002) in terms of aerosol variability over a tropical statio Pune, India," *Atmospheric Chemistry and Physics*, vol. 10, no. 1, pp. 29–37, 2010.

[76] R. Gautam, N. C. Hsu, K.-M. Lau, and M. Kafatos, "Aerosol and rainfall variability over the Indian monsoon region: distributions, trends and coupling," *Annales Geophysicae*, vol. 27, no. 9, pp. 3691–3703, 2009.

[77] O. B. Toon, "How pollution suppresses rain," *Science*, vol. 287, no. 5459, pp. 1763–1765, 2000.

[78] A. Givati and D. Rosenfeld, "Separation between cloud-seeding and air-pollution effects," *Journal of Applied Meteorology*, vol. 44, no. 9, pp. 1298–1314, 2005.

[79] S. T. Massie, O. Torres, and S. J. Smith, "Total Ozone Mapping Spectrometer (TOMS) observations of increases in Asian aerosol in winter from 1979 to 2000," *Journal of Geophysical Research D*, vol. 109, no. 18, pp. D18211–14, 2004.

[80] K. K. Moorthy, S. S. Babu, M. R. Manoj, and S. K. Satheesh, "Buildup of aerosols over the Indian Region," *Geophysical Research Letters*, vol. 40, no. 5, pp. 1011–1014, 2013.

[81] P. Kishcha, B. Starobinets, O. Kalashnikova, and P. Alpert, "Aerosol optical thickness trends and population growth in the Indian subcontinent," *International Journal of Remote Sensing*, vol. 32, no. 24, pp. 9137–9149, 2011.

[82] A. Ohmura, "Observed decadal variations in surface solar radiation and their causes," *Journal of Geophysical Research*, vol. 114, Article ID D00D05, 2009.

[83] V. Ramanathan, C. Chung, D. Kim et al., "Atmospheric brown clouds: impacts on South Asian climate and hydrological cycle," *Proceedings of the National Academy of Sciences of the United States of America*, vol. 102, no. 15, pp. 5326–5333, 2005.

[84] N. K. Lodhi, S. N. Beegum, S. Singh, and K. Kumar, "Aerosol climatology at Delhi in the Western Indo Gangetic Plain: microphysics, long-term trends and source strengths," *Journal of Geophysical Research*, vol. 118, pp. 1–15, 2013.

[85] D. G. Kaskaoutis, R. P. Singh, R. Gautam, M. Sharma, P. G. Kosmopoulos, and S. N. Tripathi, "Variability and trends of aerosol properties over Kanpur, northern India using AERONET data (2001-10)," *Environmental Research Letters*, vol. 7, no. 2, Article ID 024003, 2012.

[86] S. K. Kharol, K. V. S. Badarinath, A. R. Sharma, D. G. Kaskaoutis, and H. D. Kambezidis, "Multiyear analysis of Terra/Aqua MODIS aerosol optical depth and ground observations over tropical urban region of Hyderabad, India," *Atmospheric Environment*, vol. 45, no. 8, pp. 1532–1542, 2011.

[87] K. K. Moorthy, S. S. Babu, S. K. Satheesh et al., "Climate implications of anthropogenic aerosols and trace gases: Indian scenario," in *WCC-3 Climate Sense*, G. R. Asrar, Ed., pp. 157–160, World Meteorological Organization, Tudor Rose, UK, 2009.

[88] K. K. Dani, P. Ernest Raj, P. C. S. Devara et al., "Long-term trends and variability in measured multi-spectral aerosol optical depth over a tropical urban station in India," *International Journal of Climatology*, vol. 32, no. 1, pp. 153–160, 2012.

[89] Z. Lu, Q. Zhang, and D. G. Streets, "Sulfur dioxide and primary carbonaceous aerosol emissions in China and India, 1996–2010," *Atmospheric Chemistry and Physics*, vol. 11, no. 18, pp. 9839–9864, 2011.

[90] S. Menon, J. Hansen, L. Nazarenko, and Y. Luo, "Climate effects of black carbon aerosols in China and India," *Science*, vol. 297, no. 5590, pp. 2250–2253, 2002.

[91] R. Gautam, N. C. Hsu, K.-M. Lau, S.-C. Tsay, and M. Kafatos, "Enhanced pre-monsoon warming over the Himalayan-Gangetic region from 1979 to 2007," *Geophysical Research Letters*, vol. 36, no. 7, Article ID L07704, 2009.

[92] G. P. Ayers, "Air pollution and climate change: has air pollution suppressed rainfall over Australia?" *Clean Air and Environmental Quality*, vol. 39, pp. 51–57, 2005.

[93] P. Alpert, N. Halfon, and Z. Levin, "Does air pollution really suppress precipitation in Israel?" *Journal of Applied Meteorology and Climatology*, vol. 47, no. 4, pp. 933–943, 2008.

[94] D. Rosenfeld, "TRMM observed first direct evidence of smoke from forest fires inhibiting rainfall," *Geophysical Research Letters*, vol. 26, no. 20, pp. 3105–3108, 1999.

[95] J. C. Lin, T. Matsui, S. Pielke, and C. Kummerow, "Effects of biomass-burning-derived aerosols on precipitations and clouds in the Amazon Basin: a satellite-based empirical study," *Journal of Geophysical Research D*, vol. 111, no. 19, Article ID D19204, 2006.

[96] I. L. Jirak and W. R. Cotton, "Effect of air pollution on precipitation along the front range of the rocky mountains," *Journal of Applied Meteorology and Climatology*, vol. 45, no. 1, pp. 236–245, 2006.

[97] E. E. Hindman II, P. M. Tag, B. A. Silverman, and P. V. Hobbs, "Cloud condensation nuclei from a paper mill. 2. Calculated effects on rainfall," *Journal of Applied Meteorology*, vol. 16, no. 7, pp. 753–755, 1977.

[98] R. R. Braham Jr., "Summary of urban effects on clouds and rain," *Meteorological Monographs*, vol. 18, no. 40, pp. 141–152, 1981.

[99] G. K. Mather, "Coalescence enhancement in large multicell storms caused by the emissions from a kraft paper mill," *Journal of Applied Meteorology*, vol. 30, no. 8, pp. 1134–1146, 1991.

[100] J. Warner, "Smoke from sugar-cane fires and rainfall," in *Proceedings of International Conference on Weather Modification*, pp. 191–192, American Meteorological Society, Canberra, Canada, 1971.

[101] A. H. Woodcock and R. H. Jones, "Rainfall trends in Hawaii," *Journal of Applied Meteorology*, vol. 9, pp. 690–696, 1970.

[102] A. Hazra, V. Mandal, and J. P. Chen, "Study of cloud microphysical properties over India during CAIPEEX using a mesoscale model with new cloud microphysical scheme—part I," *Journal of Atmospheric and Solar-Terrestrial Physics*, vol. 93, pp. 29–44, 2013.

[103] K. Chakravarty, P. Mukhopadhyay, and S. Taraphdar, "Cloud microphysical properties as revealed by the CAIPEEX and satellite observations and evaluation of a cloud system resolving model simulation of contrasting large scale environments," *Journal of Atmospheric and Solar-Terrestrial Physics*, vol. 73, no. 13, pp. 1790–1797, 2011.

[104] R. Gautam, N. C. Hsu, and K.-M. Lau, "Premonsoon aerosol characterization and radiative effects over the Indo-Gangetic plains: implications for regional climate warming," *Journal of Geophysical Research D*, vol. 115, no. 17, Article ID D17208, 2010.

[105] S. J. Burian and J. M. Shepherd, "Effect of urbanization on the diurnal rainfall pattern in Houston," *Hydrological Processes*, vol. 19, no. 5, pp. 1089–1103, 2005.

[106] B. L. Lamptey, E. J. Barron, and D. Pollard, "Impacts of agriculture and urbanization on the climate of the Northeastern United States," *Global and Planetary Change*, vol. 49, no. 3-4, pp. 203–221, 2005.

[107] Y. Kim and G. Wang, "Impact of vegetation feedback on the response of precipitation to antecedent soil moisture anomalies over North America," *Journal of Hydrometeorology*, vol. 8, no. 3, pp. 534–550, 2007.

[108] E. K. Bigg, "Trends in rainfall associated with sources of air pollution," *Environmental Chemistry*, vol. 5, no. 3, pp. 184–193, 2008.